MECHANISTIC MODELING OF THE EFFECT OF PAVEMENT SURFACE PROFILE ON ROLLING RESISTANCE

FINAL PROJECT REPORT

by

Shabnam Rajaei
Karim Chatti
Michigan State University

Sponsorship
Center for Highway Pavement Preservation
(CHPP)

for

Center for Highway Pavement Preservation
(CHPP)

In cooperation with US Department of Transportation-Research and Innovative Technology Administration (RITA)

May 2020

Disclaimer

The contents of this report reflect the views of the authors, who are responsible for the facts and the accuracy of the information presented herein. This document is disseminated under the sponsorship of the U.S. Department of Transportation's University Transportation Centers Program, in the interest of information exchange. The Center for Highway Pavement Preservation (CHPP), the U.S. Government and matching sponsor assume no liability for the contents or use thereof.

Technical Report Documentation Page

1. Report No. CHPP Report-MSU#7-2020	2. Government Accession No.	3. Recipient's Catalog No.	
4. Title and Subtitle Mechanistic Modeling of The Effect of Pavement Surface Profile on Rolling Resistance		5. Report Date	
		6. Performing Organization Code	
7. Author(s) Shabnam Rajaei, Karim Chatti		8. Performing Organization Report No.	
9. Performing Organization Name and Address CHPP Center for Highway Pavement Preservation, Tier 1 University Transportation Center Michigan State University, 2857 Jolly Road, Okemos, MI 48864		10. Work Unit No. (TRAIS)	
		11. Contract or Grant No.	
12. Sponsoring Organization Name and Address United States of America Department of Transportation Research and Innovative Technology Administration		13. Type of Report and Period Covered	
		14. Sponsoring Agency Code	
15. Supplementary Notes Report uploaded at http://www.chpp.egr.msu.edu/			

16. Abstract

Rolling resistance of a vehicle plays an important role in the vehicle's fuel consumption. There are different mechanisms involved in the rolling resistance, namely, vehicle dynamics, tire bending and deformation, and tire tread deformation. Pavement surface profile is one of the factors that influences the rolling resistance and it can be divided into four scales of roughness, mega-, macro- and micro-texture. These scales influence different mechanisms of the rolling resistance. The micro-texture scale, despite being very important for friction, has a negligible effect on the rolling resistance of the tire. The macro-texture scale mostly affects the tread deformation and tire bending mechanisms of rolling resistance. The mega-texture scale, which includes both wavelengths within and beyond the tire contact patch, affects the vehicle dynamics and suspension system in addition to the tire deformation and bending. The roughness scale mostly affects the deformation in the vehicle's suspension. The main aim of this study is to evaluate the effect of these scales on the vehicle's rolling resistance. For capturing the effect of the full surface profile on rolling resistance a model that is capable of evaluating all of the mechanisms involved in the rolling resistance is required. Such a model should include the tire as well as the suspension system of the vehicle. Here, for modeling the deformations within the tire, including tire bending and tread deformation, a full 3D finite element tire model is developed and verified. For investigating the energy dissipation in the vehicle suspension system, the tire model is combined with a quarter-car mechanical model, which is a simplified system of a spring and a dashpot in parallel.

The surface profile is decomposed into different scales and characterized using root mean square (RMS) parameter. The effect of each scale of the profile on the rolling resistance is evaluated separately using the developed models. For each scale, the effect of profile on the tire as well as the suspension is assessed. Then the effects of different scales are compared with each other. The effect of macro-texture scale is found to be more on the tire deformation while roughness scale affects the suspension system more. The effect of mega-texture is found to be considerable, influencing the rolling resistance within the tire more than the suspension. A reasonable agreement is found between the developed models and the existing empirical studies for different scales.

17. Key Words Rolling Resistance, Pavement, Roughness, Texture, Finite element modeling		18. Distribution Statement No restrictions.	
19. Security Classification (of this report) Unclassified.	20. Security Classification (of this page) Unclassified.	21. No. of Pages	22. Price NA

Form DOT F 1700.7 (8-72) Reproduction of completed page authorized

Table of Contents

List of Figures

List of Tables

List of Abbreviations

CHPP Center of Highway Pavement Preservation

FE Finite element

FEM Finite element modeling

IRI International roughness index

MPD Mean profile depth

PIARC Permanent International Association of Road Congresses

RMS Root mean square

RRC Rolling resistance coefficient

RRF Rolling resistance force

Acknowledgments

This research has been supported by Center of Highway Pavement Preservation (CHPP) and funded by United States Department of Transportation (USDOT). We thank our colleague Dr. Imen Zaabar for her insightful suggestions for surface characterization. We also thank Dr. Matteo Pettinari from Danish Road Directorate for providing surface profile data to us. A special thank you to our colleague, Ali Imani Azad, for his help and support during the project.

Executive Summary

General Background

Many factors are involved in the design of a pavement including energy efficiency, safety, load capacity, ride quality, durability, noise, and cost. In 2011, approximately 71 percent of the petroleum used in the United States was used in the transportation sector, accounting for 28 percent of the U.S. energy demand (EPA, 2012). Given the increase in public awareness of global warming, the interest in improving vehicle fuel economy has escalated in the past decade. While numerous factors such as vehicle aerodynamics and engine efficiency influence the fuel consumption of the vehicle, the contact between the tire and pavement surface also affects the energy loss in the tire and the vehicle; and subsequently the fuel consumption. This energy loss is often quantified as rolling resistance of the vehicle which includes different mechanisms of vehicle dynamics (energy loss in the suspension system), tire vibration and deformation, and tire tread deformation (Bendtsen, 2004). Pavement properties such as pavement surface profile and structure can influence these mechanisms. The pavement surface profile can be divided into various scales of roughness (unevenness), mega-, macro-, and micro-textures (PIARC, Permanent International Association of Road Congresses). These scales can affect different mechanisms of the vehicle rolling resistance.

Problem Statement

The empirical studies conducted for investigating the effect of surface profile, in particular roughness and macrotexture, are mostly related to the vehicle fuel consumption (Chatti & Zaabar, 2012, Sandberg et al, 2011). These studies have empirical rolling resistance models included within their fuel consumption models. Only a few studies investigated the effect of surface profile based on the actual rolling resistance measurements (Boere, 2009).

The available numerical models, on the other hand, are more limited specially for the effect of texture on rolling resistance. Due to the wide range of the wavelengths within the pavement surface profile, and the difference between the macro-texture and roughness scales and their involved mechanisms, the existing models are only able to capture the effect of one of these scales.

The macro-texture is assumed to only affect the energy dissipation within the tire. The mean profile depth (MPD) parameter is usually used for texture characterization of the macro-texture. On the other hand, the effect of roughness on rolling resistance is considered to be more dominant on the vehicle suspension than the tire deformation. For investigation of the effect of pavement profile on vehicle suspension, the international roughness index (IRI) is usually used. It should be noted that IRI does not differentiate between roughness and mega-texture scales of the profile. It is defined based on the wavelengths higher than 250 mm, which include the full roughness scale and a portion of mega-texture scale of the profile. As the result, so far, the effect of roughness and mega-texture scales on rolling resistance has not been studied separately.

In addition, since the parameters used for surface characterization of these scales are very different, it is not possible to perform a rigorous comparison of the effect of the different scales on rolling resistance.

Therefore, to address these shortcomings in the current state of the art, the main goal of this project is to develop a mechanistic model that is able to capture the effect of the whole surface profile spectrum on the rolling resistance of the vehicle. Also, a common surface characterization parameter will be selected for assessing the relative contribution of each surface scale to vehicle and tire rolling resistance. In addition, some limitations in the existing models will be addressed.

Key Methodology

Finite element modeling has proven to be a reliable tool for mechanistic modeling of different phenomena. FE modeling of the tire has been used for many purposes, from modeling the vehicle operation conditions to the effect of pavement friction or even pavement structural influence on rolling resistance (Falk et al, 2016; Srirangam, 2015; Hernandez, 2015). However, such a model can be computationally very time consuming if the tire is in contact with profiles with very small wavelengths. Srirangam (2015) developed such a model for investigating the effect of texture on friction and reported the model to be computationally very expensive. Here, for capturing the effect of macro-texture on rolling resistance, a similar model is required as well.

The effect of roughness, on the other hand, is usually captured using simplified mechanistic models such as the quarter-car model, which consists of a simplified suspension system and tire model that is a combination of a spring and a dashpot in parallel, with their required properties found experimentally.

To include both the effect of small textures and roughness in one single model, a quarter-car FE model is proposed in this study. Such a model includes a detailed finite element model of the tire with small mesh size for capturing the effect of the macro-texture profile and a spring and dashpot suspension system for capturing the effect of surface roughness profile. Such a model can include all of the mechanisms involved in the rolling resistance of the vehicle, from tread deformation and tire bending to the vehicle dynamics.

The main purpose of this project is to develop a computational model for evaluating the effect of different scales of surface profile on rolling resistance of the vehicle. Using the developed model, the effect and importance of each scale of the profile (roughness, mega-, and macro-texture) on the rolling resistance of the vehicle can be determined. For this purpose, the surface profile will be divided into various scales, based on the standard definition of surface texture and roughness from PIARC, to evaluate their effects separately.

In addition, this model will be used to address some of the shortcomings of the existing models, including (i) having different models for the evaluation of the effect of different scales, (ii) allowing the model to lose contact with the profile if necessary, and (iii) including the effect of textures with wavelength smaller than 250 mm on the rolling resistance of the vehicle.

Major Findings and Their Implications

The obtained results show that a linear relationship exists between the RMS of different scales of macro-texture, mega-texture, and roughness and rolling resistance coefficient (RRC) of the tire and the quarter-car model. The profiles with low RMS show minimal effect on suspension of the vehicle, regardless of their scales. For higher RMS values, the mega-texture profiles and roughness profiles affect the suspension similarly. However, the effect of mega-texture on tire is much more

than roughness. Consequently, the overall effect of mega-texture on rolling resistance of the quarter is higher than roughness.

It can be argued that the higher effect of mega-texture captured by the model for higher values of RMS is due to the presence of high mega-texture along the full profiles, while in reality high values of RMS for mega-texture are related to local events only. To address this issue, a few profiles with local events of mega-texture were studied. It is found that the mega-texture's effect on rolling resistance of the tire and vehicle suspension system can be noticeable, even when the events are isolated.

The results from both the 3D FE tire model and the FE quarter-car model developed in this project are then compared with previous studies. The influence of macro-texture on the rolling resistance is compared with a few empirical studies, namely the NCHRP 720 report, the MIRIAM project, and Boere study. NCHRP 720 report and the MIRIAM project are based on the energy dissipation of the vehicle and there is a significant difference between their results. Boere's study on the other hand measured rolling resistance directly using a trailer. The tire model results are closer to Boere's study; however, it slightly overestimates the influence of macro-texture on RRC in comparison to Boere's study.

On comparison of the influence of roughness and mega-texture on rolling resistance, the results of the FE Quarter-car model are compared with mechanical quarter-car model by Zaabar et al. (2018) and NCHRP 720 report. The excess rolling resistance forces from the three models match very well for the lower IRI values (IRI<4m/km), which represents the majority of the IRI values for pavement surfaces in the US. For IRI values higher than 4m/km, the rolling resistance forces of the FE model diverges from NCHRP 720 report results, while being reasonably close to those from the mechanical quarter-car model.

The results of this project show that the mega-texture profile within the contact patch also affect the suspension of the vehicle. The current cut-off wavelength for the effect of pavement texture on displacement in the vehicle suspension and IRI calculation is considered as the contact patch length (250 mm). Therefore, further investigation is required for finding a new cut-off wavelength for the effect of texture on vehicle suspension.

The developed FE model allows the tire to lose contact with the profile if necessary. This loss of contact occurs in reality, especially in rough surfaces. However, although when the tire does not have contact with the surface and the resisting forces within the tire are minimum, the impact with the surface after contact can increase the rolling resistance. Therefore, the effect of this loss of contact is not understood fully and it should be investigated further.

CHAPTER 1
LITERATURE REVIEW

1.1 INTRODUCTION

The vehicle/tire-pavement interaction depends on three components; vehicle/tire, pavement, and operating conditions. Pavement surface profile, including surface roughness (unevenness) and texture is one of the main factors influencing different aspects of vehicle/tire-pavement interaction.

When a vehicle runs over a profile of a given unevenness, its body and axles will vibrate and the internal damping in the suspension system and tire will dissipate energy. Similarly, when a tire rolls over the pavement surface, a fraction of the texture (referred to as engaged texture) will penetrate into the rubber, which causes energy dissipation due to the viscoelastic nature of the rubber. The relationships between various engaged texture wavelengths, roughness/unevenness, and various aspects of vehicle/tire-pavement interactions are shown in Figure 1-1.

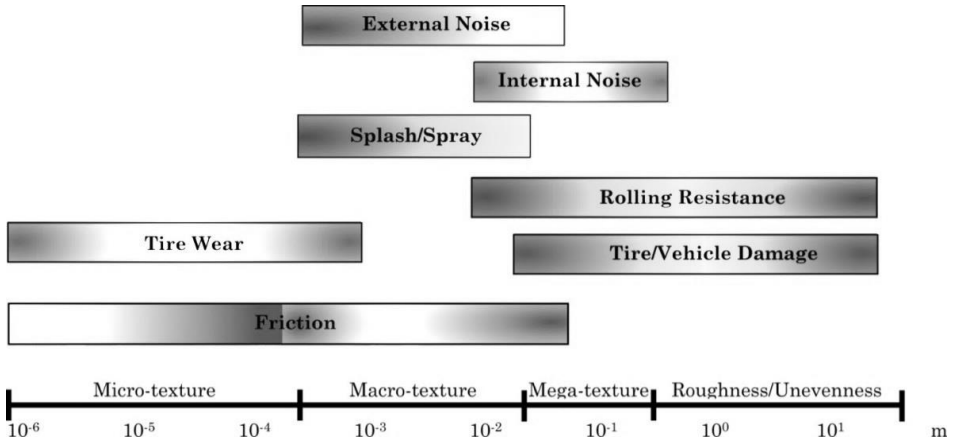

Note: Darker shading is an indicator of a more favorable effect of texture

Figure 1-1. Influence of texture and roughness wavelength on vehicle/tire-pavement interactions (after Henry, 2000 and Sandburg and Ejmont, 2000)

As it can be seen, it is widely accepted that smaller-scaled textures influence friction and tire wear, while the larger-scaled textures and roughness/unevenness affect rolling resistance and vehicle/tire damage. There is a good understanding of the effect of pavement surface texture on friction. However, the surface profile effect on rolling resistance and fuel consumption has only been investigated in a few studies.

To better understand the effect of surface profile on rolling resistance, the profile is divided into four levels of roughness, mega-, macro-, and micro-texture. The effect of each level on rolling resistance is investigated separately. Therefore, the structure of this chapter is as follows: First, previous studies on surface profile characterization, modeling, and measurement are addressed. Second, the available studies on the effect of roughness, mega-, macro-, and micro-textures on rolling resistance are discussed, respectively. It is worth noting that, as it was mentioned in the introduction chapter, due to the trade-off between friction and rolling resistance, an additional review was conducted on friction, which can be found in Appendix A.

1.2 PAVEMENT SURFACE PROFILE CHARACTERIZATION

Pavement surface profile can be divided into unevenness/roughness and texture, which has three different scales of mega-texture, macro-texture, and micro-texture (see Figure 1-2). Pavement surface texture is characterized as deviations of the surface from a true planar surface. As shown in Figure 1-2 (Sandburg, 1990), Permanent International Association of Road Congresses (PIARC) (1995) defined micro-texture as a wavelength shorter than 0.5 mm and peak to peak amplitude of 0.001 to 0.5 mm. The macro-texture is characterized by wavelengths between 0.5 and 50 mm and peak to peak amplitude of 0.1 to 20 mm, while mega-texture is defined by wavelengths between 50 and 500 mm and peak to peak amplitude of 0.1 to 50 mm. Any wavelength larger than the upper limit of mega-texture is characterized as roughness/unevenness. Figure 1-3 demonstrates a representation of texture characteristics (wavelength and amplitude).

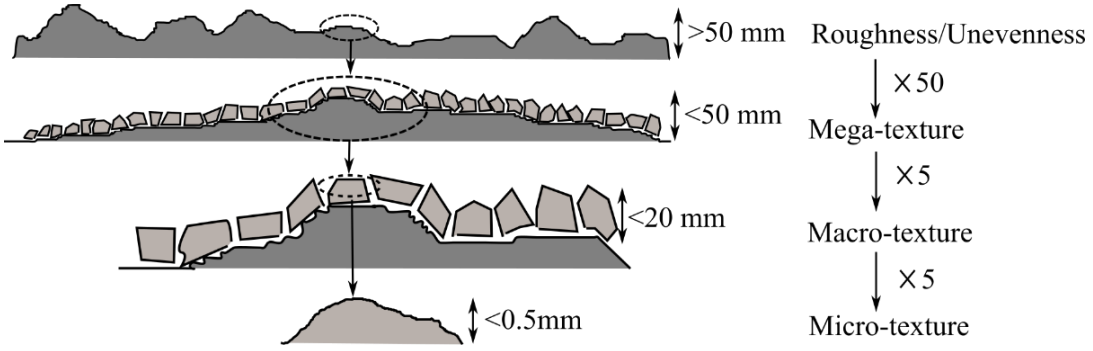

Figure 1-2. Simplified illustration of various pavement surface profile ranges (after Sandburg, 1990

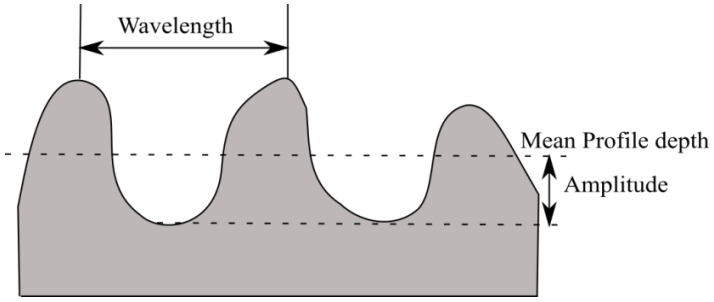

Figure 1-3. Surface texture characteristics

1.2.1 Road profile filtering

Filtering is a common way in signal processing to eliminate the unwanted voltage fluctuations from the signal. Pavement profile is very similar to a signal being in spatial domain instead of a time domain. A pavement profile includes grade, roughness/unevenness, and texture. Inclusion of the grade in the profile dominates the other two components. Therefore, filtering of the pavement profile is needed to obtain roughness and texture profiles (Gillespie and Sayer, 1981). The same process can be performed for distinguishing between surface roughness and texture, or even the different levels of texture. When studying the effect of roughness on vehicle response and performance, it is important to eliminate both grade and short wavelength textures since the experimental measurements have shown that tires filter short wavelengths from the road by

enveloping small bumps (Kenis, 1995). A moving average filter is a way to perform the long and short wavelengths filtering, in which the profile is smoothened by averaging adjacent elevation values together (see Figure 1-4). The filtered profile can be obtained by the following equation (Kenis, 1995):

$$X_H = \frac{1}{2\lambda_c}\int_{x-\lambda_c}^{x+\lambda_c} X_R(x)\ dx \qquad \text{eq. 1-1}$$

$$X_L = X_R - X_H \qquad \text{eq. 1-2}$$

where X_R is the raw profile, X_L is the low-pass profile, X_H is the high-pass profile, and λ_c is the cutoff wavelength of the moving average filter.

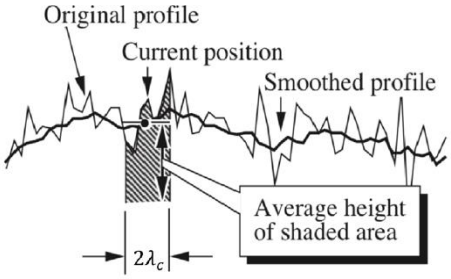

Figure 1-4. Moving average filter of a profile (Sayers and Karamihas, 1996)

Using this process, a surface profile can be divided into roughness, mega-, macro-, and micro-texture scales if required.

1.2.2 Surface profile characterization

A profile consists of a series of numbers representing the elevation of each point of the surface relative to a certain reference line. There are various methods for characterizing the surface profile. The available methods for characterization of roughness and textures are usually different from each other. Therefore, in this section they are discussed separately.

Roughness characterization

Roughness or unevenness can be defined as the wavelengths that result into excitations in the vehicle at one of its resonant frequencies at different speeds. When the amplitude of this resonant frequency is large, the vibration or vertical accelerations of the vehicle can be quite noticeable. As a result of this acceleration a significant vertical force is applied to the road, which can result in damage to the road (Hudson, 1981). Most of the vehicles in a particular class possess similar characteristics when driving at a similar speed on a given road surface. Therefore, the excitation of the vehicle can be considered as a function of the wavelength content of the road profile surface (Hudson, 1981). International Roughness Index (IRI) is based on this assumption and is the most common statistical parameter for characterizing roughness.

For defining IRI, a standard quarter-car model is introduced (see Figure 1-5). This model considers the suspension system of the vehicle as a parallel system of a spring and a dashpot, while modeling the tire with only a linear spring. Since the aim of the model is to simulate the deflection of the suspension system in response to the road roughness, the assumption of linear spring for tire modeling is considered as acceptable.

The IRI is then defined as the accumulated suspension motion or deflection divided by the length of measurement. Therefore, IRI is an index with units of slope in m/km or in/mi.

$$IRI = \frac{\sum Suspension\ movement}{profile\ length} \qquad \text{eq. 1-3}$$

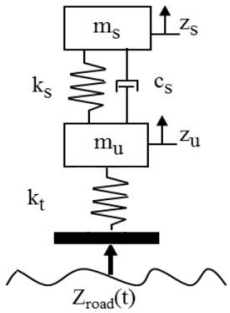

Figure 1-5. Schematic of Two DoF Quarter-Car Vehicle Model

As it was mentioned before, the surface profile is similar to a signal in spatial domain. Therefore, another useful method for representing the profile is using the Power Spectral Density (PSD) function. There are various techniques for estimating the PSD of a signal or profile, from non-parametric methods, e.g., periodogram or correlogram, to parametric methods, e.g., signal model beforehand. A common method for finding a power spectrum is using the Fast Fourier transform (FFT). FFT divides the surface into combinations of magnitudes and their corresponding frequencies. PSD can be obtained by the log-log plot of the squared magnitude versus the frequencies (see Figure 1-6).

One of the first stochastic models proposed for representation of roads is based on the PSD function (Gillespie and Sayer, 1981):

$$G_z(v) = {}^{A}/_{(2\pi v)^2} \qquad \text{eq. 1-4}$$

where $G_z(v)$ is the PSD function of elevation z, v is a wavenumber, and A is a roughness coefficient which is obtained by fitting the PSD of a measured profile to the above equation.

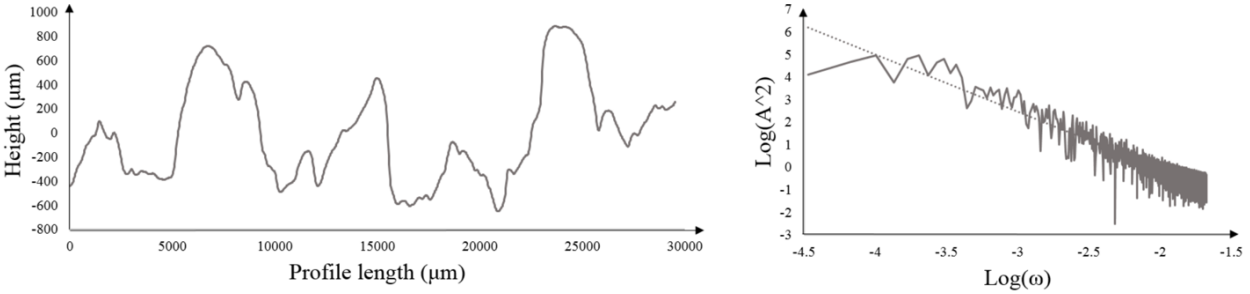

Figure 1-6. A surface profile and its corresponding PSD

Texture characterization

Seamless simulation of the pavement surfaces has been the focus of extensive studies. Characterization of the surface texture by wavelength and amplitudes into micro-, macro-, and mega-texture cannot provide sufficient information. For example, having the same macro- and micro-texture summary index (e.g. mean profile depth) in two different surfaces does not necessarily lead to similar vehicle performances like friction (Kane et al., 2015). Therefore, other

statistical parameters have been introduced to better represent the texture profile and its correlation with those performances (Yandell, 1971, Forster, 1981, Yandell, 1994, Sabey, 1959, Do, 2002).

The statistical parameters can be categorized into four groups; (i) amplitude parameters, e.g. mean profile depth, mean texture depth, root mean square, skewness, and Kurtosis, (ii) functional parameters, e.g. surface bearing index, (iii) Hybrid parameters, e.g. surface area ratio, and (iv) spacing parameters, e.g. texture aspect ratio and direction (Li et al ,2016).

Table 1-1 represents some of these parameters used for characterization of the pavement texture.

Parameters used in these formulae are illustrated in Figure 1-7.

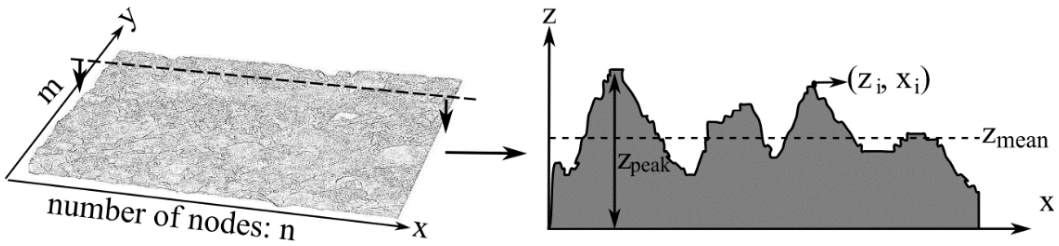

Figure 1-7. Surface texture parameters

In multi-scale surface characterization, these parameters should be defined individually for each scale since they depend on the resolution (Moore, 1975, Do and Marsac, 2002, Ergun et al. 2005, Serigos et al., 2014).

Instead of using different statistical parameters for each scale of texture, fractal techniques have been used for multi-scale characterization of pavement or aggregate surfaces. Fractal techniques were first introduced in 1982 when Benoit Mandelbrot proposed a novel idea of what he called "geometry of nature". He suggested that objects of any number of dimensions, which until then were considered to have irregular shape or texture, in fact have an inherent pattern of irregularity that repeats at all scales. This observation was a ground-breaking discovery and gave rise to a new extension of classical geometry called fractal geometry. Nowadays fractal analysis (analyzing objects in search for their fractal nature) is applied in many fields of science, engineering, and arts, enabling humans to understand nature on a deeper level.

A fractal is a pattern generated by the same geometric process repeated over and over resulting in a never-ending complex structure. In general, fractals are divided into self-similar and self-affine fractal categories. A self-similar fractal object is an object approximately or exactly equal to a part of itself. A self-affine fractal object has pieces of itself scaled by different amounts in different directions. All self-similar objects are self-affine, while self-affine objects are usually not self-similar (Russ, 1994). Figure 1-8 can show an example of self-affine surfaces in different magnifications with a scaling factor of $\zeta = L/\lambda$, where L is the minimum diameter of the contact area, A, when $A(L) \approx L^2$.

A fractal pattern gives the impression of depth, due to its inherent irregularity of boundary lines. Therefore, fractals are described with fractal (Hausdorf) dimension, D_f, which can have any non-integer value. Fractal dimension of a fractal object is always larger than its Cartesian dimension, D_C, (D_C, =1 for a line, D_C, =2 for a surface, D_C, =3 for a volume, etc.):

$$D_f = D_C + (1 - H) \qquad \text{eq. 1-5}$$

Table 1-1. Statistical parameters for surface characterization

Cat	Parameter	Description	Formula
i	MPD	Mean profile depth	$MPD = z_{peak} - z_{mean}$
i	R_a	Arithmetic mean deviation of the profile	$R_a = \frac{1}{n}\sum_{i=1}^{n} \lvert z_i \rvert$
i	R_q	Root-mean-square deviation of the profile	${R_q}^2 = \frac{1}{n}\sum_{i=1}^{n} (z_i)^2$
i	L_a	Average wavelength of profile	$L_a = 2\pi.\frac{R_a}{D_a}$
i	D_q	Root-mean-square slope of profile	${D_q}^2 = \frac{1}{n}\sum_{i=1}^{n} (\frac{\Delta z}{\Delta x})^2$
i	L_q	Root-mean-square wavelength of profile	$L_q = 2\pi.\frac{R_q}{D_q}$
i	Ssk	Skewness	$Ssk = \sum_{i=1}^{n} {z_i}^3\ (n\ R_q^3)^{-1}$
i	Sku	Kurtosis	$Sku = \sum_{i=1}^{n} {z_i}^4\ (n\ R_q^4)^{-1}$
i	SMTD	Simulated mean texture depth of an area	$SMTD = (\sum_{x=1}^{n}\sum_{y=1}^{m} z_{peak} - z(x,y))/(m\ n)$
ii	D_a	Arithmetic mean slope of profile	$D_a = \frac{1}{n}\sum_{i=1}^{n} \left\lvert \frac{\Delta z}{\Delta x} \right\rvert, \Delta z = z_{i+1} - z_i, \Delta x = x_{i+1} - x_i$
ii	γ	Profile slope at mean line	$\gamma = \frac{1}{n-1}\sum_{i=1}^{n-1} tan^{-1}(\frac{\Delta z}{\Delta x})$
ii	SAR	Surface area ratio	$SAR = \frac{A - (m-1)(n-1)\ \Delta x\ \Delta y}{(m-1)(n-1)\ \Delta x\ \Delta y}$ $A = \sum_{i}^{n-1}\sum_{j}^{m-1} A_{ij}$ $A_{ij} = \frac{1}{4}(\lvert\overrightarrow{AB}\rvert + \lvert\overrightarrow{CD}\rvert)(\lvert\overrightarrow{AD}\rvert + \lvert\overrightarrow{BC}\rvert)$
iii	S	Mean spacing of adjacent local points	$S = \frac{1}{n}\sum_{i=1}^{n} S_i$, S_i is the space between adjacent peaks
iii	TAR	Texture aspect ratio	$0 < TAR = \frac{\text{The distance that the normalized ACF has}}{\text{The distance that the normalized ACF has}}$ $\frac{\text{the fastest decay to 0:2 in any possible direction}}{\text{the slowest decay to 0:2 in any possible direction}} \leq 1$
iii	r_p	Mean radius of asperities	$r_p = \frac{2z_i - z_{i-1} - z_{i+1}}{l^2}$, where l is the length of the profile
iv	SBI	Surface bearing index of an area	$SBI = \frac{R_q}{H_{5\%}}$, $H_{5\%} = z$ at 5% bearing area

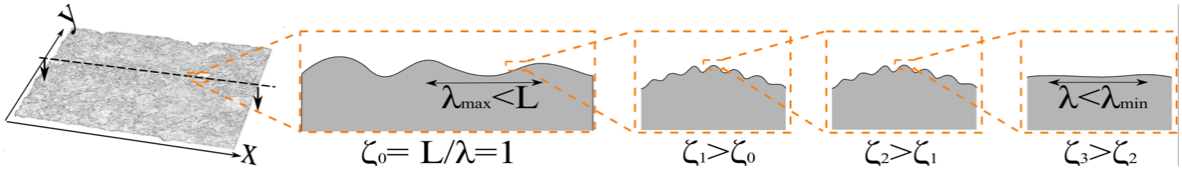

Figure 1-8. Self-affinity of pavement surface

where, 0<H<1 is the Hurst exponent. The lower the value of Hurst exponent, the rougher the fractal object appears and the more additional dimension it fills.

The fractal dimension of a profile (D_f) can be converted to the fractal dimension of a surface (D_s) by the following equations:

$$1 + D_x \leq D_s \leq D_x + D_y \quad \text{eq. 1-6}$$

$$1 + D_y \leq D_s \leq D_x + D_y \quad \text{eq. 1-7}$$

where, D_x and D_y are estimates of fractal dimension (D_f) in x and y directions and D_s is the surface fractal dimension. For isotropic self-similar and self-affine surfaces, the left side of the inequality $(1 + D_x)$ is equal to D_s. These inequalities enable one to describe (even if not exactly) a fractal surface with only one given profile (or a small number of profiles).

Fractal structures, can be defined using the fractional Brownian noise description, described as the following function:

$$f(x) = ax^{g(D_f)} \quad \text{eq. 1-8}$$

where variable x can be time in time-domain or position in spatial-domain, a is proportionality constant, and $g(D_f)$ is a negative coefficient dependent on the structure (Jahn and Truckenbrodt 2004).

Based on this function, Power law methods, such as Power spectrum, Roughness length, Tessellation, structure function, Richardson, etc., are introduced for finding the fractal dimension for a given surface (f(x)). It must be noted that some of these laws such as Richardson are limited to self-similar fractals or one-dimensional data. However, some others like power spectrum can be generalized to higher dimensions under specific conditions.

Among these laws, power spectrum is the most common method for characterization of pavement surfaces, see Figure 1-6. The slope of PSD (β) of the pavement profile has a linear relationship with fractal dimensions, which can be defined as $D_f = \frac{5+\beta}{2}$ for profiles, and $D_f = \frac{7+\beta}{2}$ for areas (Bhushan et.al. 1992).

Therefore, the fractal parameters of fractal dimension D_f and Hurst exponent (H=3-D_f), can be used for representation of the pavement surface profile. Pavement surfaces tend to be self-affine ($2.1 \leq D_f \leq 2.5$) within the lower and upper bound for length-scale, λ, shown in Figure 1-8. This range of $\lambda_{min} < \lambda < \lambda_{max}$ is often between a few millimeters and a few micrometers (Persson, 2001).

In addition to the mentioned methods, surface decomposition method has also been used for pavement surface characterization (Rado and Kane, 2014; Kane et al., 2015). Using a signal processing technique, named Hilbert-Huang transform (HHT) (Huang and Pan, 2006), the method decomposes the profile into a number of profiles (IMF). These profiles have (i) the same number

of minima, maxima, and intersect with z_{mean} and (ii) identical z_{mean} in an area between local maximum and minimum for every point. They are expressed as

$$Z(x) = r_n + \sum_{i=1}^{n} IMF_i(x) \quad \text{eq. 1-9}$$

in which r_n is the residue remained after the decomposition. Being simpler than Fourier transformation and faster to implement, the method appears to be promising for pavement characterization (Kane et al., 2015).

1.2.3 Surface profile measurements

Surface roughness measurement

Based on the roughness characterization methods mentioned, there are two types of devices for roughness measurement; response-type devices in which the vehicle response to roughness is measured, and profilometers which measure the actual profile.

The measurements of the response-type devices, which record the dynamic response of a vehicle moving on a particular pavement surface, are dependent on the characteristics of the vehicle mechanical system and the speed of the vehicle. Some of the most common devices in this category are the Bureau of Public Roads (BPR) roughometer, the Portland Cement Association (PCA) meter, and the Mays meter.

BPR roughometer, for example, is a single wheel trailer that measures the vertical movements of the damped, leaf-sprung wheel with respect to the axle using a mechanical integrator. Its result is reported in in/mi count of roughness. Although this method is one of the simplest and cheapest available methods, its measurements are dependent on the vehicle response, vehicle type, time, vehicle condition, and climate. Therefore, the accuracy of its measurements may not be as good as other devices. To solve the problem complicated calibrations are required to convert the measurements to a standard scale (Wambold et al., 1981).

The profilometers, on the other hand, measure the vertical elevation of the profile at every longitudinal point. General Motors Research (GMR) profilometer, the French Bridge and Pavement Laboratory (LCPC) longitudinal profile analyzer (APL), the Transport and Road Research Laboratory (TRRL) Beam, and CHLOE (AASHO) profilometer are some of the available devices in this category (Wambold et al., 1981).

As an example, GMR profilometer is able to measure one or two profiles at highway speeds. It consists of a small trailer under several hundred pounds of load being pulled on the given track. The displacement transducer measures the distance between surface profile and the trailer, while the accelerometer measures the vertical motion of the body of the vehicle. The profile can be obtained by subtracting the displacement signal from the double integration of the accelerometer signal for eliminating the vehicle motion (Gillespie and Sayers, 1981).

Laser scanning technology has also been used for measuring surface roughness. For example, multiple laser profiler (MLP) is a 3D laser which is able to measure multiple paths of profiles at the same time (Chang et al, 2005).

It worth noting that, as it was mentioned before, filtering is very important in roughness measurement. Therefore, nearly all of the roughness measurement devices function as mechanical filters to remove the profile grade from the measurements (Sayers and Karamihas, 1998).

Surface texture measurement

There are a wide range of methods for measurement of the texture of various surfaces such as pavements, mechanical parts, semiconductors and optics. These methods are different based on the type of evaluation, process, resolution, and presence of contact between the device and surface. Nevertheless, none of them is well-recognized as the best mean for surface measurements. This section comprises the methods which have been used in pavement engineering and briefly addresses the available methods for other fields that have been validated in similar conditions.

As the resolution of measurements increases, the speed of measurement decreases. Therefore, the devices with higher resolutions can only perform in the laboratory or at low speeds. The devices with lower resolutions can measure the surface profile in the field at highway speeds. Although the technology improvements in recent years have made the texture measuring techniques faster and more reliable, one of the major drawbacks in texture measurement methods is their time-consuming process. Here, these methods are divided into two categories: contact probes and optic or contactless probes based on the presence of contact between the device and the profile:

i. Contact probe devices

One of the common contact probe devices is the stylus profiling device which can give resolutions up to nano-scale. The device is composed of a stylus which moves along a straight line in 1-D or 2-D and records the surface profile by profiling through a grid in two perpendicular directions (Santos and Julio, 2013). The resolution of this device and the range of measurement depends on the size of the tip of the stylus.

Sand patch (ASTM E 965, ISO 10844) is a volumetric-based device which provides the mean depth of pavement surface for macro-texture only. In this test, glass beads with a known volume are spread in a circle onto a cleaned surface. Based on the volume and the diameter of the circle the mean texture depth of the surface is determined (Hall et al., 2009).

There is a strong correlation between micro-texture and friction measurements at low speed such as British Pendulum test (BPT) and Dynamic Friction tester (DFT at 20 km/hr). Hence, these two tests are often used to qualitatively characterize the micro-texture (Hall et al., 2009). These tests are explained in more detail in Appendix A.

ii. Contact-less probe devices

In contact-less probe devices, light is often used for surface profile measurements. These devices trace the light behavior, such as angle of reflection and range of scattering of the light, when it is in contact with a surface. The method is non-destructive and is often faster than contact probe methods. However, it can be too sensitive to the surface slope, direction, visibility, and scattering of the lights in the deep valleys (Vorburger et al., 2007). Optical devices have three major types which have been compared in detail in Table 1-2.

Laser scanners project a laser beam on the surface, collect the reflections and derive the coordination of the target point by triangulation. Their resolution is mainly defined by the laser spot size and some can capture textures as small as a few micrometers. In conventional laser scanners, resolution and accuracy decrease by increasing the field of view, a problem which has been addressed with recent synchronizing ability. The method has been widely used in studies on texture characterization of pavement surfaces (Serigos et al., 2014, Bitelli et al., 2012).

Image analysis systems measure the surface texture by capturing a photograph with a high-resolution camera and using triangulation to derive the coordinates. Despite being simple, finding the common points among image pairs while using more than one camera can be complicated (Ergun et al., 2005*,* Slimane et al., 2008, Masad et al., 2009).

Microscopes project a light or electron beam on the surfaces and analyze the diffracted reflections to obtain the image of the surface. Optical, electron, and scanning probe microscopy are the most well-known approaches. Microscopes can have large measurement ranges from 1nm to some millimeters (Vorburger et al., 2007). Scanning Electron Microscopy (SEM) has been often used for measuring the micro-texture of aggregates (Tourenq and Fourmaintraux, 1971, Masad et al., 2009).

Table 1-2 shows the comparison of these devices.

Table 1-2. Comparison of surface texture measurement devices

Device	Evaluation type	Resolution	Field of View	Missing data for multi-scale samples	Time	Coring	synchronizing	Portability	Cost
Stylus	Quantitative	limited to high or low resolution only	Large	Yes, cannot capture both scales	Slow	Yes	Not Built in	No	Medium
BPT	Qualitative	----	Medium	----	Fast	No	----	Yes	Low
DFT	Qualitative	----	Large	----	Fast	No	----	Yes	Medium
Laser 1D	Quantitative	up to 1 micron	Small	Yes, in the valleys	Relatively fast	Yes for high resolution ones	Not Built in	Yes for low resolution ones	Medium
Laser 2D	Quantitative	up to 1 micron	Relatively large with an encoder	Yes, in the valleys	Relatively fast	Yes for high resolution ones	Not Built in	Yes for low resolution ones	Medium
Laser 3D	Quantitative	up to 1 micron	Small for high resolution ones	No	Relatively fast	Yes for high resolution ones	Built in	Yes for low resolution ones	High for high resolution ones
Image analysis	Quantitative	up to some microns	Small for high resolution ones	Yes, in the valleys	Relatively fast	Yes	Not Built in	No- sensitive to light	High for high resolution ones
Microscope	Quantitative	up to nano scale	Small	No	Slow	Yes	Built in	No	High

Several other methods such as structured light and interferometry can be used to measure micro-texture, however, few studies have used them (Busse et al., 2010). Considering the wide range of amplitudes, e.g. deep valleys, of pavement surfaces, most methods often give missing data. The challenge of missing data becomes more relevant in rougher surfaces, such as those with chip seal preservation.

1.3 INFLUENCE OF PAVEMENT PROFILE ON ROLLING RESISTANCE

Rolling resistance is the required force for keeping an object such as a wheel or tire moving. There are different factors affecting rolling resistance such as pavement surface, vehicle/tire characteristics, vehicle/tire operating conditions, and environmental conditions.

When a vehicle is traveling along a road with a rough surface, it has to overcome additional obstacles (from the texture to roughness and bumps on the surface) in comparison to a smooth road. These obstacles result into deformation of the tire and suspension system of the vehicle. Due to the viscoelastic nature of the tire rubber and presence of damping in the suspension system, whenever there is a deformation, there exists energy loss. Therefore, the roughness- and texture-induced rolling resistance of the vehicle consists of energy loss in the suspension system of the vehicle and the tire. The losses in the suspension system are mostly affected by longer wavelengths such as roughness and mega-texture, while tire and tread deformations are influenced by surface mega-, macro-, and micro-texture, respectively (see Figure 1-9).

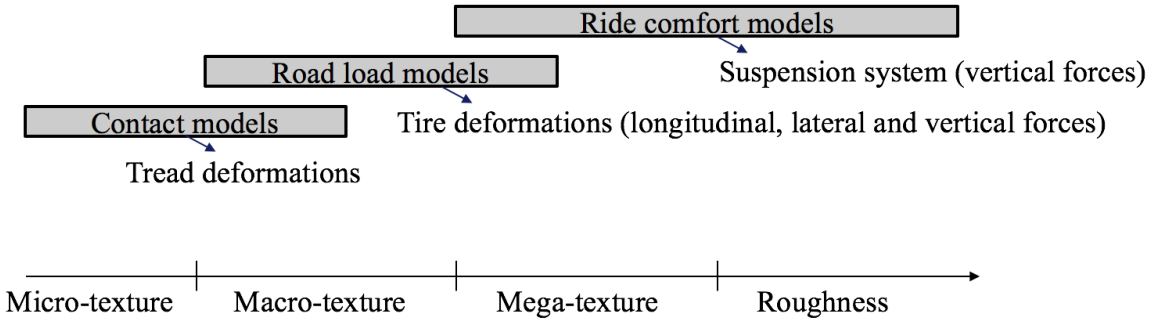

Figure 1-9. Influence of pavement profile on vehicle rolling resistance

1.3.1 Effect of surface roughness on rolling resistance of the vehicle

The effect of roughness on rolling resistance has been the focus of several studies ranging from empirical studies conducted on the effect of surface characteristics and roughness on fuel consumption (Chatti & Zaabar 2012, Hammarström et al., 2012), to mechanistic approaches aimed at roughness-induced rolling resistance (Louhghalam et al., 2015, Kim et al. 2017, Zaabar et al, 2018). These studies are summarized here.

Empirical models

There are a few models relating surface roughness to fuel consumption which often include built-in rolling resistance models. One of the most commonly used models is the World Bank's Highway Design and Maintenance Standards Model (HDM), versions HDM-3 and HDM-4 (Bennett and Greenwood 2003b). A later study, as a part of NCHRP1-45 research project, proposed a model in NCHRP 720 report by calibrating the HDM-4 model using extensive field trials (Chatti & Zaabar 2012). Another study as a part of the MIRIAM project presented an empirical model for the rolling resistance of the vehicle (Hammarström et al., 2012). These models are addressed below.

i. NCHRP 720 model

The main objective of the NCHRP1-45 research project was estimating the effects of pavement conditions on vehicle operating costs for different vehicle classes (medium car, SUV, van, light truck, articulated truck). The developed fuel consumption model is a calibrated version of the HDM 4 model (Chatti & Zaabar 2012). The effect of roughness is only accounted for in the rolling resistance model:

$$F_r = CR_2 \times \left(b_{11} \times Nw + CR_1 \times (b_{12} \times M + b_{13} \times v^2) \right) \qquad \text{eq. 1-10}$$

in which F_r is the rolling resistance force (N); CR_1 is the rolling resistance tire factor; b_{11} to b_{13} are the rolling resistance parameters related to the wheel diameter and number of wheels (Nw); v is the vehicle speed in km/h. CR_2 is the rolling resistance surface factor, which includes the effect of profile texture, roughness and pavement deflection:

$$CR_2 = Kcr_2(a_0 + a_1 \times Tdsp + a_2 \times IRI + a_3 \times DEF) \quad \text{eq. 1-11}$$

where, Kcr_2 is the calibration factor; a_0 to a_3 are the model coefficients; and Tdsp is texture depth using the sand patch method (mm): $Tdsp = 1.02 \times MPD + 0.28$, in which MPD is the mean profile depth (mm), ranging from 0.5 mm to 3 mm; IRI is the International roughness index (m/km), and DEF is the pavement deflection in mm:

$$DEF = \frac{T}{30} \times (-0.05 + 0.415 \times e^{-0.024575 \times V}) \quad \text{eq. 1-12}$$

where T is the air temperature in ^{0}C and V is the vehicle speed in km/h.

An adjustment factor is defined for rolling resistance and fuel consumption (from the baseline condition of IRI = 1 m/km) defined as $A_{IRI = x} / A_{IRI = 1}$. This adjustment factor with respect to the variation of IRI at the speed of 88km/h, temperature of 30°C, MPD of 1 mm and grade of 0% is shown in Figure 1-10 for a passenger car and an articulated truck as an example.

According to the rolling resistance and fuel consumption models developed in the NCHRP study, a 1 m/km increase in IRI causes an increase of less than 3% for a car, and less than 2% for an articulated truck in fuel consumption at 88km/h.

ii. MIRIAM model

The aim of this study was the evaluation of the effect of road surface improvements on fuel consumption. The proposed model is based on a previously developed model by (Karlsson et al. 2011) and modified using coastdown measurements data in Sweden. The rolling resistance model was developed with respect to variation of MPD, IRI, temperature, and speed, for a car, a heavy truck, and a heavy truck with trailer.

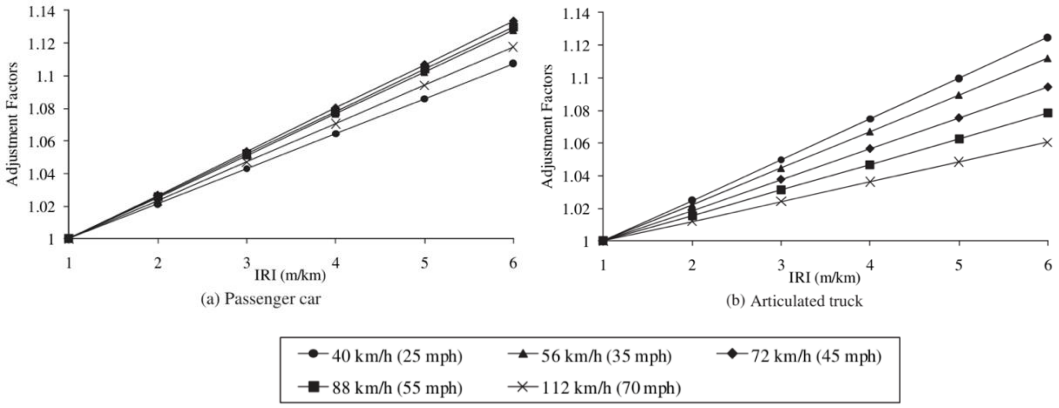

Figure 1-10. NCHRP 720 model- Relationships between IRI and Adjustment factor for fuel consumption of a) a car and b) an articulated truck at v=80km/h (Chatti and Zaabar, 2012)

The developed model for the car and trucks are similar to each other, with only the coefficient

values being different. The rolling resistance force is defined as:

$$F_r = Cr \times m \times 9.81 \qquad \text{eq. 1-13}$$

where $Cr = CR_0 + IRI \times v \times Cr_1 + MPD \times Cr_2$, and $Cr_0 = Cr_{00} + Cr_{Temp}$ (5-T); m is the vehicle mass (kg) and Cr_0, Cr_1, and Cr_2 are the rolling resistance parameters.

The effect of roughness is reported to be minimal in fuel consumption since the authors claimed that by reducing the IRI by 0.5 m/km, although the rolling resistance is reduced, the speed will increase and therefore there will be approximately no change in fuel consumption.

Mechanistic models

Mechanistic models for investigating the effect of roughness on rolling resistance and energy dissipation of the vehicle have only been developed in a few studies which are addressed in the following.

i. Louhghalam et al. model

The aim of this study was identifying the key parameters of roughness-induced fuel consumption for different vehicle classes (Medium car, SUV, Van, Light truck, and Articulated truck). In the proposed model, the surface roughness was characterized using power spectral density. The model is based on the energy loss in the suspension of a two DOF quarter-car model which is calibrated using NCHRP 720 model presented before. The calibration of the model was performed by changing the stiffness properties of the tire and the road waviness number of the surface so that the fuel consumption of the two models matches for IRI=1 m/km. Figure 1-11 shows the comparison of the relationship between roughness and fuel consumption of the two models for a passenger car at 70 and 100 km/h. As it can be seen, the relationship found in this study is non-linear ($\propto IRI^2$) while the NCHRP 720 model shows a linear trend. It should be noted that the calibration coefficient used in this model is unrealistically high for passenger cars, and the corresponding tire stiffness is almost four times the common tire stiffness.

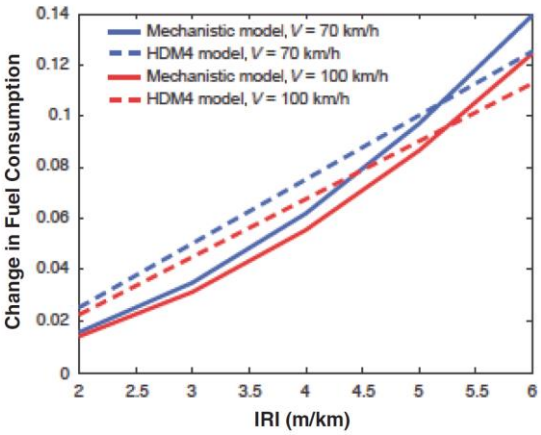

Figure 1-11. Fuel consumption variation with IRI at v = 70 and 100 km/h for a medium car (Louhghalam et al. 2015)

ii. Kim et al. model

In this study, a stochastic approach was proposed for analyzing the energy loss in a half-car model traveling on a rigid rough pavement (see Figure 1-12 (a)). The pavement roughness was

represented by a filtered white noise. The roughness was applied to the front tire directly, while it was applied to the rear tire with a delay obtained using a Padé approximation. The energy dissipation was then obtained by solving the Lyapunov equation. Similar to the previous study by Louhghalam et al., the stiffness of the tire was calibrated using the model predictions from the NCHRP 720 report. This model also shows a non-linear relationship between the energy dissipation and IRI. However, the relationship found between energy dissipation and speed is linear (see Figure 1-12 (b)).

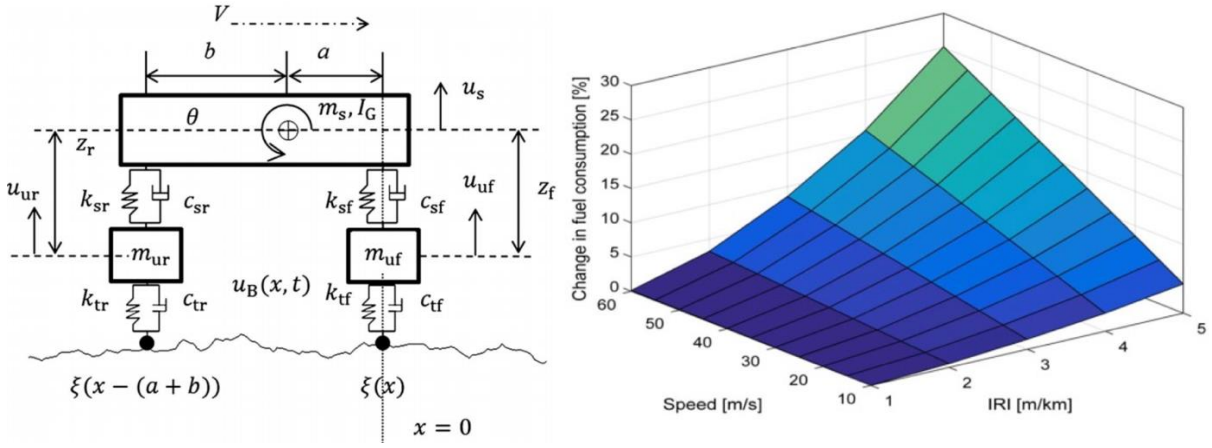

a) b)

Figure 1-12. a) Half-car model, b) Relationship between energy dissipation, roughness, and speed (Kim et al. 2017)

iii. Zaabar et al.

Zaabar et al. (2018) introduced a mechanistic approach based on a quarter-car model for evaluation of the effect of roughness on rolling resistance. They modeled the surface roughness profile as a filtered white noise. The surface profile is an input to the quarter-car model of the vehicle (see Figure 1-13).

Model parameters		
Name	Unit	Value
m_s	Kg	300
m_u	Kg	50
k_s	KN/m	28
k_t	KN/m	200
c_t	KNs/m	0.1

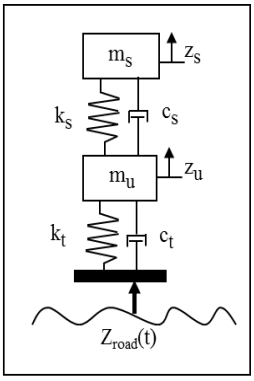

Figure 1-13. Schematic view of the Quarter-Car Vehicle Model (Zaabar et al. 2018)

Then the dissipative energy within the system is calculated using the relative velocities of the sprung and unsprung masses obtained from the quarter-car model using the following equation:

$$D = \frac{C_s}{V} E[\dot{z}_s^2] + \frac{C_t}{V} E[\dot{z}_t^2] \qquad \text{eq. 1-14}$$

in which V is the constant velocity of the vehicle, D is the energy dissipation, and $\dot{z}_s^2$ and $\dot{z}_t^2$ are the relative velocities for the suspension and tire, respectively.

Figure 1-14 shows a comparison of the results of this study and the NCHRP 720 model for a medium car. The results are presented as a normalized energy dissipation relative to the baseline corresponding to IRI=1 m/km ($RR_{IRI = x}$ / $RR_{IRI = 1}$).

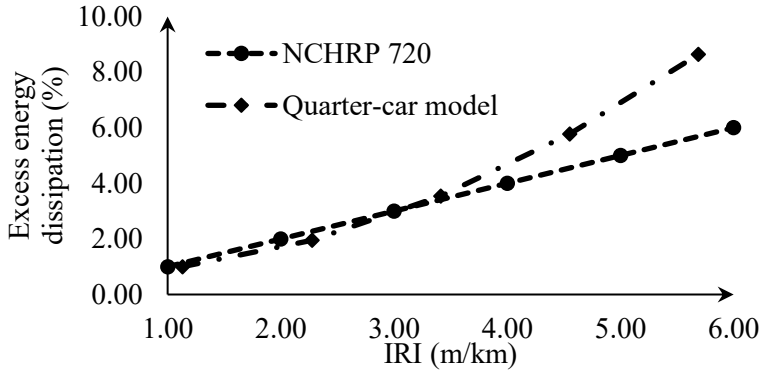

Figure 1-14. Effect of roughness on energy dissipation as a function of IRI at v=80 km/h (Zaabar et al., 2018)

The figure shows that the results of the mechanistic approach are in good agreement with the empirical results up to IRI= 3.5 m/km, without any calibration. However, the models deviate from each other at higher values of IRI and follow a non-linear trend similar to the two aforementioned studies. They also investigated the effect velocity on roughness-induced rolling resistance (see Figure 1-15).

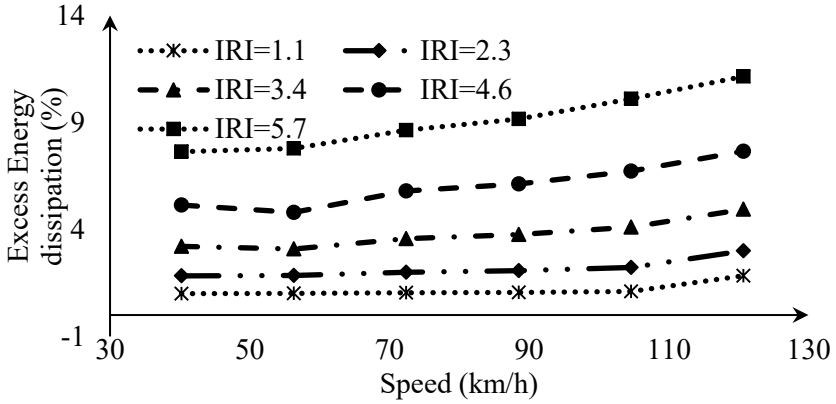

Figure 1-15. Effect of speed on energy dissipation at different roughness levels

1.3.2 Effect of surface texture on rolling resistance of the vehicle

Texture-induced rolling resistance in the tire due to tire deformations consists of three components of (1) tire deflection and bending, (2) tread slip and (3) tread surface deformation (Bendtsen, 2004, Xiong and Tuononen, 2013). Surface mega-, macro-, and micro-texture can influence these deformations.

Existing models on the effect of texture on rolling resistance or energy dissipation of the tire and vehicle can be divided into three categories of numerical models, analytical models, and empirical

models. In this study, since the focus is on the effect of different texture levels on rolling resistance the models for mega-, macro-, and micro-textures are discussed separately.

i. Effect of mega-texture on rolling resistance

Mega-texture can affect rolling resistance by creating vibration in the tire and suspension system. It has been suggested by some studies that mega-texture can have a dominant effect on rolling resistance. For example, Descornet (1990) suggested that mega-texture can be the main factor in rolling resistance and could affect fuel usage by up to 9%. In a 1990 study, Sandberg investigated the effect of different scales of the surface roughness on the vehicle fuel consumption using twenty different road surfaces, three different speeds (50, 60, and 70 km/h), and one type of car. The roughness and texture wavelengths in that study ranged from 2 to 3500 mm. The study concluded that mega-texture is influential on fuel consumption both at low and high speeds.

Despite the experimental evidence, there are no mechanistic studies specifically on the effect of mega-texture on rolling resistance. The current studies, such as the mechanistic models mentioned in the previous section, usually do not separate mega-texture from roughness and focus on the effect of IRI on rolling resistance. IRI includes wavelengths more than 250 mm; therefore, it captures the effect of a portion of the mega-texture of the surface in addition to the roughness. However, these studies neglect the effect of the lower segment of mega-texture and mostly are focused on the energy dissipation in the suspension system.

ii. Effect of macro-texture on rolling resistance

The effect of macro-texture on rolling resistance of the tire has been the focus of several studies. Due to the range of the macro-texture's wavelengths, this scale of the profile can influence all three components of the tire deformation, from tire bending to tread deformation. Therefore, a wide range of models have been introduced for investigation of the effect of macro-texture on rolling resistance, from tire models and mechanistic approaches to experimental studies.

Different tire models have been used for evaluation of rolling resistance performance of tires, ranging from simplified classical spring-damper models to detailed three-dimensional finite element (FE) models. The complexity of these models varies based on the details that have been considered in the tire assembly. The simplified models usually suffer from oversimplified representation of rubber and pavement, which are unable to consider the non-linearity of the tire performances and the details at smaller scales. However, a few current multi-scale FE simulations have been able to calculate the tire deformation along with the interaction of its components at different scales (Ghoreishy, 2008). FE models generally consider different parts for the tire (Figure 1-16) and various design and operational variables like deflection, pressure, load, and speed. A comprehensive literature review on tire models is provided by Ghoreishy (2008).

So far, existing tire models barely consider the effect of pavement surface texture, due to the high computational costs. However, there are a few studies that implemented tire models for investigating the effect of texture on vehicle performance in which they divided the problem into two parts; a tire rolling on a smooth surface, a mechanistic approach for the contact between tire tread and a rough pavement surface. Some of the existing mechanistic approaches are discussed in the following.

Figure 1-16. Various parts of a detailed tire model

Numerical Models

Wullens and Kropp (2004) proposed a 3D model of a simplified equivalent tire structure similar to the Pre-tensioned Kirchhoff's plate. In this model a Green's function (as the impulse response function) is applied at the contact nodes of the tire (see Figure 1-17). The model does not consider the curvature of the tire; however, it includes the periodic boundary conditions connecting the ends of the plate, building an infinite plate. The air stiffness and the rigid sidewalls are implemented with a spring bedding.

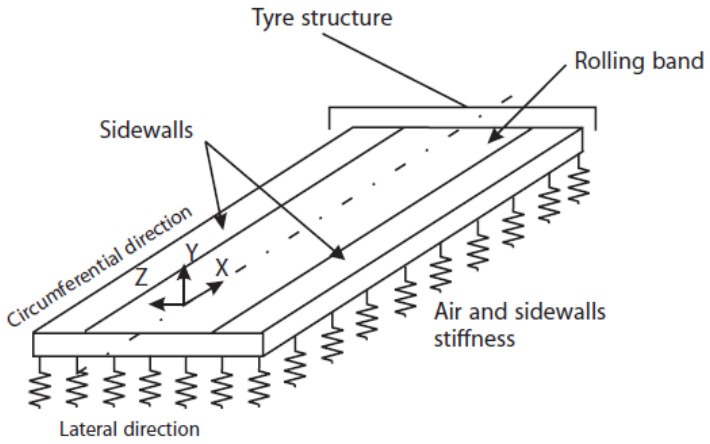

Figure 1-17. Pretensioned Kirchhoffs plate on a stiffness bedding (Wullens and Kropp, 2004)

The energy dissipation of the tire traveling on a rough surface can be predicted by this model. The results are shown to be comparable to measurements and show higher energy dissipation within the tire on a rough surface than on a smooth one. The advantage of the model is that it is able to identify the elements with the highest energy dissipation in the tire.

In another study, O'boy and Dowling (2009) considered the tire as a multi-layer viscoelastic cylinder belt (see Figure 1-18.a). The parameters of an equivalent simple bending plate model are

then obtained from the model and the Green's functions for the contact nodes are determined (Figure 1-18.b). This tire model accounts for the surface texture. The contact forces can be obtained based on the belt displacement, the height of the non-deformed tread block, and its stiffness. It should be noted that this method has been used for predicting the tire/road noise and not the tire rolling resistance.

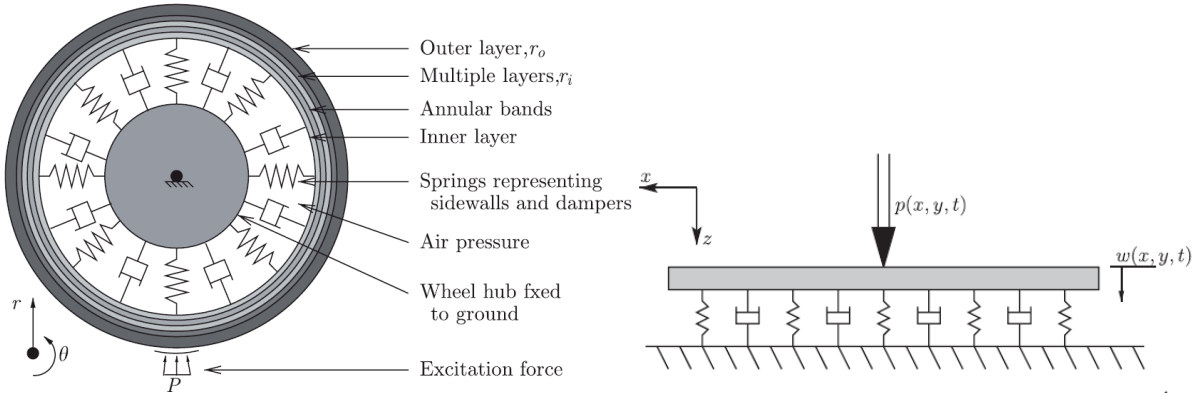

a) b)

Figure 1-18. a) viscoelastic cylindrical model of the tire belt b) simple bending plate (O'boy and Dowling, 2009)

Boere (2009) investigated the effect of macro-texture on tire rolling resistance by dividing the problem into two parts (i) a tire rolling on a smooth surface in a steady state condition and (ii) a tire moving on a textured surface. For the first part, a finite element model of the tire in steady state condition on a smooth surface was used. Then the contact forces between the tire and the smooth surface were extracted from the FE tire model and were used as an input to the mechanistic model. The mechanistic model was developed using modal analysis (Lopez et al., 2007) for capturing the effect of texture. It accounted for the texture by applying a nonlinear stiffness for the contact with the surface profile (see Figure 1-19). The total energy dissipation was then considered as the summation of the energy dissipation of the two parts.

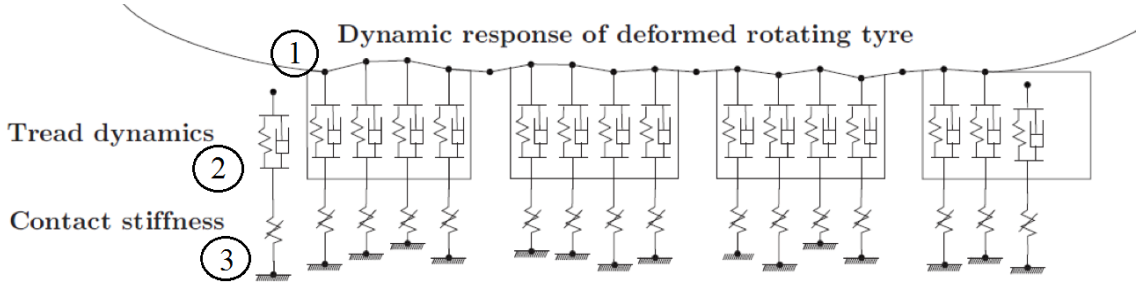

Figure 1-19. Schematic overview of the mechanistic tire-surface interaction model (Boere, 2009)

As it can be seen in Figure 1-19, the contact between the tire and the pavement surface includes three sub-systems of dynamic response of the tire, tread dynamics, and contact stiffness.

The FE tire model is a non-rotating tire; hence, its response should be converted to a rotating tire. For finding the dynamic response of the tire in the contact patch the Green's functions of the

system is determined by solving the equation of motion in the contact. As a result, the displacement of the tire points (1) in Figure 1-19 are obtained.
The tread is then modeled as a system of spring and dashpots, (point (2) in Figure 1-19). To account for the surface texture, a nonlinear spring is used for modeling the contact stiffness between the tread blocks and the surface. The equivalent stiffness of the tread material in contact is lower than the stiffness of the rubber, and it has a relationship with the indentation road texture into the tread. The results of this model are then compared with experimental results obtained from rolling resistance measurement using a trailer (see Figure 1-20). The model is in a very good agreement with the experimental results in capturing the effect of texture on rolling resistance. However, there is a difference between the initial rolling resistance of the tire and the experiment.

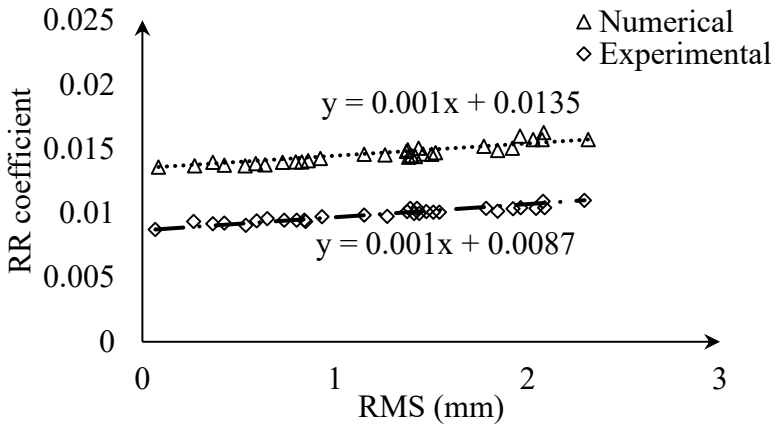

Figure 1-20. The effect of surface texture on rolling resistance of the tire (Boere, 2009)

Analytical Contact Models

Contact models have also been used for evaluation of the energy dissipation of materials in contact with rough surfaces. These models can be categorized into three main groups; (i) single-asperity, (ii) multi-asperity, (iii) multi-scale fractal models. However, these models are widely used for calculation of hysteresis part of friction rather than rolling resistance. They can be beneficial for evaluation of the energy dissipation in the contact due to tread deformation. However, they are unable to capture the tread slip and tire bending and therefore, are useful for the effect of lower textures on rolling resistance.

Single-asperity models (Greenwood, 1958; Ford, 1993; Sabey, 1958; Hui, 2000) are the most simplified contact models and consider the rough surface as simple triangles or spheres. These models cannot consider the effects of multiple contacts between two surfaces. They are beneficial only when (i) the area of effective contact is considerably smaller than the one of the nominal contact, and (ii) the distance between adjacent asperities is so large that no mutual interaction exists (Persson, 2006). These models are usually used for determining the friction coefficient as a function of the pressure in the contact area or the contact angle. In addition to theoretical models, single asperity contacts have been also modeled with Finite Element approaches, see Figure 1-21 (Mansura et al., 2017).

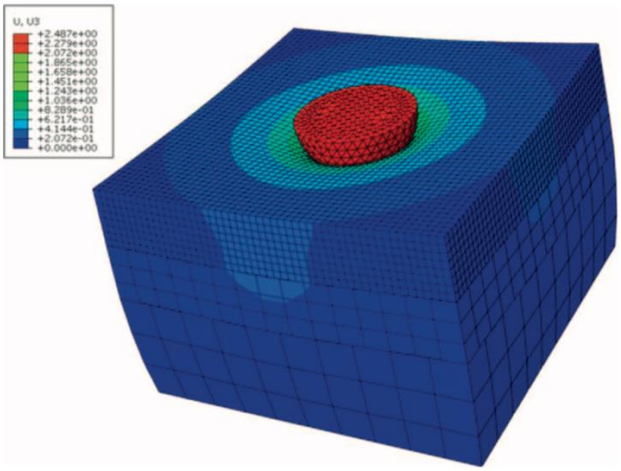

Figure 1-21. Finite element modeling of a single asperity contact

Multi-asperity models (Bush, 1975; McCool, 1986; Warren and Krajcinovic, 1995; Golden, 1981) consider that the contact occurs at more than one asperity, and thus are more reliable than single-asperity models. The original concept was introduced by Greenwood and Williamson in 1966 (Greenwood, 1966). The models cannot take into account the cases where there is the high penetration of the pavement into the rubber, since they do not consider the effect of rubber entrapment. Accordingly, the models are valid only when the ratio between effective and nominal contact area is small (Carbone, 2008).

Multi-scale contact models have been extensively studied in the past two decades. Kluppel and Heinrich (Kluppel, 2000) introduced a theoretical concept for relating the frictional force to the dissipated energy of the rubber during sliding on a self-affine surface (Figure 1-22).

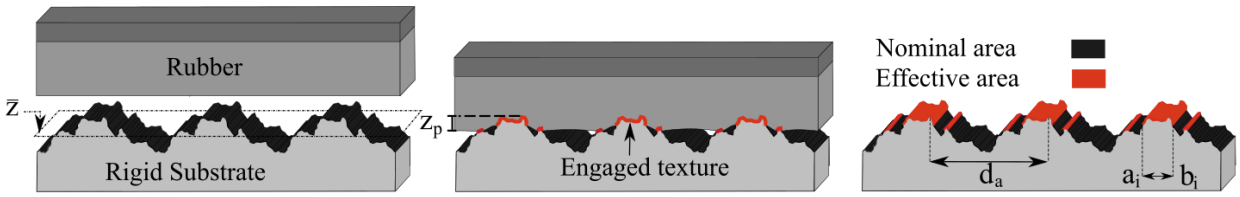

Figure 1-22. Contact of rubber with a rigid substrate as pavement

The surface was described by three shape-descriptor parameters; fractal dimension, D_f, and the correlation lengths parallel, $\xi_{\parallel}$, and normal, $\xi_{\perp}$, to the surface. Defining the friction coefficient μ as the ratio of resisting force to the normal force, it was given as

$$\mu = \frac{1}{4}\left(\frac{\xi_{\perp}}{\xi_{\parallel}}\right)^2 \left(\frac{E"_{max}}{E'(\omega_{min})}\right) \arctan\left(\frac{(v_1 - v_2)v}{v^2 + v_1 v_2}\right) \qquad \text{eq. 1-15}$$

Here, $E'(\omega_{min})$ is the storage Young modulus of the rubber corresponding to the minimum frequency of PSD of the surface, $\omega_{min} = \frac{2\pi v}{\xi_{\parallel}}$. $E"_{max}$ is the maximum loss modulus. To simplify the equations, the characteristic coupling velocities $v_1 = \frac{\xi_{\parallel}}{2\pi\tau_z}$ and $v_2 = \frac{\lambda_{min}}{2\pi\tau_z}$ were defined, where τ_z is the rubber relaxation time and $\lambda_{min} = \frac{L}{\xi_{max}}$ is the lower cut-off wavelength. The results of this model were validated by the classical friction data of Grosch (Grosch1963).

Persson theory of friction describes the energy dissipation of a perfectly elastic rubber layer with respect to the internal friction (Persson, 2001). In contrast to the theory of Kluppel model, Persson theory is three dimensional and has been used as a base concept in several models (Heinrich, 2008, Ueckermann, 2015). The theory mainly takes the hysteresis component of friction into account and excludes adhesion. Such an approach is relevant for rough or wet surfaces where adhesion has a negligible contribution to friction. Therefore, despite using a simplified assumption, the model provides a good representation of tire-pavement friction in most cases. The friction coefficient, μ, is defined with respect to the rubber vibration frequency induced by the surface texture as

$$\mu = \int_{q_L}^{q_1} q^3 C(q) R(q) dq \times \int_0^{2\pi} \cos(\phi)\, Im\, \frac{E(qv\cos(\phi))}{(1-\upsilon^2)P} d\phi \qquad \text{eq. 1-16}$$

In which $q_L = \frac{1}{\lambda_{max}}$ and $q_1 = \frac{1}{\lambda_{min}}$ are the lower and upper boundaries of wave number, q. $R(q) = \frac{A_{eff}}{A_{nom}}$ is the ratio of effective and nominal contact areas that are governed by spectral density, C(q), contact pressure, P, sliding speed, v, and rubber moduli, E, and Poisson ratio, υ.

The model has been later advanced to take into account the roughness of both rubber and pavement surface (Scaraggi, 2015). Some other studies used the model to investigate the energy dissipation at opening cracks and shearing in thin viscous film (Lorenz et al., 2011), a way to reduce the static friction (Lorenz, 2013), and friction on ice (Persson, 2015).

Pinnington model used a dynamic stiffness approach to describe the hysteresis energy loss during friction due to contact with axisymmetric asperities with radius Δ (Pinnington, 2009). He used ideal peak shape surfaces as a single asperity contact and generalized the model to consider different surfaces such as periodic array of identical peaks, randomly distributed identical peaks in one or multiple scales. The friction force, here, depends on the contact length at different slip speeds, as a function of Δ, and the slope of the peak at the contact line, $\frac{dz_{x=\Delta}}{dx}$. The friction coefficient is then defined as the mean slope of the contact, expressed as $\mu = \sin(G)(\frac{dz_\Delta}{dx})$, where G is the complex shear modulus. For a surface expressed by Fourier transformation, the friction coefficient is given as

$$\mu = \sin(G)(\frac{dz_\Delta}{dx}) = -\sin(G)\int_0^\infty \frac{P_q \sin(q\Delta)}{|G|} dq \qquad \text{eq. 1-17}$$

In which q is the wave number and P_q is the Fourier transform of contact pressure distribution.

The model was validated with measurements of Grosch (Grosch1963).

Using computational resources, residual molecular dynamics (RMD) simulations has been extensively used recently to explore rubber contact mechanics problems. While being numerically expensive, the simulation provides a detailed insight into different mechanisms involved in contact problem. The flexibility of simulation approach provides an excellent interface for validation of models, since the simulations can be validated by experiments and then be used for validation of theoretical models. The RMD method was also used to study the friction between a solid and a rough surface. In such studies, the energy dissipation during sliding of a viscoelastic material on a rough surface and the adhesive contribution to friction were investigated (Scaraggi, 2015, Scaraggi, 2016).

Empirical Models

Several experimental studies have been done for finding the influence of surface texture on rolling resistance on different types of concrete and asphalt pavements (Bester, 1984; Descornet, 1990; Delanne, 1994; Jamieson and Cenek, 1999; Boere, 2009; Chatti and Zaabar, 2012; Hammarström et al., 2012). In the following three of most recent studies are discussed.

NCHRP 720 model

The NCHRP model is explained in section 1.3.1. Similar to roughness, the effect of texture is only accounted for in the rolling resistance model. Here, some of the results of the model are presented.

The adjustment factor for rolling resistance and fuel consumption is defined with respect to the baseline condition of MPD = 0.5 mm as $A_{MPD = x} / A_{MPD = 0.5}$. The variation of the adjustment factor with respect to the variation of MPD at the speed of 80km/h, temperature of 30°C, IRI of 1 m/km and grade of 0% for a medium car (1.46t), light truck (4.5t) and articulated truck (13.6t) are shown in Figure 1-23.

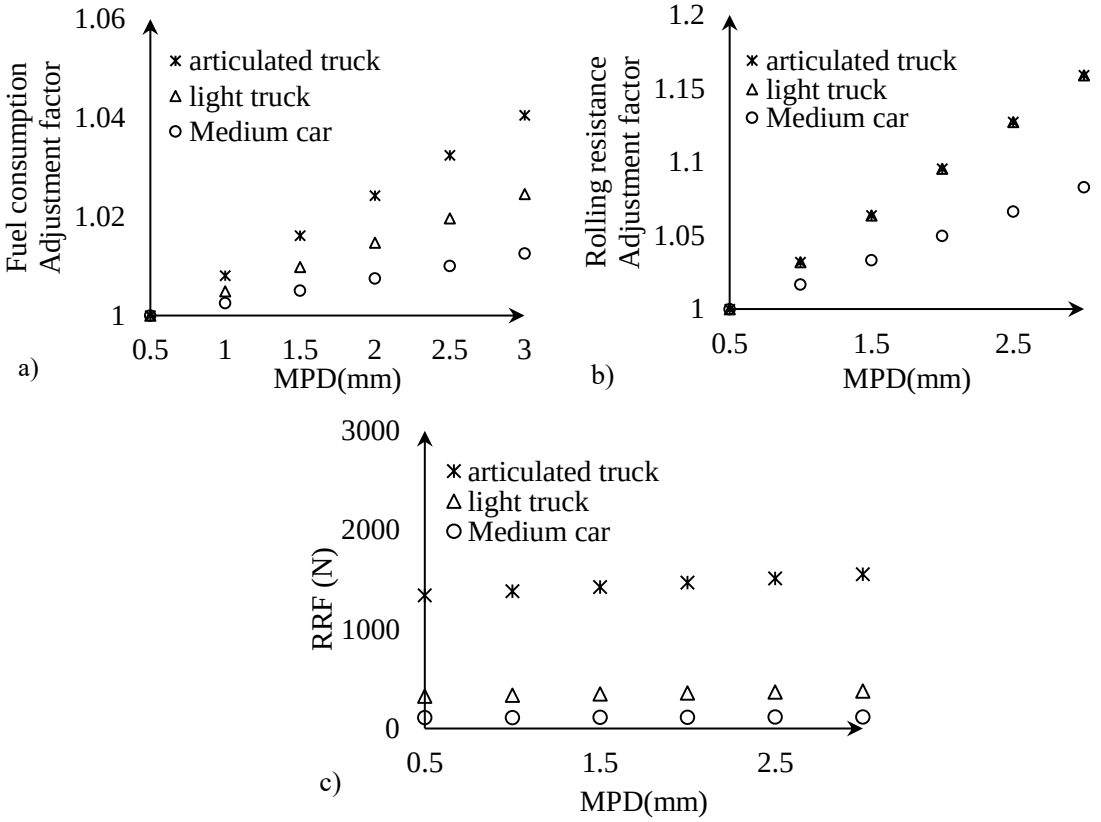

Figure 1-23. NCHRP 720 model- Relationships between pavement surface MPD and a) Adjustment factor for fuel consumption, b) Adjustment factor for rolling resistance, and c) Rolling resistance force at v=80km/h (Chatti and Zaabar, 2012)

As expected, the effect of surface texture on the adjustment factor for fuel consumption (Figure 1-23 a) is much less than that for rolling resistance (Figure 1-23 b) . It can be noted in Figure 1-23 b that the adjustement factors for the light truck and articulated truck are identical. As it is shown in Figure 1-23 c, this does not mean that the values of the rolling resistance forces for these two

vehicles are equal; the definition of the adjustment factor in the rolling resistance force (F_r) is only dependent on $a_0 + a_1 \times Tdsp$, in which the factors a_0 and a_1 change with the vehicle weight, and are the same for light truck and articulated truck (original HDM4 model). Therefore, their adjustment factors are equal.

According to the rolling resistance and fuel consumption models developed in the NCHRP 1-45 study, a 1 mm increase in MPD causes an increase in the rolling resistance of 3.2% for a car, and 6.1% for a light truck and an articulated truck. The corresponding values for the fuel consumption are 0.5% for a car, 0.98% for a light truck, and 1.6% for an articulated truck.

MIRIAM model

The rolling resistance in this study is also explained in section 1.3.1. The effect of texture as reported in the MIRIAM study is significantly higher than that reported in the NCHRP 720 report. For example, at a speed of 90 km/h, alignment standard of 1, increasing a unit value of MPD (1 mm) will cause 2.8% increase in the total fuel consumption for a car, 3.4% for a truck, and 5.3% for a truck with a trailer. These values are much higher for the rolling resistance force.

Boere study

Boere (2009) compared the results of his numerical method with measurements using a trailer on test tracks in the Netherlands. The measurements are reported in terms of a rolling resistance coefficient, which is the ratio between the rolling resistance and axle forces.

Surface texture is measured using a stationary laser profile meter with a resolution of 0.2 mm and a measurement length of 2.8 m. The root mean square (RMS_{tex}) of the surface profile is used as the surface texture measure. The relationship between the total rolling resistance and RMS_{tex} on 30 test tracks is shown using numerical simulations and experimental measurements (see Figure 1-24).

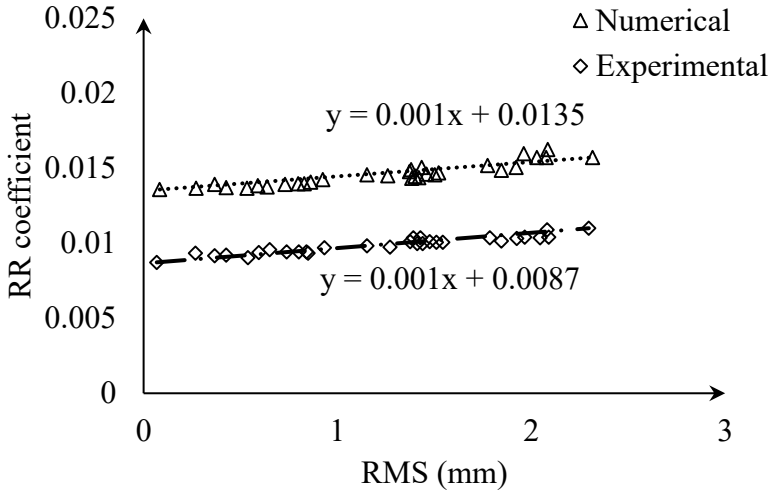

Figure 1-24. Boere model- Experimental and numerical relationships between rolling resistance and texture RMS at v=80km/h on 30 test tracks (Boere, 2009)

In Boere's study no equation was provided for this relationship. However, since a linear regression is fitted to the data, the equations for the regression lines are provided here and are considered as the Boere rolling resistance texture models. The corresponding regression equations for numerical

and empricial models, respectively, are shown below.

$$CRR = 0.001\ RMS + 0.0135 \quad \text{eq. 1-18}$$

$$CRR = 0.001\ RMS + 0.0087 \quad \text{eq. 1-19}$$

It can be seen that Boere's numerical model captures the effect of texture on rolling resistance very well. Similar results have been obtained in another study by Ejsmont et al. (2017).

iii. Effect of micro-texture on rolling resistance

All of the experimental studies suggested that the effect of micro-texture on rolling resistance is negligible. However, most of the contact mechanics models presented in the previous sub-section and the mechanistic studies on the importance of micro-texture on friction can be beneficial for investigating the effect of micro-texture on rolling resistance, if any.

1.4 ROLLING RESISTANCE MEASUREMENT

There are four standard measuring techniques for rolling resistance (Sandberg et al., 2011):

(1) Drum tests of tires in which the rolling resistance can be obtained by measuring the resistance force of the tire when it is in contact with a rotating drum. There are several standards for this method such as SAE J2452 (SAE 1999), SAE J1269 (SAE 2006), ISO 28580 (ISO 2009), ISO 18164 (ISO 2005). Although these tests are able to measure the rolling resistance force, they are not suitable for revealing the rolling resistance mechanisms and finding the effect of surface profile on rolling resistance. If the drum diameter is sufficiently large, it can be used to represent a flat road.

(2) Rolling resistance measurement trailers in which the rolling resistance can be measured by measuring the resistance of the test wheel to rolling on the pavement surface while being towed by a vehicle (Descornet, 1990, Sandberg et al., 2011, Boere, 2009). There are three different kinds of these devices, TUG, BRRC and BASt. These devices have been used for correlating rolling resistance to pavement surface characteristics.

(3) Coast-down method in which the velocity and stopping distance is measured for a vehicle that is rolling on the surface in the neutral gear, after reaching a certain speed (Preda et al, 2010). This method is usually used for finding the general condition of the vehicle and since all of the significant factors of driving resistance are involved in this method, no direct measurements are obtained for rolling resistance.

(4) Fuel consumption methods which are the most general method for assessment of rolling resistance since they include all possible factors involved in the energy loss. Therefore, it is difficult to pinpoint the rolling resistance losses using this method (Anderson et al., 2014).

Among these methods the trailer method is more common than the other ones (Anderson et al., 2014).

Moreover, new technologies have been introduced for measuring different components of rolling resistance. As an example, by using tire sensors the contact pressure of the tire can be measured even in high-speed rolling tires. Since hysteresis depends on time history of stress and strain, rolling resistance can be obtained using these sensors. Optical tire sensors can also be used for

tread deformation measurements by two laser triangulation sensors and the wheel rotation angle measurement (Xiong and Tuononen, 2013).

CHAPTER 2
SURFACE CHARACTERIZATION AND DECOMPOSITION

A surface profile can be considered as a superposition of various scales with different forms, waviness and roughnesses (Wang et al., 2018). In pavement engineering, the surface is usually divided into different scales based on its wavelengths. These wavelengths can be as small as microns or as large as several meters. The resolution and length of the measurement can affect the upper and lower limits of this range. PIARC defined four scales for describing a pavement surface profile. As it was explained before, these scales are roughness, mega-, macro-, and micro-texture (see Figure 2-1).

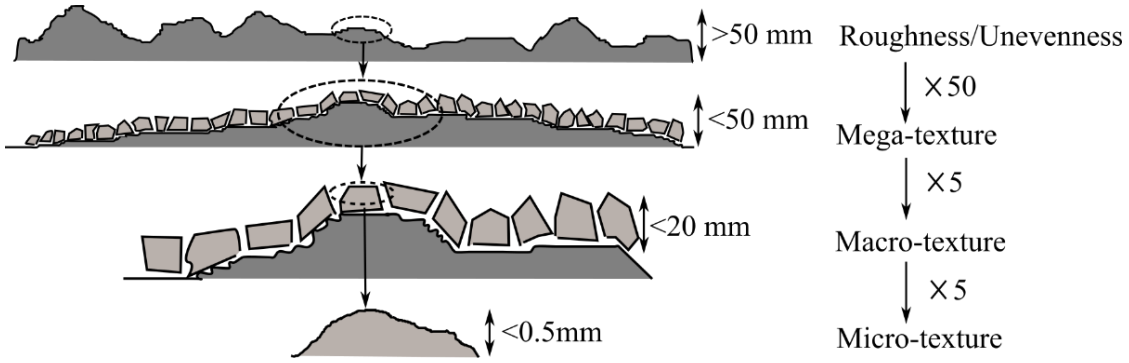

Figure 2-1. Simplified illustration of various pavement surface profile ranges (after Sandburg, 1990)

In this chapter, the range of the profile that affects the rolling resistance of the tire and vehicle will be discussed first. Then, different methods of characterization of the profile will be reviewed. After explanation of the essential modifications to the profile for achieving the required profiles for the model, samples of the profiles will be provided.

2.1 SURFACE PROFILE AND VEHICLE RESPONSE MECHANISMS

In this study, the aim is to find the effect of different scales of the surface profile on the vehicle rolling resistance. For this purpose, the surface profile should be divided into the aforementioned four scales. Roughness is described as profiles with wavelengths more than 500 mm. Mega-texture is defined by wavelengths between 50 and 500 mm. The macro-texture is characterized by wavelengths between 0.5 and 50 mm and any wavelength shorter than 0.5 mm is defined as micro-texture. Rolling resistance of the tire is related to energy dissipation and deformation of the tire and suspension system of the vehicle. The pavement profile spectrum can influence these mechanisms as follows:

- Wavelengths more than 500 mm representing roughness affect the vehicle dynamics and displacement in the suspension of the vehicle.
- Wavelengths between about 200 mm (the tire contact patch length) and 500 mm, representing the upper limit of mega-texture, also mostly affect the vehicle dynamics.
- Wavelength between 50 mm and 200 mm (within the tire contact patch), representing the lower limit of mega texture, influence the tire vibration.

- Wavelength between 0.5 mm and 50 mm, representing the macro-texture, influencing tire tread deformation and tire vibration.
- Wavelength smaller than 0.5 mm, representing micro-texture, can only affect the tread deformation. Since the effect of micro-texture on rolling resistance is usually known to be very small, it has been neglected in all of the previous studies. In this study also, this effect is considered as negligible.

2.2 AVAILABLE DATA SETS

Due to the wide range of the pavement profile spectrum, from micrometers to meters, it is usually not possible to capture the whole profile using one measuring device. The devices with high resolution have small field of view; therefore, they are unable to measure the roughness and a wide portion of mega-texture spectrum. On the other hand, the low-resolution devices used for roughness measurements cannot measure smaller scales.

In this study, different sets of data have been obtained:

- Surface profiles from NCHRP 1-45 study (Chatti & Zaabar, 2012), which only contains roughness and mega-texture, with a distance between two consecutive points of 3 inches.
- Data from surface texture measurements of chip seal surface profiles with profile lengths of 43 cm, which are mostly rougher than the other types of pavements and include macro-texture and the majority of the mega-texture spectrum.
- Data provided by the Danish Road Directorate, with 100 m sample lengths and a distance of 0.5 mm between different points. However, the samples are mostly from new low-rolling resistance pavements and therefore are very smooth.

To obtain an acceptable range of wavelengths and amplitudes for different scales, the profile spectrum in this study is considered as the summation of all of these databases.

2.3 DECOMPOSITION OF THE PROFILE INTO DIFFERENT SCALES

A common method for separating the different scales of the profile from each other is filtering. This operation can be performed using a built-in command in MATLAB, namely, BUTTER command. In this command the normalized cutoff frequency (W_n) for upper and lower limits can be defined by:

$$W_n = \frac{\text{cutoff frequency}}{\frac{\text{sampling frequency}}{2}} \qquad \text{Eq. 2-1}$$

where the cutoff frequency is defined as the upper and lower limit frequency of each scale, while the sampling frequency is the frequency of the experimental data.

Using this method, it is possible to eliminate the wavelengths higher and lower than the limits of each scale in a way that the remainder of the profile only includes the required wavelengths. It should be noted that after filtering the wavelengths, the amplitudes of the profiles for each scale fit within the ranges defined by PIARC in section 1.2 as well.

Figure 2-2, Figure 2-3, and Figure 2-4 depict samples from NCHRP, chip seal surfaces, and Danish road directorate databases, respectively.

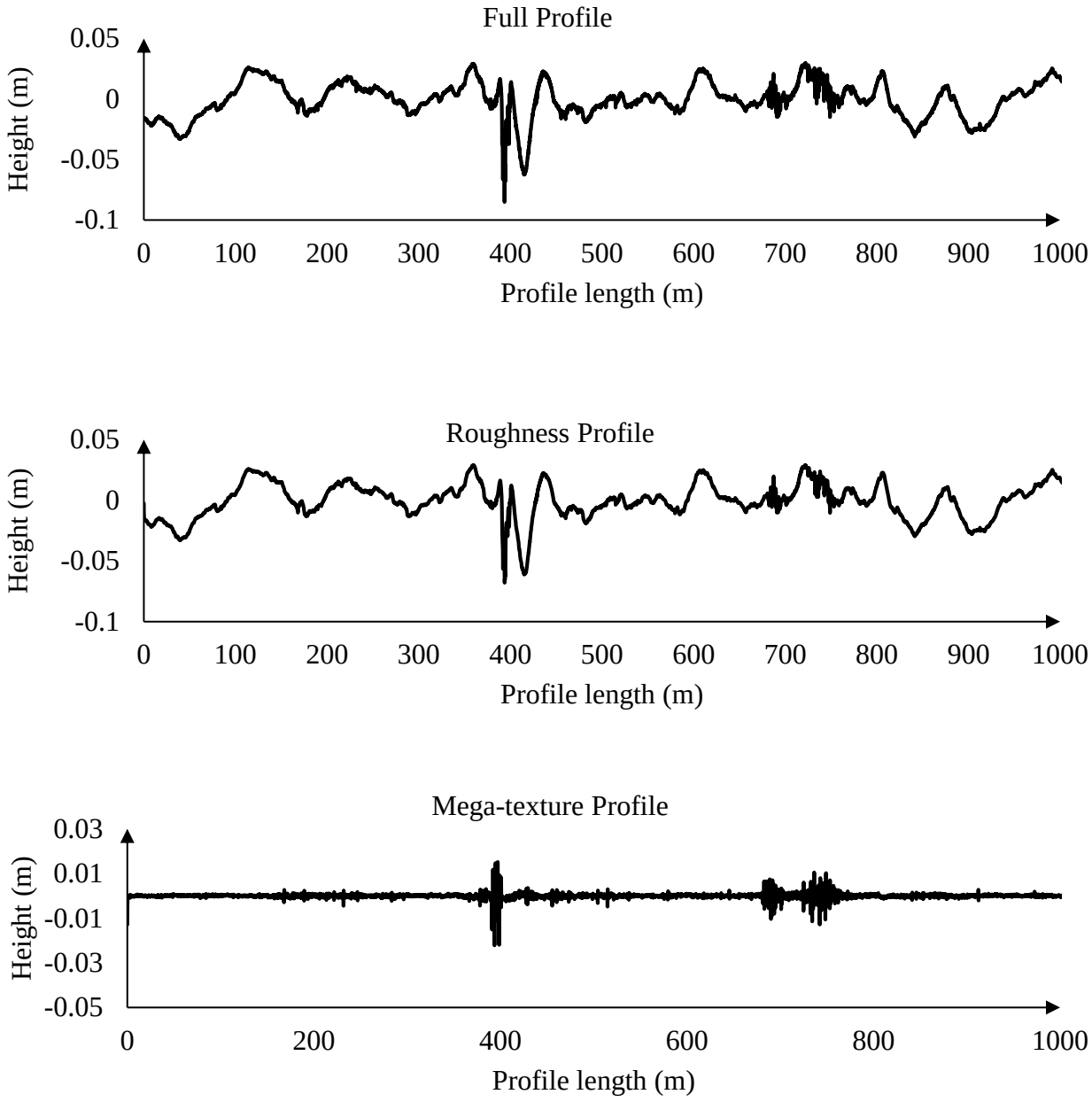

Figure 2-2. Division of the surface into different scales (data from NCHRP 720 report

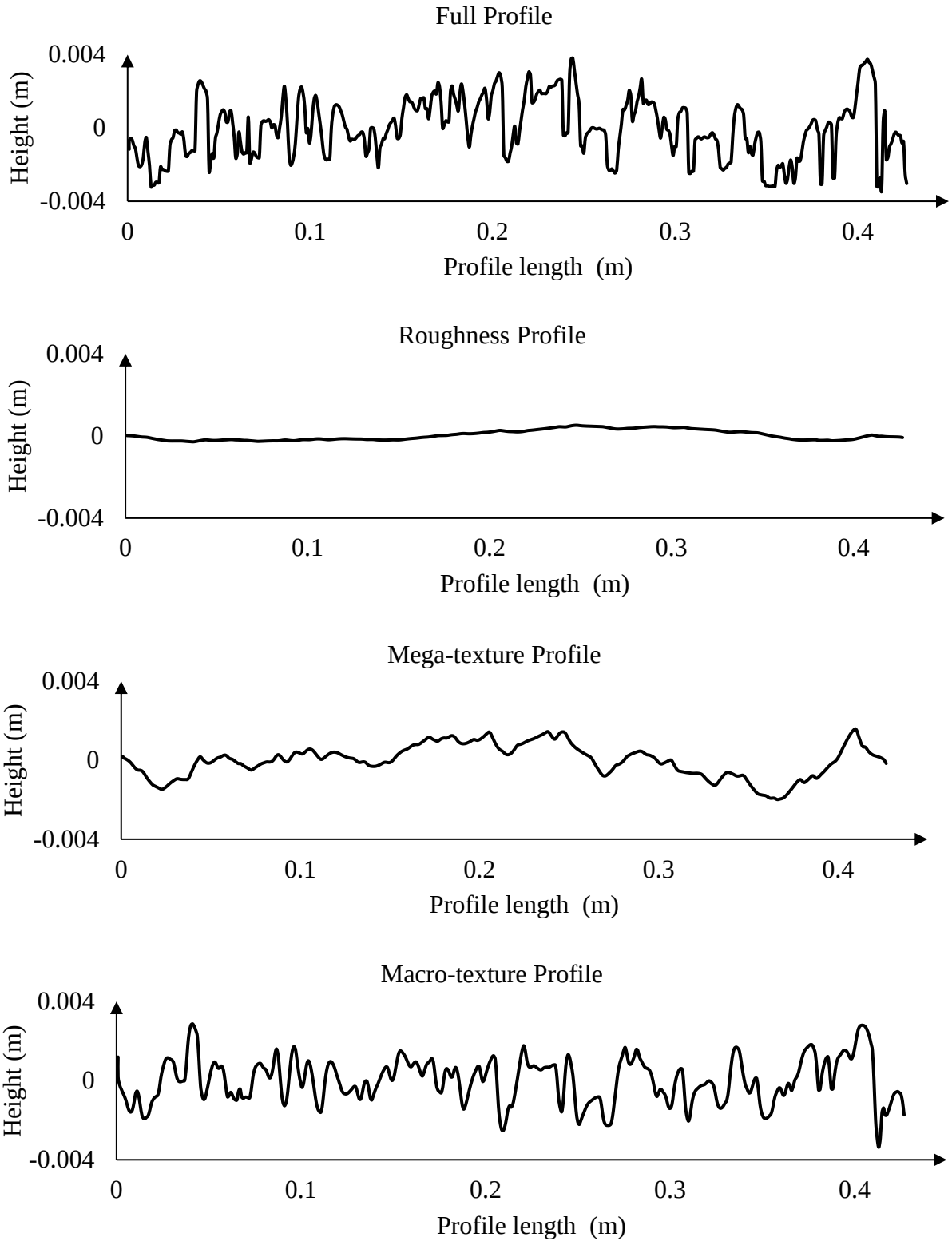

Figure 2-3. Division of the surface into different scales (Chip seal surfaces)

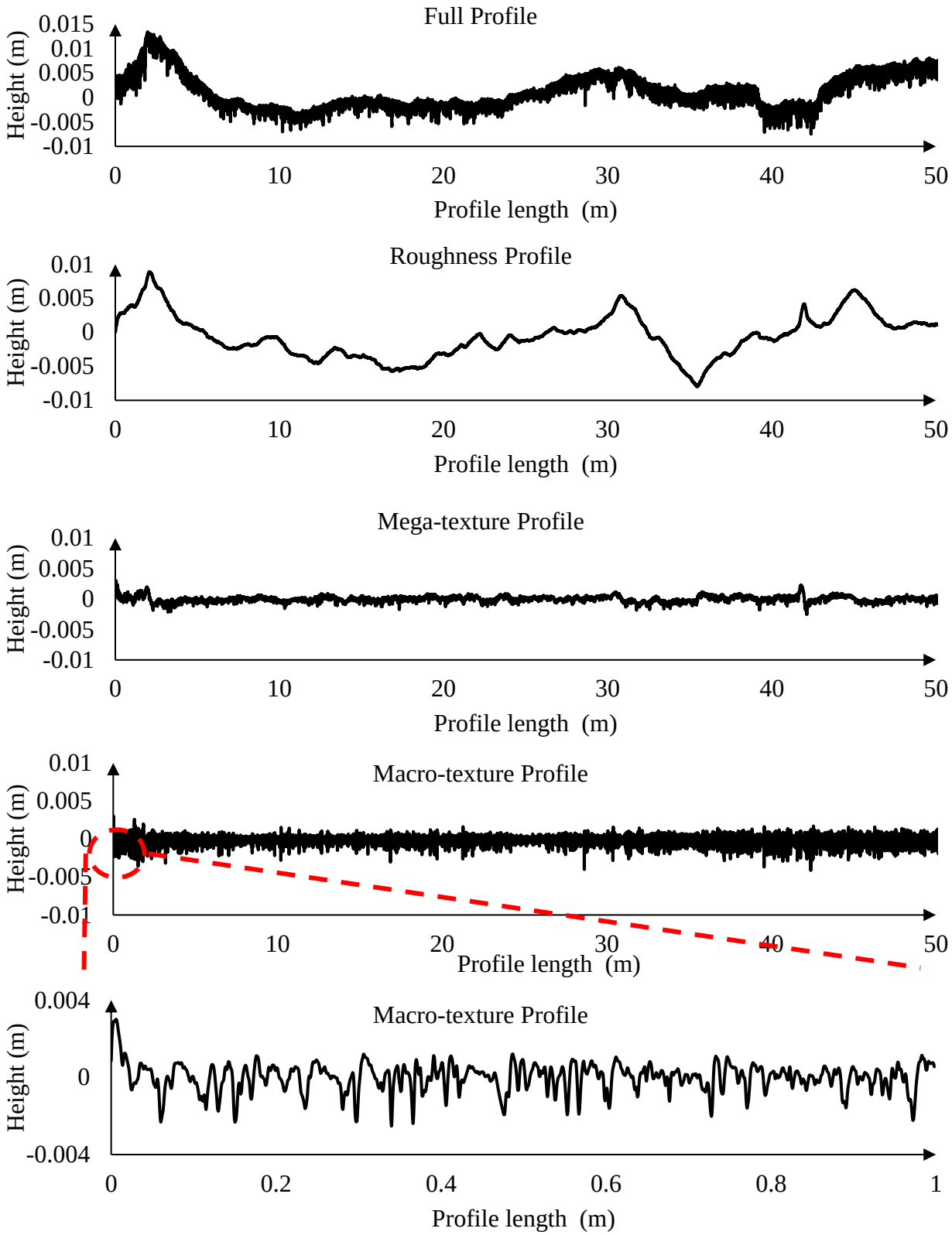

Figure 2-4. Division of the surface into different scales (Data from Danish road institute)

As it can be seen, the following is true for these databases:

- The NCHRP study database, does not include macro-texture, because the distance between the measured data points is 7.5cm.
- The chip seal database does not have roughness in its spectrum since the profile length is less than 50cm.
- The Danish database includes all of the spectrum since the resolution of the measurement is high and the length of the profiles are 100m. However, because the profiles are new and built to be low-rolling resistance, they do not cover the whole range of the roughness and texture spectrum.

After separation of different scales, the required modifications such as outlier removal and grade removal should be applied to the surfaces to prepare them for characterization.

2.4 OUTLIER REMOVAL

Optical instruments and lasers are the most common devices for surface profile measurements. The raw data from these measurements usually contain some missing points and outliers due to high speed scanning, the intensity of the light, transparency of the material, local slopes, etc. Outliers can be defined as the points within a data set that are inconsistent with the remainder of the data (Wang et al. 2018).

The presence of these outliers within the data test can influence the value of the characterization parameters. Therefore, prior to characterization, they should be removed from the data sets. MATLAB programming software can be used for this purpose. The outlier removal command (filloutliers) is used and the results demonstrate the capability of this command in recognition and removal of the outlier points. Figure 2-5 shows a sample of the performed outlier removal for a given surface.

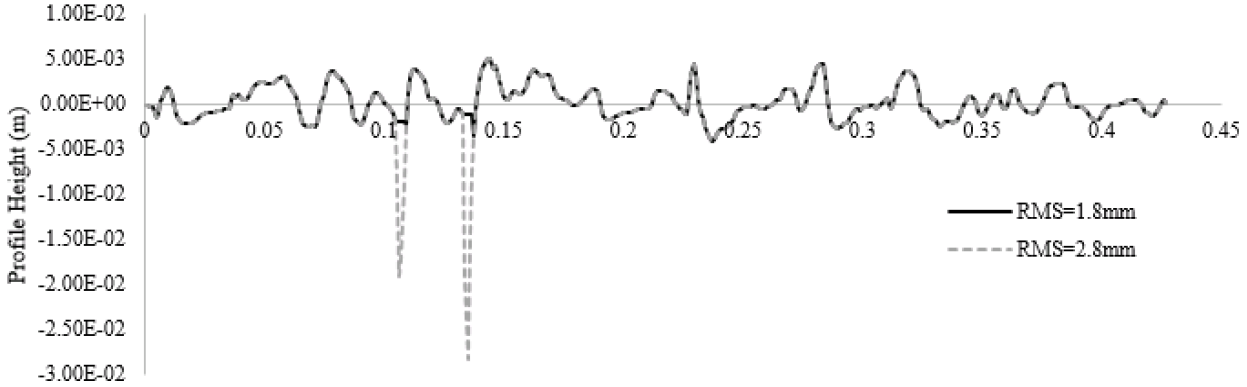

Figure 2-5. Outlier removal from the surface profile

As it can be seen, for this surface which only includes macro-texture of the profile, outlier removal omits two extreme points from the profile. This omission resulted in a decrease in the root mean square of the surface profile, changing the value from 2.8 mm with the outliers to 1.8 mm without outliers. This result indicates the necessity of outlier removals from surface profiles before characterization.

2.5 GRADE REMOVAL

After removal of the outliers within the profile, the mean of the profile is set to zero and any existing grade is removed from it. This task should be performed before surface characterization because, similar to outliers, the grade of the profile can also influence the surface characterization. For this purpose, the slope of the fitted linear line to the data is found using fitting toolbox in MATLAB and eliminated from the data. Figure 2-6 shows a sample of grade removal from a surface profile.

After removal of the grade or any outliers, surfaces should be characterized. However, for generation of the surface profile in the finite element model, no other modifications are required to be performed on the surfaces. Therefore, the filtered profiles can be imported directly into the finite element model as inputs with a process that will be explained in section 3.1.

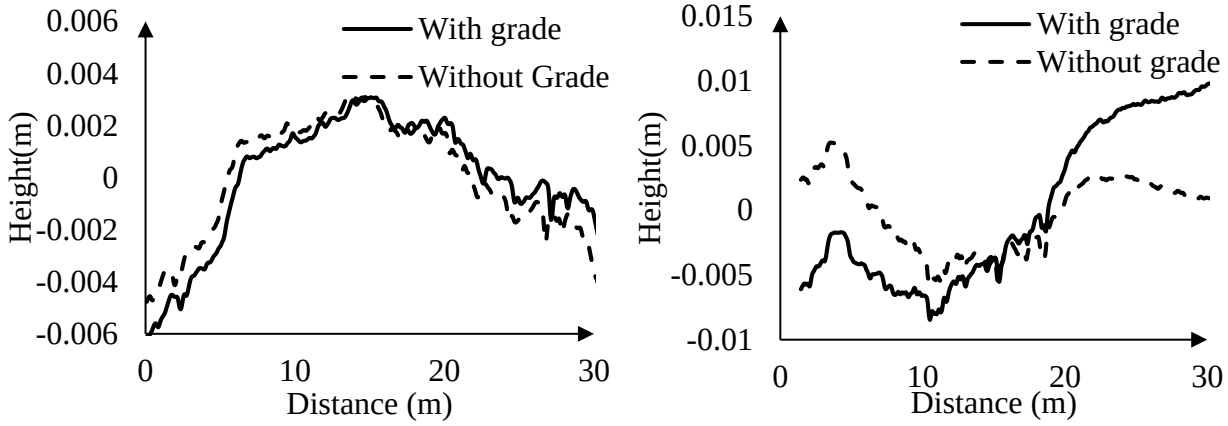

Figure 2-6. Grade removal from surface profiles

2.6 SURFACE PROFILE CHARACTERIZATION

To better represent the results of the study and show the influence of different scales on rolling resistance, the profiles need to be characterized. In this study, statistical parameters are used for surface characterization. As it was mentioned before, statistical parameters are scale dependent and their value depends on the sample size. Having one parameter for the entire sample results in missing information in smaller scales. Therefore, these parameters should be defined for each scale independently. Hence, after division of the profile into the four aforementioned scales and performing the required modifications on each profile, an adequate parameter should be chosen for surface characterization.

Roughness or unevenness is usually defined by the International Roughness Index (IRI) which is the accumulated motion of the suspension of the vehicle divided by the length of measurement. For calculation of the IRI, a standard quarter-car model is used for capturing the deflection of the suspension (see Figure 2-7). This quarter-car model considers the internal resistance of the suspension as a combination of a spring and a dashpot, while assuming only a spring for the tire. The deflections in the suspension can be found by solving the two following equations of motion:

$$m_s\ddot{z}_s = -c_s(\dot{z}_s - \dot{z}_u) - k_s(z_s - z_u) \qquad \text{Eq. 2-2}$$

$$m_u\ddot{z}_u = c_s(\dot{z}_s - \dot{z}_u) + k_s(z_s - z_u) - k_t(z_u - z_r) \quad \text{Eq. 2-3}$$

IRI is then defined as

$$IRI = \frac{\sum Suspension\ movement}{profile\ length} \quad \text{Eq. 2-4}$$

IRI is an index with units of slope in m/km or in/mi.

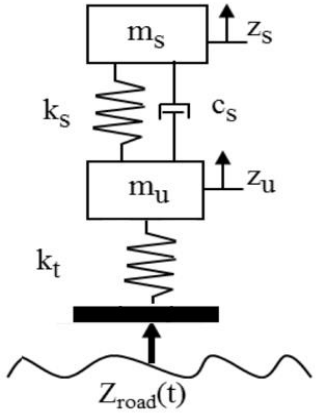

Figure 2-7. Standard Quarter-car model for IRI calculation (Zaabar et al, 2018)

For calculation of the IRI, ProVAL software can be used. This software is built for viewing and analyzing surface profiles, and it can provide the IRI of any given profile, over fixed or variable lengths. This software uses a 250 mm filtering routine to omit the effect of any portion of the profile smaller than the contact patch. This is a common practice in IRI calculation, since it is assumed that any wavelength smaller than the contact patch does not affect the deflections in the suspension of the vehicle.

For characterization of macro-texture, the most common parameter is the mean profile depth (MPD). MPD is defined over a 10 cm length of the profile, as the average of the difference between the maximum height of first and second half of the profile and the mean of the profile (see Figure 2-8):

$$MPD = \frac{Elv1+Elv2}{2} \quad \text{Eq. 2-5}$$

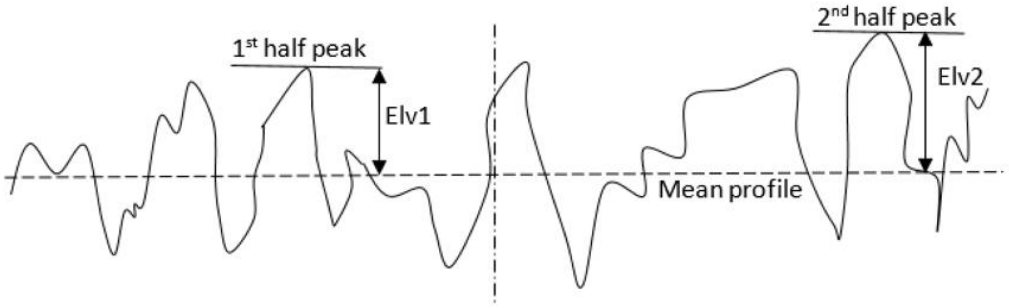

Figure 2-8. Surface texture MPD calculation

As it was mentioned, IRI is related to the vehicle response and is not a characteristic of the surface by itself. On the other hand, MPD is representing the textures with a 10 cm range of profile, so it is not sufficient for characterization of the higher scales of the profile. In this study, the main purpose is comparing the effect of different scales of the profile on rolling resistance of the vehicle.

Therefore, for consistency between different scales of roughness, mega-, and macro-texture, it is beneficial to use the same parameter for the different scales. For this purpose, among the statistical parameters mention in Table 1-1, the root mean square (RMS) is selected. RMS or Rq of the profile can be defined as

$$R_q{}^2 = \frac{1}{n}\sum_{i=1}^{n}(z_i)^2 \qquad \text{Eq. 2-6}$$

where z_i is the height of each point of the profile, when the mean of the profile is set to zero, and

n is the number of available points in the profile.

Avaik et al. 2013, investigated the relationship between MPD and RMS of the macro-texture of the pavement surface and obtained the following linear relationship:

$$\text{MPD} = 1.729\ \text{RMS} + 0.019 \qquad \text{Eq. 2-7}$$

Figure 2-9 shows a comparison between MPD and RMS of the macro-texture data sets available in this study. As it can be seen the relationship found for the two data sets are quite different. For the Danish database with smoother surfaces, the MPD values are lower than the MPDs for the same RMS value of the Chip seal surfaces. If both databases are considered together, the relationship in Figure 2-10 is obtained.

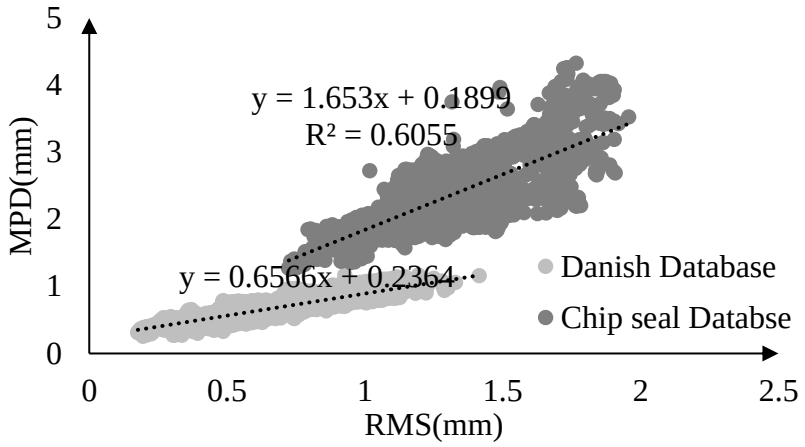

Figure 2-9 Relationship between RMS and MPD values for Danish and Chip seal databases

In addition, the relationship between IRI and RMS is also investigated for roughness data from the NCHRP 1-45 study. Figure 2-11 shows that a non-linear relationship can be assumed between these two parameters. The data points available for this comparison are fewer due to the longer process of obtaining IRI values from ProVAL software.

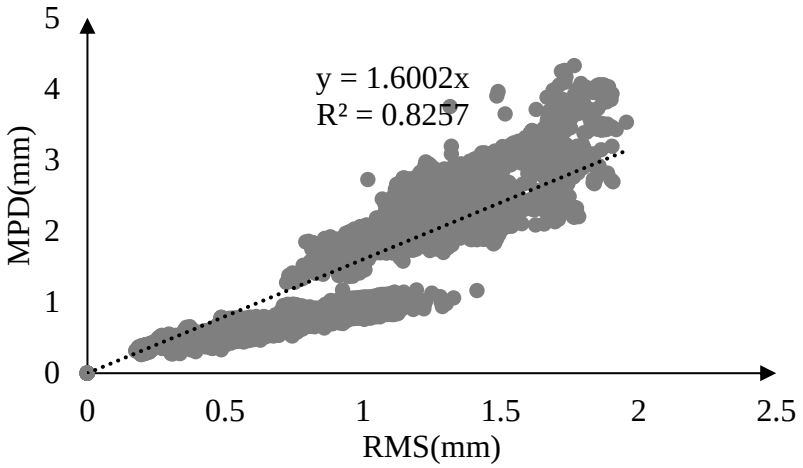

Figure 2-10. Relationship between RMS and MPD values for all databases

This relationship is consistent with the results from Marcondes et al. (1991) (see Figure 2-12). Similar to Figure 2-11, Marcondes et al. show smaller variation of IRI (less than 2 m/km) for RMS values less than 3mm. It should be noted that the values of RMS and IRI reported are in inch and inch/mile units. However, the ranges are similar.

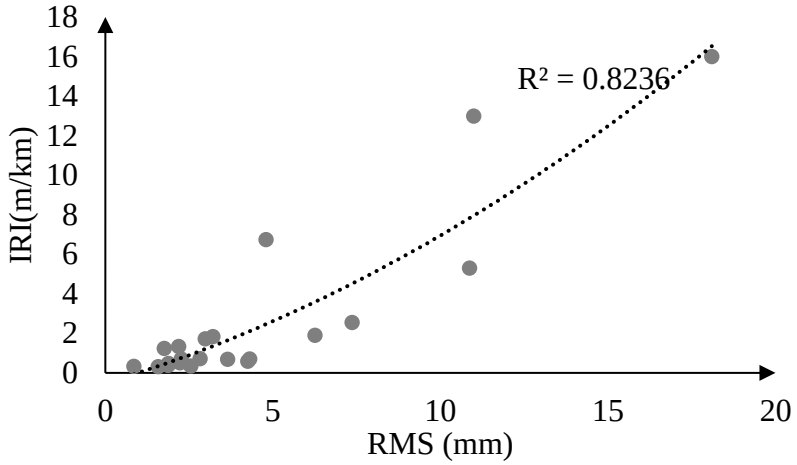

Figure 2-11. Relationship between RMS and IRI values

As it can be seen, the standard deviation of the relationships between RMS and MPD and IRI is not low and the two relationships cannot be considered as very strong ones. Also, RMS is a statistical parameter and it is dependent on the length of the profile. However, these limitations exist for any statistical parameter. Therefore, although RMS is not an ideal parameter, it is used in this study as the common parameter in different scales for comparison of the results.

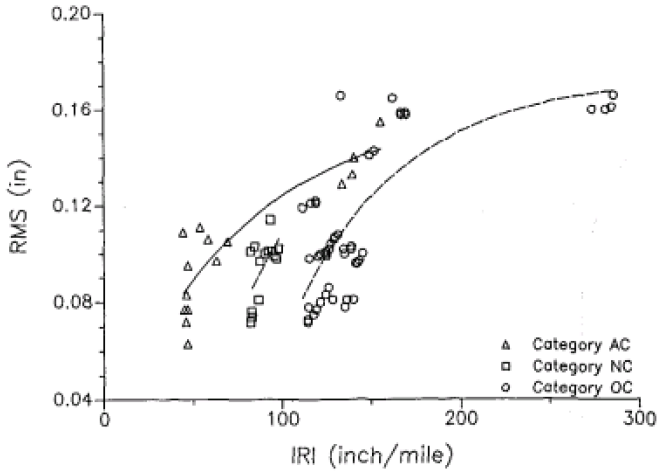

Figure 2-12. Relationship between RMS and IRI values for asphalt and new and old concrete surfaces (Marcondes et al, 1991)

2.7 SAMPLE SIZE SELECTION

Considering a statistical parameter such as RMS for surface characterization, the size of the sample profile is of great importance. The selected surfaces should be large enough to represent the whole spectrum of the specific scale. In addition to the surface profile, the finite element model can also affect the considered profile length. The profile should be long enough for the tire to reach the steady state condition. However, it should not be too large to increase the computational time of the model unreasonably. Hence, this length is related to some of the model characteristics, such as the size of the tire and the rolling velocity. In this section the required sample size for each scale at 80km/h for a tire with a diameter of almost 2 m is defined. This size should be the maximum of (i) minimum required length (ii) length of available profiles (iii) required tire model length

2.7.1 Macro-texture

- Minimum length: 10 cm (2 times of the maximum wavelength)
- Available data: 43 cm available data from chip seal samples
- Tire model requirement: At least 6 meters (3 cycle of the tire rolling)

Therefore, the minimum length of the profile for macro-texture profiles is chosen as 6 meters.

2.7.2 Mega-texture

- Minimum length: 1 m (2 times of the maximum wavelength)
- Available data: no limit
- Tire model requirement: At least 12 meters (6 cycle of the tire rolling)

Therefore, the minimum length of the profile for mega-texture profiles is chosen as 12 meters.

2.7.3 Roughness

For roughness, there is no minimum based on the definition of roughness. Based on the effect of frequency on vehicle response (Figure 2-13), the maximum wavelength that can affect the vehicle response can be considered as 100 meters (far left point in the figure). However, the available

studies suggest a length of 30 meters to be sufficient for capturing the effect of the roughness (Sayers and Karamihas, 1998). Considering 30 meters as the maximum wavelength instead of 100 m, it can be evident from Figure 2-13 that the error in the response can be limited to 2% only. Therefore, 30m can be considered as the required length for the roughness profiles.

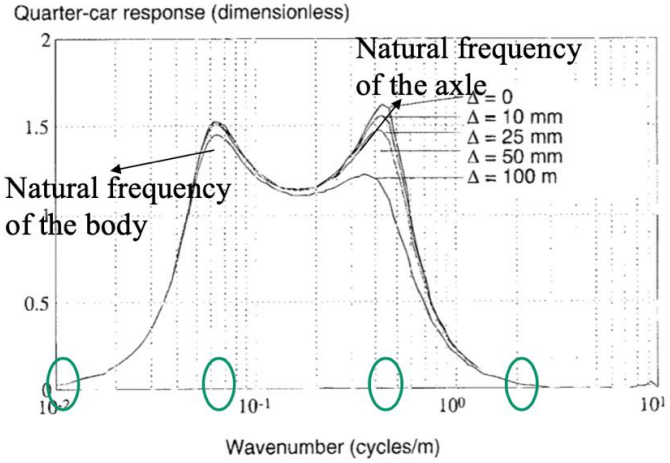

Figure 2-13. Effect of frequency on vehicle response (Mann et al. 1997)

2.8 FINAL SELECTED SURFACES FOR THE SIMULATION

2.8.1 RMS variation for each scale

For capturing the effect of each scale on rolling resistance, performing only a limited number of finite element analyses is practical due to the high computational time of the analysis. Therefore, it is necessary to know the range of the variation of surface profile parameter RMS, to be able to choose the surfaces in high, low and middle of the ranges. For this purpose, using the available data sets the RMS values are calculated for different scales of roughness, mega-, and macro-texture individually, and based on the obtained ranges, the final surfaces are selected. Figure 2-14, Figure 2-15, and Figure 2-16 show the variation ranges for the RMS values of roughness, mega-, and macro-texture, respectively.

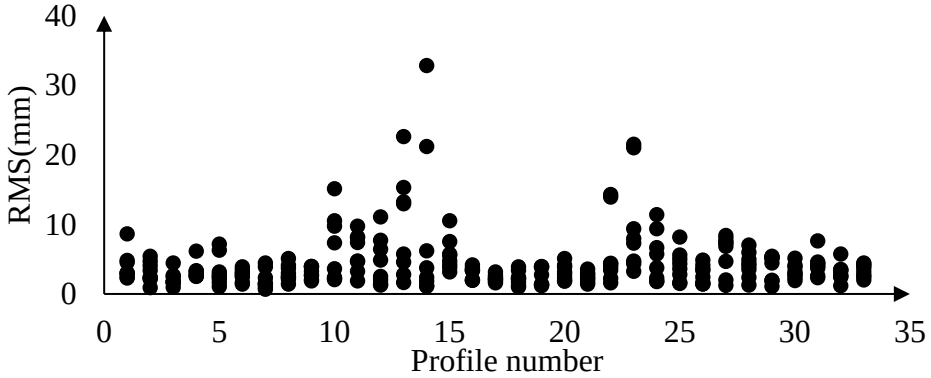

Figure 2-14. RMS variation for roughness profiles of 30 meters long

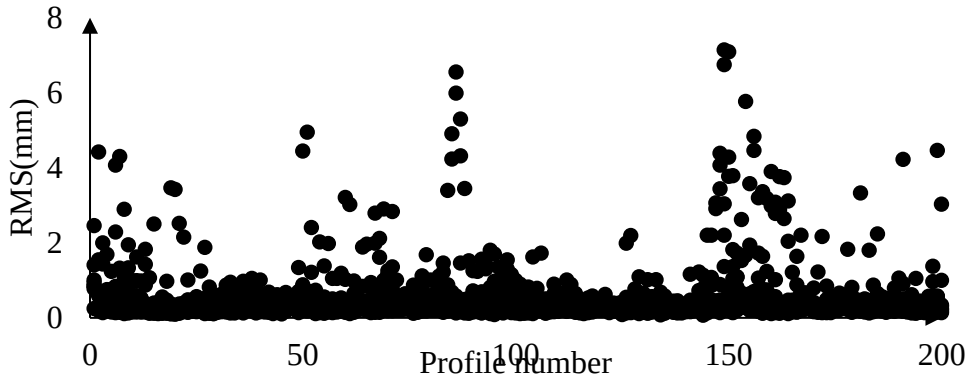

Figure 2-15.RMS variation for mega-texture profiles of 12 meters long

As it can be seen, RMS values of roughness profiles are mostly less than 12 mm. However, in some instances they can go up to values as high as 20 mm, which can be the result of local major distresses on the road. Mega-texture profiles show RMS as high as 7.5 mm, but the majority of the values are less than 4mm. The RMS values for macro-texture for both databases of smooth Danish roads and chip seal surfaces are below 2mm after outlier removal. It is evident that roughness range has the largest range, while macro-texture has the smallest one.

2.8.2 Comparison of surface profiles with similar RMS

RMS is a statistical parameter; therefore, it is possible for a surface with one single large event to have the same RMS value as a surface with uniformly distributed smaller events. The effect of local events is not the purpose of this study. Hence, here, although the surfaces are selected randomly, the profiles with single events have been removed from the database. Figure 2-17, Figure 2-18, and Figure 2-19 show a comparison of profiles with different RMS values within the ranges of each roughness, mega-, and macro-texture scales.

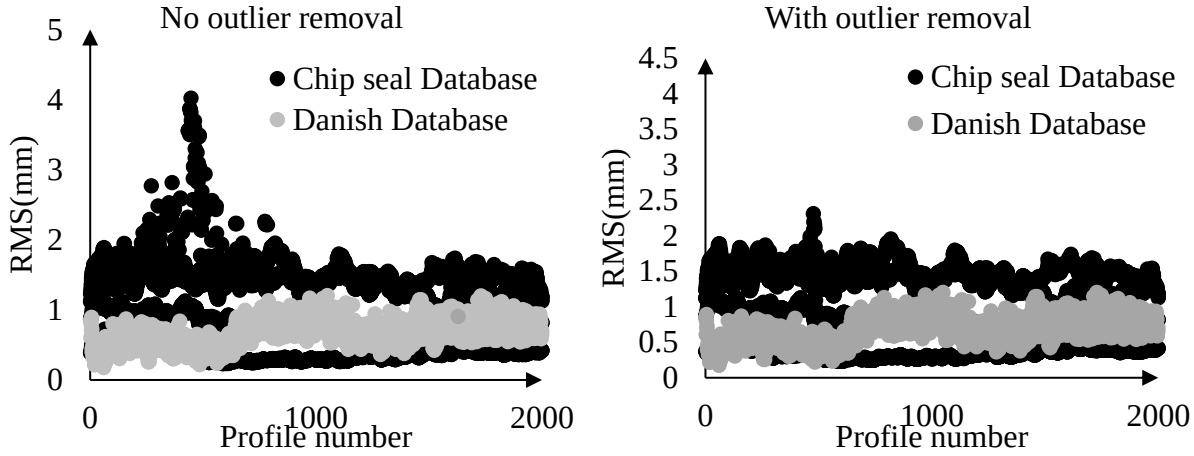

Figure 2-16. RMS variation for macro-texture profile of 0.45m long (data base maximum length)

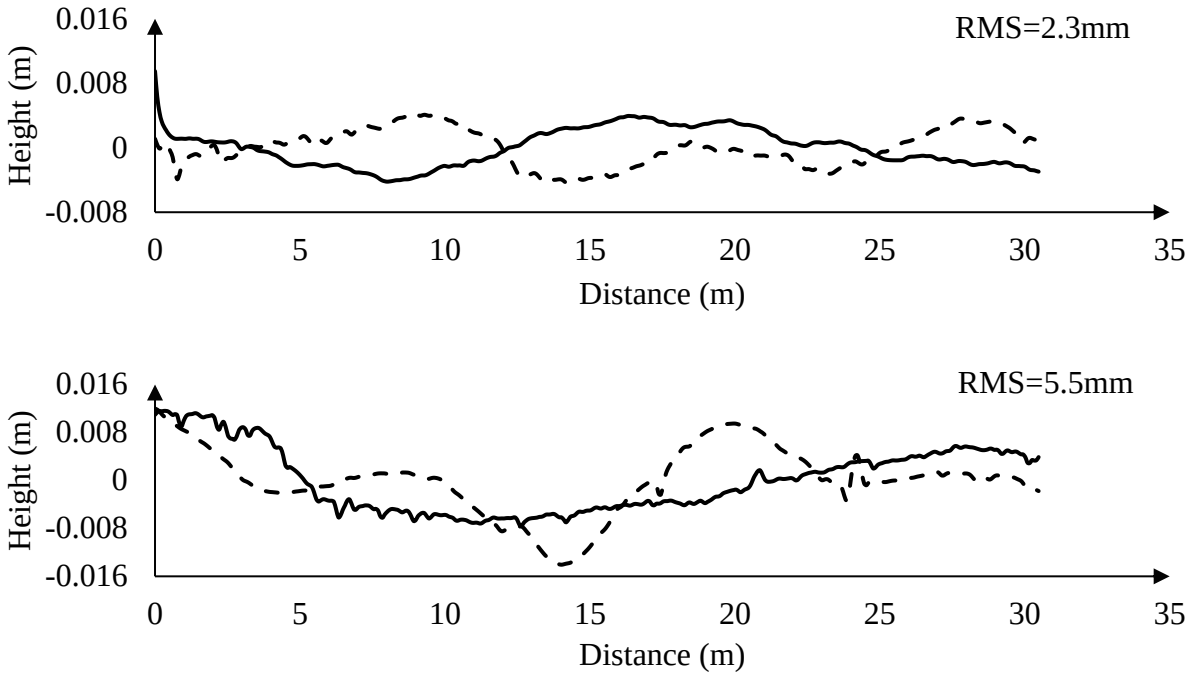

Figure 2-17. Comparison of different roughness profiles with the same RMS values

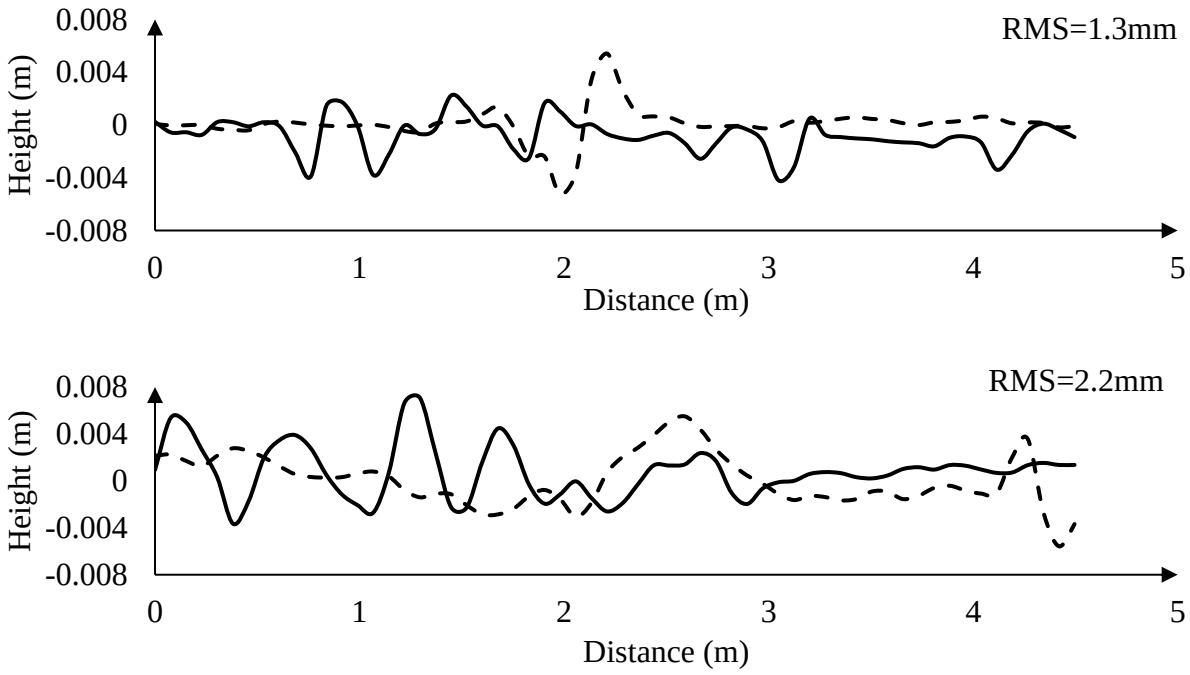

Figure 2-18. Comparison of different mega-texture profiles with the same RMS values

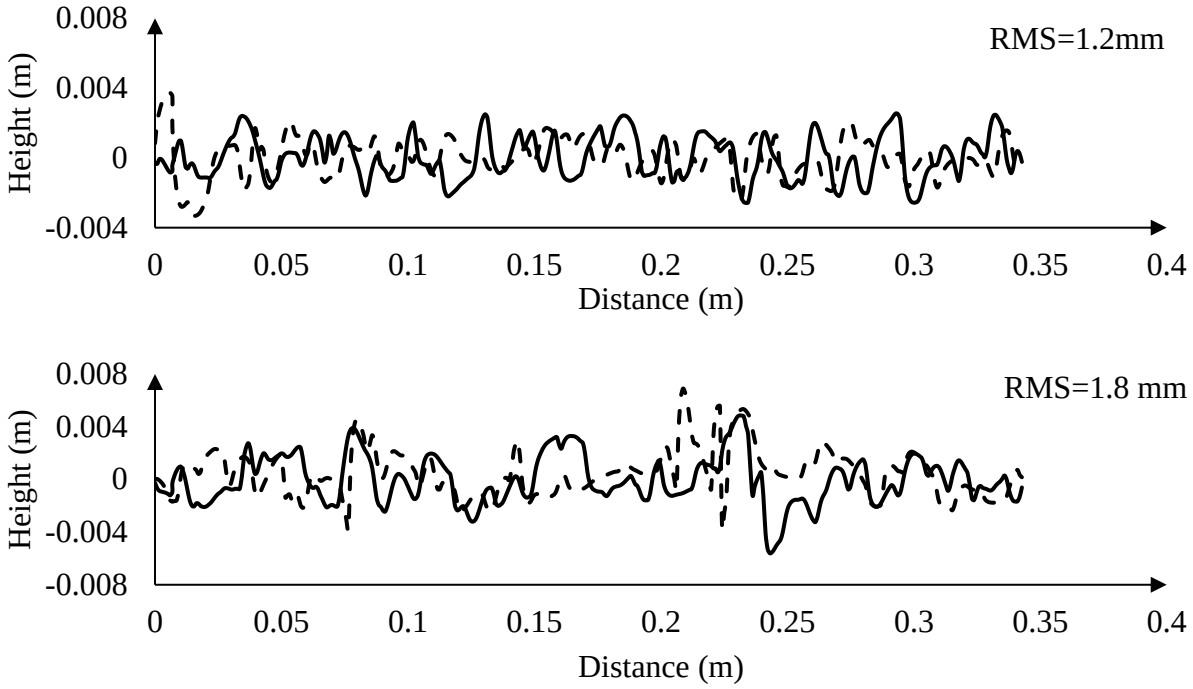

Figure 2-19. Comparison of different macro-texture profiles with the same RMS values

2.8.3 Occurrence frequency of mega-texture events

Macro-texture of the surface is related to the aggregate and mix properties of the top pavement layer; therefore, for a given profile, its value does not change dramatically. However, high mega-texture values can be related to specific distresses on the road, and therefore, they can be localized events. To better understand the frequency of these localized events, here, a profile of 100 m is depicted in Figure 2-20, along with filtered roughness and mega-texture profiles.

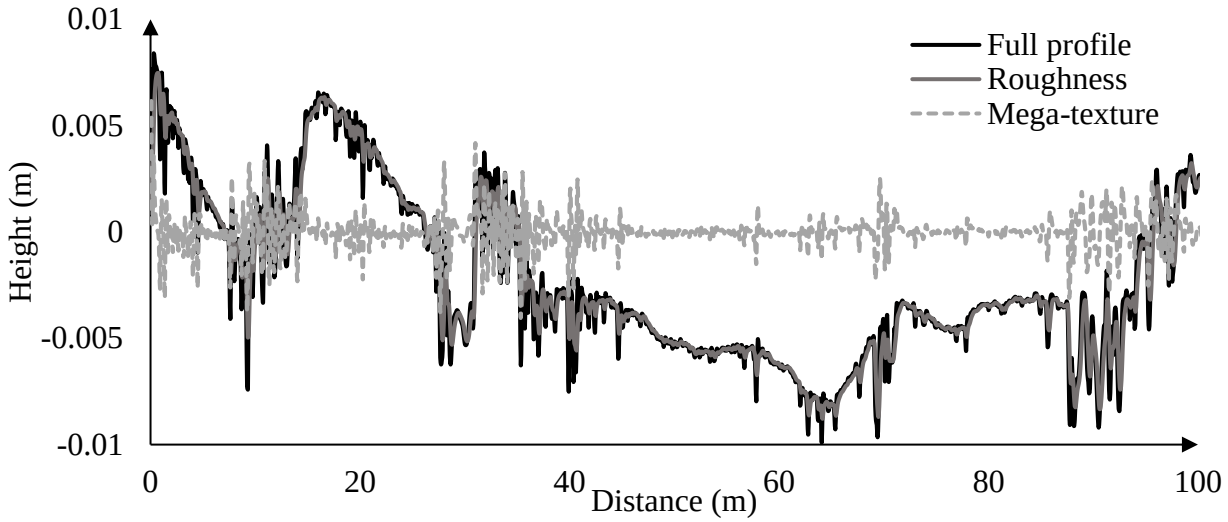

Figure 2-20. Frequency of the high mega-texture in the profile

As it can be seen, in a few locations, the mega-texture of the profile increases. To prevent overestimation of the effect of mega-texture, the effect of the occurrence frequency of the mega-texture on rolling resistance should also be investigated.

2.8.4 Selected surfaces for each scale

Considering the mentioned ranges, different surfaces are selected randomly, in order to properly cover the range of RMS values for each scale. Figure 2-21, Figure 2-22, and Figure 2-23 depict the selected surfaces used for the analysis of the effect of each scale on rolling resistance of tire and vehicle in the future chapters. RMS values are presented for each one of the surfaces.

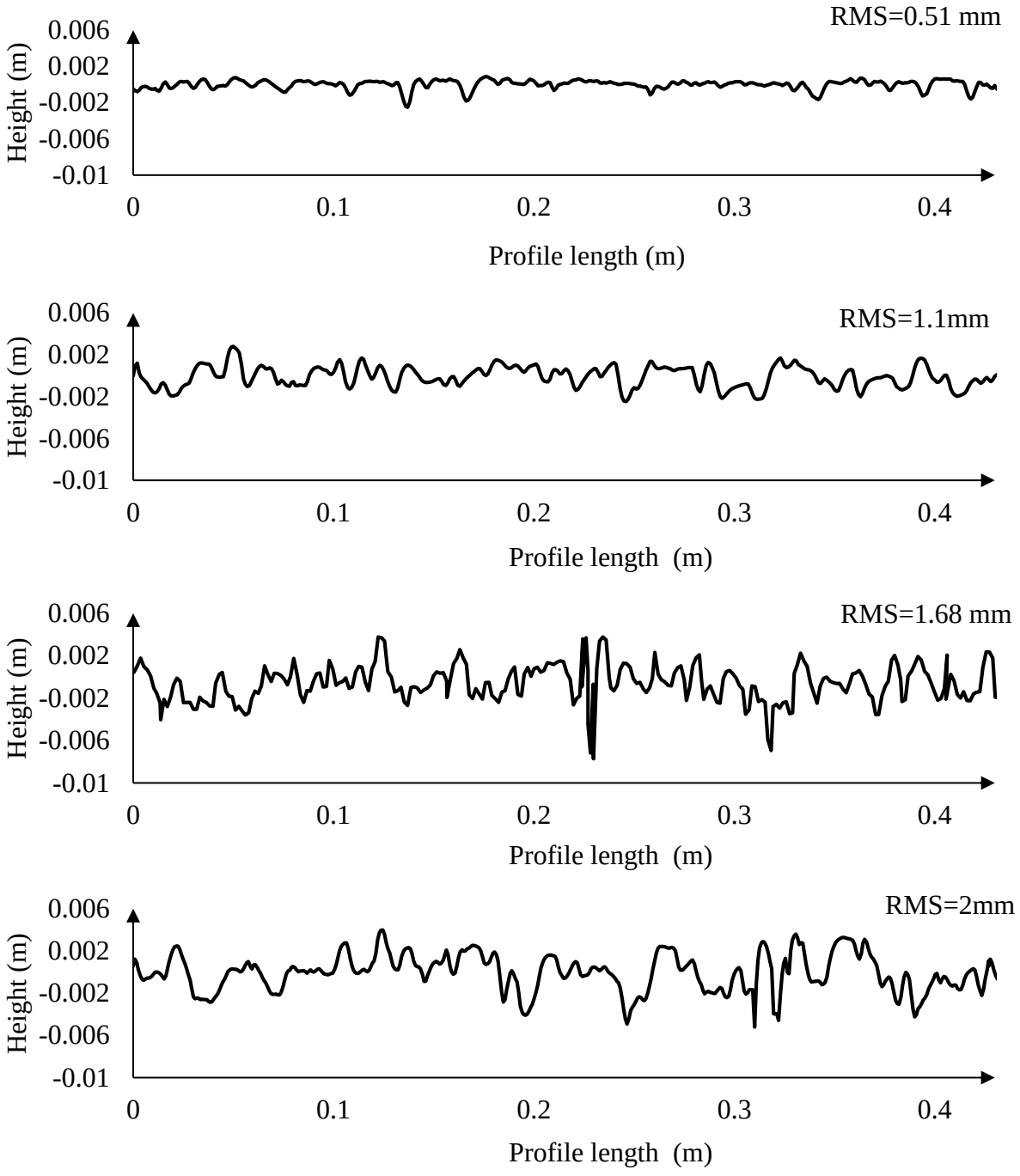

Figure 2-21. Selected profiles for macro-texture scale, with different RMS values

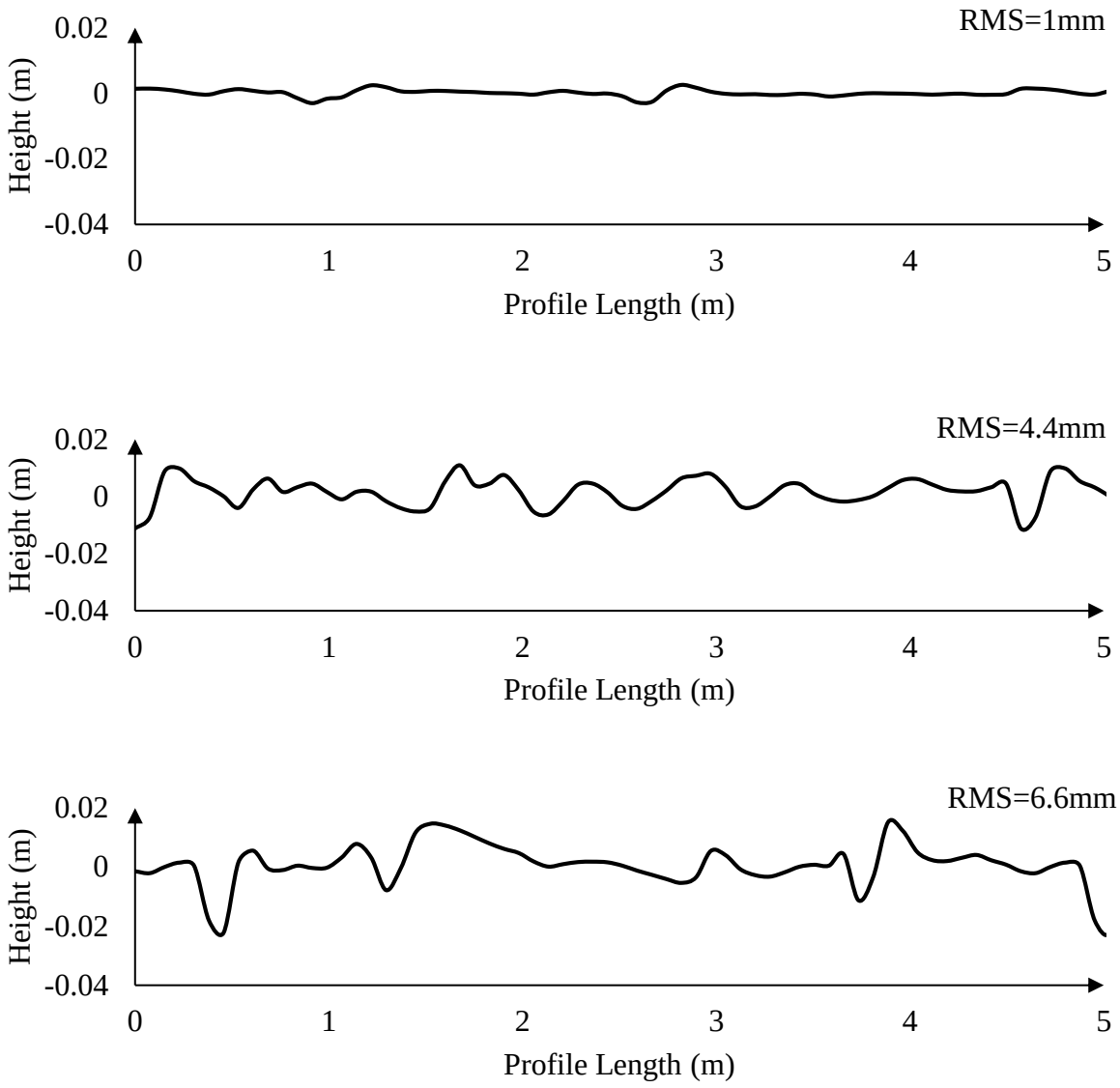

Figure 2-22. Selected profiles for mega-texture scale, with different RMS values

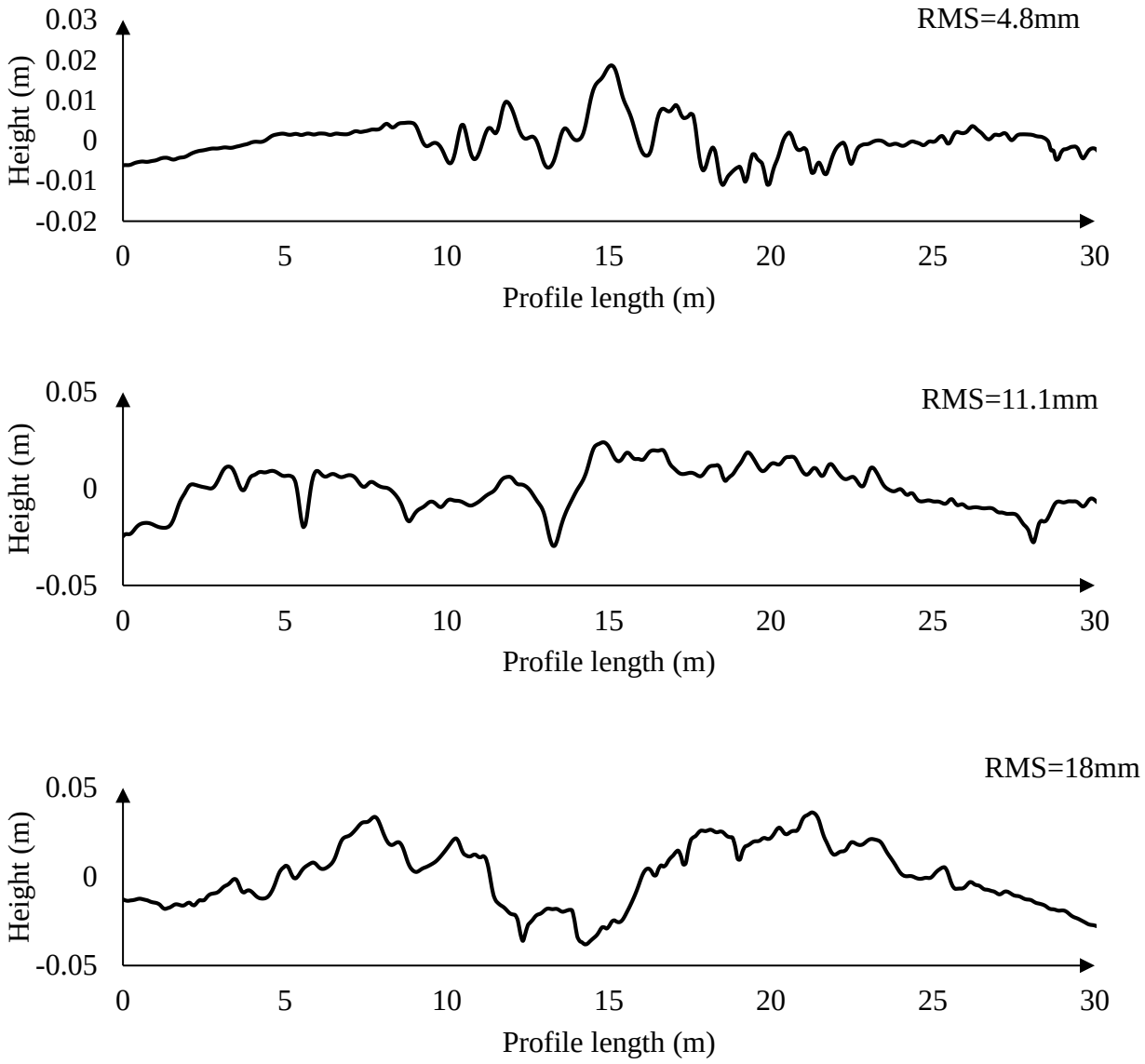

Figure 2-23. Selected profiles for roughness scale, with different RMS values

CHAPTER 3
FINITE ELEMENT MODEL DEVELOPMENT AND VERIFICATION

Tires can include more than 200 materials, such as carbon black, silica, sulfur, plasticizers, volcanizing agents and many different cords (steel, fabric polestar (fabric plies), etc.). These materials are generally used in different parts of the tires such as ply, belts, beads, sidewalls, tread, rim, etc. The tire manufacturers use various layers with different material properties and reinforcements to enhance the performance of their tires. Figure 3-1 depicts a sample of these parts along with a common tire manufacturing process.

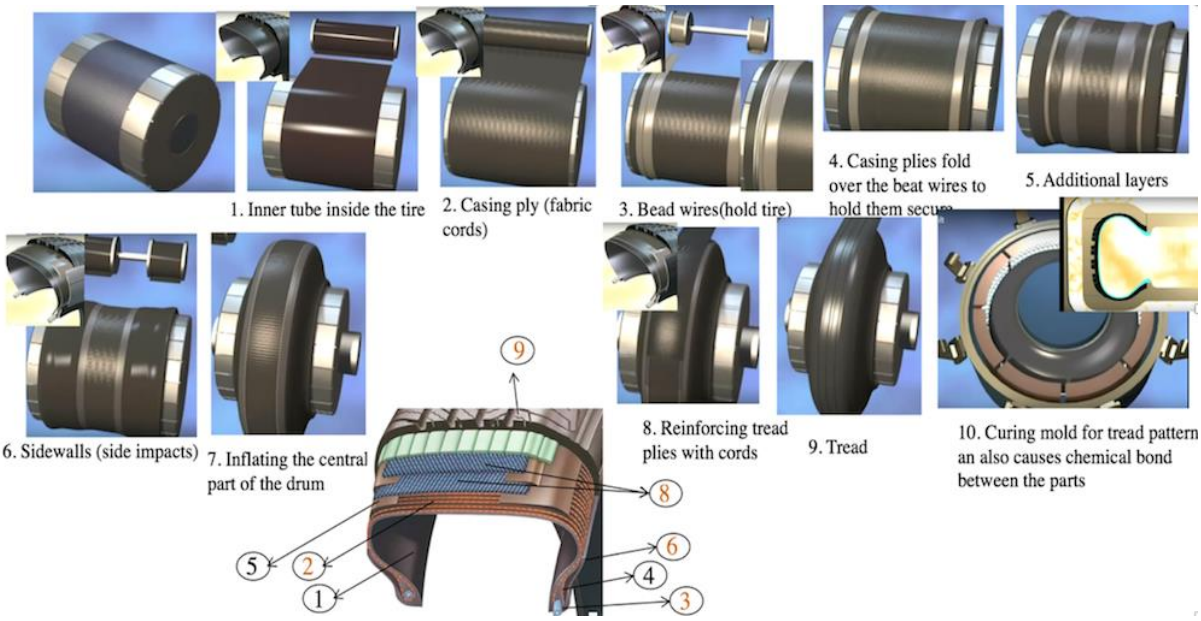

Figure 3-1. Tire manufacturing process and various parts (made from photos from Michelin's tire website)

Most of the published finite element models of tires consist of a simplified tire model including only the main parts of the tires such as ply, belts, beads, sidewalls, tread, and rim (Srirangam, 2015, Hernandez, 2015). For developing such models, the geometry of the different parts, their material properties and mesh type, the contact properties between the tire and the pavement surface, and the required boundary conditions for the problem should be determined.

None of the tire industry companies publish the details of their tire design. Therefore, most of the available studies for FE tire models either obtained this information by performing the required experiments or got limited access to the tire industry designs without the right to publish. For this study, none of these options were available. Therefore, the tire properties (geometry and material properties) had to be taken from another study which published the details of their tire cross section and material properties. The tire model developed by Wei and Olatunbosun (2016), from a 235/60 R18 tire, is chosen as the reference tire for this study due to the availability of (i) thorough details of the tire model and (ii) results of a controlled test performed in the laboratory, which is required for validation of the FE model. After development and verification of the tire model, the main objective of the research is to find the effect of pavement surface profile (roughness, mega-texture, and macro-texture) on rolling resistance. To achieve this goal, since there is no study that covers the whole spectrum of the profile, the results from this study are compared with different studies

that considered different wavelength ranges within the profile. First, the tire model is rolled over various macro-texture profiles, as mentioned in the previous chapter, and the results of the study are compared with experiments taken from Boere's (2009) study. The tire that was used in Boere study is a 225/60 SR16 tire. Therefore, after validation of the FE model, the tire size was changed to a 225/60 SR16 tire, with the same material properties and a similar geometry but with different size. In the next step, the model set up was changed in order for it to be compared with the results from the NCHRP 1-45 project (Chatti and Zaabar, 2012), which includes roughness and mega-texture. For this purpose, the properties of the model were changed to match those used in the NCHRP model, and the suspension system of the vehicle was added to the tire model to build a quarter-car FE model. To compare the effect of different texture spectrums, the final model was used for rolling over surfaces with different texture levels.

The details of the Wei and Olatunbosun model and required changes for comparison with Boere study and developing the quarter-car model are discussed in the following subsections.

3.1 TIRE GEOMETRY

The tire used in the initial part of this study is a 235/60 R18 tire. This tire has a width of 235mm, aspect ratio (height to width ratio) of 60%, and diameter of 18 inches (457.2 m). For the FE model, the structure of the tire is simplified to include the following parts: Tread, Sidewall, Apex, Two belt layers, Cap layer, Carcass layer, Reinforcements, and Rim. The cross section (excluding the tread pattern) is shown in Figure 3-2.

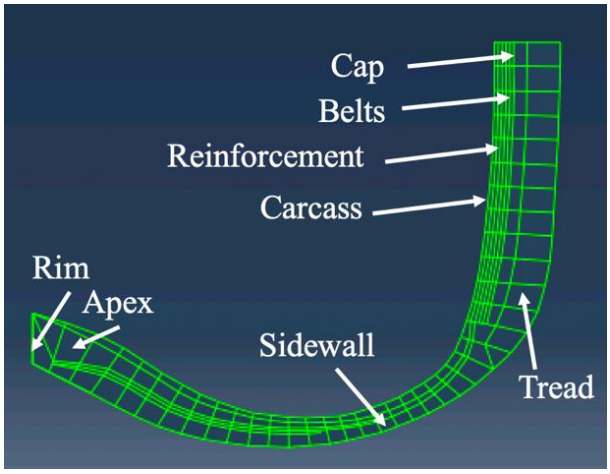

Figure 3-2. Tire cross section

Wei and Olatunbosun obtained the geometry of these parts by measuring their actual dimensions from the tire. Therefore, the tire geometry in this study is based on the figures provided in their study.

In the tire manufacturing process, reinforcements are embedded within layers of rubber, with different areas and orientations. There are five different reinforcements considered in this study: Cap layer, two steel belts, carcass layer, and a reinforcement strip. For modeling these reinforcements, similar to the actual construction process, they should be embedded within the rubber materials. Therefore, their area, spacing and orientations should be provided. Wei and Olatunbosun (2016) measured the reinforcement areas and diameters using a micrometer gauge. Their spacings and orientations were obtained using image processing techniques. A schematic

representation of the reinforcement distribution in the tread layer used in this study is shown in Figure 3-3. The orientation of the reinforcement, their areas, and the spacing between them are given in Table 3-1.

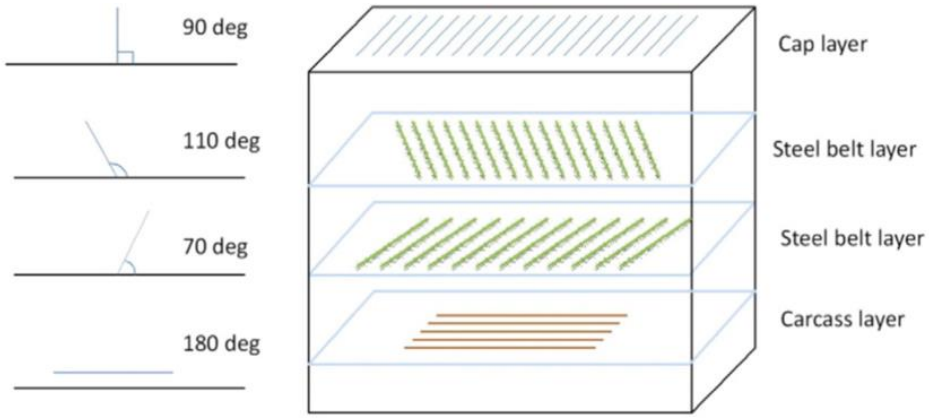

Figure 3-3.A schematic representation of reinforcement distribution in the tread layer (Wei and Olatunbosun, 2016)

Table 3-1.Reinforcements detail

	Area (mm^2)	Spacing (mm)	Orientation angle (°)
Cap	0.1521	0.5128	90
Steel belt 1	0.3165	1.2983	110
Steel belt 2	0.3165	1.2983	70
Carcass	0.2917	0.5928	0
Reinforcement strip	0.1898	0.8055	80

This tire is later converted to a 225/60 SR16 tire keeping a similar geometry as it can be seen in Figure 3-4.

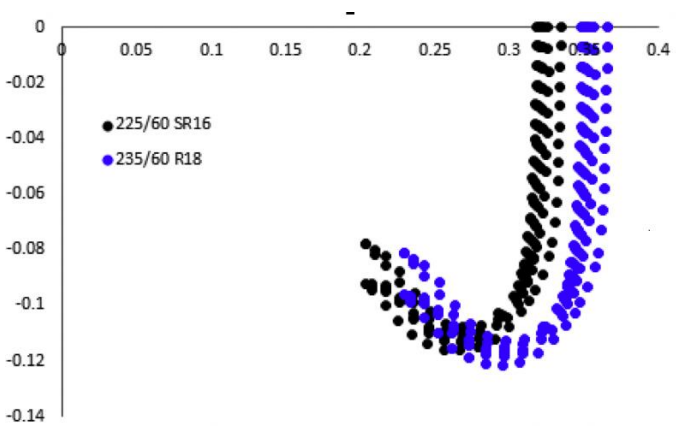

Figure 3-4. Conversion of the geometry of a 235/60 R18 tire to a 225/60 SR16 tire

3.2 MATERIAL PROPERTIES

3.2.1 Rubber material properties

Wei and Olatunbosun (2016) considered the rubber materials as hyper-viscoelastic. For obtaining the material properties, two sets of tests were performed. The required rubber samples were extracted from the tire. Due to the difference between the rubber materials used in different parts of the tire, three different rubber material properties were considered, separating the tread rubber material from sidewall and apex materials. The specimens acquired from the tire were in straight narrow strips shapes, which satisfy the ASTM-D412 requirements (for test specimen requirements); where, the required minimum length of the samples is 10 times of their width and thickness. For defining a material as hyper-viscoelastic, the hyperelastic and viscoelastic properties should be obtained separately since they describe different components of the response of the material. Hyperelastic properties correspond to the non-linear elastic response of the rubber while viscoelastic properties define the viscous component of the material response, related to the dependency of the material strain rate on time.

Hyperelastic material property

For obtaining the hyperelastic material properties of the three rubber materials (tread, sidewall, and apex), the uniaxial extension method was used. In this test, before data collection, the rubber sample was stretched for more than 10 cycles to have a stable stress-strain relationship. Then, the uniaxial process was repeated at least three times, and the final result was the average of the three sets (with test temperature of 23 °C). For characterization of the material properties, different constitutive models can be used. For this purpose, Wei and Olatunbosun (2016) considered Yeoh hyperelastic model, which is one of the common strain energy functions for hyperelastic materials; that produced a good fit to the test data (Figure 3-5). This model can be defined as

$$\psi(\alpha_1, J) = \sum_{i=1}^{3} c_{i0}\,(\alpha_1 - 3)^i + U(J) \qquad \text{eq. 3-1}$$

$$U(J) = \frac{1}{D_1}(J^2 - 1 - 2\ln(J)) \qquad \text{eq. 3-2}$$

where, J=det(C) is the Jacobian, C is the right Cauchy-Green strain tensor, c_i are the material constants related to deviatoric response of the material, $\alpha_1 = J^{\frac{2}{3}}(C:I)$, where, I is the identity tensor, and $U(J)$ is the volumetric part of the strain energy (Holzapfel, 1996).

Considering the nearly incompressible property of the rubber material, the volumetric part ($U(J)$) is usually small, in which D_1 is the material constants related to volumetric response of the material and it can be considered as $D_1 = \frac{2}{K}$, where K is the Bulk modulus of the material. Consequently, the stress can be obtained by getting the derivative of the strain energy with respect to the strain tensor, as it is shown in the following equation:

$$S = \frac{2\partial\psi}{\partial C} \Longrightarrow S_{iso}^{\infty} = \frac{2\partial \sum_{i=1}^{3} c_{i0}(\alpha_1 - 3)^i}{\partial C},\ S_{vol} = \frac{2\partial U(J)}{\partial C} \qquad \text{eq. 3-3}$$

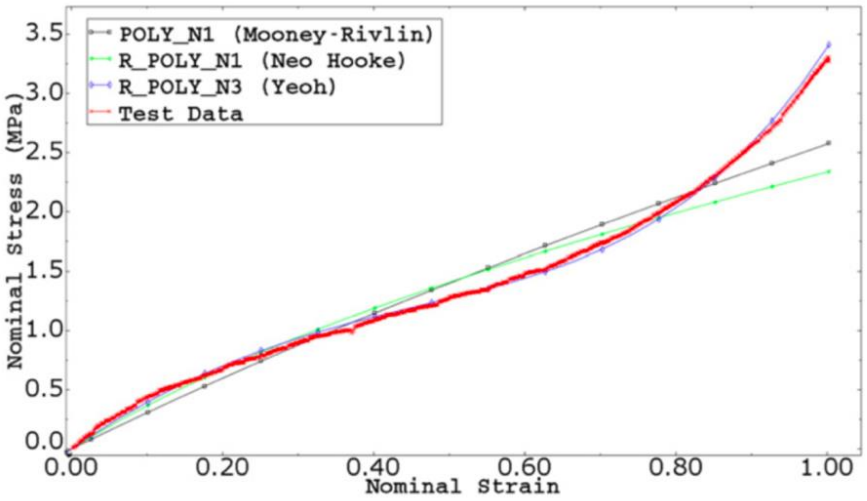

Figure 3-5. Yeoh model comparison to the test data (Wei and Olatunbosun, 2014)

The Yeoh constants (c_{1i} constants) used to define the hyperelastic material properties of the three rubbers are presented in Table 3-2.

Table 3-2. Yeoh constitutive model constants

	c_{10}	c_{20}	c_{30}
Tread	0.73	− 0.18	0.0796
Sidewall	0.71	− 0.28	0.13
Apex	1.28	-1.25	1.20

Viscoelastic material properties

For providing the viscoelastic material properties of the rubber, Wei and Olatunbosun (2016) used Prony series, a constitutive equation in the form of a series for determining the time-dependent stress-strain relationship of a linear viscoelastic material. Both Creep and relaxation test can be used for defining the viscoelastic properties of the material using Prony series. For obtaining the parameters required for the Prony series, Wei and Olatunbosun performed a stress relaxation test. The relaxation function was then represented in the form of the Prony series to fit the test data as follows:

$$G_R(t) = G_0(1 - \sum_1^N g_i(1 - e^{-t/\tau_i}) \qquad \text{eq. 3-4}$$

where g_i is the shear relaxation modulus ratio and τ_i is the relaxation time for each term of the series. In this study a two-term Prony series was used and the parameters obtained to fit this series to the test data (see Figure 3-6) are presented in Table 3-3. In addition to g_i and τ_i, the normalized bulk moduli (k_i) should be defined for each term as well. Due to the incompressibility of the rubber materials, the normalized bulk moduli (related to the initial bulk modulus and the total volumetric strain) are considered to be zero since the volumetric strain is assumed to be zero.

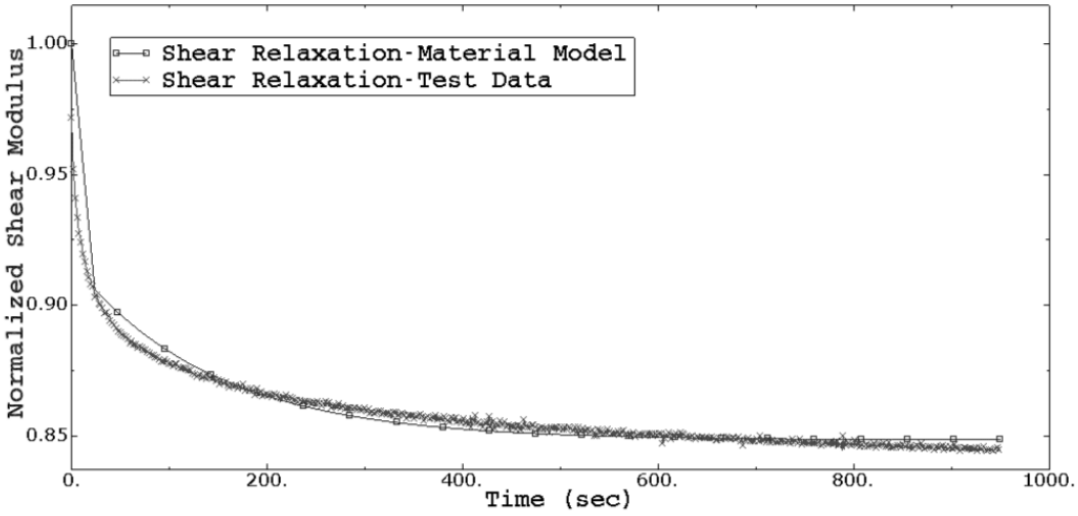

Figure 3-6. Prony series comparison to the test data (Wei et al, 2016)

Table 3-3. Prony series constants

	g_1	k_1	τ_1	g_2	k_2	τ_2
Tread	0.08	0	2.39 e-5	0.07	0	142.83
Sidewall	0.1	0	2.07 e-6	0.07	0	146.11
Apex	0.15	0	5.76	0.08	0	220.41

Effect of temperature on viscoelastic material properties

Viscoelastic materials are time and temperature dependent. In the previous section the Prony series was used for defining the time-dependent material properties of the three rubbers at the constant temperature of 23°C. Therefore, the effect of temperature is not considered. However, as the rolling velocity of the tire increases, the tire temperature rises. As a result, the response of the rubber material changes. Hence, in the following, the effect of temperature on rubber material properties is addressed and a method for implementation of this effect into the developed FE model of the tire is presented.

Rubber materials exhibit a glass transition state in which their material behavior changes from hard and glassy to viscous and rubbery. The temperature at which this transition occurs is called the glass transition temperature. At temperatures above glass transition, the material exhibits a more pronounced viscoelastic behavior, where material's modulus and damping change dramatically. At the glass transition temperature, the relaxation time of the material reaches its maximum, therefore the energy dissipation is highest (maximum $\tan(\delta) = {E_{loss}}/{E_{storage}}$). As the temperature rises, molecular frictions reduce and as a result the loss modulus decreases, and less energy is dissipated. As the rate of the molecular motion increases, the relaxation time is inversely affected and reduced.

Rubber materials can be considered thermorheologically simple; in which temperature is affecting all of the relaxation times in the same way. Therefore, it is possible to use the Time-Temperature

Superposition Principle (TTSP) (Leaderman, 1943; Schwarzl & Staverman, 1952). By applying the TTSP, master curves can be generated for including the effect of temperature and time on the material properties. Master curves are used for converting a series of creep and relaxation tests performed at different temperatures into one single curve by horizontally shifting the data with respect to a reference temperature (See Figure 3-7) (Roylance, 2001).

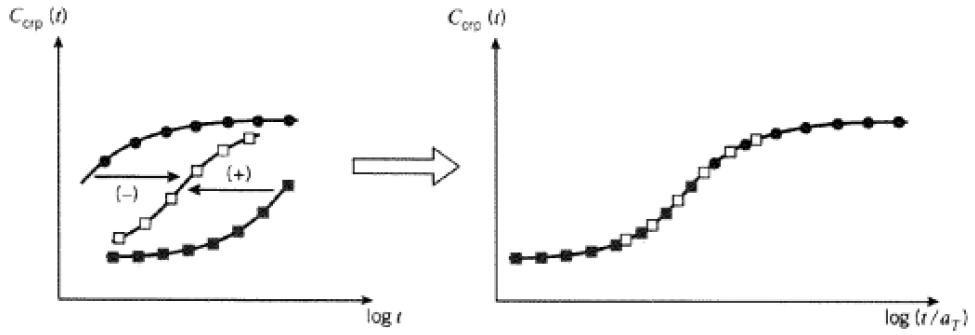

Figure 3-7. Master Curve (Roylance, 2001)

As it was mentioned before, as the temperature increases the relaxation time decreases. Therefore, the tests performed at higher temperatures than the reference temperature should be shifted to the left toward the lower times. The opposite holds for tests performed at lower temperatures (see Figure 3-7). Using a technique developed by Williams, Landel and Ferry (1955), for each curve and temperature, a shifting factor (a_T) can be defined for all of the relaxation times at that temperature. Every master curve is only valid at the corresponding reference temperature. However, having the data at different temperatures, the master curve can be obtained for different reference temperatures as long as the correct shift factor is used. The shift factor is defined as:

$$\log a_T = \frac{-C_1(T-T_{ref})}{C_2+(T-T_{ref})} \qquad \text{eq. 3-5}$$

where, C_1 and C_2 are characteristic material properties and T_{ref} is the reference temperature. If the glass temperature is considered as the reference temperature, the values of C_1 and C_2 can often be assumed as universal values for a wide range of polymers (Roylance, 2001), as:

$$C_1 = 17.4$$

$$C_2 = 51.6$$

In order to include the temperature effect on the modulus $G_R(t)$, defined previously, the relaxation times in the Prony series equation should be modified and multiplied by the shift factor (Corollaro et al., 2014, Pacheo et al. 2015).

$$\tau_{i,T}^G = a_T \tau_i^G \qquad \text{eq. 3-6}$$

Hence, the Prony series is converted to the following

$$G_R(t) = G_0(1 - \sum_1^N g_i^p(1 - e^{-t/a_T\tau_i^G}) \qquad \text{eq. 3-7}$$

In this study, the stress relaxation test was performed only at T=23 °C. Therefore, no additional information is present for obtaining the Master curve at different temperatures and the corresponding shift factors. Hence, for implication of the effect of temperature on the viscoelastic material properties with a good estimation, the glass transition temperature, the shift factors at

T=23 °C, the temperatures at the corresponding velocities (T_v), and the characteristic properties at T_{ref}=glass transition temperature ($C_1 = 17.4, C_2 = 51.6$) are considered as the basis for finding the relationship between the relaxation times, as follows:

$$\tau_{T=23^\circ} = a_{23}\tau_g \rightarrow \tau_g = \tau_{T=23^\circ}/a_{23}$$

$$\tau_{T_v} = a_{T_v}\tau_g \rightarrow \tau_{T_v} = \tau_{T=23^\circ} * (a_{T_v}/a_{23}) \qquad \text{eq. 3-8}$$

where $\tau_{T=23^\circ}$ are the relaxation times obtained from the stress relaxation test by Wei and Olatunbosun (2016); τ_g and τ_{T_v} are the relaxation times at the glass transition temperature and required temperatures corresponding to the rolling velocities, respectively.

In order to use this method for implementation of the effect of temperature into the Prony series, the glass transition temperatures for the rubber materials and the tire temperature at each velocity should be found. For an estimation of the glass transition temperature for the rubber materials, the data published by PerkinElmer, Inc is used [1]; in which the variation of the elastic modulus and tan (δ) by temperature are given for tire tread and sidewall materials (see Figure 3-8). tan (δ) is the ratio of the loss modulus to the storage modulus which is maximum at the glass transition temperature. Based on this data, temperatures of -30 °C and – 50 °C are chosen for tire tread and sidewall materials, respectively.

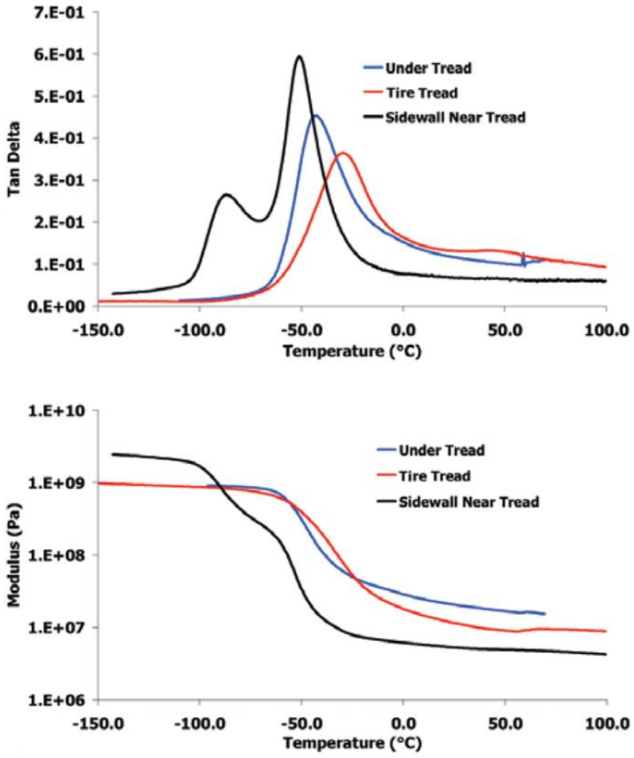

Figure 3-8. Glass transition of tire (by PerkinElmer, Inc)

[1] https://www.perkinelmer.com/lab-solutions/resources/docs/APP_007771B_15_Characterization_of_Car_Tire_Rubber.pdf

For finding the temperature of the rubber material at different velocities, the results from a study by Lin and Hwang (2004) are used; in which the relationship between the temperature and rolling velocity of the tires for inner and outer surfaces under different loads at 200kPa inflation pressure is given (Figure 3-9).

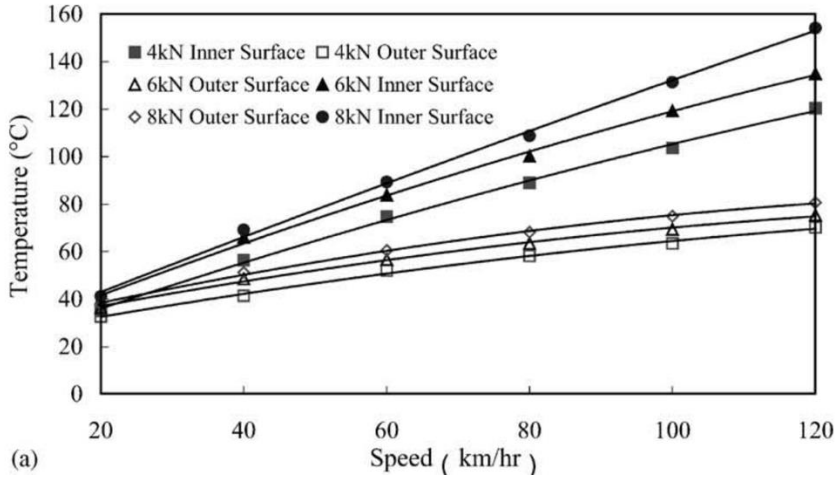

Figure 3-9. Variation of tire temperature with tire speed (Lin and Hwang, 2004)

Due to the geometry of the tire defined in this study, average temperature values of 74 °C and 60 °C are considered for the rubber materials at the speed of 80km/h and 55km/h, respectively.

Based on these considerations the Prony series constants presented in Table 3-3 are modified to the coefficients in Table 3-4.

Table 3-4. Prony series constants considering the effect of temperature

	g_1	k_1	τ_1	g_2	k_2	τ_2
Tread	0.08	0	2.95E-06	0.07	0	17.62
Sidewall	0.1	0	2.55E-07	0.07	0	18.02
Apex	0.15	0	7.10E-01	0.08	0	27.19

By decreasing the relaxation times, the response of the material is changed. Figure 3-10 shows the changes applied to the normalized tire tread shear modulus and shear compliance as a function of time for different temperatures. As it can be seen, by increasing the temperature the modulus of the material is decreased.

As it can be seen, the effect temperature on the modulus at very short relaxation time (in the first few seconds) is negligible. Moreover, after approximately 8 minutes the values of the modulus in both temperatures reach the infinite modulus. However, it should be noted that even if the effect of temperature itself may not be as important in a steady state analysis, it still affects the inflation pressure of the tire. Therefore, in addition to assessing the effect of temperature on energy dissipation, the effect of temperature on inflation pressure and the effect of inflation pressure on energy dissipation within the tire should be investigated as well.

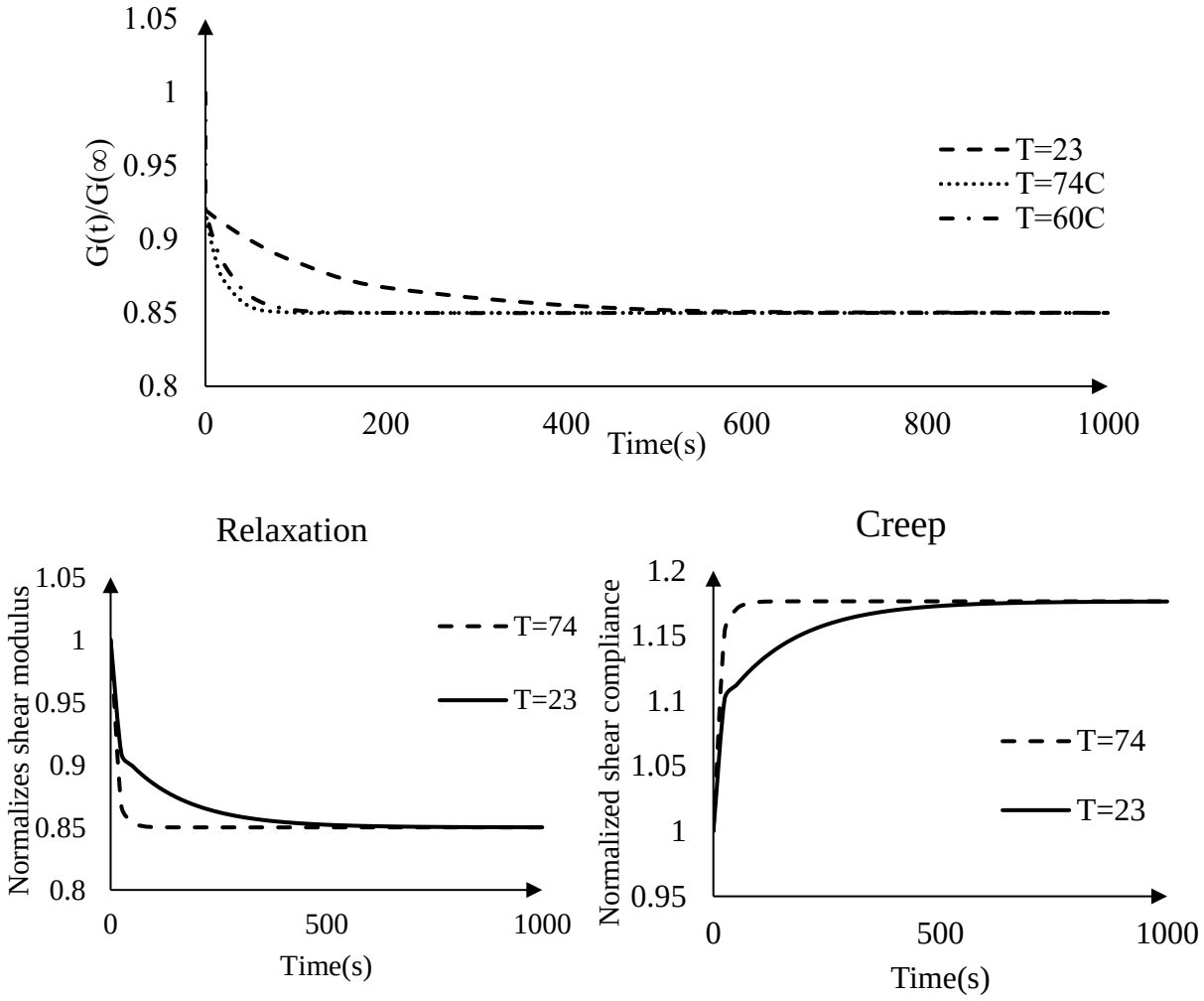

Figure 3-10. Effect of temperature on tire tread rubber material properties

Density

The density of all of the rubber material properties for tread, sidewall, and apex have been chosen to be 1100 kg/m^3.

Rayleigh damping

Rayleigh damping is a viscous damping used for imposing additional damping in modeling of material damping of a structure. It is usually used for matching the model's response to the experimental data, and it is defined as a linear combination of mass and stiffness of the material in the following form:

$$C = \alpha M + \beta K \qquad \text{eq. 3-9}$$

In which M and K are the mass and stiffness matrices of the material, respectively, and α and β are proportionality coefficients for mass and stiffness, respectively. The mass component of the Rayleigh damping adds additional damping to the rigid body motion. Therefore, usually it should be neglected for a structure that undergoes a large rigid body motion.

In finite element modeling, and specifically in transient analysis of dynamic impacts, Rayleigh damping can be used for imposing additional damping to the structure for the following two reasons: (i) to fit the results of the simulation to the experimental results and (ii) to control the numerical oscillations caused by the impact. The Rayleigh damping coefficients are not necessarily unique from one simulation to the other and different studies have assumed different values with large differences for these parameters (Haung et al. 2018).

In this study, the Rayleigh damping coefficients are defined in order to fit the response of the developed tire model to the experimental results from two studies by Wei and Olatunbosun (2016) and Boere (2009). Since the tires used in these two experiments are different from each other, the Rayleigh damping coefficients should be found each one of them separately. To find the appropriate coefficients a sensitivity analysis should be performed. For this purpose, the value of coefficients should be changed, and the rolling resistance force or coefficients should be compared with the experimental results from the given studies. Due to the large rigid body motion of the tire along the driving direction, the mass coefficient of α is not considered. Therefore, the stiffness coefficient β is changed to match the results to the test data. The results of the sensitivity analysis are presented in section 3.3.1.

3.2.2 Reinforcement material properties

There are 5 different layers of reinforcement considered in this tire model; A cap, two belts, carcass, and additional reinforcements (Figure 3-2). The reinforcements are generally defined as elastic materials. Two material properties are considered for modeling these 5 layers. The cap and belts are considered as steel material with elastic modulus of 172e9 Pa, Poisson ratio of 0.3, and density of 5900 kg/m^3, while the carcass and additional reinforcements are made of a softer material and have elastic modulus of 4.5e9 Pa, Poisson ratio of 0.3, and density of 1500 kg/m^3.

3.2.3 Rim

The tire rim is made of steel and it does not experience any deformation while traveling on the pavement surface profile. Therefore, in this study, the rim is considered as a rigid body with no deformation. No material properties definition is required for modeling the behavior of a rigid body part in ABAQUS. However, the density of the rim should be defined for considering the gravity force. Here, the density of the rim is considered as 7800 kg/m^3.

3.3 ANALYSIS TYPE

The analysis type affects the element type, contact definition and boundary conditions. Therefore, in this section a brief explanation of the analysis process is provided. This process will be discussed thoroughly in section 3.7.

For dynamic analysis of a full 3D tire in ABAQUS, the analysis can be divided into 6 different steps that follow each other and are based on the imported results from the previous step. Four of these steps are performed within ABAQUS standard (implicit analysis), while the last two steps are performed in ABAQUS explicit analysis mode. These steps are as follows:

i. 2D half tire model, which is a 2D model of half of the cross section of the tire.

ii. 3D half tire model, which is obtained by revolving the 2D cross section axisymmetrically.

iii. 3D full tire model, which is developed by mirroring the 3D half tire model from the previous step along the vertical plane.

iv. Steady state analysis of the tire, to reach the rolling velocity of the tire to the required velocity.

v. Transient analysis of the tire, to include the dynamic effect of the contact between the tire and pavement surface profile.

vi. Transient analysis of the tire with suspension (Quarter-car model), to capture the effect of longer wavelengths within the pavement surface profile (mega-texture and roughness).

3.4 MESH

For deciding about the mesh of any part in finite element modeling two factors are involved; the type of element that should be used and the mesh fineness. Here both of these factors are addressed.

Element type

iii. Rubber

Rubber material is considered as nearly incompressible. The incompressibility of the material and limitation on volume change, causes shear locking in the elements. Fully integrated elements with the ability to bend show this behavior when they are used for incompressible materials. For modeling such materials in ABAQUS standard, Hybrid elements are usually used. However, in this study, in addition to the four initial steps in ABAQUS standard for steady state analysis, the last two transient analysis steps are performed in ABAQUS explicit to capture the dynamic effects of the contact between the tire and the surface; subsequently, only the elements that are common between the two analysis types can be used. Since Hybrid elements are not available in ABAQUS explicit, reduced-integration solid elements should be used. These elements have one point less than the fully integrated elements in every direction; e.g. for a quadrilateral element with eight points, the reduced integrated version only has four points. Since the initial model is a 2D model that is revolved in axisymmetrically in the following steps, the elements should also be axisymmetric elements.

Hourglassing is also another issue that should be considered. It is defined as the distortion of the element in reduced integration elements when the strains at the integration point are all zero, which can lead to uncontrolled distortion of the mesh. ABAQUS has a built-in control on hourglassing which can be used for reduced integration elements. In addition, the mesh size should be kept small in case hourglassing occurs.

Therefore, for the rubber materials in this study 4-node bilinear, reduced integration axisymmetric element with hourglass control is chosen.

iv. Reinforcement

Reinforcements including the cap, belts, carcass and reinforcement layers are considered as 2-node linear axisymmetric surface element, that are embedded within the rubber materials as their host elements.

v. Rim

No deformation is allowed in the rim of the tire. Therefore, the rim is considered as a 2-node analytical rigid element for which no meshing is required.

Mesh Fineness

There are a few factors that can influence the number of required meshes or the minimum required mesh size in a model; the geometry of the part, boundary conditions, and the contact between that part and any other part or surface are among these factors. In this model, the contact is the main controlling factor for mesh size. When the tire is in contact with the road profile, the mesh size in rolling direction should be small enough to accurately capture the effect of the profile on the tire deformation and dissipated energy. Therefore, as the wavelength of the profile and the distance between the two points on the profile decreases (e.g., going from roughness to macro-texture), the mesh size should also decrease. Consequently, the mesh size within the tire cross section should also be reduced to keep a reasonable aspect ratio within the elements.

For this reason, a mesh sensitivity analysis is performed after verification of the tire model for determining the minimum radial mesh size for reasonably capturing the energy dissipation for the small wavelengths of the profile spectrum.

It is worth mentioning that the time increment and computational time are the limiting factors for the mesh size. While decreasing the mesh size as much as possible can be beneficial for taking the effect of the smallest wavelengths in the profile into account, it can increase the computational time dramatically. Therefore, a trade off needs to be considered between the two factors.

Considering all the above-mentioned factors, the final mesh of the tire in this study is shown in Figure 3-11.

3.5 CONTACT

The contact between the tire and pavement is defined as a penalty contact. This contact searches for node-into-face penetrations in the current configuration and is less stringent in enforcing the contact constraints. Therefore, it is suitable for modeling complex contacts. It also allows to define contact damping to reduce the noises in the solution and it uses a small amount of viscous contact damping to soften the contact.

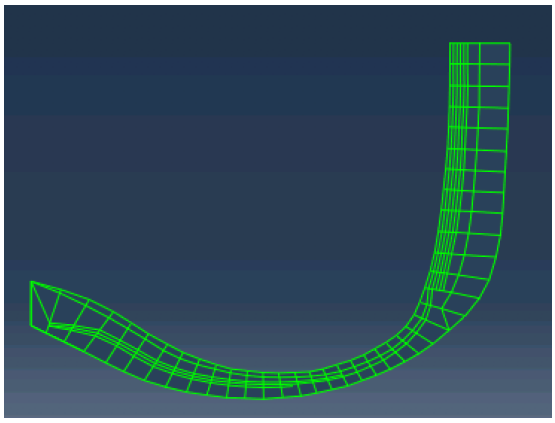

Figure 3-11. Final tire mesh

3.5.1 Friction coefficient

Friction exists between any two surfaces that are in contact with each other. Therefore, in modeling the contact between the tire and the pavement surface, a friction coefficient should be applied.

Since, the rolling resistance tests are performed in dry condition, the chosen friction coefficient should be a representative of such a contact. Several studies have been conducted for evaluating pavement friction coefficient; however, most of them are related to wet condition, where friction is critical. A few studies measured friction on dry surfaces. Horne and Leland, (1962), presented an average value between 0.7 to 0.8 for friction coefficient on dry surfaces (see Figure 3-12).

In two other studies by Oberg (1994) and Wallman (1995), that were conducted to investigate the reaction of drivers to road's friction in summer condition, a friction coefficient of 0.8 was reported.

Moreover, Do et al. (2013) also reported a friction coefficient between 0.8 and 1 for dry condition (see Table 3-5).

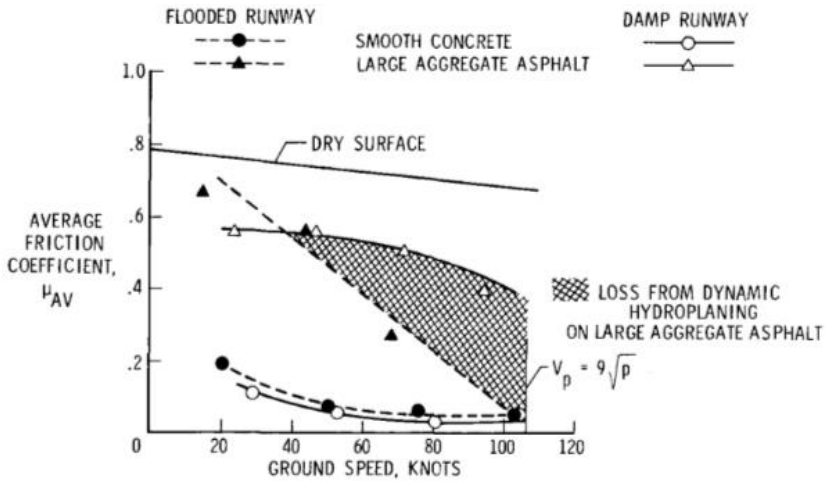

Figure 3-12. Friction coefficient on dry surfaces (Horne and Leland, 1962)

Table 3-5. Friction coefficient values for different surfaces (Do et al, 2013)

Surface type	Friction coefficient
Dry bare surface	0.8-1.0
Wet, bare surface	0.7-0.8
Parked snow	0.2-0.3
Loose snow/ slush	0.2-0.5
Black ice	0.15-0.3
Loose snow on black ice	0.15-0.25
Wet black ice	0.05-0.10

Based on these studies a friction coefficient of 0.8 is considered for the contact in dry condition.

3.6 BOUNDARY CONDITIONS

Here only the general boundary conditions are mentioned. Individual boundary conditions for each step are discussed separately in their subsections.

3.6.1 Inflation pressure

The air inside the tire does not carry any load. However, the resulting pressure from it applies tension to the tire walls. This inflation pressure has an effect on the deformation of the tire (see

Figure 3-13). In an under inflated tire, the shoulder is in contact with the road, while in the over inflated one there is a lot of pressure on the inner side of the tire. These changes in inflation pressure, besides having an effect on tire wear (shoulder wear and inner side wear), can affect the contact patch length and as a result the rolling resistance of the tire. As the inflation pressure increases, the contact patch and the deformation of the tire decreases. Correspondingly, the rolling resistance decreases. In contrary, when the pressure decreases, bending and shearing occur in the tire sidewall and tread which results in more energy dissipation (Redrouthu & Das, 2014). Figure 3-14 depicts the influence of inflation pressure on rolling resistance on different surfaces.

Under inflated Over inflated Properly inflated

Figure 3-13. Effect of inflation pressure on tire deformation[2]

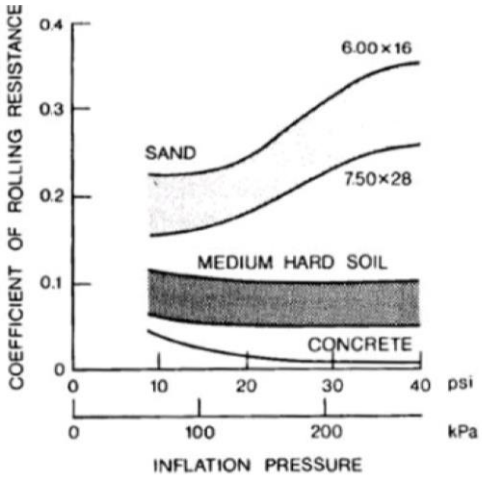

Figure 3-14. Effect of tire inflation pressure on rolling resistance on different surfaces (Wong, 2008)

[2] https://info.duraturntires.com/blog/over-inflated-tires-are-a-problem

It is apparent that the tire rolling resistance decreases on concrete roads by increasing the tire inflation pressure. It is worth mentioning that in calculation of rolling resistance on deformable surfaces, the energy loss in the pavement layers and subgrade soil is also considered, and therefore, an increase in the rolling resistance can be seen.

A recommended range for the tire pressure of a passenger car is between 200-240 kPa (30-35 psi). This inflation pressure changes by temperature (increases at high temperatures and decreases at low temperatures). As a result, in summer it is recommended to lower the inflation pressure while in winter the pressure should be adjusted to a higher value, to keep the tire in a reasonable shape.

As the speed of rolling changes, the temperature of the tire also changes. Correspondingly, the inflation pressure changes. Rao et al (2006), attributed the inflation pressure of 240 kPa to 80km/h while considering 210 and 180 kPa for 60 and 40 km/h, respectively; considering a linear relationship between velocity and inflation pressure. However, in a study by Michelin an inflation pressure of 210 kPa is considered for 80km/h velocity. Redrouthu & Das (2014) also considered 210 kPa inflation pressure for their simulations. Most of these inflation pressures are in the range of recommended pressures for the tires, and it may not be possible to find an absolute value for the inflation pressure at a specific velocity. It is suggested that the tire stiffness changes dramatically with tire pressure; therefore, any assumption about the tire inflation should be done carefully (Calrson and Gerdes, 2002). Since it is assumed that the rolling resistance should not change dramatically with speeds below 80km/h, the changes in the inflation pressure should not either. Therefore, for considering different values for inflation pressure for different velocities, it is assumed that the tire inflation pressure is at the bottom of the recommended range in the stationary condition (200 kPa). For 80km/h, the inflation pressure suggested by Michelin and Redrouthu & Das (2014) is used (210 kPa). A linear relationship between the velocity and inflation pressure is considered between 200 kPa and 210 kPa, similar to Rao et al (2006). As a result, the inflation pressure for 55km/h is considered as approximately 207 kPa.

In this study, for investigation of the effect of surface profile on rolling resistance the inflation pressure has been set to 200 kPa. However, the effect of inflation pressure on rolling resistance is investigated for pressure values of 200, 210 and 240 kPa.

For applying the inflation pressure to the tire, a uniform pressure should be applied to the inner surface of the 2D half tire model, in the first step. This pressure should be kept constant in the following steps.

3.6.2 Vertical load

The vertical load is applied gradually after formation of the half 3D tire model. After developing the full 3D tire model in the third step of the analysis, the vertical load should be equal to a quarter of the vehicle weight. In the steps before addition of the suspension the vertical load is applied to the wheel.

Any boundary condition that should be applied to the wheel is applied through the rim of the tire. The rim of the tire is a rigid part defined along with a reference point. All of the nodes on the rim element follow the reference point displacement. Therefore, if a boundary condition is applied to this point, it is transferred to the rest of the nodes in the rim. For example, any longitudinal or vertical displacement of the reference point causes the same displacement in all of the nodes of the rim. In this study the centroid of the rim is considered as the reference point. As a result, for

applying the vertical load to the wheel, a concentrated load should be applied to the centroid of the rim.

In the presence of the suspension, the vertical load is divided into two parts: (i) a mass that is applied on top of the suspension, as the sprung mass, which is equal to the load of the vehicle; and (ii) a concentrated load that is applied to the centroid of the rim, as the unsprung mass, which is equal to the axle load. It is worth mentioning that since the gravity is applied to the whole model the tire mass should be deducted from the axle load.

In this study, as it was mentioned before, the model is compared with different studies. In each one of these comparisons, the characteristics of the model are changed to fit the corresponding study. Therefore, the values of the vertical load have been changed accordingly. The vertical load in the verification phase is equal to 3,000N applied on the rim to match Wei et al, 2016. For comparison of the model's results to Boere study (2009), a vertical load of 4,100N, which corresponds to a mass of 417 kg, is used. For final comparison of the relative effect of different spectrums of surface profile with each other, and to simulate a quarter-car model thoroughly, the model is set to be based on the quarter-car model from Dixon (2008). In such a model, as it can be seen in Figure 3-15, two masses are required (sprung and unsprung masses). To fully model this quarter-car model, the sprung mass is selected as 300kg, similar to the Dixon (2008) study. For the unsprung mass, the weight of the FE tire and axle are separated.

Model parameters		
Name	Unit	Value
m_s	Kg	300
m_u	Kg	50
k_s	KN/m	28
k_t	KN/m	200
c_t	KNs/m	0.1

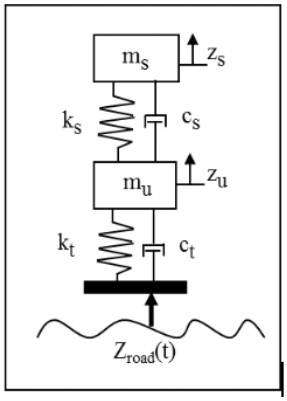

Figure 3-15. Quarter car model (Dixon, 2008)

It is not easy to calculate the tire model's weight based on the densities defined, due to the geometrical complexity of the model. Therefore, for measuring the weight of the tire an additional model is generated. In this model after applying the vertical load, a step is defined for applying the gravity to the tire. The difference between the vertical reaction of the road in the two steps is the actual weight of the tire model. Figure 3-16 depicts this difference. The difference in the vertical reaction is 135 N which corresponds to 13.85 kg.

Therefore, from the 50 kg unsprung mass mentioned in Figure 3-15, 13.85 kg corresponds to the tire weight and is included by applying gravity in that step. The remaining 36.15 kg is considered as the axle load and is applied as a concentrated load on the tire rim centroid. In this stage, the total vertical load applied on the tire (including both sprung and unspring masses) is equal to 3432.6 N.

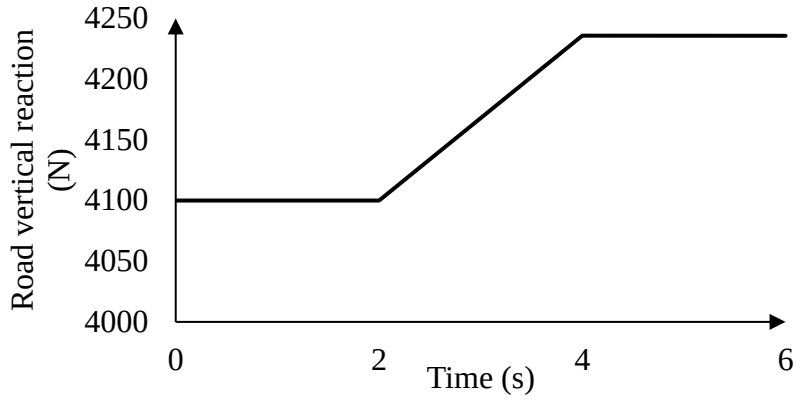

Figure 3-16. Weight of the FE tire model

3.6.3 Velocity

For rolling a tire at a constant velocity, both horizontal and angular velocities should be applied to the tire rim centroid to be transferred to the tire nodes. The horizontal velocity is equal to the named velocity in m/s, e.g. for 80km/h speed, the horizontal velocity is equal to 22.224 m/s.

In this study braking and traction modes are not of interest; hence, the tire is set to roll in free rolling condition. Free rolling angular velocity corresponds to a velocity in which there is no horizontal force applied to the tire rim centroid to maintain that velocity. To find this velocity, in step IV (steady state analysis of the tire) the velocity that corresponds to zero horizontal force or resistant moment is selected. Figure 3-17 shows a sample of variation of longitudinal force by changes in angular velocity.

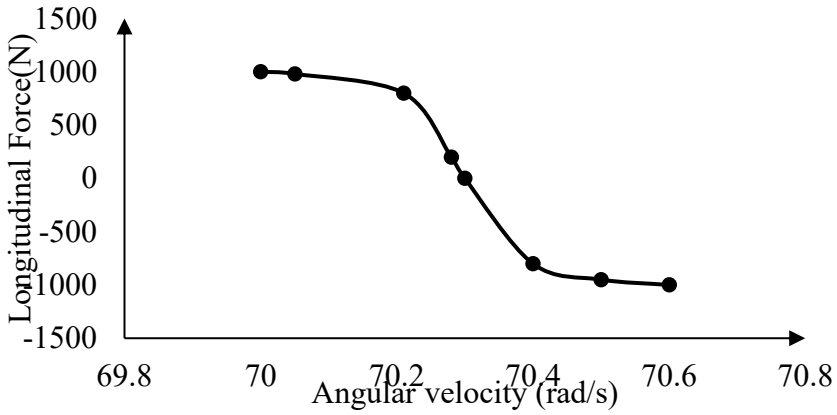

Figure 3-17. Variation of longitudinal force by angular velocity in steady state analysis

The angular velocity changes by the radius of the tire; therefore, the free rolling velocity should be calculated again when the tire dimension is changed from 235/60 R18 tire to a 225/60 SR16 tire.

3.7 STEPS

As it was mentioned in section 3.3, the analysis includes six steps. The last increment in each step is the initial point for the next step. Different models are developed for each step, due to the

difference in analysis type or computational time restrictions. The first four models are performed in ABAQUS standard and in static or steady state analysis. Therefore, they do not include the time dependency of the rubber material properties. To include the viscoelastic response of the rubber and the energy loss due to the contact between the tire and the pavement, transient analysis should be run. The last two steps are transient analysis in ABAQUS explicit. These steps are discussed in the following subsections.

3.7.1 2D half tire model

The first step in tire modeling is a 2D model of the tire. The geometry of the tire, cross section mesh, material properties, damping, and inflation pressure are defined in this step. Since the tire is symmetric around the vertical line that passes through the tire axle, only half of a tire section with axisymmetric elements can be sufficient for modeling the tire (see

Figure 3-18). Inflation pressure on the inner surface of the tire is the only load that is applied in this step. After loading the model, a circumferential deformation is generated due to the anisotropic nature of the tire construction. Consequently, a fully three-dimensional stress field is developed.

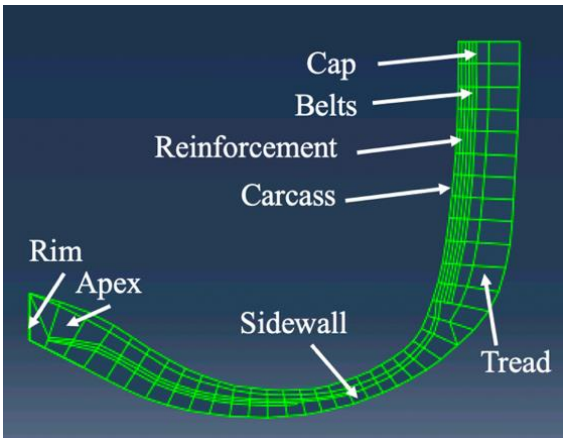

Figure 3-18. Generated 2D tire model

3.7.2 3D half tire model

In this step, a 3D model is generated by revolving the deformed axisymmetric cross-section imported from the 2D model, around the axis of revolution. The revolving command cannot be performed in the graphical version of ABAQUS, and it has to be written in command version. So, the whole modeling process should be performed in ABAQUS command. A smooth pavement surface is generated as an analytical rigid surface, and the contact between the tire and the surface is defined in this step. A vertical load is applied to the tire rim centroid to initiate the contact between the tire and the surface.

To base the initial state of this model on the previous one, the axisymmetric solution from the 2D model should be transferred to the new mesh. Since in this step only half of the tire is modeled, the skew-symmetric boundary conditions must be applied along the mid-plane of the cross-section to account for antisymmetric stresses that result from the inflation loading and the concentrated load on the axle (ABAQUS manual).

In this step the number of meshes in the driving direction is defined. Since the tire has to roll over the pavement profile the mesh discretization should be the same for every point of the circumference (see Figure 3-19). To capture the effect of the pavement surface profile a sensitivity

analysis should be performed for different scales of surface profile. This sensitivity analysis will be done in section 3.3, for both smooth and textured surfaces.

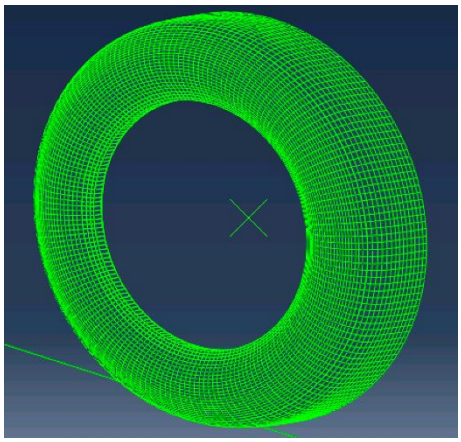

Figure 3-19. Generated 3D half tire model

3.7.3 Full 3D tire model

The solution from the half 3D tire model should be imported to the full 3D model as an initial point. The full tire model can be generated by mirroring the half tire around the vertical plane (see Figure 3-20). The vertical load is applied to the rim centroid to reach the final vertical load for the analysis.

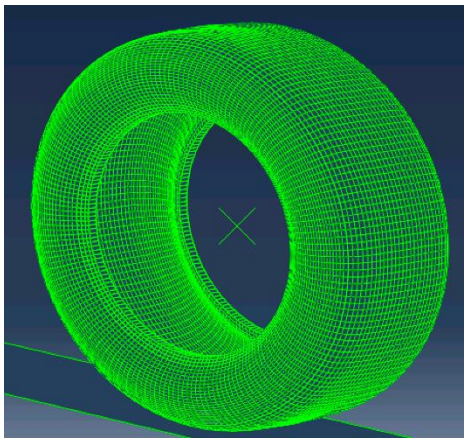

Figure 3-20. Full 3D tire model

3.7.4 Steady state analysis of the tire

Any changes to the model should be applied gradually so that the model stays in steady condition. So far, the tire inflation pressure and vertical loading are applied in the previous steps and the deformed tire under the vertical load is the initial state for this step. However, the tire is still stationary.

For the tire to reach a velocity such as 80km/h (22.224 m/s) in a steady condition, the tire should roll for a long time in a moving frame analysis. Therefore, it is very beneficial to use fixed frame analysis instead of a moving one. In ABAQUS such analysis exists for rolling objects, called as steady state analysis. In this analysis, the mesh is kept stationary while the material rotates within

the mesh. In this step, longitudinal and angular velocities should be applied to the tire rim centroid. As it was mentioned before in section 3.6.3, the free rolling angular velocity should be defined for the tire not to be in braking or traction modes and prevent the tire from slipping over the surface. This velocity will be applied as the initial velocity in the following steps.

3.7.5 Transient analysis of the tire

The steady state analysis is a stationary model in which the tire is not actually rolling. To capture the effect of pavement profile on the tire deformation and rolling resistance, the tire should be rolling over the surface. Moreover, the effect of the viscoelastic material properties is only considered in transient analysis. Therefore, a transient analysis should be performed, using the steady state analysis results as the initial point. The transient analysis is available in ABAQUS explicit. Therefore, the finial state from the previous step should be imported to the new model. Here only the deformed mesh can be imported from the previous model and the contact, boundary condition, imbedded reinforcements, and pavement surface should be defined again. Since the model is changing from steady state to transient mode, adequate time should be allocated so that the model could get to a steady response rolling over the smooth surface. After reaching a steady state mode, another model is generated to roll the tire over the pavement profile, using the steady response of the transient analysis as the initial state. The surface profile causes deformation in the tire and resisting forces which leads to energy loss in the tire.

As the profile length increases, depending on the details of the profile, the computational time required for the analysis can be increased dramatically. Therefore, to reduce the computational cost, the model can be divided into a few models having shorter spans of the pavement profile.

3.7.6 Transient analysis of the tire with suspension (Quarter-car model)

The previous step, having no suspension in the model, and applying the vertical load on the tire rim centroid, is not very similar to the vehicle system in reality. In addition, the tire model alone, can only capture the effect of pavement macro-texture and a portion of mega-texture which is within the contact patch of the tire. The effect of any texture beyond the contact patch cannot be captured thoroughly by the tire model. To have a more accurate and realistic model for investigation of the effect of roughness and full range of the mega-texture, the suspension of the tire should also be included in the analysis. A portion of the vertical load which is related to the weight of the vehicle should be moved to the top of the suspension, while the axle load should be applied at the rim centroid. The suspension of the vehicle can be modeled by a combination of a spring and a dashpot to build a Quarter-car model. A schematic view of a tire with suspension is shown in Figure 3-21. The suspension should move along with tire in longitudinal direction, while being able to move freely in vertical direction. This vertical movement due to the contact between the profile and the tire, causes energy loss in the suspension.

The stiffness of the spring and the damping in the dashpot are chosen from common values found empirically by Dixon (2008) as 28 KN/m and 2000 Ns/m, respectively (see Figure 3-15).

3.1 PAVEMENT SURFACE GENERATION

The pavement profile in this study is only considered along the longitudinal direction and is uniform in the transverse direction. For generation of the pavement profile, straight lines are used between consecutive profile points. The pavement surface is considered as a rigid surface, and the

deformation of the pavement under the tire load is neglected. A sample of the generated profile underneath the tire model is shown in Figure 3-22.

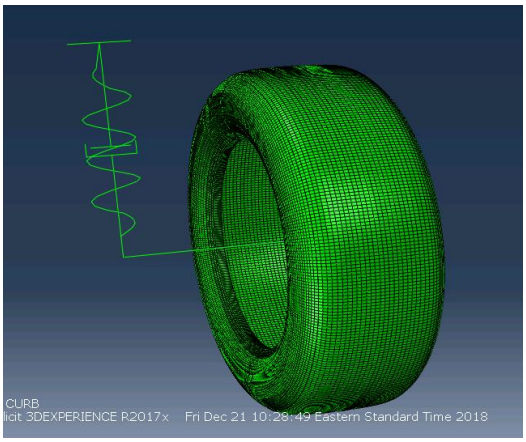

Figure 3-21. Schematic view of FE Quarter-car model

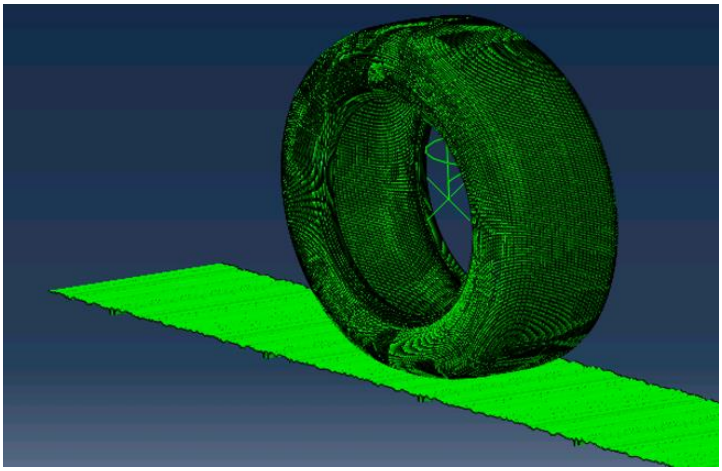

Figure 3-22. Tire model rolling on a textured surface

3.2 VERIFICATION OF THE TIRE MODEL

The first step after developing the tire model is its validation. For this purpose, it is beneficial to compare the model with an experiment with a controlled test set up. As it was mentioned before, the material properties in this study are borrowed from a study by Wei and Olatunbosun (2016). In their study, they also provided the test results for a controlled experiment, rolling a tire over a drum with a large diameter of 2.44 m to represent a flat road (with less than 0.1% error in contact patch length, comparing to a flat road), as it can be seen in Figure 3-23. In the test setup, the tire is fixed, and the drum is rotating. A step obstacle is built on the drum, and the longitudinal and radial forces at the center of the tire are measured. The tire inflation pressure is 200KPa and the vertical load applied on the tire is 3000N.

For simulating this experiment, instead of the drum rolling, the tire is rolling over the surface (see Figure 3-24). Similar to the test, the vertical degree of freedom for the rim reference point

(centroid) is fixed in the transient step, after deforming the tire under the vertical load in the steady state analysis. The suspension is not included in this part. The friction coefficient is set to 1.

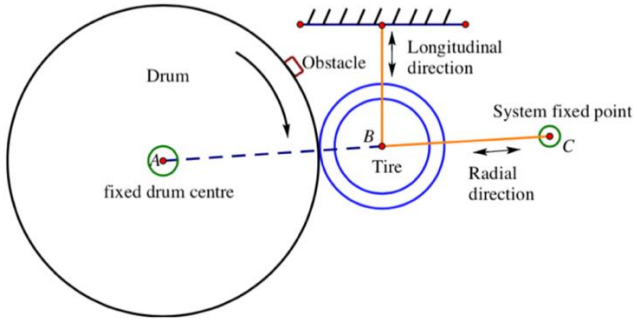

Figure 3-23. Schematic test setup for transient rolling of tire over an obstacle (Wei and Olatunbosun, 2016)

The tire is rolling with free rolling velocity with velocities of 10km/h, 20km/h and 30km/h over an obstacle with dimension of 25mm width and 20mm height (see Figure 3-24). The longitudinal forces are then compared with the measurements from Wei and Olatunbosun (2016). The comparisons of the results are depicted in Figures Figure 3-25, Figure 3-26,and Figure 3-27.

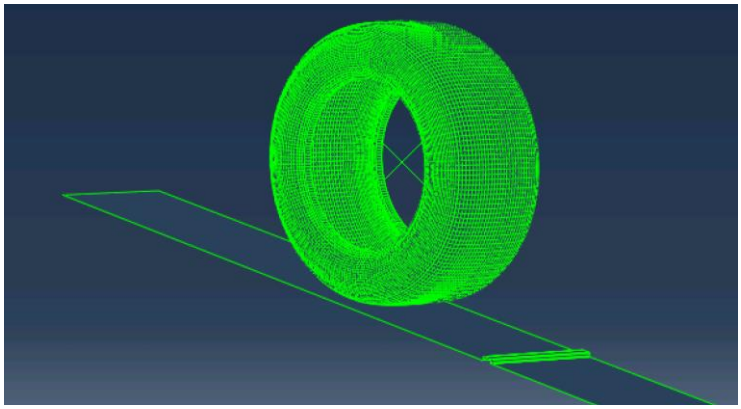

Figure 3-24. FE tire model rolling over a step

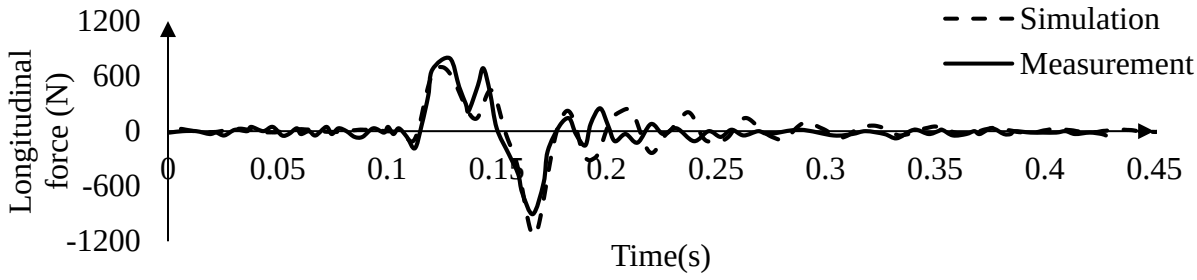

Figure 3-25. Comparison of the FE model with experimental measurements of Wei and Olatunbosun (2016), at velocity of 10km/h

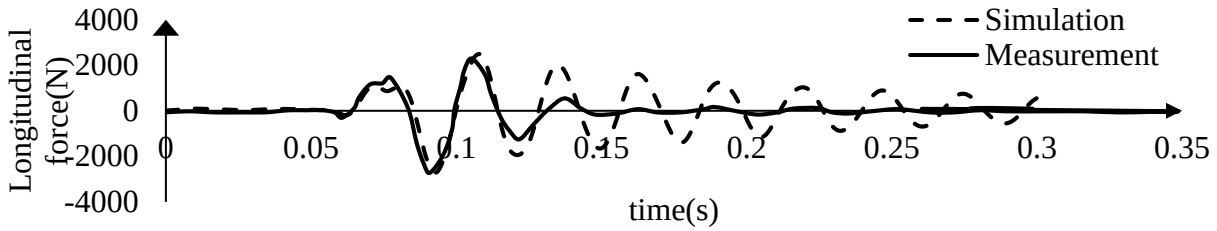

Figure 3-26. Comparison of the FE model with experimental measurements of Wei and Olatunbosun (2016), at velocity of 20km/h

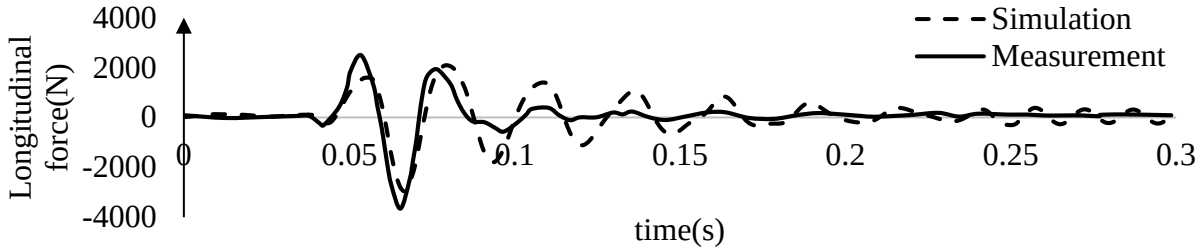

Figure 3-27. Comparison of the FE model with experimental measurements of Wei and Olatunbosun (2016), at velocity of 30km/h

As the results show, the FE model captures the effect of the impact with the step well and the longitudinal forces from the FE model match the measurements. Therefore, the FE model is verified.

3.3 TRANSFORMING THE TIRE TO BOERE'S EXPERIMENTAL TIRE

After validation of the model, the tire model is converted to a 225/60 SR16 tire as explained in section 3.1. For this purpose, the size of the tire is changed to the new tire, keeping a similar structure to the previous tire. In addition to the size of the tire, the vertical load on the tire is changed to 4100N to match Boere's study. The tire is free to move in vertical and longitudinal directions. The velocity is changed to 80km/h and the corresponding free rolling angular velocity is obtained. The friction coefficient is set to dry pavement coefficient of 0.8, as it was explained in section 3.5. In Boere's study, the pavement profile includes only macro-texture. As it was mentioned in section 3.4, the mesh size of the tire depends on the pavement profile texture. Therefore, mesh sensitivity analysis should be performed to choose the mesh size resulting in accurate results. Although the tire size is the same as that of Boere's experiment, the details of the two tires can be very different. Since there are no information provided by Boere about the tire detail, to match the models with the measurements, Rayleigh damping can be used for this purpose. To find the corresponding Rayleigh damping a sensitivity analysis should also be done.

3.3.1 Rayleigh damping sensitivity analysis

Rayleigh damping is a numerical damping applied to the material properties to match the model to the experimental results (as it was explained in section 3.2.1). There are two sets of results available in this study;

(i) The longitudinal reaction at the rim centroid of the tire rolling over a step, for verification of the initial developed tire model with the size of 235/60 R18, from Wei and Olatunbosun (2016).

(ii) The rolling resistance coefficient resulting from a 225/60 SR16 tire rolling on surfaces with different textures, from Boere (2009).

As mentioned before, there is no information available on the structure of the test tire in Boere study, and the only available data is the size of the tire. Therefore, first the Rayleigh damping coefficients are found by performing a sensitivity analysis on the 235/60 R18 tire rolling over a step and comparing the results with Wei and Olatunbosun study. Thereafter the model size is changed to the 225/60 SR16 and the sensitivity analysis is performed again to match the results of the new tire model to the Boere experimental data. Since the purpose of the study is the evaluation of the effect of texture on rolling resistance, to avoid any effect on the final results, the smooth surface is chosen for selection of Rayleigh damping coefficients.

Sensitivity analysis for 235/60 R18 tire

As it was explained before, due to the rigid body motion of the tire, the mass coefficient of α is neglected and β coefficient is changed for all three rubber material properties to match the experimental results. Figure 3-28 Shows the results of the sensitivity analysis for β coefficients changing from 0 to 6e-4.

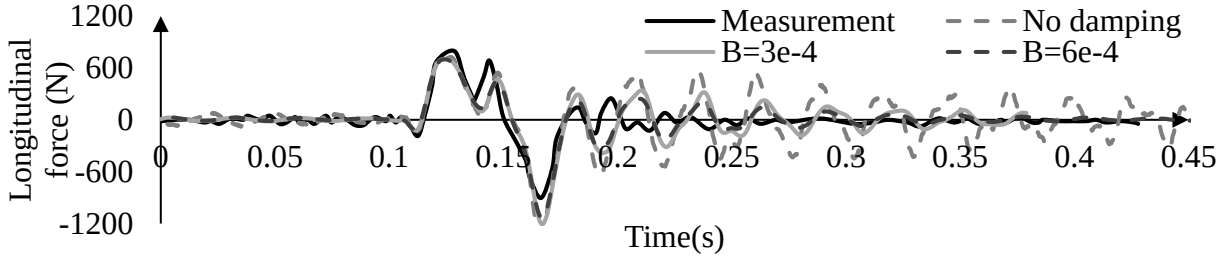

Figure 3-28. Variation of tire longitudinal force rolling over a 10mm *25mm step with 10km/h speed for different Rayleigh damping coefficients

As it can be seen, the additional damping does not affect the maximum force caused by the impact significantly, but as the Rayleigh damping increases the oscillations after the impact decreases.

It is worth mentioning that as the Rayleigh damping coefficient increases, the model computational time also increases. Therefore, since the variation of the results between β of 3e-4 and 6e-4 are not very significant, β= 3e-4 is chosen as the final Rayleigh damping coefficient for this part of the analysis.

Sensitivity analysis for 225/60 SR16 tire

After changing the tire size and rolling conditions, the tire is rolled over a smooth surface with speed of 80km/h, the average rolling resistance force after reaching the steady state condition is compared with the experimental results from Boere, 2009. In his study, the corresponding rolling resistance coefficient for the tire rolling at RMS=0 is 0.0087. The rolling resistance coefficient is defined as the ratio between the rolling resistance force and normal force applied to the tire. Having a normal load of 4100kN on the tire the average rolling resistance force should be about 35.7 N. In the initial model, β= 3e-4 is considered as matching the final value from the previous part.

Thereafter, the value of β is varied between 2e-4 and 6e-4 to investigate its effect on the final results. Figure 3-29 shows the variation of the rolling resistance force along the driving direction by changes in rubber Rayleigh damping.

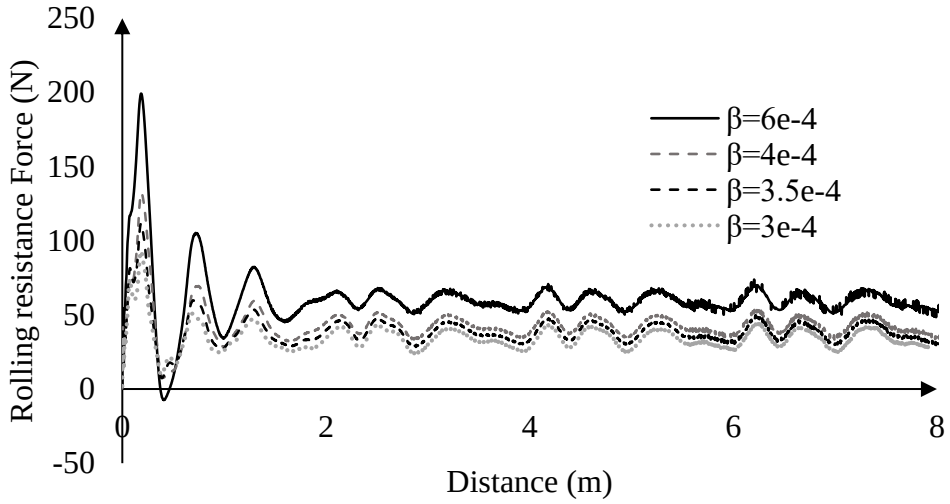

Figure 3-29.Variation of tire rolling resistance force rolling over a smooth surface with 80km/h speed for different Rayleigh damping coefficients

For better understanding the effect of β on rolling resistance force, their relationship is depicted in Figure 3-30, for tire models with 180 and 540 radial sections.

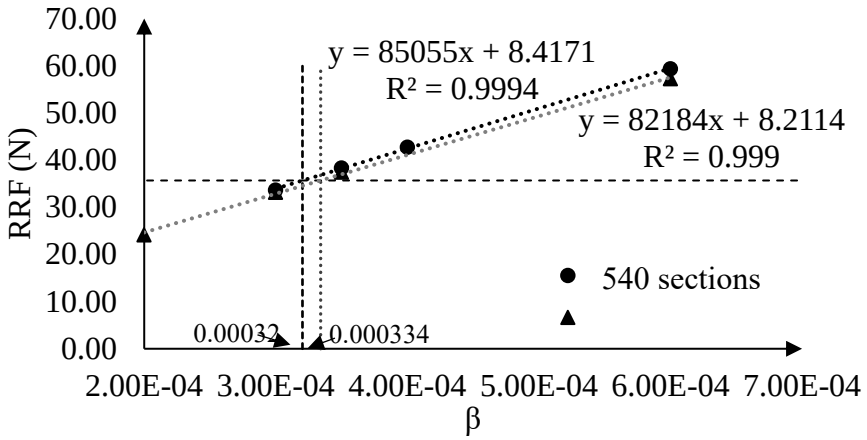

Figure 3-30. Relationship between the tire rolling resistance force and β rolling over a smooth surface with 80km/h speed

As it can be seen, there is a linear relationship between β and the rolling resistance coefficient. Therefore, the equivalent β value corresponding to a rolling resistance force of 35.7 N can be calculated using regression. As a result, the final value of β=3.2 e-4 is chosen for the tire model.

3.3.2 Mesh sensitivity analysis

The mesh sensitivity analysis is performed on both smooth and textured surfaces. For this purpose, different numbers of radial sections have been considered, from 90 sections to 540 radial sections

(see Figure 3-31). The largest element size is for the 90 sections (2.2 cm) and the smallest one is for 540 sections (3.7 mm). The macro-texture wavelength range is from 0.5mm to 5cm, and that for the mega-texture is between 5cm and 50cm. Due to the limited computational time allowed (even by using 32 parallel cores), smaller mesh than 3.7 mm is not feasible. The minimum distance between the pavement points used in this study is considered as 1mm for macro-texture and 7.5cm for mega-texture and roughness. Going from the largest mesh size to the smallest, the mesh analysis shows (i) how much the pavement texture is going to affect the final rolling resistance and (ii) how much error is caused by excluding the wavelengths smaller than the mesh size. Since the distance between the pavement nodes is different for macro- and mega-texture, the mesh size for the corresponding models does not need to be the same necessarily. To decrease the computational time, the sensitivity analysis is performed for both macro- and mega-textures to investigate the possibility of using a larger mesh size for mega-texture and roughness surfaces.

Rolling resistance force and coefficient are used for comparing the results of different models. Rolling resistance force (RRF) is usually defined as the longitudinal force applied to the tire rim centroid for overcoming the energy dissipation in the tire. Correspondingly, the rolling resistance coefficient (RRC) is defined as the ratio between the average rolling resistance force and normal force applied on the rim centroid.

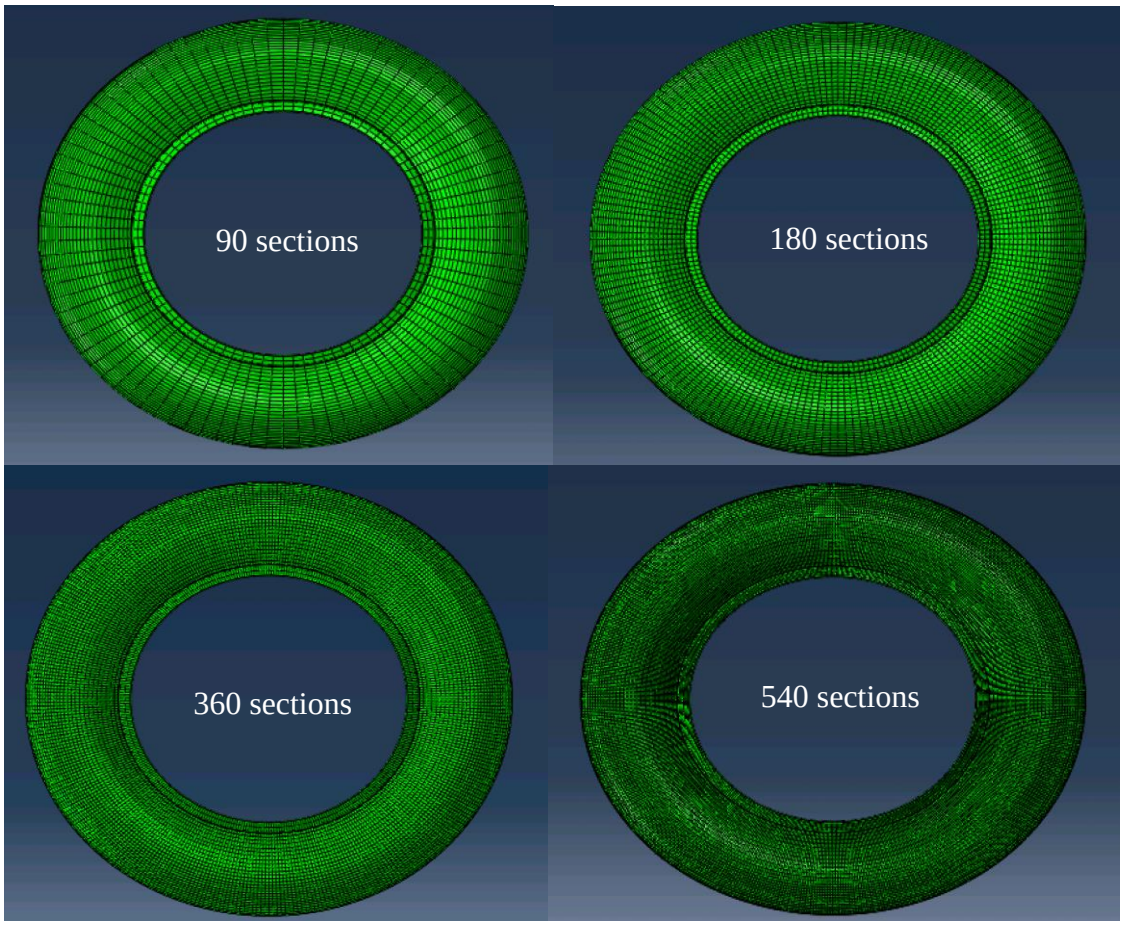

Figure 3-31. Different number of radial sections used in the mesh sensitivity analysis

Figure 3-32 and Figure 3-33 show the variation of rolling resistance force (longitudinal force at the rim centroid) over time on smooth and textured (including macro-texture only) surfaces,

respectively. As it can be seen, while the average of the rolling resistance force is similar for different mesh sizes, the oscillations are decreased. Therefore, the rolling resistance is calculated more accurately.

This can also be observed in Figure 3-34 and Figure 3-35, where the variation of rolling resistance coefficient with the number of radial sections (in other words, mesh size) is depicted. As it can be seen RRC variation by number of radial sections on a smooth surface is about 5% between 90 and 540 radial sections, while this difference is much more evident for textured surface (more than 20% difference between 90 and 540 radial sections). It should also be noted that the difference between 360 and 540 number of sections is small, and the results tend toward a plateau value. This is an indication that the effect of the wavelength less than 3.7 mm is small. As a result, for the effect of macro-texture, the number of sections is chosen as 540, for achieving a more accurate result.

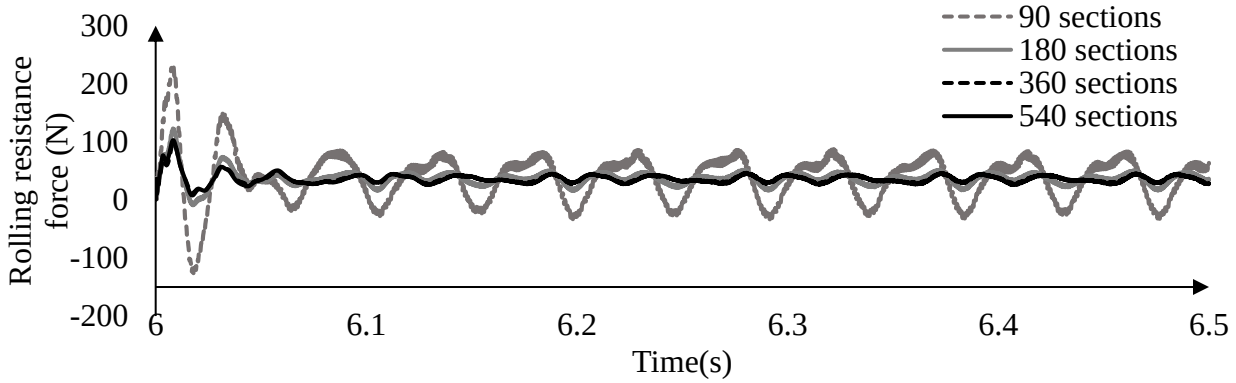

Figure 3-32. Variation of tire rolling resistance force rolling over a smooth surface with 80km/h speed for different number of radial sections

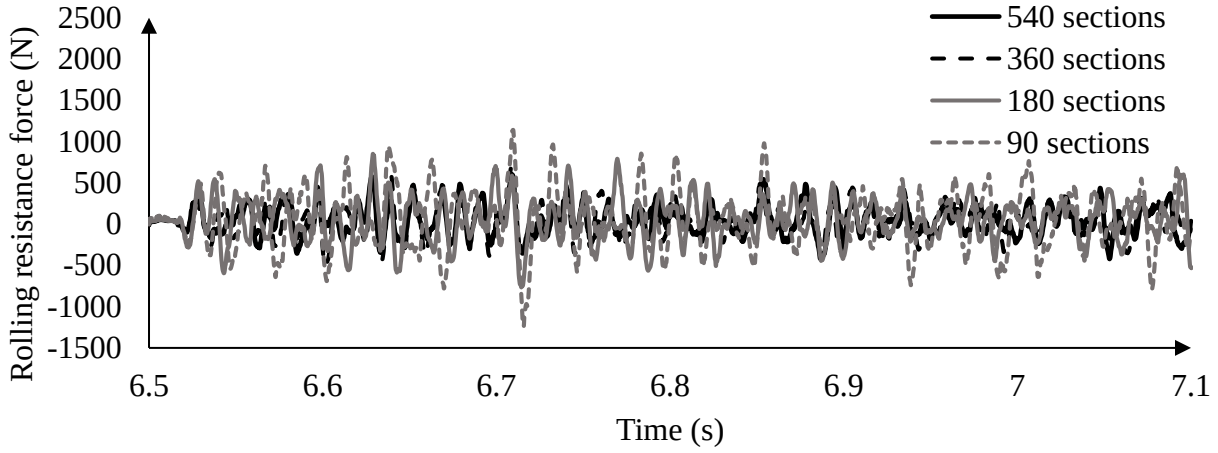

Figure 3-33. Variation of tire rolling resistance force rolling over a textured surface with macro-texture with RMS of 1.68 mm and speed of 80km/h for different numbers of radial sections

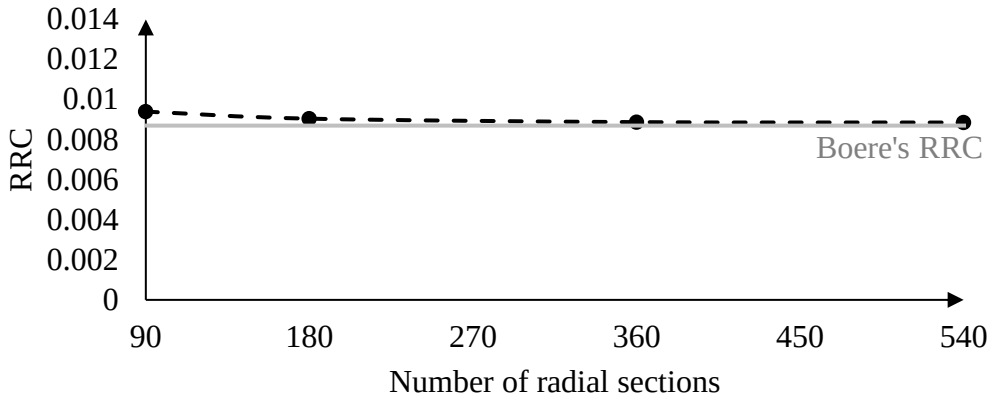

Figure 3-34.Variation of tire rolling resistance coefficient rolling over a smooth surface with 80km/h speed for different numbers of radial sections

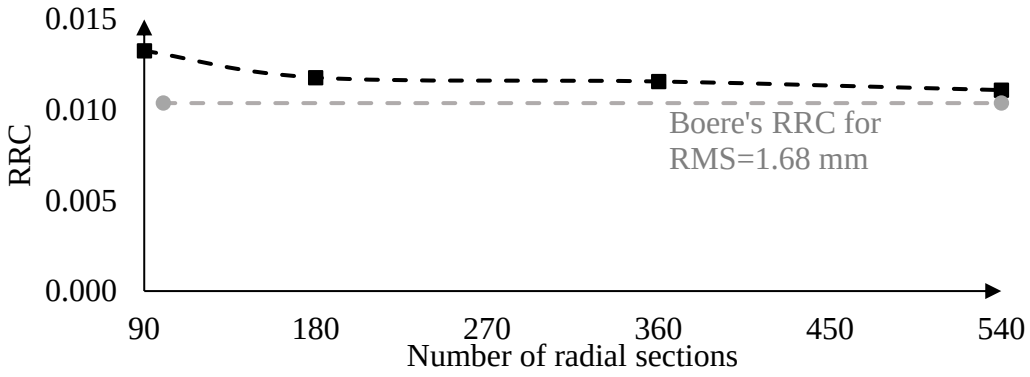

Figure 3-35.Variation of tire rolling resistance coefficient rolling over a textured surface with macro-texture RMS of 1.68 mm and speed of 80km/h for different numbers of radial sections

For mesh sensitivity analysis for mega-texture and roughness, the number of sections of 540 with mesh size of 5mm is not necessary since the smallest mega-texture wavelength is 5cm. Therefore, here the results of 360 and 180 sections are compared with each other (see Figure 3-36 and Figure 3-37).

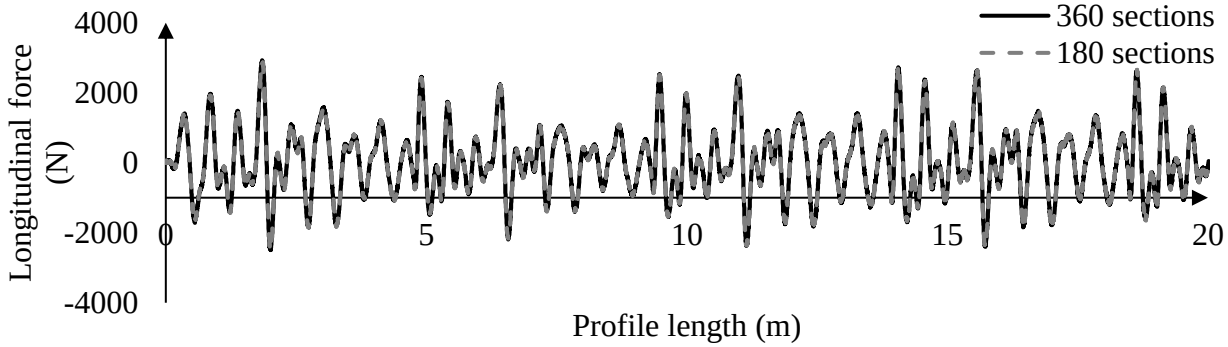

Figure 3-36.Variation of tire rolling resistance force rolling over a textured surface with mega-texture with RMS of 4 mm and speed of 80km/h for different numbers of radial sections

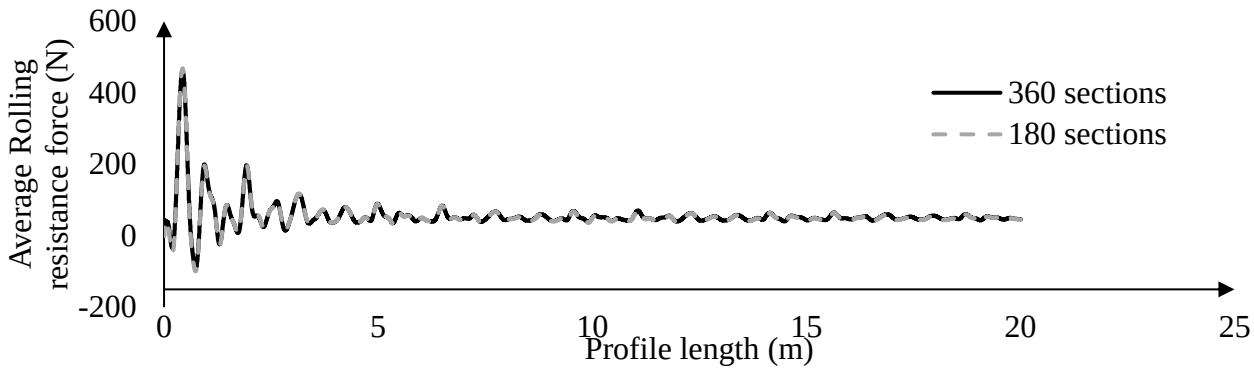

Figure 3-37. Variation of average rolling resistance force of the tire rolling over a textured surface with mega-texture with RMS of 4 mm and speed of 80km/h for different numbers of radial sections

As it can be seen in Figure 3-36 and Figure 3-37, the results for the number of radial sections of 180 and 360 are perfectly matching. Therefore, the larger radial mesh size (180 radial sections with 1.1 cm, almost 1/5 of the smallest mega-texture wavelength) is sufficient to capture the effect of mega-texture and is chosen as the final mesh size for mega-texture and roughness models.

3.4 VERIFICATION OF THE QUARTER-CAR MODEL

As the wavelength of the profile increases (wavelengths more than tire contact patch), its effect goes beyond the tire deformation to the suspension of the vehicle. The suspension of the vehicle dampens the vibration caused by the contact between the pavement surface and the vehicle and as the result the passengers experience a smoother ride. This damping causes energy dissipation and therefore it should be accounted for in the calculation of the rolling resistance of the vehicle. For this purpose, a simple suspension system (combination of a mass, spring and a dashpot) is added to the model to build a quarter car model as it was explained in section 3.7.6. Having this system in place, it is possible to distinguish between the sprung and unsprung masses in the vehicle. After building the model based on the parameters given in Figure 3-15, the model should be verified again. For verification the vertical displacement of the sprung mass (car) is evaluated. Considering no damping in the dashpot, the deformation of the spring under a mass (m) is defined as

$$\Delta = mg/K \qquad \text{eq. 3-10}$$

where K is the stiffness of the spring, and g is the gravity. Therefore, it is expected that by the presence of the dashpot in the model, the deformation of the spring and displacement of the sprung mass will be close to Δ. Figure 3-38 shows the displacement of the sprung mass obtained from FE model, along with a 5% boundary from the analytical Δ value. As it can be seen, after reaching the steady state condition, the displacement is within the 5% limit from Δ, which is an indication of the model working properly.

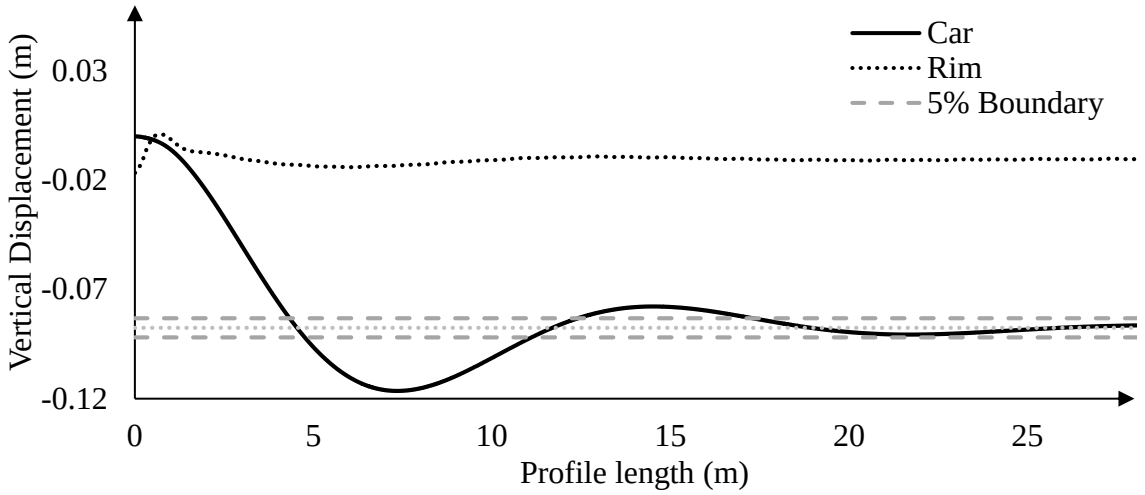

Figure 3-38. Vertical displacement of the spring mass under the vehicle load

After reaching the steady state condition (within the 5% limits) the tire can be rolled over different surfaces, and the effect of texture and roughness on the deformation of the tire and suspension can be considered as the rolling resistance.

The relevance of the effect of suspension for mega-texture and roughness may be obvious. However, to evaluate its necessity or benefit for the macro-texture, another mesh sensitivity analysis is performed for a macro-texture surface with RMS of 1.68mm. Figure 3-39 shows a comparison between the rolling resistance coefficients obtained from the tire model with suspension (Quarter-car model) and without suspension.

As it can be seen, the results are very similar after 180 radial sections. Since the addition of the suspension does not change the computational time of the analysis, for consistency between the models, even for the macro-texture surfaces, the Quarter-car model is used.

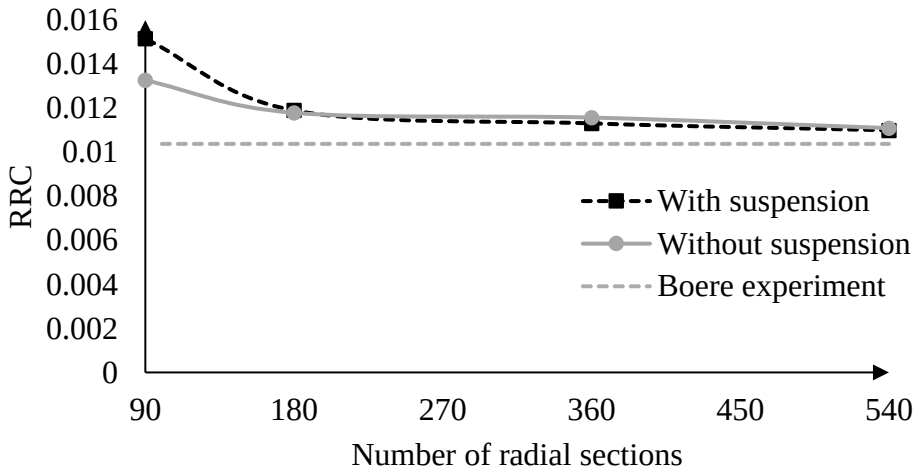

Figure 3-39. Mesh sensitivity analysis for the Quarter-car model on textured surface with RMS=1.68mm

CHAPTER 4
RESULTS

Pavement surface profile is one of the factors that can influence the rolling resistance of the vehicle. The macro-texture, the lower wavelengths within the profile spectrum, affect the deformation within the tire, e.g., tread deformation and tire bending. Mega-texture includes wavelengths as small as 5cm (within the tire contact patch) up to 50cm. Therefore, in addition to the tire deformation, it also influences the suspension of the vehicle. Roughness of the profile that consists of wavelengths beyond 50cm only affects the body and suspension of the vehicle. The main purpose of the study is to determine the effect of each scale of profile (roughness, mega-, and macro-texture) on the rolling resistance of the vehicle. To achieve this goal, as it was mentioned in the previous chapter, two finite element models are developed: (i) Finite element model of the tire to capture the effect of textures that only affect the tire deformation; and (ii) Finite element model of the tire combined with a quarter-car mechanical model, which is a simplified vehicle suspension system that is comprised of a spring and a dashpot in parallel. The second model is able to capture the effect of the wavelengths that goes beyond the tire deformation. With these two models, it is possible to evaluate the effect of different scales of the surface profile spectrum on rolling resistance of the tire and suspension system separately.

It is obvious that textures larger than the tire's contact patch affect the suspension system of the tire. Therefore, to assess the effect of roughness, the quarter-car FE model will be used. Mega-texture includes textures with wavelengths both smaller and larger than the contact patch. So, to capture the effect of mega-texture on rolling resistance, similarly to the roughness, the quarter-car FE model will be used.

Most of the current models consider the contact patch size (25 cm) as the cut-off wavelength for the effect on suspension. Even in IRI calculation, textures smaller than 25 cm are neglected and removed from the surface profile. The textures between 25 cm and 5 cm are within the mega-texture limits and will be evaluated by the quarter-car FE model, as mentioned above. However, although negligible, to investigate the macro-texture's effect on the suspension of the vehicle, both of the models will be used, and their results will be compared.

Then, the results of different scales will be compared with each other to evaluate the relative importance of each scale. As it was mentioned in chapter 3, mega-texture can be a result of localized events and allocating a high RMS value for mega-texture can be sometimes misleading. Therefore, to completely understand the effect of mega-texture, the importance of these local events should be evaluated along the profile length. For this reason, the rolling resistance of a profile with roughness and mega-texture will be compared with the one with roughness only. The difference is related to the mega-texture of the surface. Although surfaces can have different levels of roughness and mega-texture, this model can provide an understanding of the localized high mega-texture events.

Afterward, the results of the macro-texture's effect on rolling resistance will be compared with two empirical studies: NCHRP 1-45 project (NCHRP 720 report) and MIRIAM project. The effect of roughness and mega-texture will be also compared with the NCHRP 720 report and a mechanical model presented by Zaabar et al (2018).

4.1 ROLLING RESISTANCE DEFINITION

4.1.1 Rolling resistance of the tire

When a tire is rolling at a certain velocity, to compensate any force that is resisting the tire rolling, a force should be applied to the tire rim centroid. Therefore, the rolling resistance force of a tire is defined as the average work per unit length or average longitudinal force that should be applied to the centroid of the tire rim to roll it at the corresponding velocity.

$$RRF = \frac{\sum F.d}{d} \qquad \text{eq. 4-1}$$

If the rolling distance is sufficiently long, the average rolling resistance for the surfaces goes toward a constant number (with small fluctuations related to local events).

4.1.2 Rolling resistance of a quarter-car FE model

When the profile affects the vehicle dynamics, the energy loss in the suspension system of the vehicle and tire vibration should both be considered. There are various models for tackling this problem, from two degree-of-freedom quarter-car model to complex finite element models. In this section of the study, the finite element tire model is combined with the two degree-of-freedom quarter car model (see Figure 4-1). Therefore, the model consists of a detailed finite element tire model attached to a 300 kg mass via a spring and dashpot system as the suspension.

As it can be seen the system consists of two parts; (i) the dynamic response of the tire in contact with the surface profile, where the FE tire model replaces the simplified spring and dashpot system of (k_t and c_t) used in the simple mechanical models, and (ii) the response of the suspension system between the axle (unsprung mass) and the vehicle mass (sprung mass), which is modeled in the same way as simple mechanical models, considering k_s and c_s.

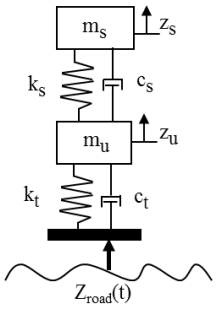

Figure 4-1. Schematic of Two DoF Quarter-Car Vehicle Model (Zaabar et al., 2018)

For defining the rolling resistance force, the resistance forces in tire and suspension should be both accounted for. The rolling resistance force in the tire is defined previously as the longitudinal force at the rim centroid. The resistance in the suspension, however, is related to the energy dissipated in the dashpot. Therefore, it should be defined accordingly.

When the surface is combined with the quarter-car model the relative displacements and velocities of the sprung and unsprung masses can be obtained by solving the following system of two equations:

$$m_s\ddot{z}_s + c_s(\dot{z}_s - \dot{z}_u) + k_s(z_s - z_u) = 0 \qquad \text{eq. 4-2}$$

$$m_u\ddot{z}_u + c_t(\dot{z}_u - \dot{z}_r) + k_t(z_u - z_r) - c_s(\dot{z}_s - \dot{z}_u) - k_s(z_s - z_u) = 0 \qquad \text{eq. 4-3}$$

in which, m_s and z_s are the mass and the displacement of the sprung mass and $m_u$and z_u are the mass and displacement of the unsprung mass. The parameters c_s and k_s are the damping and stiffness of the suspension. The parameters c_t and k_t are the damping and stiffness of the tire, and z_r is the road profile elevation.

The dissipative energy of the system per unit distance is related to the relative velocities between the two masses, which can be defined by

$$D = \frac{C_s}{V}E[\dot{z}_s^2] + \frac{C_t}{V}E[\dot{z}_t^2] \qquad \text{eq. 4-4}$$

in which V is the constant velocity of the vehicle, D is the energy dissipation, and $\dot{z}_s$ and $\dot{z}_t$ are the relative velocities for the suspension and tire, respectively.

Therefore, the energy dissipation in the suspension is defined in this study as

$$D_s = \frac{C_s}{V}E[\dot{z}_s^2] \qquad \text{eq. 4-5}$$

The average rolling resistance force is equal to the average energy dissipated over the unit length. The total rolling resistance coefficient is then defined as the ratio between the summation of the rolling resistance forces in both tire and suspension and the applied normal force.

4.2 EFFECT OF MACRO TEXTURE PROFILE ON ROLLING RESISTANCE OF THE TIRE

For understanding the effect of each scale of the surface profile (macro-, mega-texture and roughness), the rolling resistance corresponding to each scale will be obtained separately. The macro-texture of the profile is defined as wavelengths between 0.5mm and 50mm. The macro-texture is known to only affect the tire tread deformation and bending and not the suspension. In this section, the effect of macro-texture on tire rolling resistance is investigated. For this purpose, different macro-texture profiles with different RMS values are defined in the finite element model. The tire is rolled over each profile for 6 meters (Section 2.7.1) to reach a steady state condition. The goal is to find a relationship between RMS of each scale and their rolling resistance coefficient, if any. As it was mentioned in section 3.3.2, for capturing the effect of macro-texture, a smaller mesh should be used. Therefore, the tire model with 540 radial sections is used. The rolling resistance coefficients of the tire rolling on surfaces with RMS values of 0.51 mm, 1.1 mm, 1.68 mm, and 2.1 mm are obtained. The RMS value of zero corresponds to the tire rolling on a smooth surface. The final results are shown in Figure 4-2.

As it can be seen, a linear relationship (with a slope of 0.0012) can be considered for the effect of macro-texture profile on tire rolling resistance. The obtained result is compared with the experimental results reported by Boere (2009). Although the two results are very similar, there is a difference between the slope of the two lines. The finite element model is demonstrating a slightly higher influence of the macro-texture profile on the rolling resistance of the tire than the experimental results. It should be mentioned that it may not be possible to find the source of this difference, since it can be related to a range of assumptions and simplifications considered in this study that may be different from the experimental set up; from simplifications in the geometry of

the tire to neglecting the effect of temperature, or inflation pressure, or any other differences between the two studies.

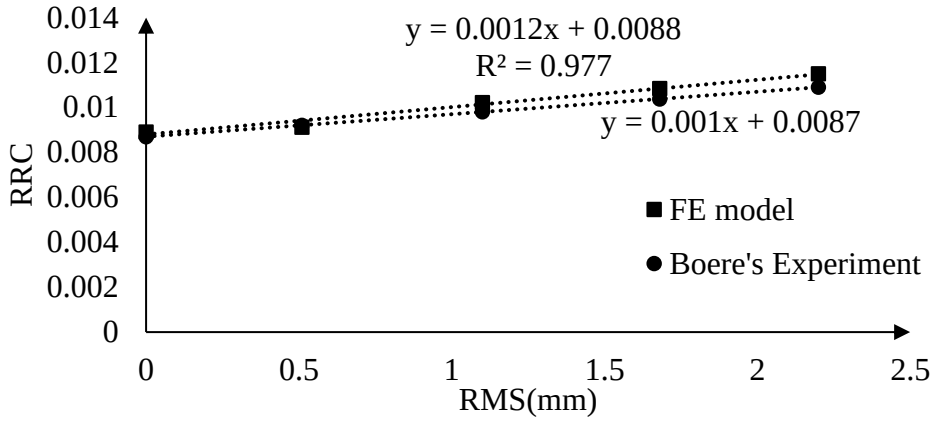

Figure 4-2. Effect of macro-texture profile's RMS on tire rolling resistance coefficient

4.3 EFFECT OF MACRO-TEXTURE PROFILE ON ROLLING RESISTANCE OF THE QUARTER-CAR FE MODEL

For investigating the effect of macro-texture on the quarter-car FE model rolling resistance, the model's properties are changed to the properties of a model by Dixon (2008). For this purpose, besides the addition of the suspension to the model, the normal load on the system is changed to 3433 N (combination of 300 kg sprung and 50 kg unsprung masses, see Figure 3-15). Then, the quarter-car FE model is rolled over surfaces with different macro-texture profiles. The rolling resistance coefficients (RRC) obtained from the model for profiles with RMS values of 0.51mm, 1.1mm, 1.68mm, and 2.1mm are shown in Figure 4-3. To better understand the effect of macro-texture on the suspension system, in addition to the RRCs of the quarter-car FE model (tire and suspension), the RRCs of the tire alone are also shown. As it can be seen, both tire and quarter-car FE model show a linear relationship with the RMS of macro-texture, with very similar slopes. This is an indication that the surface macro-texture mainly affects the tire deformation and its effect on suspension can be neglected.

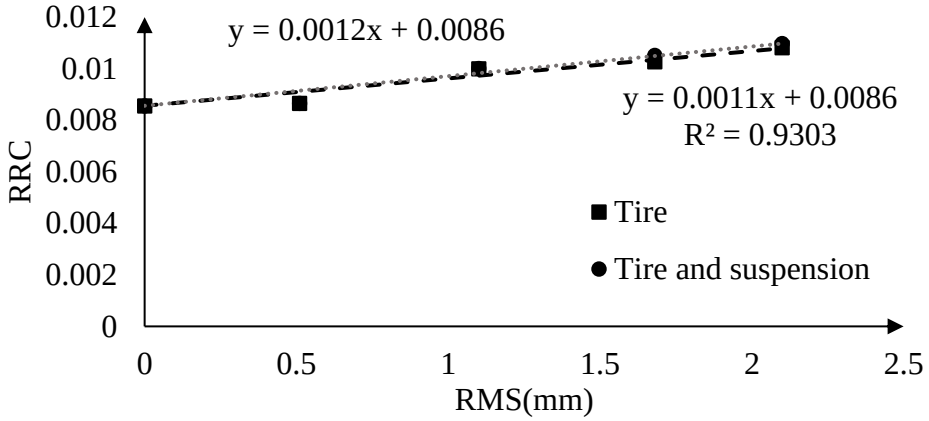

Figure 4-3. Effect of macro-texture profile's RMS on RRC of the tire and the quarter car model

Moreover, the relationship between rolling resistance and mean profile depth (MPD) of the profiles is also found, see Figure 4-4.

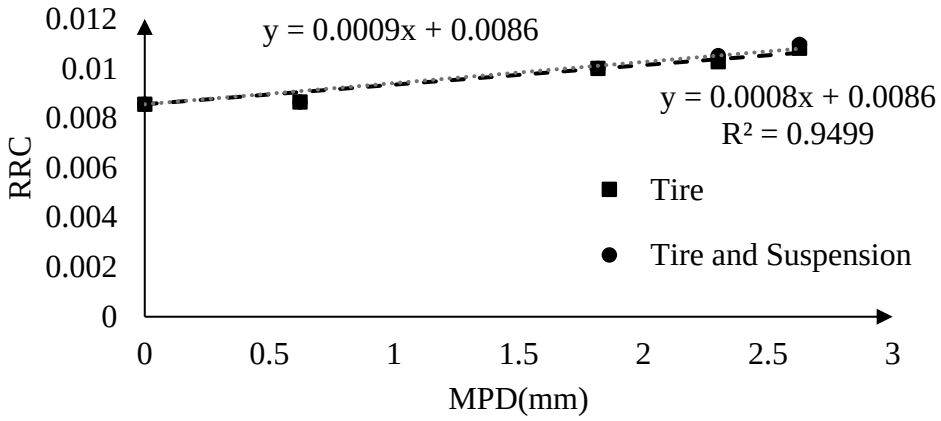

Figure 4-4.Effect of macro-texture profile's MPD on RRC of the tire and the quarter car model

As it can be seen, a similar relationship to RMS vs RRC is obtained for MPD vs RRC for the selected surfaces. However, RRC seems to have a slightly better relationship with MPD than RMS. RMS is the root mean square of the whole profile while MPD is related to the maximum points within a profile. When the tire is moving on macro-texture at 80km/h speed, it is not able to have contact with all of the textures within segments below the mean of the profile. But it can capture the effect of the textures at the peak of the profile. Therefore, the MPD shows a better relationship with RRC than RMS. However, since the difference is not significant, RMS can still be considered as an acceptable parameter for characterization of the surface macro-texture profile.

The effect of the normal load on rolling resistance will be addressed in section 4.10.1.

4.4 EFFECT OF MEGA-TEXTURE PROFILE ON ROLLING RESISTANCE OF THE QUARTER-CAR FE MODEL

The mega-texture is defined as wavelengths between 50 mm and 500 mm with peak to peak amplitude of 0.1 to 50 mm. For modeling the effect of mega-texture on the rolling resistance of a vehicle and tire, two ranges should be considered (1) wavelengths larger than the contact patch (≈ 250 mm – 500 mm), and (2) wavelengths smaller than the contact patch (≈ 50 mm – 250 mm). The upper part of the mega-texture spectrum affects the vehicle dynamics. However, the textures within the contact patch (≈ 50 mm – 200 mm) are known to not have a big influence on the suspension of the vehicle, and their effect is limited to the tire vibration. The quarter-car FE model, including both tire and suspension, should be capable of capturing the effect of both mega-texture spectrums.

For investigating the influence of the mega-texture on rolling resistance, the filtered mega-texture profiles of 12m length are imported into the quarter-car FE model. Similar to the previous section, the effect of mega-texture on both tire and the combination of tire and suspension is evaluated. Figure 4-5 shows the relationship between the RMS values of the selected mega-texture profiles

and their corresponding rolling resistance coefficients. Figure 4-6 shows the same relationship for the IRI values of the profiles.

As it can be seen the effect of the mega-texture on the suspension of the vehicle is negligible for smaller RMS and IRI values, while its effect can be quite noticeable for rougher surfaces. Here, for distinguishing between the effect of mega-texture on rolling resistance in tire and its effect on rolling resistance in the suspension, ΔRRC parameter is introduced. ΔRRC of suspension and tire at any given RMS value can be defined based on y_1 and y_2 relationships given in Figure 4-5:

$$\Delta RRC_{suspension} = RRC_{tire\ \&\ suspension,RMS=x} - RRC_{tire,RMS=x} = y_{2,RMS=x} - y_{1,RMS=x} = 0.0006\ RMS \quad \text{eq. 4-6}$$

$$\Delta RRC_{tire} = y_{tire,RMS=x} - RRC_{RMS=0} = y_{1,RMS=x} - y_{1,RMS=0} = 0.0013\ RMS \quad \text{eq. 4-7}$$

Therefore, the ratio between the effect of mega-texture on rolling resistance of suspension and its effect on tire is $\Delta RRC_{suspension}/\Delta RRC_{tire} = 0.0006/0.0013 \approx 0.46$. This result shows that the effect of mega-texture on the tire is more than its effect on the suspension.

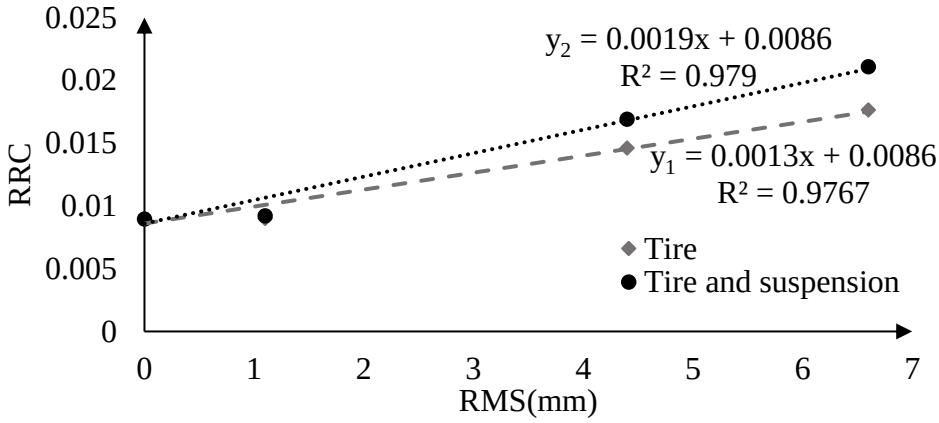

Figure 4-5. Effect of mega-texture profile's RMS on RRC of the tire and the quarter car models

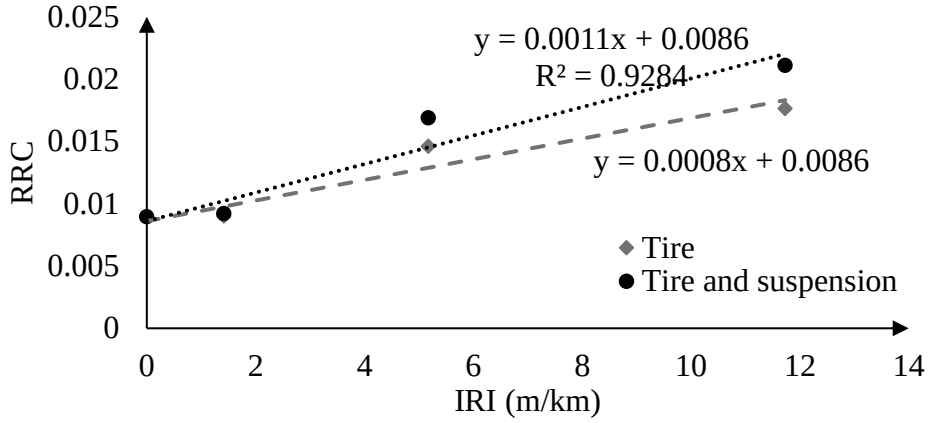

Figure 4-6.Effect of mega-texture profile's IRI on RRC of the tire and the quarter car models

It is worth mentioning that the equivalent IRI for the RMS of 6.6mm is quite high (12m/km). Usually, IRI values around 5 or 6m/km are considered high for pavement management purposes and preservation strategies should be suggested for such surfaces. However, in this part of the study, it should be considered that the length of the profile is only 12 m while in practice the IRI

is measured for much longer profile lengths. Mega-texture profiles with high IRIs do exist along a road profile; however, since they do not occur as often, the measured IRI values in the field are usually not as high. An assessment of the effect of occurrence of these kinds of events with high mega-texture on rolling resistance will be done in section 4.7.

A comparison between Figure 4-5 and Figure 4-6 shows that the relationship between RMS and RRC is a better one than RRC and IRI. In calculation of IRI, a 250 mm filter is used to eliminate the effect of the profile within the contact patch. The exclusion of mega-texture wavelengths between 50 and 250 mm from the profile can be the reason for the weaker relationship between IRI and mega-texture-induced RRC. To verify this suggestion, the wavelength smaller than 250 mm are filtered from the roughest profile in this section with RMS of 6.6mm (applying the high pass filtering of 250 mm), see Figure 4-7.

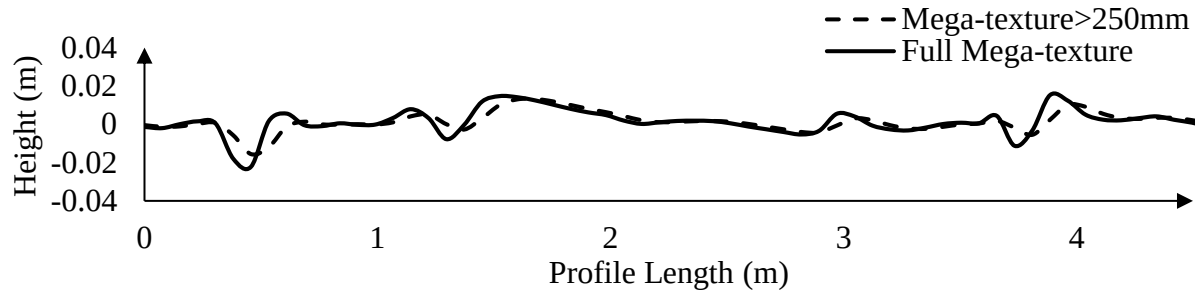

Figure 4-7. Filtered mega-texture profile (RMS=6.6mm)

The RMS value of the new filtered profile is reduced to 5.3 mm. The rolling resistance force (RRF) of the new profile is then compared with the RRF of the full mega-texture profile, in Figure 4-8.

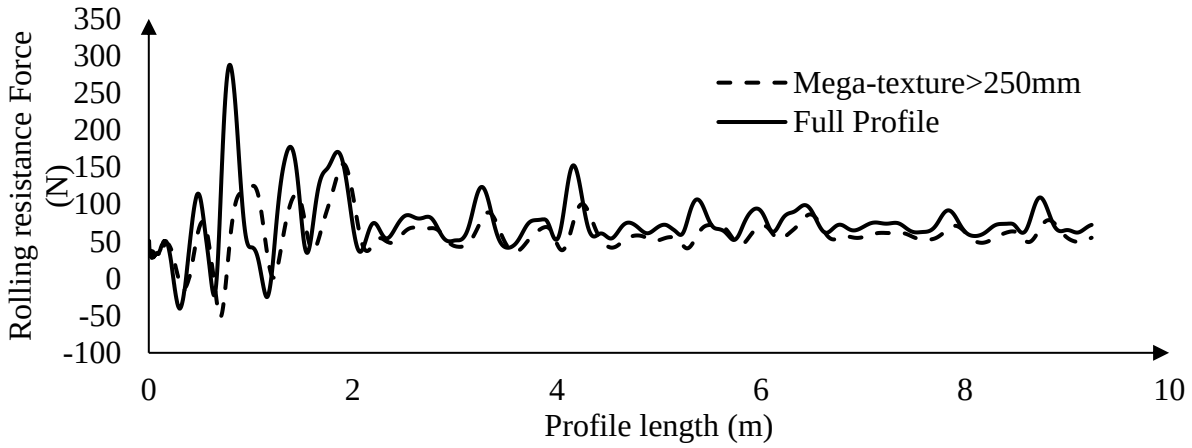

Figure 4-8. Effect of 250mm filtering of mega-texture on the rolling resistance force of the quarter-car FE model

Table 4-1 shows the variations in the rolling resistance forces in the tire, suspension, and the quarter-car FE model.

Table 4-1. Summary of the effect of 250 mm filtering of mega-texture on the rolling resistance force of the quarter-car FE model

Profile	RMS (mm)	Tire RRF (N)	Suspension RRF (N)	Total RRF (N)
Full Profile	6.6	60.54	11.88	72.42
Filtered	5.33	50.31	10.82	61.31
Ratio (Filtered/Full)	0.808	0.83	0.91	0.84

For the given profile, the total rolling resistance force decreases by 16% after filtering out the wavelengths less than 250 mm. The rolling resistance force in the suspension is reduced by 8.9 %, while the RRF of the tire is decreased by almost 19%. This result shows the significance of the effect of the 250 mm filtering on the rolling resistance of the quarter-car FE model. Also, it is noticeable that the filtering affects the tire rolling resistance more than the suspension. This is an expected result, since the wavelengths less than 250 mm are within the contact patch of the tire and their effect should be more on the tire than the suspension.

4.5 EFFECT OF ROUGHNESS PROFILE ON ROLLING RESISTANCE OF THE QUARTER-CAR FE MODEL

The roughness of a profile is defined as any wavelength larger than 500 mm. Similarly to the upper segment of mega-texture, the roughness profile affects vehicle dynamics. Therefore, a quarter-car FE model is required for calculating the roughness-induced rolling resistance force. Hence, the filtered roughness profiles of 30 m length are imported into the quarter-car FE model. The relationships between the RRC of both tire and quarter-car FE models and the RMS values of the roughness profiles are shown in Figure 4-9.

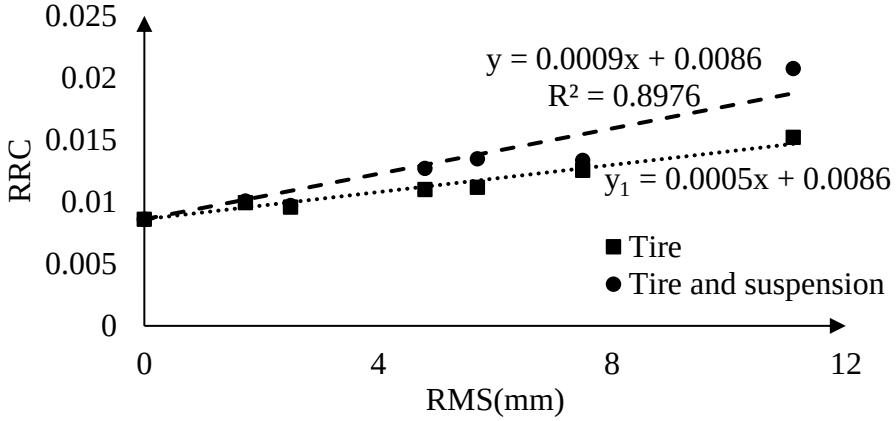

Figure 4-9. Effect of roughness profile RMS on RRC of the tire and the quarter car models

As it can be seen the slope of the relationship between RRC and roughness RMS for the total rolling resistance of the quarter-car FE model is lower than the one for mega-texture found in the previous section. However, the effect of roughness on suspension can be more pronounced in some cases: The RRC variation in the suspension can be as high as 80% of the changes in RRC of the

tire, using eq.5.6 and eq.5.7 ($\Delta RRC_{suspension}/\Delta RRC_{tire} = \frac{0.0004}{0.0005} = 0.8$). As a result, it can be assumed that the RRC of the roughness should have a strong relationship with IRI of the profile, which is related to the displacements in the suspension.

The available studies on the relationship between IRI and RRC, have considered both linear and non-linear relationships. As an example, the empirical results from NCHRP 720 report show a linear relationship between rolling resistance and IRI. However, the mechanistic models developed by Zaabar et al (2018), Louhghalam et al. (2015) and Kim et al. (2017) showed a non-linear relationship. Here, to get a better understanding, both relationships are considered for the rolling resistance coefficient and IRI of roughness profile (see Figure 4-10). It can be seen that the non-linear relationship is stronger than the linear one.

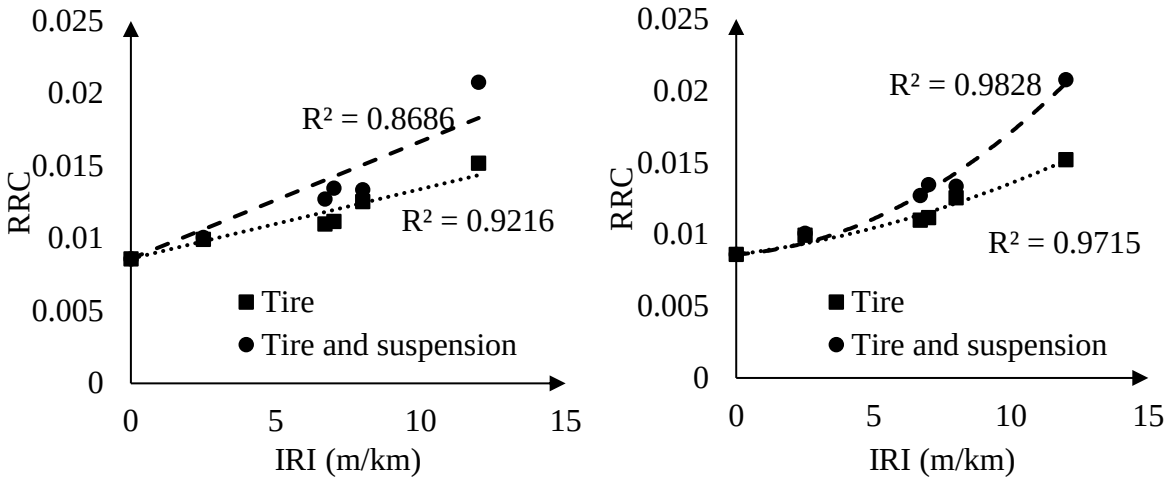

Figure 4-10. Effect of roughness profile IRI on RRC of the quarter car model with linear and non-linear relationships

Similarly to the mega-texture, the roughness profiles with high RMS values result in higher than normal IRI values, which can be explained by the presence of local events within portions of the profile length, that do not necessarily occur regularly in measurements over longer surface profiles.

4.6 COMPARISON OF ROLLING RESISTANCE IN DIFFERENT SCALES

So far, the relationships between the rolling resistance coefficient of the quarter-car FE model and the profile for each scale of macro-texture, mega-texture, and roughness have been found. In this section, the obtained results are compared with each other to assess the relative importance of each one of the scales. For this comparison, the RMS parameter which is the common parameter between all of the scales is used and only linear relationships are considered. Figure 4-11 and Figure 4-12 show this comparison for tire and quarter-car FE models, respectively. For better visualization of the results and comparison of the RRC values of the different scales for lower RMS values (less than 2 mm) for quarter-car FE model, the log x-axis format is used (see Figure 4-13).

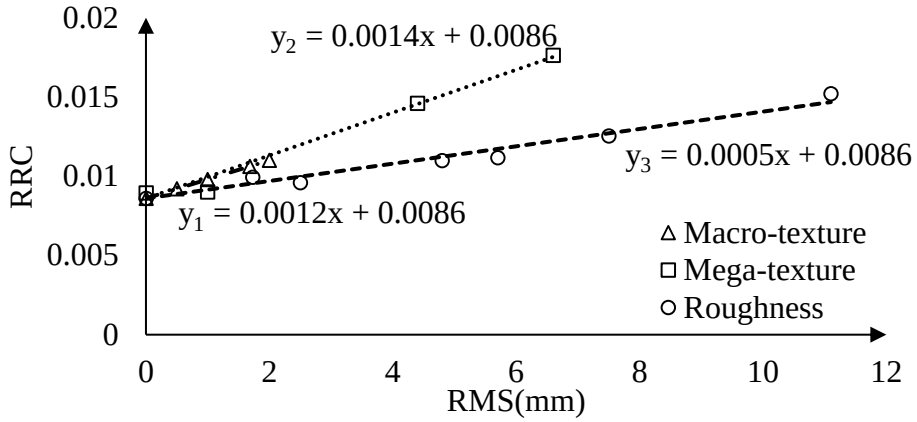

Figure 4-11.Comparison of the effect of macro-texture, mega-texture, and roughness on rolling resistance coefficient of the tire

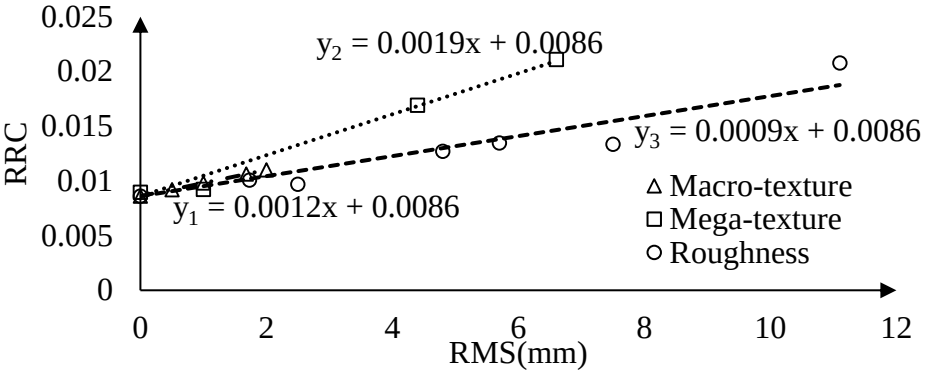

Figure 4-12. Comparison of the effect of macro-texture, mega-texture, and roughness on rolling resistance coefficient of quarter-car FE model

As it can be seen, for lower RMS values within the macro-texture range (less than 2mm), the RRCs for all of the scales are very similar to each other. Also, the profiles in this range affect the suspension only slightly. Therefore, whether the profile includes roughness or texture, for profiles with RMS values less than 2 mm, the rolling resistance is limited to the energy dissipation in the tire. In another words, when the amplitude is low, regardless of the frequency of the wave, the response is similar, and the profile only affects the tire.

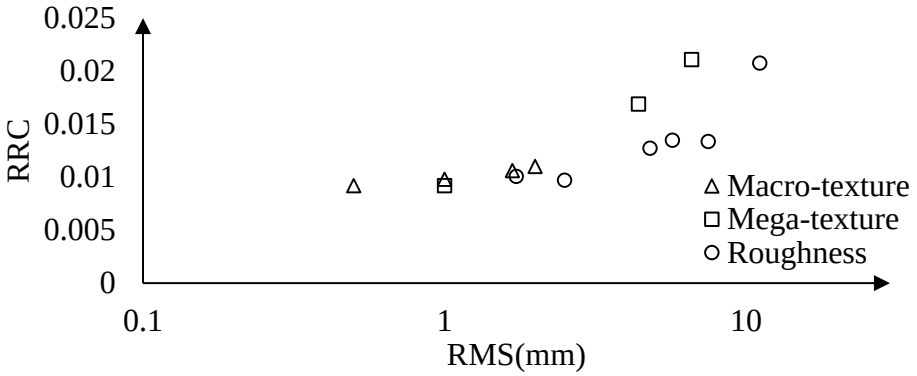

Figure 4-13.Comparison of the effect of macro-texture, mega-texture, and roughness on rolling resistance coefficient of quarter-car FE model in semi-log space

However, for higher RMS values (higher amplitudes), mega-texture shows a higher rolling resistance than roughness. For a better understanding of the effect of these two scales on rolling resistance, two profiles with similar RMS values are selected and their results are compared: (i) mega-texture profile with RMS of 4.4 mm (ii) roughness profile with RMS of 4.8 mm. A comparison of the profiles of these two surfaces is shown in Figure 4-14.

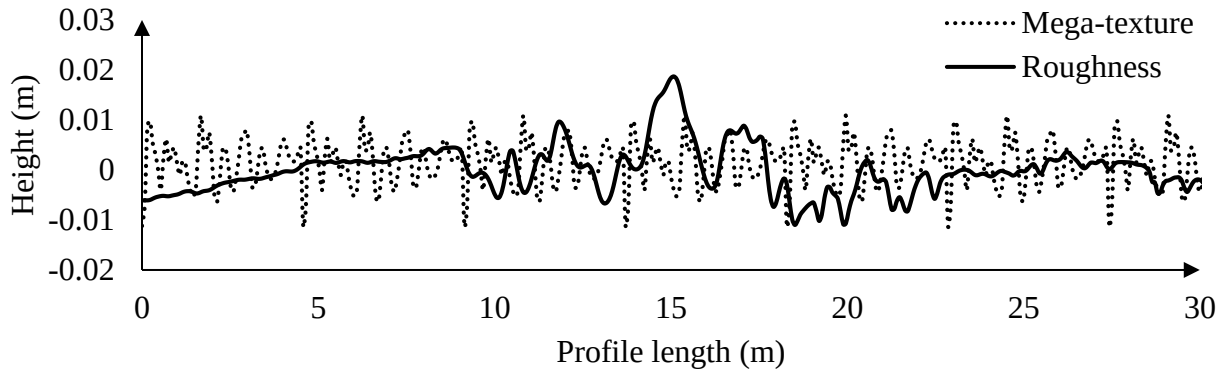

Figure 4-14. Comparison of mega-texture profile with RMS of 4.4 mm with roughness profile with RMS of 4.8 mm

Table 4-2 shows a summary of the rolling resistance coefficients for the two profiles. It can be seen that the mega-texture profile's effect on the tire RRC is significantly higher than that of the roughness profile (a factor of 2.6). As a result, the total RRC due to mega-texture is also higher (about 70%) than that due to roughness. It is expected that the mega-texture will influence the tire deformation more than the suspension. However, it has generally been assumed that roughness affects the suspension response more than mega-texture. In this case, the results show that the RRC due to mega-texture is still about 30% higher than that due to roughness. Although the absolute effect of mega-texture on RRC on the suspension response is still slightly higher than that from roughness, the ratio of $\Delta RRC_{Suspension}$ / ΔRRC_{Tire} for roughness (78%) is higher than that for the mega-texture (38%). This result indicates that the roughness effect on RRC in the suspension can be in the same order as that in the tire, while the mega-texture's effect on RRC in the tire is much higher than that in the suspension.

Table 4-2. Summary of the rolling resistance coefficients of the quarter-car FE model for mega-texture and roughness profiles with similar RMS values

Profile	RMS (mm)	Initial RRC	ΔRRC_{Tire}	$\Delta RRC_{Suspension}$	Total RRC
Mega-texture	4.4	0.0086	0.006	0.0023	0.0169
Roughness	4.8	0.0086	0.0023	0.0018	0.0127

4.7 EFFECT OF MEGA-TEXTURE AND ROUGHNESS ON ROLLING RESISTANCE

As it was mentioned in section 2.8.3, high values of RMS for mega-texture can be related to local events in the road profile. Based on the results shown in the previous section mega-texture variation has the highest effect on RRC considering a constant presence of high mega-texture

features all along the profile (Figure 4-14). However, if high mega-texture RMS values only appear a few times within a longer profile length, its overall effect may not be as dominant as it was found in the previous sections. Therefore, it is necessary to investigate the effect of mega-texture on rolling resistance more thoroughly and in a more realistic way. For this purpose, two profiles with 30 m length have been chosen randomly (namely, profile 1 and 2). Table 4-3 shows the IRI and RMS values of the full profile, as well as of the roughness and mega-texture portions only. To fully understand the effect of mega-texture, the rolling resistance forces are obtained for (i) the full profile including both roughness and mega-texture and (ii) the profile including only the roughness after removing the mega-texture.

Table 4-3. Summary of surface characterization parameters for effect of mega-texture repetition on rolling resistance

Profile	IRI (m/km)	Full Profile RMS (mm)	Roughness RMS (mm)	Mega-texture RMS (mm)
1	5.06	9.12	8.58	2.86
2	3.85	7.7	7.5	1.3

The profiles and their filtered roughness and mega-texture profiles are shown in Figure 4-15 and Figure 4-16 for profile 1 and 2, respectively. As it can be seen, profile 1, includes higher mega-texture with several local events, while the mega-texture of profile 2 is lower and only consists of one event around x=22m of the profile.

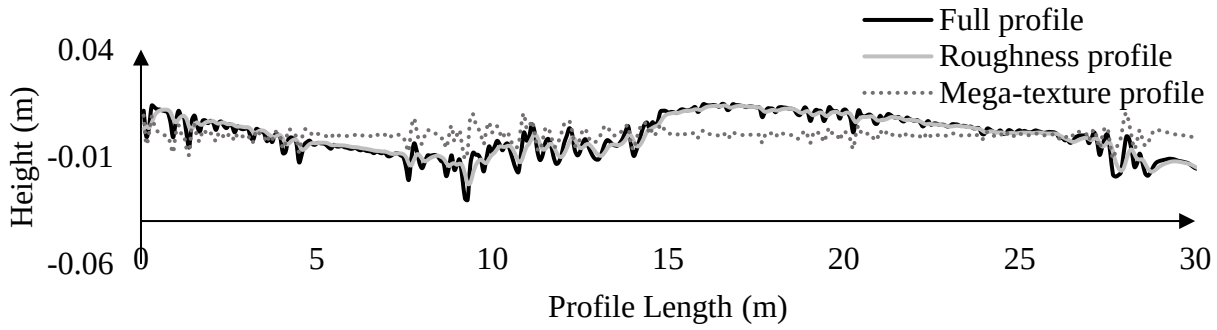

Figure 4-15. Profile 1, IRI= 5m/km

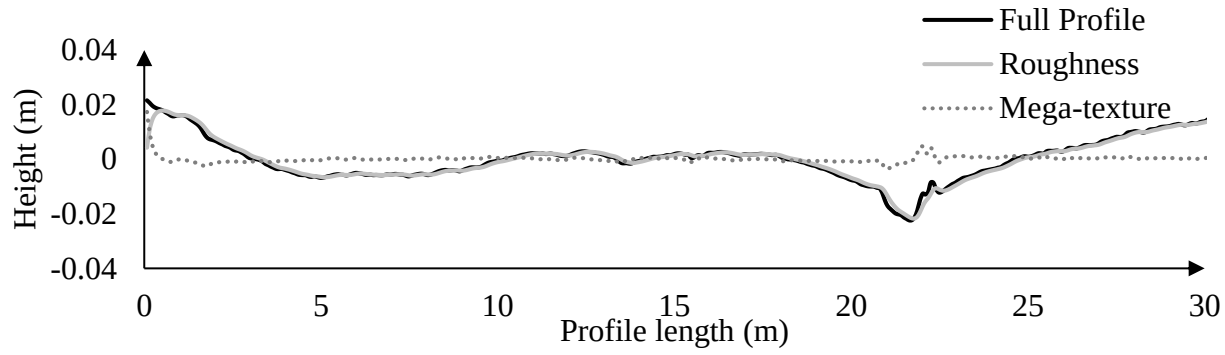

Figure 4-16. Profile 2, IRI= 3.85m/km

The corresponding rolling resistance force (obtained from the full FE model with tire and suspension system) for these profiles, with and without mega-texture, are shown in Figure 4-17 and Figure 4-18 for profiles 1 and 2, respectively. A summary of the results is given in Table 4-4.

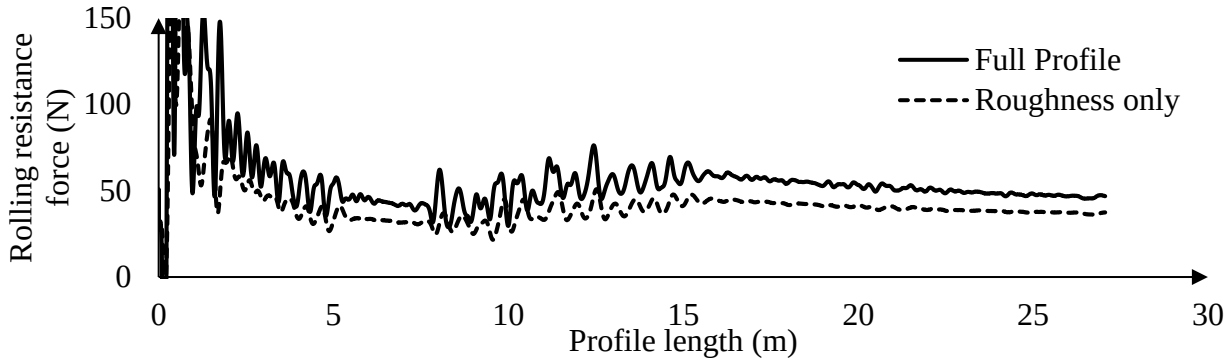

Figure 4-17. Rolling resistance forces for full profile and filtered roughness profile of profile 1 with IRI=5m/km

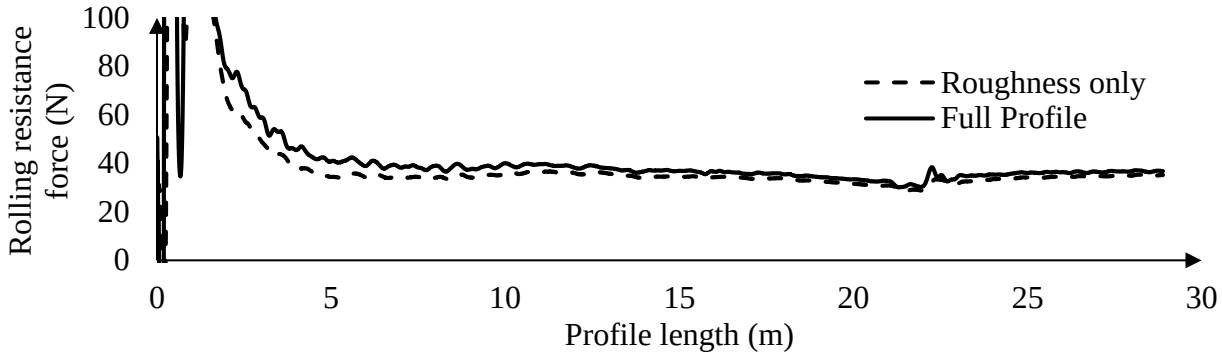

Figure 4-18. Rolling resistance forces for full profile and filtered roughness profile of profile 2 with IRI=3.85 m/km

For understanding the effect of the mega-texture and roughness of the profile on rolling resistance force, the rolling resistance force of the smooth surface is considered as the base line ($RRF_{IRI=0}$ =29.52 N). The effect of the different profiles on the rolling resistance force can then be defined as the difference between the RRF of the profiles and the smooth surface ($RRF_{IRI=x}$ - $RRF_{IRI=0}$).

Table 4-4. Summary of rolling resistance forces and coefficients for effect of mega-texture repetition on rolling resistance

Profile	IRI (m/km)	RRF Full profile (N)	RRF roughness profile (N)	RRC Full profile	RRC roughness profile
1	5.06	57.89	42.2	0.0169	0.0123
2	3.85	44.69	40.04	0.0130	0.0117

Therefore, it can be noted that for profile 1, from almost 28.39N increase in rolling resistance force because of the full surface profile, only 12.7 N is related to roughness portion of the profile (45%). Therefore, although mega-texture is not high everywhere and its RMS is only 2.86 mm, its effect

on rolling resistance is more than roughness. For profile 2, however, the mega-texture's RMS is 1.3mm and it includes only one large event. As a result, the roughness portion of the profile imposes the majority of the effect on rolling resistance, causing 10.56 N increase in rolling resistance force out of the total of 15.17 N (69.6%).

These results are an indication of the importance of mega-texture on the rolling resistance of the vehicle, even when the events are isolated.

4.8 COMPARISON OF THE RESULTS ON THE EFFECT OF MACRO-TEXTURE ON ROLLING RESISTANCE WITH EMPIRICAL STUDIES

There are a few empirical models on the effect of macro-texture on rolling resistance which were discussed in section 1.3.2, namely NCHRP 720 report, MIRIAM project, and Boere study. There seems to be a significant difference between the results of NCHRP 720 report and the MIRIAM project. The main focus of both of these studies is energy dissipation. Therefore, here, their results are compared with those from Boere's study, in which the rolling resistance forces were measured directly. The results from the quarter-car finite element model developed in this study were already compared with Boere's experiments. In this section, they will be compared with the other two studies as well.

The NCHRP 720 report includes a wide range of vehicles. But, the MIRIAM project only covers three vehicle types: car, truck, and truck with trailer. On the other hand, the measurements reported by Boere were performed using a trailer. The normal load applied on the trailer is 4100 N, which is equivalent to a 417 kg mass. Since this weight is on only one tire, the total vehicle mass (considering 4 wheels) is about 1668 kg. Based on the tire model and the axle load, the equivalent vehicle type for the Boere study can be considered as a medium car. Therefore, the common vehicle type for all three studies can be considered as the medium car.

Both NCHRP 720 report and MIRIAM project presented equations for rolling resistance definition based on factors such as texture, roughness, deflection, load, and velocity (section 1.3.1). The results of Boere's experimental study, however, are more limited, since the experiment was only performed at one velocity under a specific load. Therefore, for performing the comparison, the rolling resistance force is found at 80km/h speed and under a load corresponding to 1,668 kg in order to match Boere's experimental study.

The results of Boere's study are based on the RMS of the profile texture while the other two are based on MPD. Therefore Boere's results are converted to MPD, using the following equation (Avaik et al. 2013):

$$MPD = 1.729\ RMS + 0.019 \qquad \text{eq. 4-8}$$

Figure 4-19 shows the rolling resistance forces and coefficients for different MPD values for full vehicles of different types: car, light truck, and articulated truck from NCHRP 720 report.

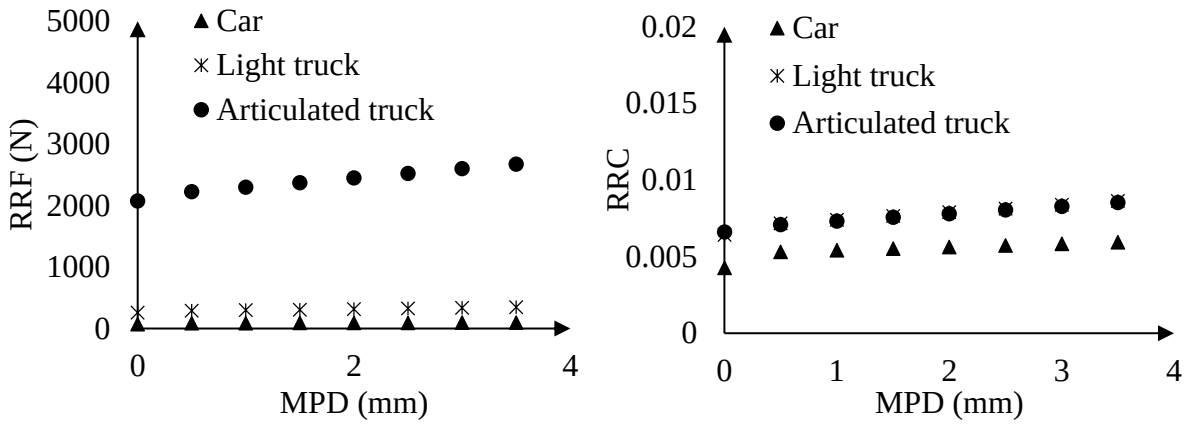

Figure 4-19. Rolling resistance force and coefficient for full car, light truck, articulated truck, from NCHRP 720 report

As it can be seen, the rolling resistance force of the articulated truck is much higher than the other two. However, when converted to rolling resistance coefficient the articulated truck and light truck have similar values. This is because in NCHRP 720 study the parameters used for rolling resistance calculation are the same based on vehicles weight class, and both light truck and articulated truck are considered in the same weight class.

Figure 4-20, depicts the rolling resistance forces and coefficients for MIRIAM project for a car and a truck with trailer for different MPD values. The rolling resistance force for a truck with trailer is much higher than the car, due to the difference between the weight of the two vehicles. However, the final rolling resistance coefficient (RRF/ Normal force) of the car is higher than the truck and trailer. This is because all of the coefficients used for rolling resistance calculation (e.g. rolling resistance, texture, IRI, and temperature coefficients) are higher for the car than the ones for the articulated truck.

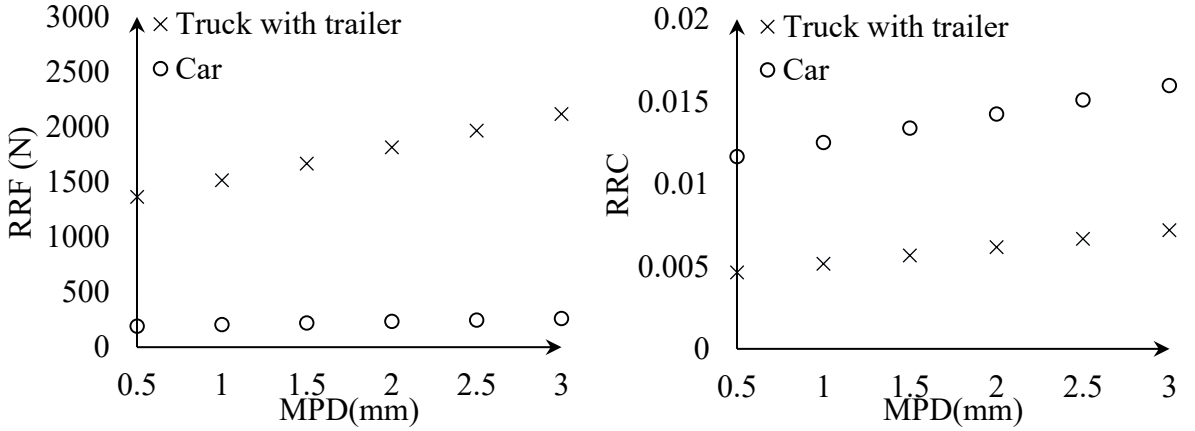

Figure 4-20. Rolling resistance force and coefficient for a full car, and equivalent articulated truck, from MIRIAM project

Since various factors affect the rolling resistance of the vehicle (espicially in empirical studies), for comparison of different studies a parameter should be used that is able to isolate the effect of one factor only. NCHRP 720 report introduced an adjustment factor for this purpose which can be defined as the ratio of the rolling resistance at any MPD value with respect to the rolling resistance

at a base MPD. In this study, the smooth surface is considered as the base point, therefore the ajustment factor is defined as $RRC_{MPD = x}$ / $RRC_{MPD = 0.0}$. Since the effect of macro-texture is important in this section, the IRI and deflection values are set to zero.

Figure 4-21 shows the comparison of the rolling resistance coefficients for the mentioned studies. It can be seen that the NCHRP 720 report underestimates the rolling resistance for zero texture condition (intercept of the line) and the effect of texture on rolling resistance (slope of the line) while MIRIAM project overestimates them. The FE results are similar to Boere's results as it was stated before.

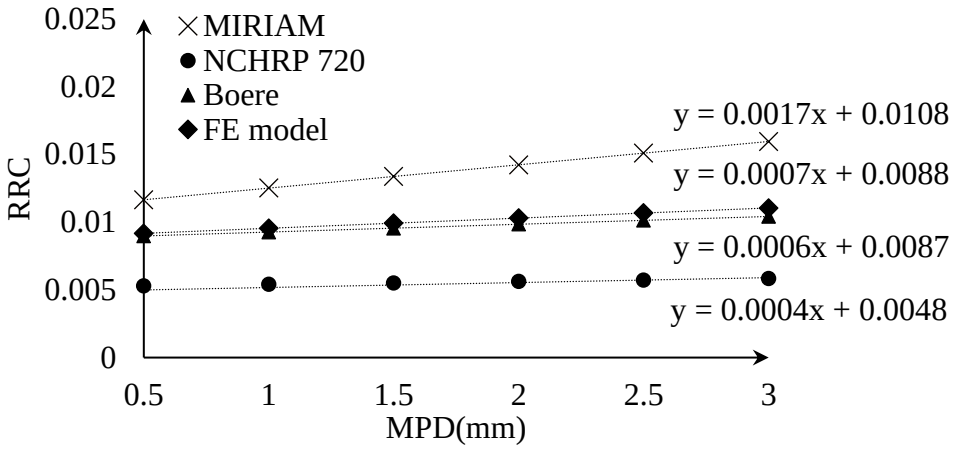

Figure 4-21. Comparison of rolling resistance coefficients of MIRIAM, NCHRP 720, Boere study and quarter-car FE model for a car at v=80 km/h

For having a better comparison, the adjustment factor is used, which considers the effect of both slope and intercept of the relationships, but eliminates the other factors involved (see Figure 4-22). It can be seen that considering both initial rolling resistance and the effect of texture on rolling resistance, the NCHRP 720 results are closer to those from Boere's study than the MIRIAM project. However, the FE model results are more similar to those from Boere's study.

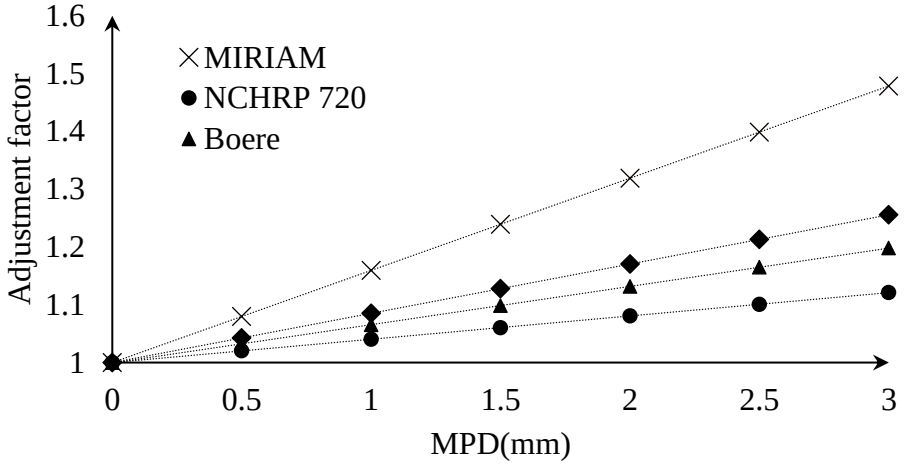

Figure 4-22. Comparison of rolling resistance adjustment factor of MIRIAM, NCHRP 720, Boere study and quarter-car FE model for a car at v=80 km/h

4.9 COMPARISON OF THE RESULTS ON THE EFFECT OF IRI ON ROLLING RESISTANCE WITH PREVIOUS STUDIES

In the previous sections, the effect of roughness and mega-texture on rolling resistance have been investigated separately. However, most of the available studies have not differentiated between these two scales and instead evaluated the effect of IRI on rolling resistance. As it was mentioned previously, IRI is related to the summation of displacements in the suspension, and it takes the effect of any wavelength larger than 250 mm into account. Therefore, it captures a combination of the effect of roughness and mega-textures with wavelength larger than 250 mm.

Among the studies that evaluated the effect of IRI on vehicle rolling resistance, the empirical model presented in NCHRP 720 report and a mechanical quarter-car model by Zaabar et al. (2018) have been chosen for comparison in this study. As it was mentioned previously, the NCHRP 720 model is an empirical model for predicting fuel consumption of the vehicle, which comprises a rolling resistance model based on texture (MPD) and roughness (IRI). The mechanical quarter-car model, on the other hand, considers the tire and suspension of the vehicle as a combination of a spring and a dashpot. A comparison of the results from these two studies is shown in Figure 4-23.

As it can be seen, there is a good agreement between the results of the two studies for lower IRI values (less than 3 m/km). However, for higher IRI values, the mechanical model shows a non-linear relationship and diverges from the NCHRP 720 results.

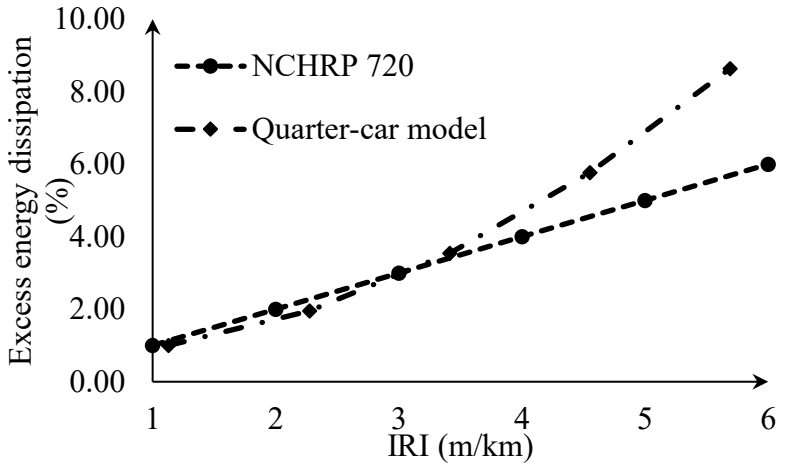

Figure 4-23. Comparison of the effect of IRI on energy dissipation of a car for NCHRP720 report and mechanistic quarter-car model at v=80 km/h (Zaabar et al. 2018)

The parameters used in the quarter-car finite element model in this study are similar to the mechanical model by Zaabar et al. (2018). However, there are three differences between the two studies: (i) the mechanical model considers the tire as a combination of a spring and dashpot, but in this study a full finite element model of the tire is used; (ii) in the mechanical quarter-car model enveloping of the surface profile is done to exclude the wavelengths within the contact patch, while the finite element model can consider the full surface profile; and (iii) the mechanical quarter-car model enforces full contact between the tire and the profile, while the FE model allows the tire to

lose contact with the profile, if necessary. The issue of loss of contact is looked at in an example shown at the end of this section.

Different profiles with various IRI values have been chosen from the NCHRP 720 surface profile database. The quarter-car FE model is used for the evaluation of the rolling resistance of these profiles. To compare these results with those presented in Figure 4-23, the excess rolling resistance force should be calculated. For this reason, the IRI=0 is considered as the base line. Figure 4-24 shows the results of this comparison.

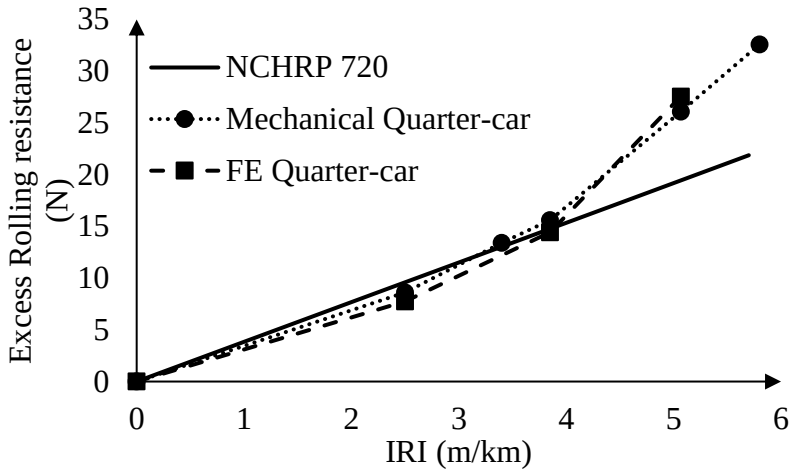

Figure 4-24.Comparison of the effect of IRI on rolling resistance of a car for quarter-car FE model and previous studies.

It can be seen that the three models are in a good agreement. The FE quarter-car model shows a non-linear trend with IRI similar to the mechanical model. The results from the three models match very well for IRI values lower than 4m/km. It should be noted that almost 93.5% of the road surfaces in the United States have IRI values less than 4m/km, where the results of all three studies are in good agreement (see Figure 4-25).

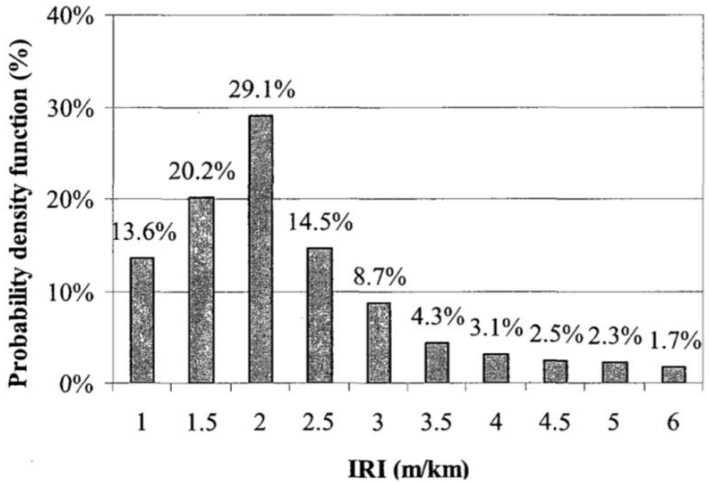

Figure 4-25. Histogram of the distribution of IRI in United states (Zaabar, 2010)

On the other hand, for IRI values higher than 4 m/km, the rolling resistance forces of the FE model and the mechanical quarter-car model start diverging from NCHRP 720 report results. It can be hypothesized that this difference may be due to the loss of contact between the tire and the pavement surface. To investigate this hypothesis, the vertical displacement of the rim centroid and the profile are compared with each other for IRI values below and above 4m/km (Figure 4-26 and Figure 4-27). The longitudinal forces at the rim centroid are also depicted in Figure 4-28 and Figure 4-29.

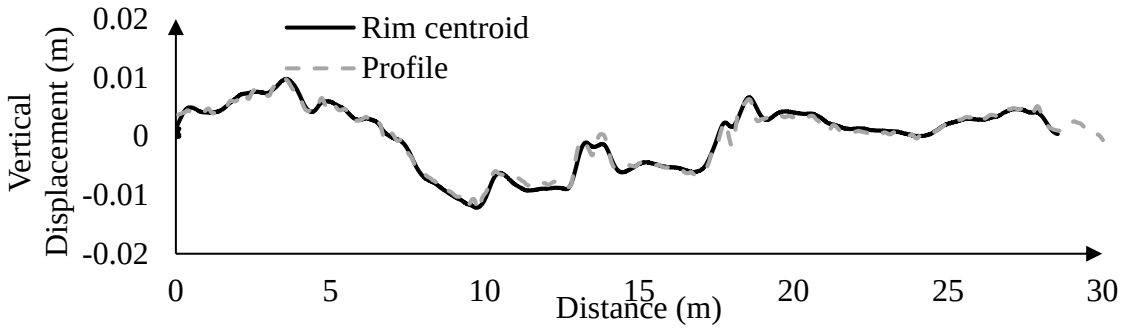

Figure 4-26. The vertical displacement of the rim centroid and the profile for IRI=3.3 m/km

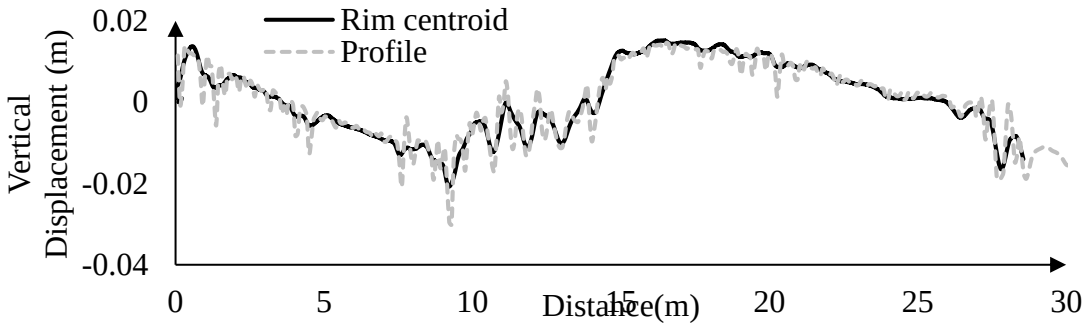

Figure 4-27. The vertical displacement of the rim centroid and the profile for IRI=5 m/km

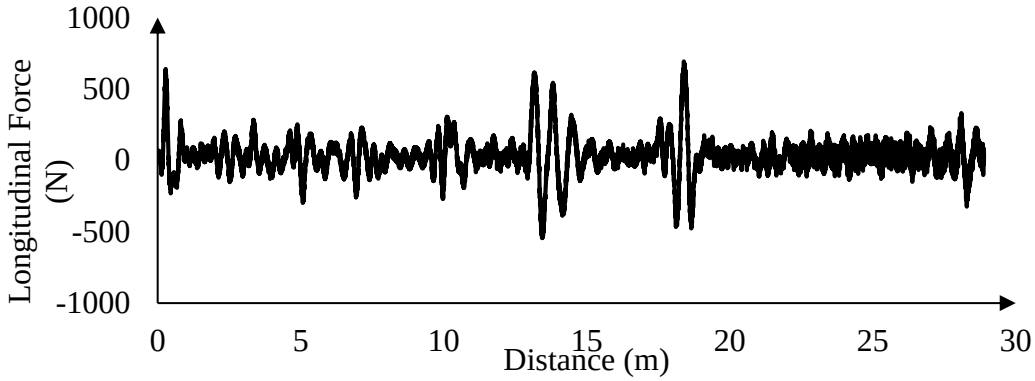

Figure 4-28. Longitudinal forces for IRI=3.3 m/km

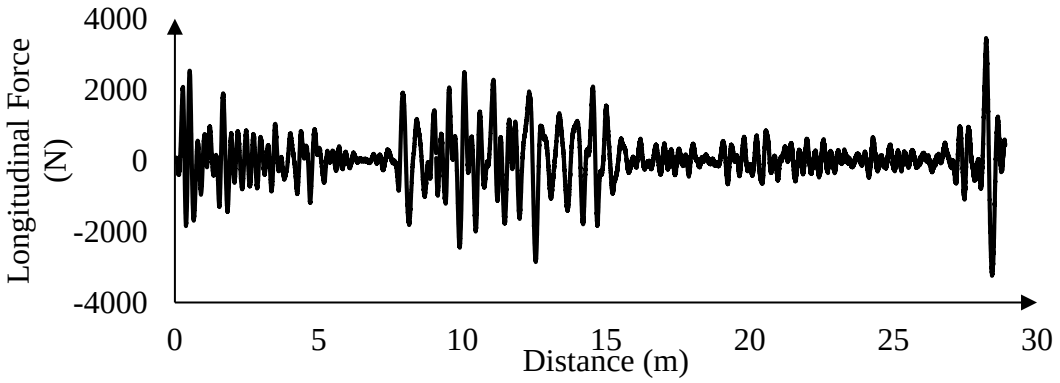

Figure 4-29. Longitudinal forces for IRI=5 m/km

As it can be seen in Figure 4-26 and Figure 4-27, for the profile with IRI= 3.3 m/km the vertical displacement of the rim centroid is very similar to the profile. However, for the profile with IRI=5 m/km, there are differences between the rim displacement and the profile. For the points where the profile is below the vertical displacement of the rim, the tire does not have contact with the profile. Therefore, there is a partial loss of contact at these points. For the points where the profile is above the rim displacement, the tire deformation is local, and their effect is evident on the longitudinal forces depicted in Figure 4-29. It is worth mentioning that even though the loss of contact is partial, a reduction in the longitudinal force can be observed at these points.

However, since no complete loss of contact is seen in these examples, it is not expected to have a reduction in the rolling resistance forces due to loss of contact. Therefore, the results of the FE quarter-car model are agreeing more with the mechanical model than the experiments.

It should be noted that the rolling resistance of the FE quarter-car model is a little higher than the mechanical quarter-car model (see Figure 4-24). This difference is due to the effect of mega-texture within the contact patch that is included in the FE model and excluded from the mechanical quarter-car model due to the enveloping of the profile.

4.10 IMPORTANCE OF VEHICLE OPERATING CONDITIONS ON ROLLING RESISTANCE

There are a few factors beside the geometry and material properties of the tire and suspension that affect the rolling resistance of the vehicle. For example, the vehicle's mass and velocity, and the tire's inflation pressure and temperature have been considered in different empirical studies as some of the factors that influence the vehicle's rolling resistance. The rolling resistance is expected to decrease by reducing the normal load on the tire and vehicle velocity and increasing the tire inflation pressure and temperature. In this section, the aim is to investigate the influence of these factors on the effect of surface profile on rolling resistance.

4.10.1 Effect of applied load on the influence of texture on rolling resistance of the vehicle

As the weight of the vehicle or normal load applied on the tire and suspension decreases, the tire deformation and displacement in the suspension decreases. As a result, it is expected that the rolling resistance of the vehicle decreases. In this study, the effect of macro-texture on rolling resistance is found under two axle loads of 4100N (similar to Boere's study) and 3433 N (similar

to the mechanical quarter-car model), which are within the acceptable range for a medium car. The effect of macro-texture on rolling resistance is shown for both of these cases (see Figure 4-30).

As it can be seen in the figure, the rolling resistance coefficient at zero RMS decreases by decreasing the normal load from 4100N to 3433N (a reduction of about 3.5%). Considering the absolute rolling resistance force values, decreasing the load by about 16.3%, a reduction of about 19% is observed in rolling resistance forces. This result is in agreement with other studies which suggest similar changes in rolling resistance force with respect to variations in normal load (Hernandez, 2015).

However, comparing the effect of macro-texture's RMS on RRC in these two cases, it can be seen that decreasing the normal load by 16.3% only causes a very small change in RMS-RRC relationships, since the slope of the two relationships are very similar.

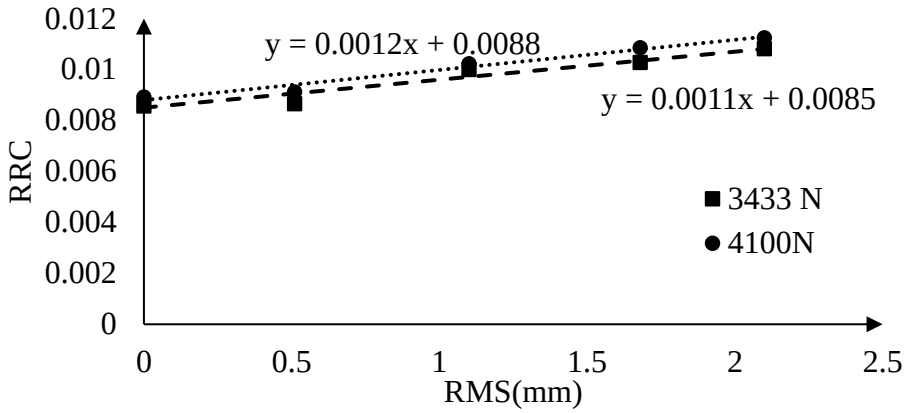

Figure 4-30. Effect of applied load on variation of rolling resistance with surface macro-texture

Therefore, it can be concluded that although the normal load affects the absolute RRC value, it does not affect the variation of rolling resistance with texture (i.e., the effect of texture on rolling resistance).

4.10.2 Effect of velocity on the influence of texture on rolling resistance of the vehicle

The results presented so far correspond to a vehicle velocity of 80km/h. As the velocity decreases, the rolling resistance on a smooth surface is also expected to decrease. The variation of RRC is assumed to be higher for higher speeds (see Figure 4-31).

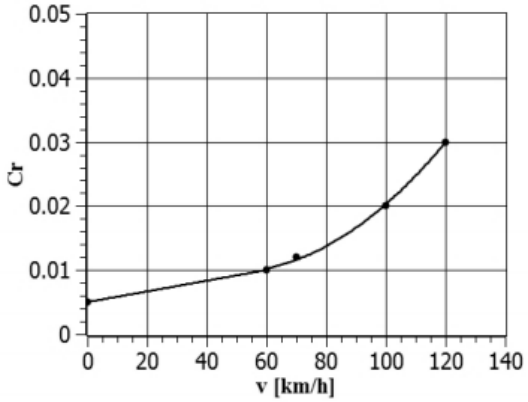

Figure 4-31. Effect of speed on rolling resistance coefficient (Mozharovskii et al. 2007)

In this section, the RRC is obtained for vehicle velocities of 20, 55, and 80 km/h on a smooth surface (see Figure 4-32). A similar trend is observed.

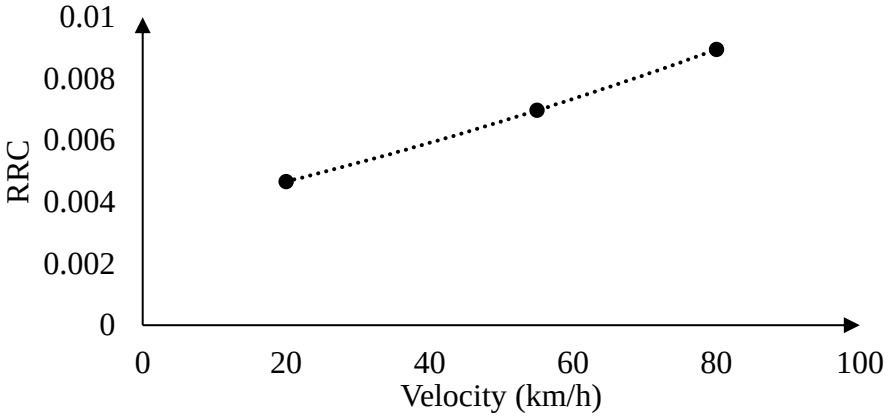

Figure 4-32. Variation of rolling resistance coefficient by velocity on a smooth surface

In previous sections, the effect of mega-texture on rolling resistance was found to be more pronounced than the other two scales. Therefore, evaluating the effect of velocity on the relationship between surface profile and rolling resistance, mega-texture surfaces with RMS values of 1.1, 4.4, and 6.6 mm are used.

The quarter-car FE model is rolled over the surface profiles with a velocity of 55km/h (15.2778 m/s) and the results are compared with those at 80km/h (22.224m/s). Figure 4-33 shows the effect of mega-texture on RRC for the tire and quarter-car FE model at 55km/h velocity.

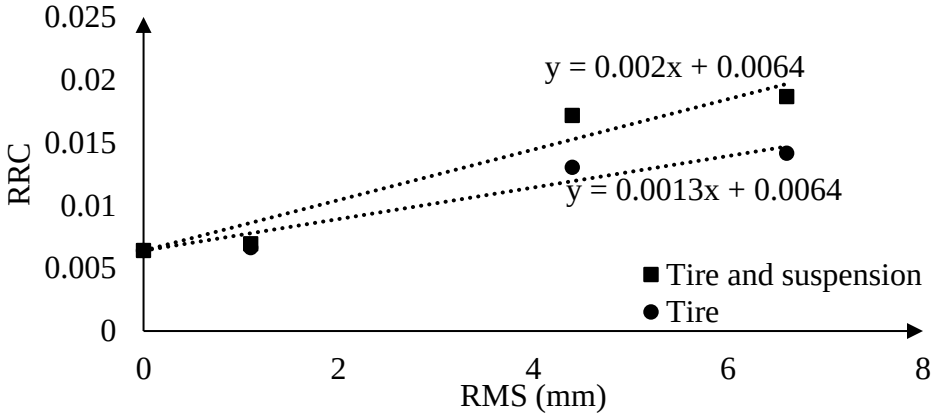

Figure 4-33. Effect of mega-texture on rolling resistance coefficient at V=55km/h

Comparing these results with those from Figure 4-5, it can be seen that by decreasing the vehicle velocity, the effect of mega-texture on tire rolling resistance is decreased, while the effect of suspension is increased. The increase in the suspension's effect is because energy dissipation in the suspension (D_s) has a reverse relationship with vehicle velocity (V):

$$D_s = \frac{C_s}{V} E[\dot{z}_s^2] \qquad \text{eq. 4-9}$$

where $\dot{z}_s$ is the relative velocity in suspension.

Therefore, although the average relative velocity in the suspension is decreased, for the given mega-texture profiles, this reduction is less than the reduction caused by the vehicle velocity. Figure 4-34 shows the comparison between the rolling resistance coefficients of the quarter-car FE model at 55 and 80 km/h velocities.

It can be seen that the RRC at 55km/h is lower than that at 80km/h, but the slope of the line is very similar. Therefore, it can be concluded than the rolling resistance coefficient is reduced by decreasing the vehicle speed; however, vehicle speed does not affect the variation of rolling resistance with texture (i.e., the effect of texture on rolling resistance).

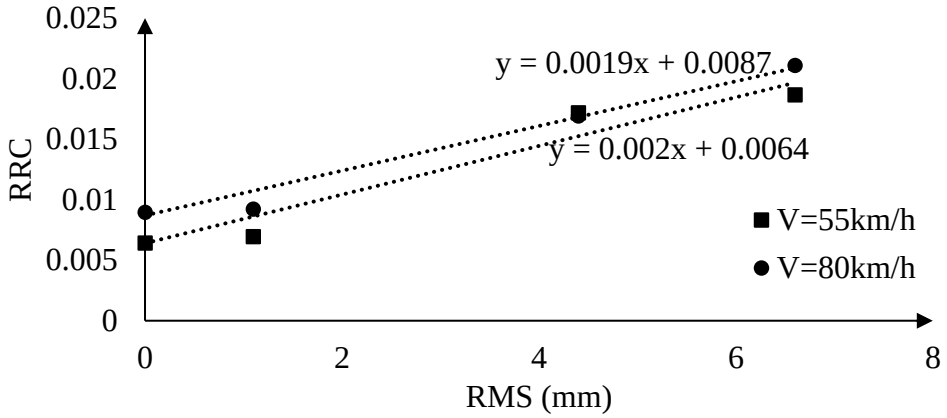

Figure 4-34. Effect of vehicle velocity on variation of rolling resistance with RMS of surface mega-texture

4.10.3 Effect of temperature on the rolling resistance of the vehicle

As the temperature within a tire increases, the stiffness of the rubber material changes. A lower loss modulus for the rubber material results in a lower rolling resistance. Furthermore, the tire temperature increases with increasing velocity. Changing the temperature within the model is possible if thermo-mechanical material properties are used. In this study, such material properties were not available. Therefore, in order to include the effect of temperature variation in the model, the rubber material properties are modified to the corresponding values for a given temperature. As it was mentioned in Section 3.2.1, for including the temperature's effect on material properties, the coefficients of the Prony series can be changed. The original coefficients are obtained from experiments performed at 23°C. Considering that by increasing the velocity to 80 km/h the temperature within the tire can rise to 74°C (explained in section 3.2.1,), the Prony series coefficients are changed accordingly. The effect of temperature on the rolling resistance forces was investigated for two profiles: (1) smooth surface with RMS=0 mm and (2) mega-texture surface profile with RMS=4.4 mm. Table 4-5 shows a summary of the variation of rolling resistance force and coefficient with changes in temperature for these two profiles.

As it was expected, the rolling resistance slightly decreases by increasing the temperature. The results show that the effect of temperature on the smooth surface is more than on the textured surface for the given profile. Variation of tire temperature also affects the inflation pressure of the tire. Therefore, any considerations for the temperature should also include the changes in the inflation pressure.

Table 4-5. Summary of effect of temperature on rolling resistance of the tire

Profile	RMS (mm)	Temp (°C)	RRF (N)	RRC	Difference
1	0	23	30.7	0.0087	3% decrease
1	0	74	29.78	0.0086	
2	4.4	23	49.42	0.00144	0.2% decrease
2	4.4	74	49.30	0.00143	

4.10.4 Effect of inflation pressure on the rolling resistance of the vehicle

The changes in the temperature of the tire affect the tire inflation pressure. Rising the temperature within the tire increases the inflated air temperature and correspondingly its pressure. The effect of tire inflation on energy dissipation is known to be more than the effect of temperature itself.

Different parts of the tire usually have different temperatures, but some studies suggested that the temperature of the inflated air is similar to the one of the tire shoulders (Nielsen and Sandberg, 2002 and Janssen and Hall, 1980).

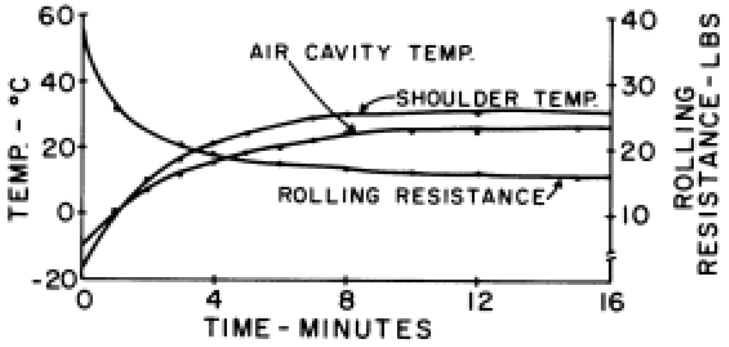

Figure 4-35. Inflated air temperature variation with tire shoulder temperature (Janssen and Hall, 1980)

The suggested temperature for the tire shoulder in different studies is around 50 ^{o}C (Nielsen and Sandberg, 2002; Lin and Hwang, 2004). Some studies suggested a 10 Kpa increase in tire inflation pressure for every 10 °C increase in the air temperature (Schuring, 1985).

As the inflation pressure increases, the contact area between the tire and the surface decreases, and the stiffness of the tire increases, which reduces the tire deformation. Therefore, less rolling resistance is expected within the tire. Figure 4-36 depicts the variation of rolling resistance with tire inflation pressure at a velocity of 60 mph (Schuring, 1985).

As it can be seen, the relationship is non-linear when we can consider the entire range for inflation pressures (changing from 10 psi to 65 psi). However, the common inflation pressure for passenger car tires is usually between 30 to 35 psi (200 to 240 kPa) and pressures as high as 65psi or as low as 10psi do not occur in normal conditions. Therefore, in this section, only the variation of the inflation pressure within the common range of 200 kPa to 240 kPa is considered. Figure 4-36

shows an average decrease of about 7% in rolling resistance for a 10% increase for this range of tire pressure at 60 mph.

In this study, the inflation pressures of 200, 210, and 240 kPa are considered and the rolling resistance in each condition is calculated on a smooth surface at 80km/h velocity. Figure 4-37 shows the variation of rolling resistance forces and coefficients by changing the inflation pressure from 200 kPa to 240 kPa on a smooth profile (RMS=0). The results show a linear relationship, which can be due to the narrow range that is considered for the variation of the inflation pressure.

In Figure 4-36, also, although the whole trend is nonlinear, a linear relationship can be assumed between 30 and 35 psi inflation pressures. In addition, in the FE model, the rolling resistance coefficient decreases by 8.5% for a 10% increase in inflation pressure, which is close to the results shown in Figure 4-36.

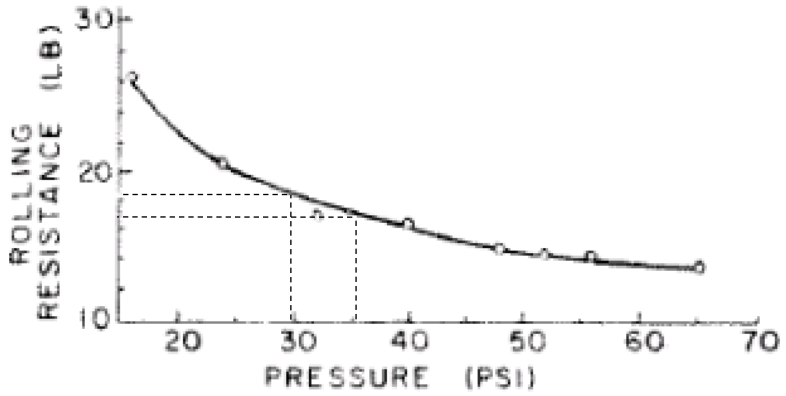

Figure 4-36. Relationship between tire inflation pressure and rolling resistance (Schuring, 1985)

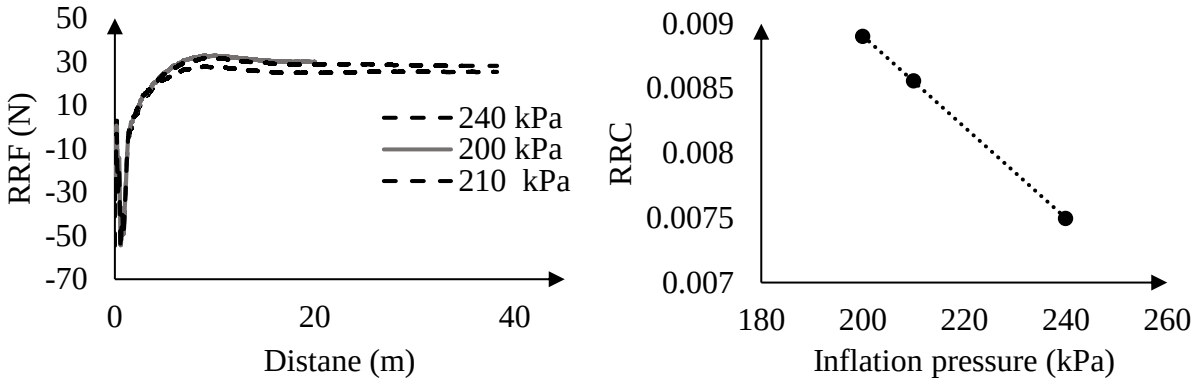

Figure 4-37.Effect of inflation pressure on rolling resistance force and coefficient on a smooth surface at 80km/h

In addition to the smooth surface, the mega-texture profiles with RMS of 1.1, 4.4 and 6.6 mm used in the previous sections are selected to investigate the variation of texture-induced rolling resistance with variation of the inflation pressure. To observe the effect better, the maximum inflation pressure of 240 kPa is considered.

Figure 4-38 shows the comparison between the effect of texture on rolling resistance coefficient for two inflation pressures of 200 and 240kPa. As it can be seen, the slope of the RRC-RMS relationship has not changed by changing the inflation pressure. Therefore, it can be concluded

that although the inflation pressure affects the energy dissipated within the tire in the smooth surface condition, it doesn't influence the effect of texture on rolling resistance.

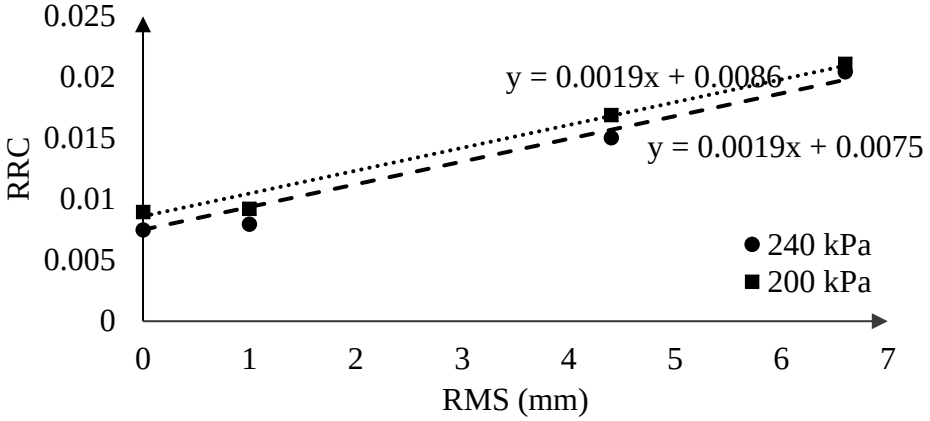

Figure 4-38. Effect of inflation pressure on variation of rolling resistance by surface mega-texture at 80km/h

CHAPTER 5
SUMMARY, CONCLUSIONS, AND FUTURE WORK

5.1 SUMMARY

Pavement surface profile is one of the factors that can influence the rolling resistance of the vehicle. There are different mechanisms involved in the rolling resistance, namely, vehicle dynamics, tire bending and deformation, and tread deformation. The surface profile can be divided into four scales of roughness, mega-, macro-, and micro-texture. These scales influence different mechanisms of the rolling resistance. The effect of micro-texture, which includes wavelengths smaller than 0.5 mm, is known to be negligible on vehicle rolling resistance, but important in surface friction and road safety. The macro-texture scale, wavelength between 0.5 mm and 50 mm, affects the tread deformation and tire bending. The mega-texture scale, wavelengths between 50 mm and 500 mm, includes both wavelengths within and beyond the tire contact patch. Therefore, in addition to the tire deformation and bending, it also affects the vehicle dynamics and deformation in the vehicle's suspension system. The roughness scale consists of any wavelengths larger than 500 mm. Hence it is expected to mostly affect the rolling resistance within the suspension of the vehicle. The main purpose of the study is to determine the effect of these scales of profile (roughness, mega-, and macro-texture) on the vehicle's rolling resistance.

To capture the effect of the profile on tire deformation, including tire bending and tread deformation, a full 3D finite element tire model is developed and verified. For investigating the influence of the profile on the energy dissipation in the vehicle suspension system, the tire model is combined with a quarter-car mechanical model. Such a model is a simplified vehicle suspension system, comprised of a spring and a dashpot in parallel. These two models are capable of evaluating the effect of different scales of the surface profile spectrum on rolling resistance of the vehicle.

The surface profile is decomposed into the above-mentioned scales. For a robust comparison of the effect of these scales, a common parameter should be considered for surface profile characterization between these scales. For surface texture characterization, the mean profile depth (MPD) is usually used, which is based on the texture variation within a 10 cm length of the profile. However, since the roughness affects the suspension of the vehicle, for its characterization, IRI index is used. This index is related to the vertical displacement within the suspension induced by the surface profile. Since the mechanisms involved in the definition of these two parameters are totally different and not applicable for one another, the root mean square of the profile at each scale is considered as the common parameter.

A FE tire model is used for evaluating the effect of macro-texture on rolling resistance, while the quarter-car FE model is used for the mega-texture and roughness scales.

In addition to evaluating the effect of different scales on rolling resistance of the vehicle, some of the shortcomings in the current state of the art are also addressed using the developed models.

Moreover, the influences of vehicle operating conditions including applied load, driving velocity, and tire temperature and inflation pressure on the effect of surface profile on rolling resistance are investigated.

5.2 CONCLUSIONS

The following conclusions are drawn based on the presented analysis and results.

5.2.1 Effect of individual scales of the surface profile on rolling resistance

The effects of each individual scale of the pavement profile (macro-texture, mega-texture, and roughness) are investigated and the following conclusions are obtained:

- On the effect of macro texture profile on rolling resistance of the tire, the analysis shows that a linear relationship exists between the macro-texture RMS and rolling resistance coefficient (RRC) of the tire. The obtained results are similar to the experimental results by Boere (2009). However, the FE model slightly overestimates the influence of macro-texture on RRC, which can be because of the differences between the model and the experimental study, such as simplifications and assumptions within the developed model.
- The effect of macro-texture on the suspension of the vehicle is also investigated. The quarter-car FE model shows that the surface macro-texture mainly affects the deformation within the tire and its effect on suspension can be neglected.
- In comparison of the relationship of the two surface characterization parameters of RMS and MPD with tire RRC, MPD shows a slightly better correlation than RMS.
- Mega-texture profile affects the energy loss both within the tire and the suspension system. For smaller RMS values, similar to the macro-texture, the effect of the mega-texture on the suspension of the vehicle is negligible. Although for rougher mega-texture, the energy dissipation in the suspension is more noticeable, the rolling resistance within the tire is still higher. The mega-texture-induced rolling resistance in the suspension can be as high as 23% of the total rolling resistance.
- The relationship between RMS and RRC for mega-texture is found to be better than that between RRC and IRI. This can be related to the exclusion of the lower portion of mega-texture spectrum from IRI calculation.
- The mega-textures within the contact patch (wavelength smaller than 250 mm), influence the rolling resistance in both tire and suspension and its effect on the tire energy dissipation is more significant than the suspension.
- The effect of roughness profile on the total rolling resistance is found to be lower than the one for mega-texture. However, its effect on suspension is more pronounced than mega-texture and it can be as high as 45% of the total rolling resistance.
- Roughness-induced RRC is found to have a strong non-linear relationship with IRI.

5.2.2 Comparison of the rolling resistance of different scales

The results for the different scales are compared with each other:

- For low RMS values (less than 2 mm), i.e., low amplitudes, all of the scales show similar results and there is not a big difference between the effect of different wavelengths. Also, the profiles of different scales in this range barely affect the suspension. However, for higher RMS values, mega-texture shows a higher rolling resistance than roughness. This means that for higher amplitudes, lower wavelengths affect the rolling resistance more.

- Mega-texture profile affects the rolling resistance in the tire much more than the suspension. However, the effect of roughness on rolling resistance in the suspension can be in the same order as that in the tire.
- High values of RMS for mega-texture can be related to local events in the road profile and therefore they only appear a few times within a longer profile length. In an investigation of the importance of the frequency of occurrence of high mega-texture within the profile, it is found that the mega-texture can affect the rolling resistance of the vehicle, even when the events are isolated.

5.2.3 Comparison of the finite element results with empirical studies

The influence of macro-texture on the rolling resistance as predicted by the FE model is compared with a few empirical studies, namely the NCHRP 720 report, the MIRIAM project, and the results reported by Boere. NCHRP 720 report and the MIRIAM project are based on the energy dissipation of the vehicle and there is a significant difference between their results. Boere's study on the other hand measured rolling resistance directly using a trailer. Here, the three studies are compared with the developed FE model:

- The results show that considering both the initial rolling resistance (on the smooth surface) and the effect of texture on rolling resistance, the NCHRP 720 results are closer to those from Boere's study than the MIRIAM project.
- The results of the developed FE model in this study are closer to those from Boere's study than the other two studies.

Most of the available studies on the effect of roughness have not differentiated between roughness and mega-texture scales and evaluated the effect of IRI on rolling resistance. The empirical model presented in NCHRP 720 report and a mechanical quarter-car model by Zaabar et al. (2018) are compared with the results of the FE model.

- The FE quarter-car model and the mechanical model show a non-linear trend with IRI, while NCHRP 720 has a linear relationship.
- The excess rolling resistance forces from the three models match very well for the lower IRI values (IRI<4m/km), which represents the majority of the IRI values for pavement surfaces in the US. For IRI values higher than 4m/km (about 6.5% of the pavement surfaces in the US), the rolling resistance forces of the FE model diverges from NCHRP 720 report results, while being reasonably close to those from the mechanical quarter-car model.

5.2.4 Importance of vehicle operating conditions on rolling resistance

Besides the geometry and material properties of the tire and suspension, other factors related to the vehicle operating conditions, such as the vehicle's mass and velocity, and the tire's inflation pressure and temperature affect the rolling resistance. The effect of these factors on the texture-induced rolling resistance is investigated in this study and the following conclusions are obtained:

- The vehicle weight or the normal load applied on the quarter-car model, affects the absolute value of rolling resistance. Decreasing the load, reduced the rolling resistance. However, the variation of the load does not influence the effect of texture on rolling resistance.
- While the tire rolling resistance is reduced by decreasing the velocity, the rolling resistance in the suspension is increased for the range considered. But the total, combined rolling

resistance is reduced by decreasing the velocity. In addition, the velocity does not affect the variation of rolling resistance with texture.

- The rolling resistance slightly decreases by increasing the temperature. The effect of temperature on the smooth surface is found to be more than the textured surface for the given profile.
- Variation of tire temperature affects the inflation pressure of the tire. Increasing temperature increases the tire inflation pressure and reduces the contact area between the tire and the surface as well as the tire deformation, and as a result the rolling resistance. However, it does not influence the effect of texture on rolling resistance.

5.3 FUTURE WORK:

- RMS is a statistical parameter and may not be the best parameter for characterizing the surface profile and capturing the effect of profile on rolling resistance of the vehicle. Another parameter that also includes the frequency of the high amplitude texture or roughness can be more beneficial.
- The current cut-off wavelength for the effect of pavement texture on displacement in the vehicle suspension and also IRI calculation is considered as the contact patch length (250 mm). However, the results of the study show that the mega-texture profile within the contact patch also affect the suspension of the vehicle. Therefore, further investigation is required for finding a new cut-off wavelength for the effect of texture on vehicle suspension.
- The developed FE model allows the tire to lose contact with the profile if necessary. This loss of contact occurs in reality, especially in rough surfaces. However, although when the tire does not have contact with the surface, the resisting forces within the tire are minimum, the impact with the surface after contact can increase the rolling resistance. Therefore, the effect of this loss of contact is not understood fully and it should be investigated further.
- It is also beneficial to further investigate the effect of operating conditions, including the interaction of velocity (within the city and on highways), temperature and tire inflation pressure on the effect of texture and roughness.
- The pavement surface is considered as rigid in this study and the deformation of the pavement under the load is neglected. Further investigation into the effect of two-way interaction between the vehicle and pavement (considering the deformability of both tire and pavement) can be beneficial, especially for chip seal surfaces.

APPENDIX A- LITERATURE REVIEW ON EFFECT OF PAVEMENT SURFACE MICRO-TEXTURE ON FRICTION

Friction is a macro-scale empirical representation of a multi-scale deformation mechanism which results from three parallel phenomena; adhesion, hysteresis, and shear (Figure A1-1).

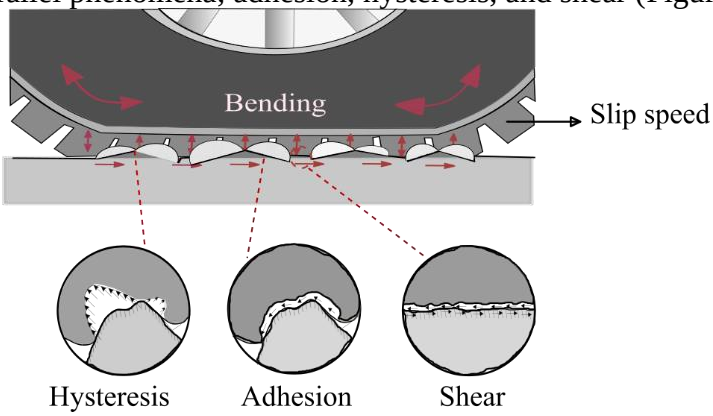

Figure A1-1. Friction mechanism

Adhesion is induced by interlocking and bonding of rubber compound to pavement surface. In the exposure of micro-asperities and irregularities of tire and pavement surfaces to each other, an attractive force due to Van der Waals or dipole forces keeps the two materials together and prevents their movements (Dewey et al., 2001, Persson, 1998). Adhesion is a function of the contact area and the shear strength of the contact surface (Hall et al., 2009).

Hysteresis, or internal friction, is a multi-scale phenomenon which highly influences the overall response of tires ranging from friction and noise to rolling resistance. It results from the viscoelastic response of the rubber material to the cyclic loading. Thus, the bulk deformation of the rubber and the deformation of the tire tread due to engaged texture yields hysteresis (Hall et al., 2009, Choubane et al., 2004, Lindner et al., 2004).

Defining the cascade of hysteresis in tire-pavement contact, three separate length-scales can be identified and associated to (i) tire deflection and bending, (ii) tread slip, and (iii) tread surface deformation (Bendtsen, 2004, Xiong and Tuononen, 2013).

The shear force of a rigid surface in contact with another material is small, and thus negligible. However, in the presence of a fluid scattered between the two surfaces, the shear force, which is mainly induced by the viscosity of the fluid, is more significant. The viscosity of water is less than snow, which leads to (i) lower shear forces in the contact area, and (ii) faster escaping rate of water from within the contact area and correspondingly smaller shearing contact area in comparison to the presence of snow. Therefore, the role of shear in friction between tire and rigid pavement is usually neglected except in the existence of snow (Hall et al., 2009). The contribution of friction components at different environmental conditions is depicted in Figure A1-2 (Hall et al., 2009).

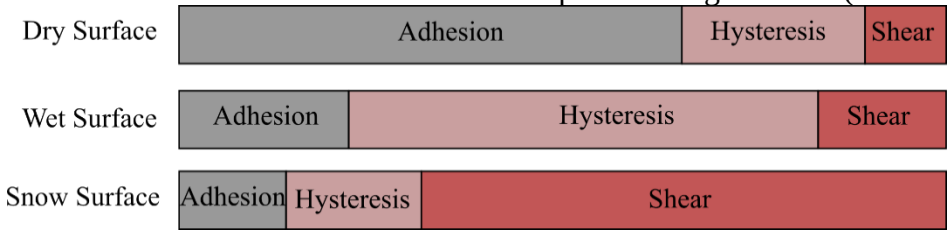

Figure A1-2. Compositions of Major influences on braking slip conditions (Hall, 2009)

Hysteresis is correlated to the volume of the deformed material and adhesion to the contact area (Kummer, 1966, Do and Marsac, 2015). Therefore, these phenomena are governed by characteristics of the pavement surface, the tire properties, and the loading conditions due to environmental factors and vehicle performance (see Table A1-1).

In contrast to macro-texture, the contribution of micro-texture to adhesion is more significant than to hysteresis (Leu and Henry, 1978, Henderson et al., 2006, Hall et al, 2009). Nevertheless, there is a difference between the hysteresis of these two textures. The hysteresis of macro-texture contributes to rolling resistance and noise, in addition to friction (Bendtsen, 2004). However, the micro-texture mainly affects friction (Boere, 2009).

Beside the surface texture, the friction depends on other factors among which sliding velocity, temperature, normal load, and presence of contaminations are the most prominent ones. In the following, the influence of these factors on the contribution of surface texture to friction will be discussed. These factors are not necessarily independent of each other.

Table A1-1. Important factors in pavement friction (after Hall et al., 2009)

Pavement surface characteristics	**Vehicle Operating Parameters**	**Tire Properties**	**Environmental factors**
▪ **Surface-texture** ▪ **Material properties** ▪ Temperature	▪ **Slip speed** **(**Vehicle speed, Braking action) 1. Driving maneuver (Turning, Overtaking)	▪ **Tread design and condition** ▪ **Inflation pressure** ▪ Tire Foot print ▪ Rubber composition and hardness ▪ Load ▪ Temperature	▪ Climate (Wind, **Temperature, rainfall and condensation, Snow and Ice)** 2. **Contaminants** like: Anti-skid material (salt, sand), Dirt, mud, debris)

Note: Critical factors are shown in bold.

The velocity of the vehicle influences the role of surface texture in friction by affecting the viscoelastic behavior of the tire. In tire-pavement interaction, two velocities of free rolling (static) and sliding velocity during cornering or ABS-braking (kinetic) are involved. The velocity of rolling tire directly influences the viscoelastic properties of the rubber. As the velocity increases the rubber becomes stiffer. Therefore, the contribution of different surface textures in friction varies with vehicle speed and the deformation rate (Persson, 2001). The influence of micro-texture on friction is more at lower speeds (soft tread) while the one of macro-texture is more at higher speeds (stiff tread) (Dewey et a., 2001, Hall et al., 2009). The changes in the engagement of textures affect the contact area between the tire and the pavement surface and thus the friction

coefficient. At higher velocities, the contact area decreases due to the reduction of the engaged texture (Persson, 2001).
Temperature affects the viscoelastic properties of the rubber, similar to velocity. The tire pressure increases with temperature and consequently, the area of contact and the friction decreases (Lin and Wang, 2004).
Bazlamit et al, (Bazlamit and Reza, 2005) suggested that the decrease in hysteresis due to the increase in temperature occurs in all surfaces with different textures. But, the effect of surface texture on adhesion is more dominant in comparison to temperature. However, there are still some challenges in understanding the effect of temperature on the friction since the temperature in friction measurements are influenced by friction test method, pavement type, and climate (Flintsch et al., 2012)
Considering the effect of normal load on friction, increasing the load leads to an increased contact area due increase in the engaged texture. Whilst, the rate of penetration is defined by the rubber stiffness. The relationship between the applied load and the contact area is the topic of many recent theoretical studies (Heinrich and Klupple, 2008, Persson, 2001, Persson, 2002, Klupple and Heinrich, 2000). Most of the available theories define this relationship to be linear when the contact area in comparison to nominal contact area is small. As the load increases the area approaches to the nominal contact area in a continuous manner (Persson, 2006).
However, representing the contact to be similar to the real contact between a solid and a rough surface, and also considering the coupling of adjacent asperities under a reasonable load has been a challenge (Archard, 1957, Greenwood, 1966, Bush et al., 1975, Persson, 2006). Such a relationship has been developed by Persson (Persson, 2001).
Contaminations also influence the role of surface texture in friction. As an example, in the presence of water the contact zone is divided into three zones: (i) tire lifting zone, (ii) thin water film zone, and (iii) full contact zone (Figure A1-3) (Moore, 1975). Since the friction force is only generated in the full contact zone, there is a reduction in friction due to the decrease in contact area. Surface micro- and macro-texture along with tire tread help the water to escape through the contact surface and therefore they could increase the contact area (Do and Cerezo, 2015). At high speeds, the available time for water evacuation decreases, thus, the loss of friction becomes more significant. If there is no contact maintained between the tire and the surface, aquaplaning[3] occurs.

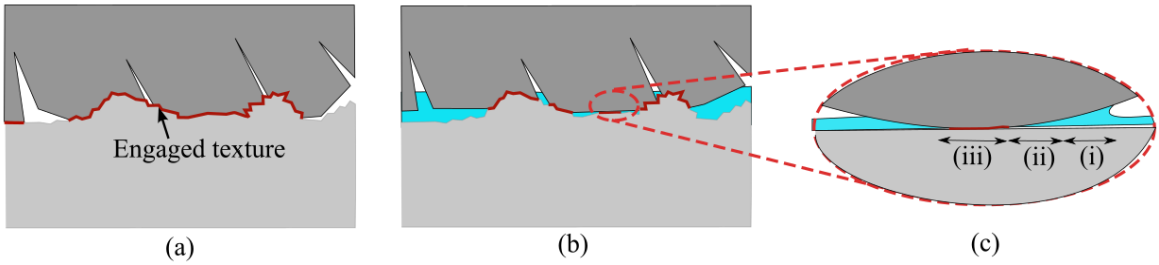

Figure A1-3. Effect of water presence on contact area (a) contact without water, (b) contact in presence of water, and (c) contact zone

Similarly, other contaminants (such as dust and dirt particles) decrease the friction because they prevent the contact between the tire tread and the smallest micro-textures of the surface. This effect

[3] Aquaplaning occurs when enough water is trapped under the tire tread at high speeds to detach the entire tire tread from the pavement surface.

is more significant on adhesion component since the influence of micro-texture on adhesion is more dominant than hysteresis. Therefore, adhesion is usually assumed to be important on clean and relatively smooth surfaces (Persson, 2001). It worth mentioning that in presence of detergents the friction coefficient is even less since they prevent the direct contact at the interface.
Grosch (Grosch, 1963) investigated the effect of dust, water and detergent on friction coefficient as depicted in Figure A1-4.

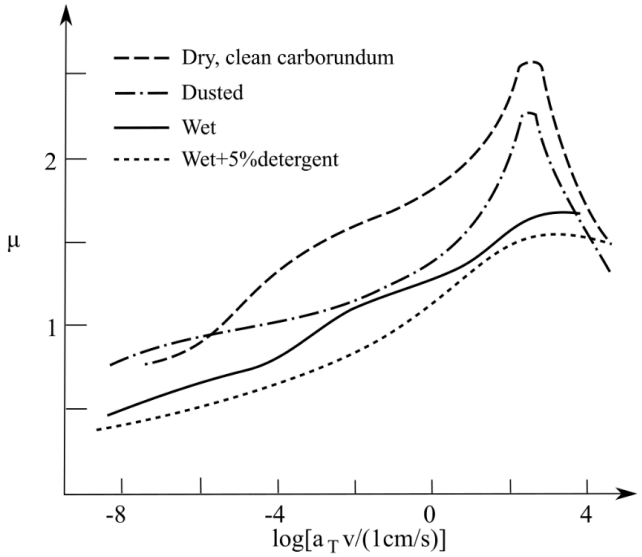

Figure A1-4. The kinetic friction coefficient for rubber sliding on a carborundum surface under different conditions (Grosch1963)

- **Friction Measurements**

Friction measurement devices are founded on the principle of rubber sliding over the wet surface and the measurement of the resistance force. These devices follow different measurement mechanisms depending on the type of the measured friction force, the performance speed, and the slip ratio of the tire. The two different frictional forces measured with these devices are (i) longitudinal and (ii) lateral frictional forces, which help the driver to control and maneuver the vehicle safely. The longitudinal forces occur between the tire and the pavement surface when it is moving in the longitudinal direction in the free rolling or constant-braked mode. The lateral friction forces occur when the vehicle is changing direction or moving on a cross-slope road or facing a cross-wind effect.
Most devices are capable of measuring friction at various speeds up to highway limit. Some of them can even perform in variable slip ratio of the tire. Other factors can also influence the friction measurements, such as tire loading, size, tread design and construction, and inflation pressure. For controlling these tire-related factors standard tires are used after ASTM E501.
So far, there is no well-accepted universal friction measurement approach. The popular approaches vary depending on the region (Wallman et al., 2001). Here, the most popular friction measuring devices are reviewed.

i. Stationary devices

The two devices that are used commonly for friction measurement at low speeds (which require the traffic to stop) are British Pendulum Tester (BPT) (AASHTO T 278 or ASTM E 303) and the Dynamic Friction Tester (DFT) (ASTM E 1911). In these devices, a slider (pendulum or rotating

disc) slides over the pavement surface at a specific speed. The friction between the slider and the surface forces the slider to slow down. This friction is then measured tracing the dissipation of the kinetic energy of the slider which is governed by a decrease in the momentum of the pendulum or the disc (Hall et al.,2009). A good agreement has been found between the coefficient of friction of the DFT and the British Pendulum Number (BPN) at different speeds (Saito et al., 1996). The results of these methods are usually attributed to micro-texture of the surface because the effect of micro-texture on friction is more dominant at lower speeds.

ii. Pulling devices

The friction measurement devices which can work at higher speeds are mostly categorized in four groups of locked-wheel, fixed-slip, variable-slip and sideway-force or cornering mode. The locked-wheel devices measure the friction when the tire is moving in the vehicle direction, the wheels are locked, and the slip ratio is 100%. The friction in fixed-slip devices is measured in vehicle direction and constant slip ratio up to 20%, similar to anti-lock braking condition. The variable-slip devices are capable of measuring the frictional force at predetermined slip ratios in vehicle direction. In sideway-force devices, there is a constant angle between the tire and the vehicle direction which is necessary to assess the rotational resistance and the controlling ability of the vehicles in curves at constant slip ratio (Nordstroem, 1998).

Among these devices locked-wheel (ASTM E 274) is widely used in the U.S. (Choubane et al., 2004). It characterizes the friction by a friction number (FN) that depends on the tire velocity, the horizontal and the vertical loads and the friction coefficient (Henry, 2000, Hall et al.,2009).

Despite being popular, locked-wheel devices have limited performance due to the required long distance between two readings. These devices provide only one reading of friction over a long distance. Also, the locked-wheel condition is not a proper representation of the braking condition of the current vehicles equipped with ABS systems. Therefore, continuous friction measuring equipments (CFME) (ASTM E2340) as slip-wheel devices (fixed-slip or variable-slip) are more preferable, e.g. Grip tester (Najafi et al., 2013). These devices can measure the friction in higher frequencies and operate similarly to the ABS systems with a critical slip ratio of 10-20%. However, still, the current CFME devices are not able to measure the lateral friction at curves.

The ability of these devices to measure the friction at various speeds, is useful for investigating the effect of velocity on friction (Hogervorst, 1974, Noyce et al., 2005, Matilainen and Tuononen, 2012). At higher speeds, friction is mainly governed by hysteresis while at lower speeds, it is governed by adhesion (Masad et al., 2009). Accordingly, it could be possible to find the contribution of hysteresis and adhesion by performing friction test at different speeds.

The main limitation of the high-speed friction measurement devices is the consumption of a large amount of water for wetting of the surface (Ueckermann et al., 2015). Therefore, in the more recent friction measurement devices, the focus is on reducing the amount of required water as much as possible. The presence of water affects the measurements by reducing the engaged texture. Moreover, other factors such as temperature, speed of measurement, and age and wear of the rubber can affect the friction measurements, while being difficult to control during the measurement process. To address these limitations, the concept of contactless friction measurement based on optical texture measurements has been introduced. The method relates the surface texture measurements to the friction of the surface (Dunford, 2008). They are founded on the current friction prediction models based on surface data.

The tests presented here, evaluate friction by a friction coefficient or friction number, as a function of speed and tire load. Many equations have been developed by different studies to define the correlation between friction numbers and various factors such as surface texture, velocity, and

temperature (Bazlamit et al., 2005, Hall et al., 2009). Some studies developed models to correlate the results of different tests. Some of these correlations are presented in Table A1-2.
A schematic comparison of the pavement friction devices and their mechanisms are presented in Figure A1-5.
Theoretical studies on rubber-surface contact characterization use different devices to measure the friction. Lorenz et al. (Lorenz et al., 2011) developed a new instrument for validating their friction theory. It included a rubber block attached to an aluminum plate and a rough surface moving with a specific speed. Tension and compression load cells were used to measure the friction force in the interface. They used this device for measuring friction on concrete (Lorenz et al., 2011) and asphalt (Lorenz et al., 2013) surfaces.

Table A1-2. Correlation between different friction test results

Friction coefficients	Correlation	Validation	Author
BPN and DFT	DFT=0.0078 BPN	R=0.97	Steven_-2009
	BPN=57.9 DFT+23.1	R=0.86	henry2000
BPN and SN	SN_{40}= 0.862 BPN – 9.69	-----	Kissoff1988
	SN_0=1.32 BPN-34	R=0.95	henry1983
BPN and CST	BPN=179.67 CST	R=0.99	Steven_-2009
SN and Mu	Mu_{40}=1.21 SN_{40}^{a}-14.9	R=0.99	burns1973
	Mu_{40}=2.14 SN_{40}^{b}-17.8	R=0.92	burns1973
SN and SFC	SFC_{50}=0.388 $SN_{80}^{1.425\ c}$	R=0.93	Henry1986
	SFC_{50}=1.52 SN_{80}^{d}-1.4	R=0.9	Henry1986

BPN: British pendulum tester, DFT: Dynamic friction tester, SN: Locked-wheel ([a] New Mexico Locked-Wheel, [b] California Locked-Wheel, [c] Stuttgarter Reibungsmesser, [d] Skiddometer BV 8), CST: California Skid tester (Stationary device), Mu: Mu Meter (Side-force), SFC: SCRIM tester (Side-force)

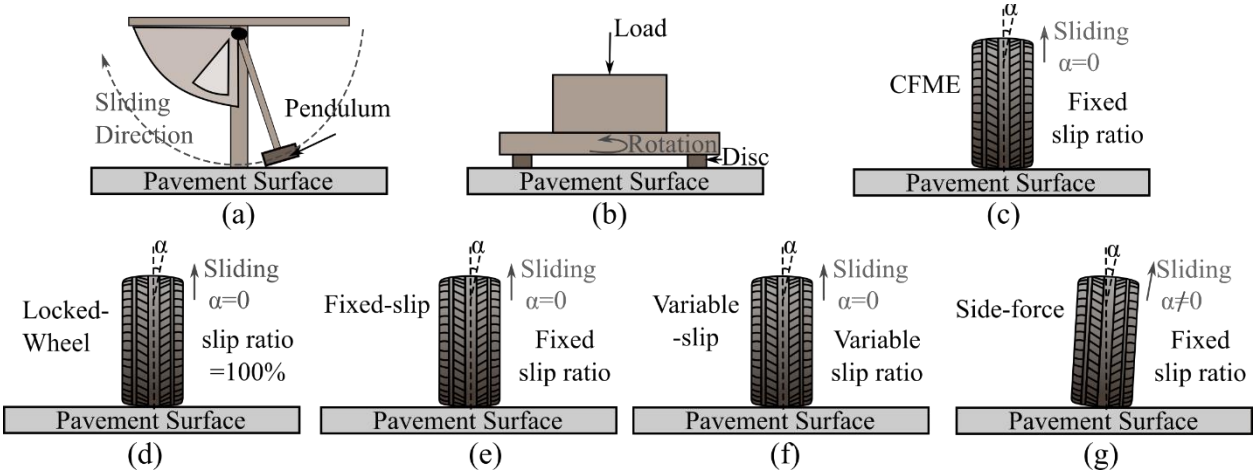

Figure A1-5. Friction measurement devices: (a) BPT (b) DFT (c) CFME (d) Locked-wheel (e) Fixed-slip (f) Variable-slip (g) Side-force

- **Texture-Friction Relationship**

Friction coefficient, μ, has long been known to be a function of the texture and adhesion of the contact surface. On the smooth surfaces, the friction coefficient can be attributed to adhesion.

On the rough surfaces, μ is attributed to deformation and hysteresis. In most of the existing studies the adhesion and hysteresis components of friction have been studied separately. While the surface texture directly influences the hysteresis, its contribution in adhesion is limited to the increase in the nominal surface area.

In pavement surface, micro- and macro-texture both affect the hysteresis, and consequently friction. While there are few models that can correlate the friction to the texture, it remains a challenge to define the exact geometrical parameters that contribute to friction.

The complexity of tire-pavement interaction, lack of detailed texture profiles, and in compatibility of tire and pavement models makes the development of a multi-scale contact model for predicting the pavement friction difficult (Li et al., 2005). Existing contact models are mostly phenomenological and can be divided into three categories (i) tire models, (ii) theoretical contact models, and (iii) empirical or semi-empirical models.

The tire models and hysteresis contact models used for friction modeling are similar to the models for rolling resistance mentioned in section 2. However, in dry or poorly lubricated contacts, adhesion is also present due to the molecular interaction between the two surfaces. In the presence of adhesion, the breakage of the adhesive bonds in the contact interface in addition to adhesional friction, can also cause adhesional hysteresis. While few studies have incorporated the effect of adhesion into the contact problem (Persson et al., 2015, Busse et al., 2010), it remains a challenge to describe the friction as the result of concurrent hysteresis and adhesion mechanisms.

Theoretical Adhesion Models

If loading and unloading process occurs at a very low speed, rubber can be assumed elastic. Thus, some studies employed adhesion theories for elastic materials for the contact between rubber and rough surfaces (Carbone and Bottiglione, 2008, Persson, 2015). Among the existing elastic theories for adhesion, DMT theory (Derjaguin, 1934) and JKR theory (Johnson et al., 1971) have been used for this contact. In DMT theory, adhesion is considered as a force applied to the solid in addition to the normal force. The contact area is then defined by the classic theory of Hertz (Hertz, 1881). This theory includes the adhesion in non-contact zones near to the contact zone as well as the contact area and is valid for elastically hard solids which are weakly interacting with each other. However, in JKR theory, the adhesion is only limited to the extent of the contact area and the adhesional energy is defined as $U_{adh} = \Delta\gamma A$. In which γ is the work of adhesion, which represents the required energy for separation of a unit area of the interface between two materials. This theory is valid for elastically soft solids which are strongly interacting with each other. Here, the deformed shape of the solids after the contact can be calculated by minimizing the total energy, sum of adhesional and elastic energies $U_{adh} + U_{el}$.

Carbone model (Carbone et al., 2015) is based on JKR theory and it considered the penetration of an elastic rubber layer into a fractal rigid surface. The hysteresis loop induced by a randomly rough adhesive contact was investigated. The total energy was defined as the sum of adhesion and elastic energies. The adhesion energy was obtained from

$$U_{adh} = -\gamma \sum_{i=1}^{n_c} \int_{a_i}^{b_i} \sqrt{1 + [z'(x)]^2} dx$$

where γ is the work of adhesion. $z'(x) = z - \bar{z}$ is the height of the profile measured from its mean plane. n_c is the number of contact regions and a_i and b_i are the limit lengths of each contact. They found that the contact area has a linear relationship with the work of adhesion (Carbone et al., 2015).

Busse model (Busse, 2010) described friction coefficient as the summation of individual contribution of hysteresis, μ_{hys}, and adhesion mechanisms, μ_{adh}. Accordingly,

$$\mu = \mu_{hys} + \mu_{adh}$$

Here, the hysteresis friction is given by describing the surface by two different fractal dimensions, dividing it into two scaling ranges, expressed as

$$\mu_{hys} = \frac{< \delta >}{2Pv} \left(\int_{\omega_{min}}^{\omega_2} E''(\omega) C_1(\omega) \omega \, d\omega + \int_{\omega_2}^{\omega_{max}} E''(\omega) C_2(\omega) \omega \, d\omega \right.$$

where $\delta = b.z_p$ is the mean excitation depth in which b is a fitting parameter. C_1 and C_2 are the PSDs in two different scaling ranges, namely $\{\omega_{min}\text{-}\omega_2\}$ and $\{\omega_2\text{-}\omega_{max}\}$.

Adhesion friction coefficient was defined as the ratio between the adhesion force F_{adh} and normal force F_N.

$$\mu_{adh} = \frac{F_{adh}}{F_N} = \frac{\tau_s A_{eff}}{P A_{nom}}, \qquad \tau_s = \tau_0 (1 + \frac{E_{inf}/E_0}{(1 + \left(\frac{v_c}{v}\right))^n}$$

where τ_s and τ_0 are the interfacial shear stress at v and 0 velocities, respectively. E_{inf} and E_0 are long term and instantaneous elastic moduli. Here, v_c is the critical velocity where the shear stress is at maximum, and n is related to the exponent of the relaxation time spectra of the elastomer.

Persson and Scaraggi (2014), investigated the effect of surface roughness on adhesion between two elastic solids, implementing JKR and DMT theories into Persson theory of friction. They verified their theory results with exact numerical calculations using RMD.

Empirical Models

Empirical modeling is another popular approach to describe the correlation between the texture of the surface and friction measurements through fitting of the results to pre-assigned formulas. Micro-texture and its role in friction is often neglected in empirical models of friction since most of the shape descriptor parameters considered in empirical models cannot detect micro-texture. For many parameters listed in table 1, micro-texture presence only results in micro-variations in their magnitudes. Therefore, for inclusion of micro-texture effect, its characterization should be implemented separately.

In 1978, Dahir and Henry proposed the first empirical model that incorporated micro texture into friction by using BPN values as a surrogate for micro-texture. While their study suggests the existence of a correlation between friction and micro-texture, they could not formulate it (Luce, 2006). The relationship between BPN and surface texture has been the focus of several studies (Forster, 1989, McLean and Foley, 1998, Do, 2000, Ergun, et al. 2005, Serigos et al.,2014}, and

BPN was found to be governed by both micro- and macro-texture (see Figure A1-6) (Serigos et al., 2014).

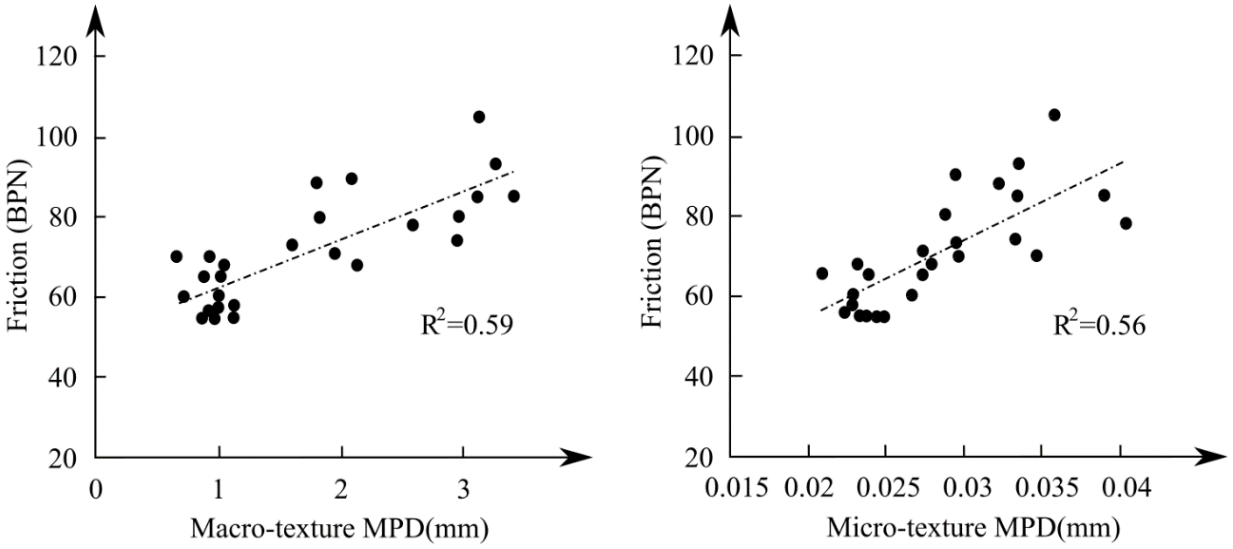

Figure A1-6. Relationship between Skid resistance and Macro- and Micro-texture (Serigos et al., 2014)

In another approach, Kokkalis and Panagouli (1998) described the friction at 40 mi/h SN_{40}, with respect to micro-texture as

$$SN_{40} = \frac{9.4m \times \bar{z} - 38}{4.25 \times d_a^{0.1} e^{\left(\frac{0.14}{\bar{z}_{macro}^{0.72}}\right)}}$$

where $\bar{z}_{macro}$ is the average macro-texture depth expressed in millimeters and d_a is the distance between adjacent asperities. Later, Kokkalis et al. (2002) suggested that SN values are directly correlated to the fractal dimension (Figure A1-7).

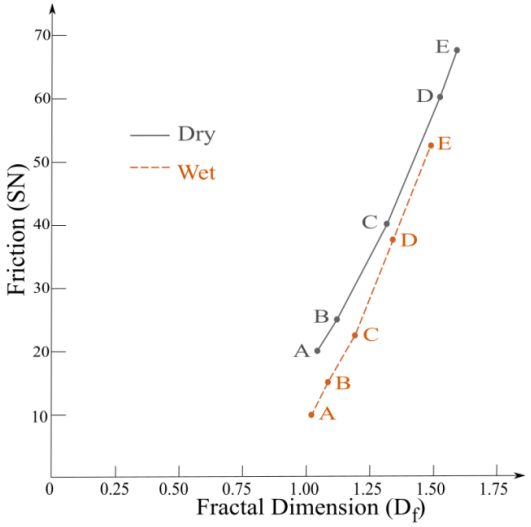

Figure A1-7. Correlation between the fractal dimension and the friction for dried and wet surfaces (Kokkalis et al., 2002)

Ergun et al. (Ergun et al., 2005) presented a model to correlate friction coefficient and surface texture as follows

$$\mu(s) = (0.37 + \frac{0.11}{MPD_{mac}} + \frac{0.15}{La_{mic}}) \times e^{(\frac{s}{149+91\log(MPD_{mac})+80\log(Rq_{mic})})}$$

where s is the slip speed and MPD_{mac} is the mean profile depth of macro-texture. Here, La_{mic} and Rq_{mic} are the average wavelength and the root-mean-square of micro-texture, respectively. They suggested the average wavelength of the profile as the most reliable texture parameter for predicting the friction coefficient at no slipping.

Recently, Kanafi et al. (2014) have extensively studied the correlation between friction and the fractal and non-fractal surface parameters. They found that none of the current fractal parameters can be considered to be directly correlated with the friction (see Figure A1-8).

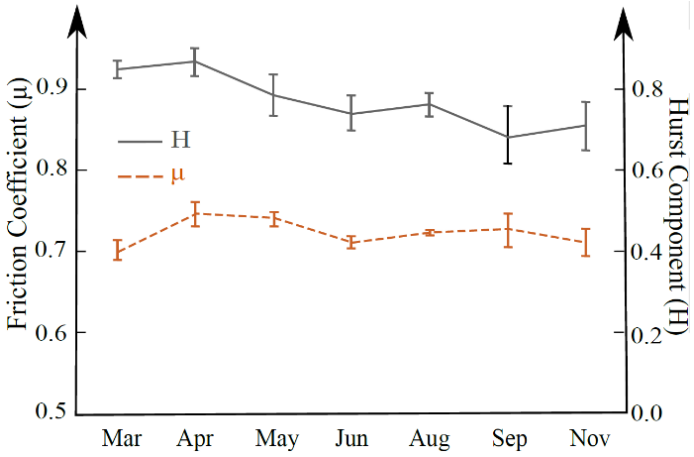

Figure A1-8. Friction variation relationship with Hurst exponent

Noyce et al. (Noyce et al, 2005) demonstrated the variation of wet skid resistance of pavement in different speed by changing micro or macro-texture, while keeping the other factor constant, as illustrated in Figure A1-9. On the basis of these results, it can be concluded that the need for adequate macrotexture does not reduce the need for high micro-texture in pavement surfaces. Both textures contribute to the wet friction although their magnitudes vary with speed (Noyce et al., 2005).

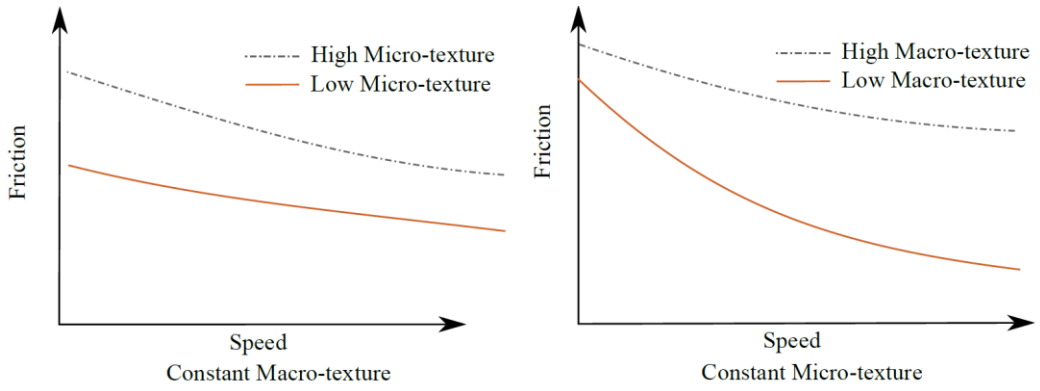

Figure A1-9. Wet skid resistance versus speed for constant (a) macro- and (b) micro-textures (Noyce et al., 2005)

Micro-texture plays a significant role in tire-pavement friction particularly in low speeds, and has to be understood (Forster, 1989, Serigos et al., 2014). Moreover, there has been very limited efforts on coupling of existing tire and surface models together. Since the influence of both elements on friction is evident, such efforts are necessary for thorough understanding of friction mechanism.

APPENDIX B- EFFECT OF PAVEMENT SURFACE MICRO-TEXTURE ON ROLLING RESISTANCE OF TIRE - A PRELIMINARY STUDY

Introduction

In the previous chapters the effect of roughness, mega-, and macro-texture scales of the pavement surface profile has been investigated. The effect of micro-texture is very important on friction as it was stated in Appendix A. Many studies have been performed and different models have been generated for capturing this effect. The hysteresis portion of the friction is related to the effect of the energy dissipation due to deformation of the rubber on the friction between the two surfaces in contact. There is no mechanistic study on the effect of micro-texture on rolling resistance, since is effect is often known to be negligible.

Therefore, here, instead of a thorough investigation, a rough estimate of the effect of micro-texture on rolling resistance is presented. Further investigation is not performed based on the preliminary results; however, the full procedure is explained.

Methodology

Micro-texture is referred to wavelengths from 0.001 to 0.5 mm. Due to the small size of the textures at this level, their effect is only evident on tire tread deformation. Therefore, the problem can be defined as contact between a rubber block and the surface texture, which can be approached by finite element analysis using ABAQUS software.

Considering that the micro-texture goes down to 0.001 mm wavelengths, generation of a contact with the whole spectrum can be computationally very expensive and sometimes even not possible. Therefore, in this study a multi-scale approach is considered, in which the surface is divided into a reasonable number of scales of sinus waves; assuming that the final surface is the summation of these sinus waves, see Figure A2-1.

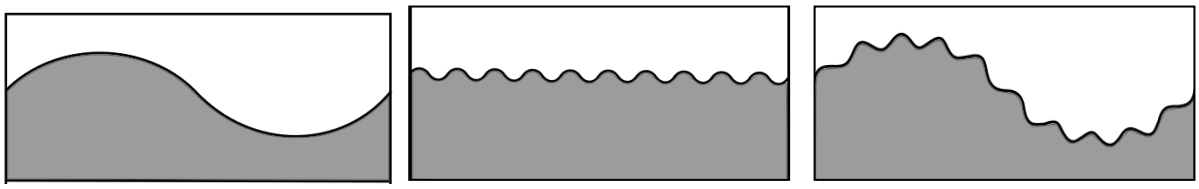

Figure A2-1. A sample of wavelength combination for pavement surface simulation in FE model

Then, in each scale, the contact between the sinus wave and the rubber block with the same width as the wavelength of the sinus wave is modeled, see Figure A2-2.

For a full multi-scale simulation, the pressure applied at each scale should be defined based on the contact force in the upper scale and the energy dissipation at each scale should be dependent on the lower scales. Therefore, in the analysis of this model, the contact forces should be similar to the forces applied in the upper scale (macro-texture scale) as an input for the largest scale. In the first step of the process, a top-down analysis of the scales should be performed to obtain the contact pressure at each scale. Then, in the second step, a bottom-up analysis should be done to calculate the energy dissipation of each scale, by importing the stresses inside the block to the upper scale.

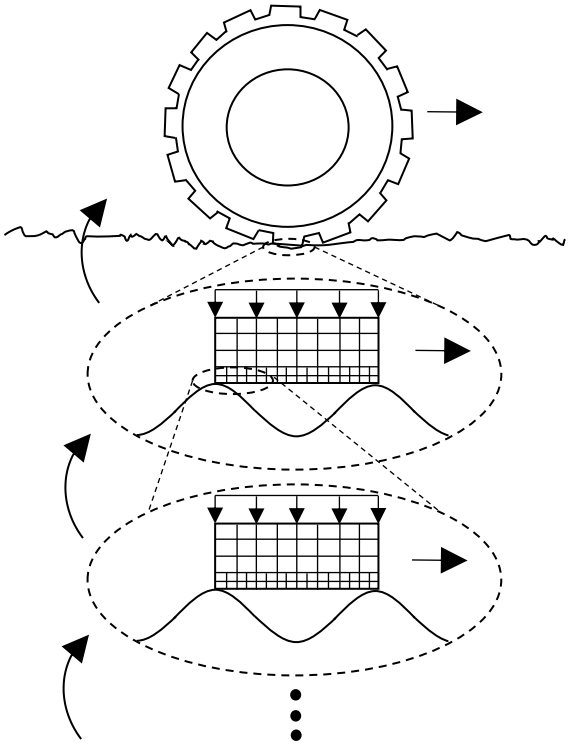

Figure A2-2. A schematic view of multi-scale modeling of micro-texture effect on rolling resistance

However, as it was mentioned, this procedure is not fully followed due to the preliminary results which demonstrate the negligible effect of micro-texture on rolling resistance.

Model development

The process of model development at each scale is explained in the following.

For generating the surfaces in ABAQUS, the coordinates of the surface are obtained from a MATLAB code, the surface is constructed in Auto-cad, and then imported into the ABAQUS model. In order to decrease the computational cost, the smallest required size for the rubber block, which satisfies the boundary conditions, should be found. The width of the block should be limited to the surface wavelength (λ) at each scale because, for any lower values, the boundary conditions on the two ends of the block will not be the same (loss of contact at one end). The height of the rubber should be big enough to ensure that the load application zone does not affect the contact zone. Therefore, after performing a sensitivity analysis, the height of the rubber block is considered to be $\lambda/2$. A schematic view of the problem at each scale is shown in Figure A2-3.

For completely defining the problem the following boundary conditions should be applied:

- As a rigid element, the pavement surface requires the boundary condition defined at only one point. Therefore, a reference point should be defined for the part. Since in the model, the rubber block is sliding on the pavement surface, the pavement surface (reference point) is considered fixed in all directions.
- In Sliding, the top surface of rubber is constrained to move perfectly horizontally.

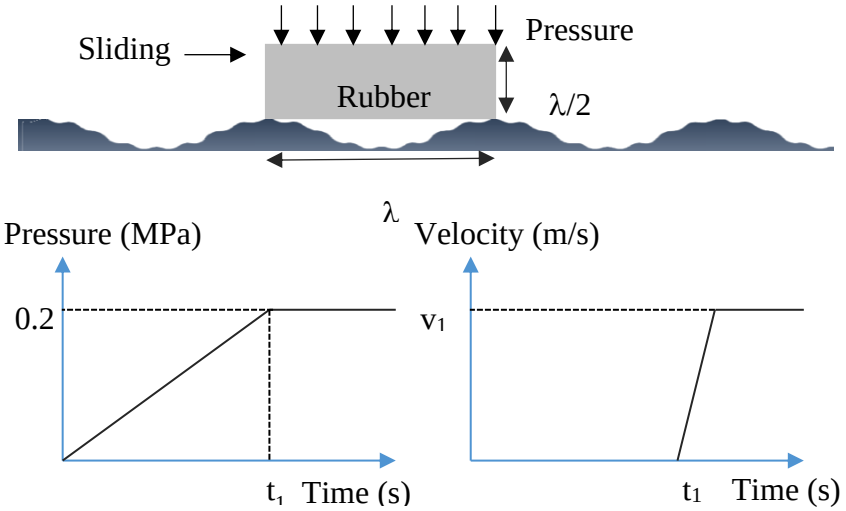

Figure A2-3. Schematic view of the FE model and applied loads for each micro-scale

- When a large system is in contact with repeated events, it is possible to capture the effect of the events by considering the system as one finite representative element, using periodic boundary conditions (PBCs). Therefore, PBCs have been applied to the nodes on the two walls of the rubber block, as follows:

$$u_{left} = -u_{right}$$

where, u is the displacement of the node (see Figure A2-4).

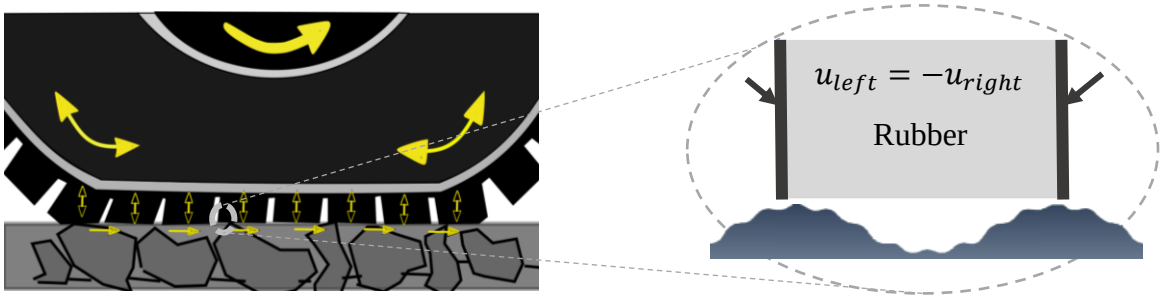

Figure A2-4. Periodic Boundary condition

This PBC should be applied in both horizontal and vertical directions. For implementing PBCs equation constrains have been used. Using this periodic boundary condition on the sides, all of the corresponding points on the two side of the walls (that are in the same elevation and location) are forced to have the same strain and stress distribution.

For reducing the computational time, a finer mesh should be used near the contact. However, it should be considered that in order to be able to define the PBCs, the mesh should be structured so that every point on one side the block has an equivalent point on the other side of the block (see Figure A2-5).

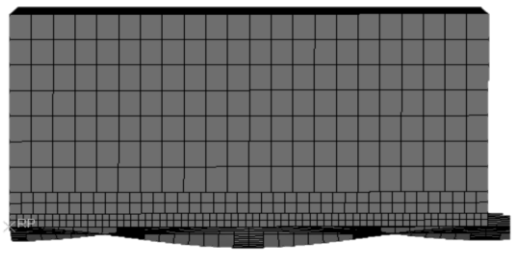

Figure A2-5. Rubber block mesh

The micro-scale model is generated with the following procedure: First a 2D FE model was developed, which was then converted to a 3D model for considering the effect of texture in both directions. The first step after generation of the model is finding the required size of the block; i.e., the block height after which the effect of the surface on tread deformation is negligible. For this purpose, a sensitivity analysis is performed, and its results are shown in Figure A2-6. As it can be seen, for height less than 0.5 λ (λ= wavelength of the surface and width of the block), the energy dissipation decreases which indicates that the height of the block that is influenced by the texture is 0.5 λ.

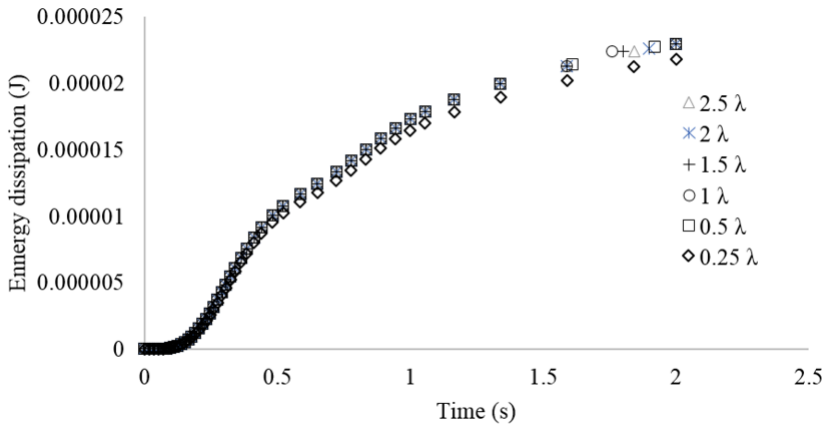

Figure A2-6. Sensitivity analysis for finding the optimum rubber block height

Also, the performance of the 2D and 3D models are compared with each other. For this purpose, the penetration depth under a certain load is compared between the two models, see Figure A2-7.

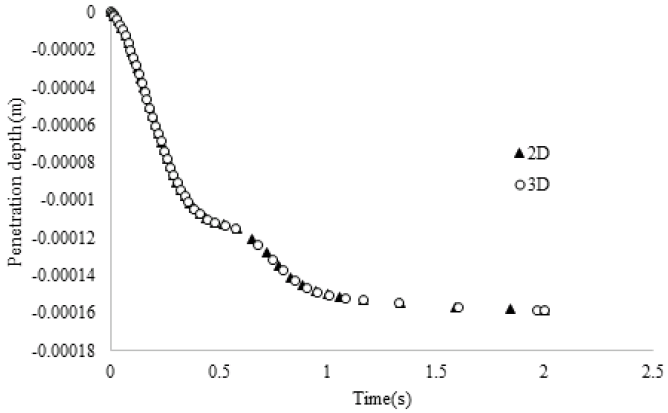

Figure A2-7. Comparison of penetration depth between 2D and 3D models

It can be seen that both models generate similar results.

Model validation

For validation of the model, some of the assumptions of the contact theory presented by Persson (2001) for hysteresis friction are assessed for the 2D model in the following:

Investigation of the relationship between contact area and applied pressure

Persson theory of hysteresis friction suggests that the contact area and applied load should have a linear relationship when (i) the load is small and (ii) the contact area is not close to the nominal contact area, A0. After running the model for a certain surface, with different applied loads and obtaining the contact area in each case, a linear relationship has been found between the contact area and applied load. Figure A2-8 demonstrates this relationship. Graphs on the left show the variation of contact area for different loads with time and the graphs on the right show the linear relationship between the load and contact area. Also, the contact area for a certain load is known to be more for a smooth surface in comparison to a rough one.

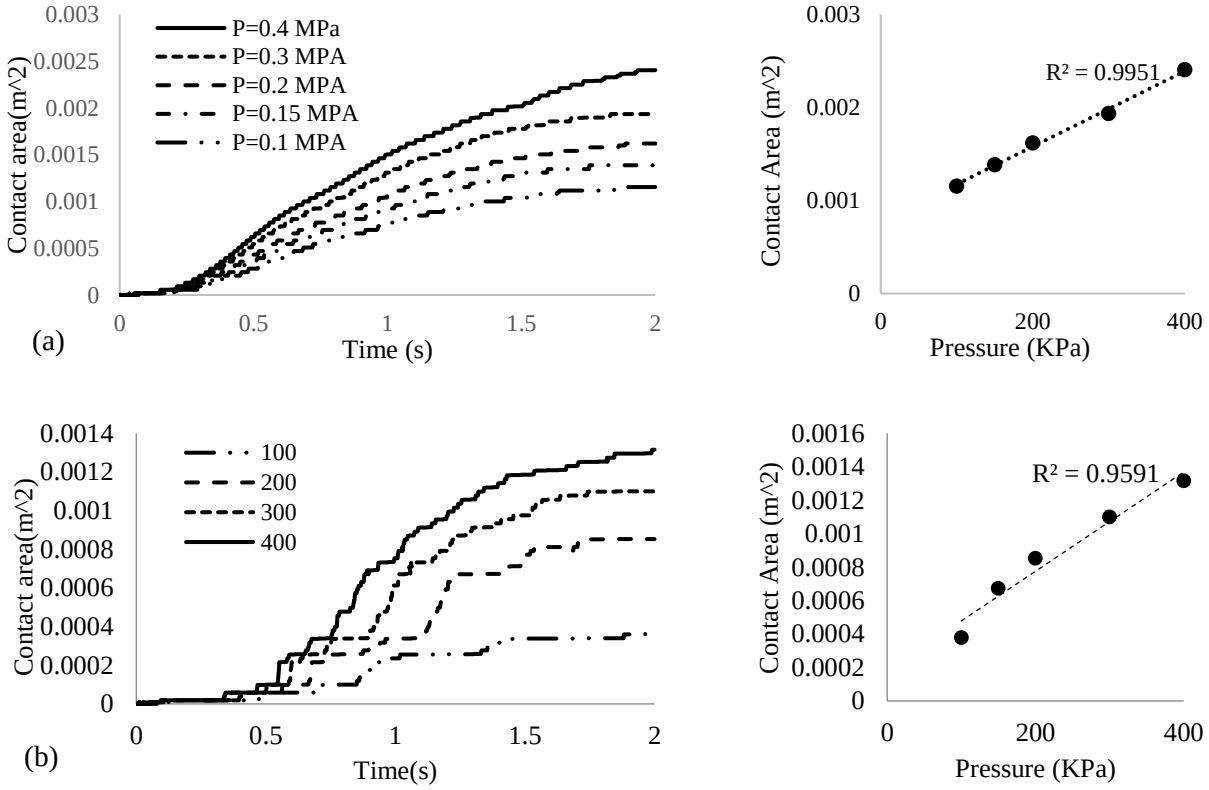

Figure A2-8. Load-contact relationship (a) for λ=4mm (b) for combination of λ=4mm, λ=1mm and λ=0.25mm.

Figure A2-9 shows a comparison between the contact area of a smooth surface (a sinus wave with wavelength of 4mm) and a rough surface (summation of three sinus waves with wavelengthes of 4,1, and 0.25 mm). As it can be seen in Figure A2-9, the contact area for the smooth surface is larger than the rough surface.

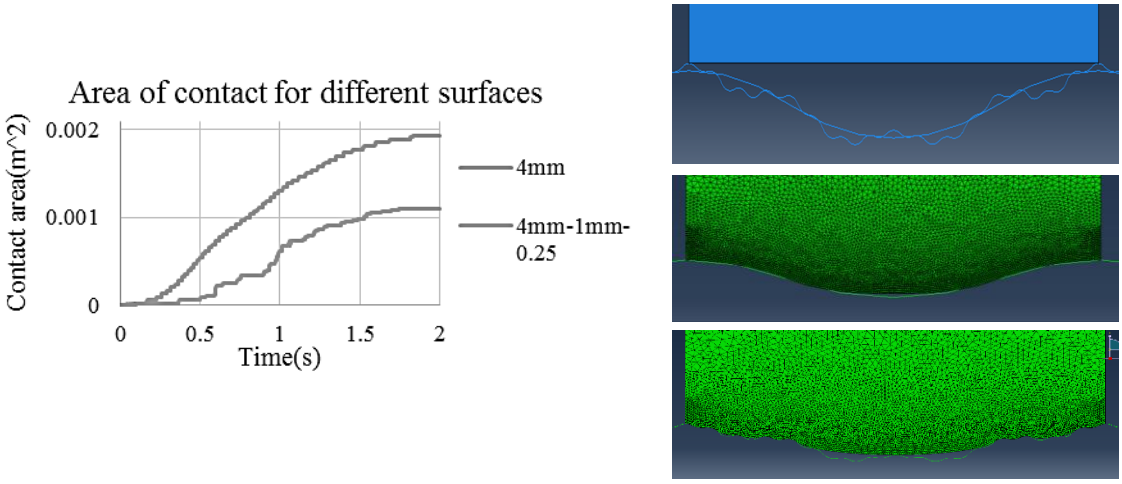

Figure A2-9. Comparison of area of contact for a smooth (sinus wave) and a rough surface (summation of three sinus waves) under equal load

Investigation of the relationship between penetration depth and applied pressure

The relationship between the penetration depth and applied pressure is also known to be linear. As it can be seen in Figure A2-10, this assumption holds in this model as well.

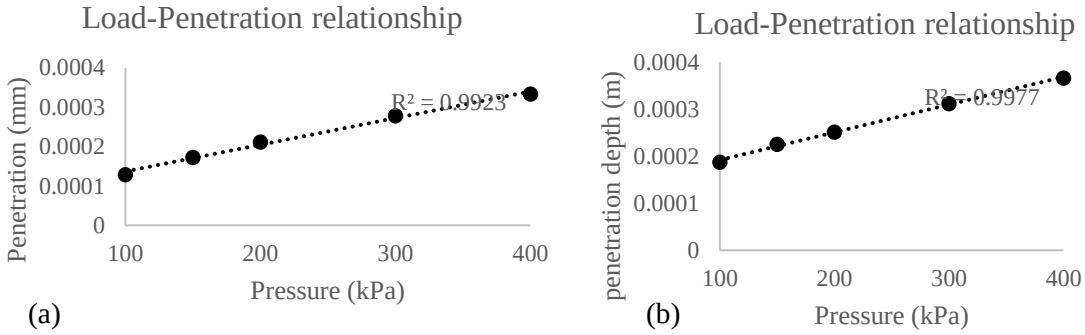

Figure A2-10. Load-Penetration relationship for (a) λ=4mm and (b) combination of λ=4mm, 1mm, and 0.25 mm

Investigation of the relationship between h/λ and applied pressure

It is assumed that if the ratio between the amplitude and the wavelength is related to the ratio between the applied pressure and the elastic modulus of the rubber (h/λ α σ/E), the full contact between the rubber and the surface should be reached. Also, if h/λ is the same for two different surfaces, the load required for the full contact would be the same. After running the model, it can be seen that these assumptions are valid (see Figure A2-11(a)). In addition, a linear relationship has been found between the required pressure for full contact and h/λ ratio (see Figure A2-11 (b)).

Model preliminary results

For performing the multi-scale modeling of the effect of texture on the energy loss in a rubber block, the contact forces are required from the macro-texture scale. Therefore, here, the model is

built (see Figure A2-12); however, the presented results are preliminary results because performing the final simulation without the correct contact force and pressure is not possible.

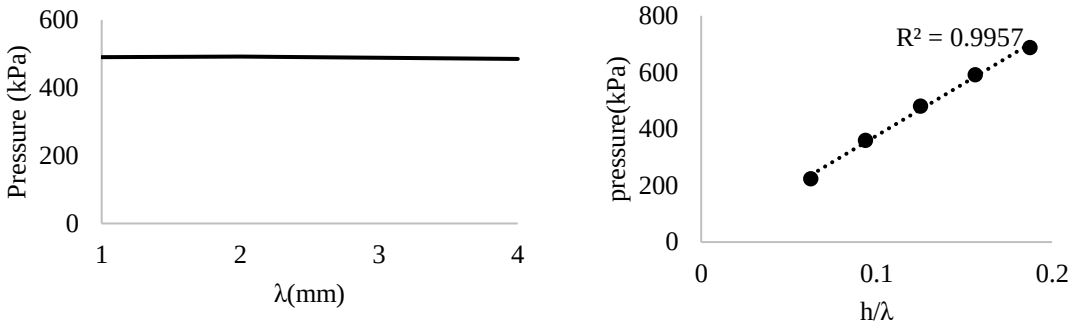

Figure A2-11. (a) λ-Pressure relationship for different surfaces with the same h/λ ratio when they reach the full contact, (b) relationship between the required pressure for full contact and h/λ ratio.

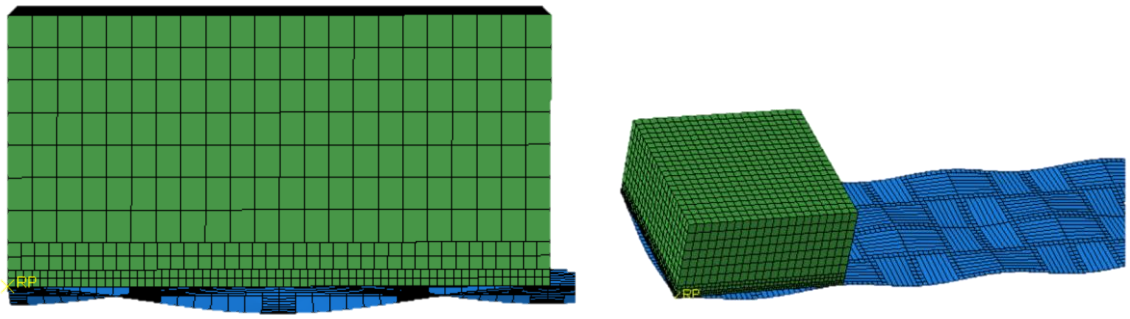

Figure A2-12. 3D rubber block model in contact with a sinusoidal surface

Therefore, in the following, some very preliminary results on the effect of texture amplitude on energy dissipation are provided (Figure A2-13).

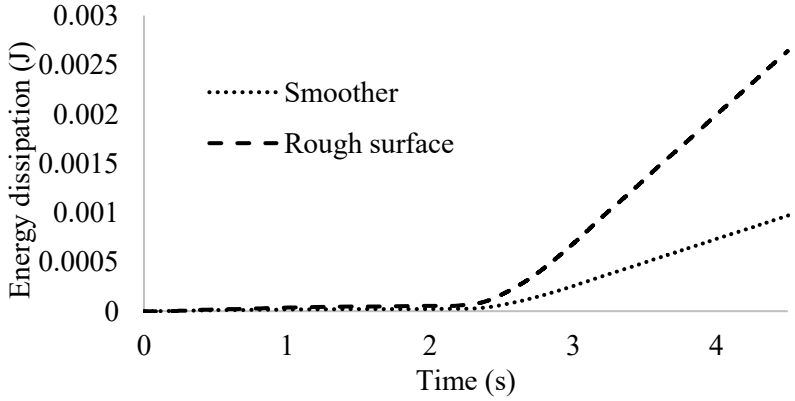

Figure A2-13. Energy dissipation in a rubber block with 4mm width for a rough and smooth surface

Figure A2-13 shows the dissipated energy variation for a rough and a smooth surface. The amplitude ratio of the two surfaces (A_{rough}/A_{smooth}) is 2; however, the energy dissipated in the

rougher surface is more than twice of the smoother surface. This is an indication of the importance of the surface texture amplitude on energy dissipation.

Here, for evaluating the validity of the proposed approach, a simplified conceptual example is given. In this example, the effect of texture at the lower range of the macro-texture (1-5 mm) is simulated with the micro-texture approach presented here (without considering the multi-scale modeling). Therefore, a *very rough* estimate of the effect of a continuous sinusoidal texture on the rolling resistance of the rubber block can be obtained. This result can be then compared with the NCHRP 720 model for the effect of macro-texture on rolling resistance. For this comparison, the rolling resistance coefficient defined as the ratio between the rolling resistance force and the normal force is used.

NCHRP 720 provides the rolling resistance force. For an MPD of 0.5mm, the rolling resistance coefficient (rolling resistance force/normal force) for a car is almost 0.01 N/N.

For the rubber-texture interaction model, the rolling resistance force can be obtained by dividing the energy dissipation by the sliding distance of the rubber. Therefore, the rolling resistance coefficient for a rubber block with width of 3 mm (moving with 0.01 m/s speed and sliding a distance of 15 mm) is equal to 0.007 N/N. However, this model considers a continuous sinusoidal surface throughout the sliding distance (in this case over 5 cycles; i.e., with 5 contact points). Considering the distribution of micro-texture peaks in Figure 3-3 (only 5 peaks in 100 mm), a more reasonable rolling resistance force for this model can be around (15/100)(0.007 N/N) = 0.0011 N/N, or about 15% of the macro-scale rolling resistance force obtained from NCHRP 720 model. Considering that the wavelength in the FE model is only 3mm, while macro-texture in the NCHRP 720 model includes wavelength up to 50 mm, the result of the proposed model is reasonable.

It is worth mentioning that the wavelength of 3 mm used in this example is more than 5 times larger than the upper limit of the micro-texture range. Therefore, the effect of micro-texture will be even smaller than what is estimated here, since the results show that the rolling resistance force decreases with decreasing wavelength.

These results give a rough estimate of how small the effect of micro-texture on rolling resistance of the tire is. Since development of the full multi-scale model is computationally very expensive, further investigation of the effect of micro-texture on rolling resistance deemed to be unnecessary.

BIBLIOGRAPHY

BIBLIOGRAPHY

- Aavik, A., Kaal, T. & Jentson, M. (2013). "Use ofpavement surface texture characteristics measurement results in Estonia." The XXVIII International Baltic Road Conference. Vilnius, Lithuania.

- ABAQUS manual.

- American Association of State Highway and Transportation Officials (AASHTO). 1976. Guidelines for Skid-Resistant Pavement Design, Task Force for Pavement Design, AASHTO, Washington, D.C.

- Andersen, L. G., Larsen, J. K., Fraser, E. S., Schmidt, B., & Dyre, J. C. (2014). Rolling Resistance Measurement and Model Development. Journal of Transportation Engineering, 141(2).

- Archard, J. F. (1957), "Elastic Deformation and the Laws of Friction," Proceedings of the Royal Society of London A, 243, pp 190-205.

- Bazlamit, S. M., & Reza, F. (2005). Changes in asphalt pavement friction components and adjustment of skid number for temperature. Journal of Transportation Engineering, 131(6), 470-476.

- Bendtsen, H. (2004). Rolling resistance, fuel consumption-a literature review. Rolling resistance, fuel consumption-a literature review, (23).

- Bester, C. J. (1984). Effect of pavement type and condition on the fuel consumption of vehicles (No. HS-039 023).

- Bennett, C. R. & Greenwood, I. D. (2003b). Volume 7: Modeling Road User and Environmental Effects in HDM-4, Version 3.0, International Study of Highway Development and Management Tools (ISOHDM), World Road Association (PIARC), ISBN 2-84060-103-6.

- Bitelli, G., Simone, A., Girardi, F., & Lantieri, C. (2012). Laser scanning on road pavements: A new approach for characterizing surface texture. Sensors, 12(7), 9110-9128.

- Boere, S. (2009). "Prediction of road texture influence on rolling resistance." M.S. thesis, Eindhoven Univ. of Technology, Eindhoven, Netherlands.

- Bhushan, B. (1992). Tribology of magnetic storage systems.

- Bush, A. W., Gibson, R. D., and Thomas, T. R. (1975), "The Elastic Contact of Rough Surfaces," Wear, 35, pp 87-111.

- Busse, L., Le Gal, A., & Klüppel, M. (2010). Modelling of dry and wet friction of silica filled elastomers on self-affine road surfaces. In Elastomere Friction (pp. 1-26). Springer, Berlin, Heidelberg.

- Carbone, G., & Bottiglione, F. (2008). Asperity contact theories: Do they predict linearity between contact area and load. Journal of the Mechanics and Physics of Solids, 56(8), 2555-2572.

- Carbone G., Pierro, E., and Recchia, G. Loading-unloading hysteresis loop of randomly rough adhesive contacts. Physical Review E, 92(6):062404, 2015

- Carlson, C. R., & Gerdes, J. C. (2002, September). Identifying tire pressure variation by nonlinear estimation of longitudinal stiffness and effective radius. In Proceedings of AVEC 2002 6th International Symposium of Advanced Vehicle Control.

- Chang, J. R., Chang, K. T., & Chen, D. H. (2005). Application of 3D laser scanning on measuring pavement roughness. Journal of Testing and Evaluation, 34(2), 83-91.

- Chatti, K. & Zaabar, I. (2012). Estimating the effects of pavement condition on vehicle operating costs. NCHRP Report 720. Transportation Research Board.

- Choubane, B., Holzschuher, C. R., & Gokhale, S. (2004). Precision of locked-wheel testers for measurement of roadway surface friction characteristics.Transportation Research Record: Journal of the Transportation Research Board, 1869(1), 145-151.

- Corollaro, A., Russo, M., & Ciaravola, V. (2014). Essentiality of temperature management while modeling and analyzing tires contact forces.

- Delanne, Y. (1994). The influence of pavement evenness and macrotexture on fuel consumption. ASTM special technical publication, 1225, 240-240.

- Derjaguin, B V. (1934). Untersuchungen u¨ber die reibung und adha¨sion, iv. Colloid & Polymer Science, 69(2):155–164.

- Descornet, G. (1990). Road-surface influence on tire rolling resistance. Surface characteristics of roadways: International research and technologies, ASTM STP, 1031, 401-415.

- Dewey, G. R., Robords, A. C., Armour, B. T., & Muethel, R. (2001, July). Aggregate wear and pavement friction. In 80th Transportation Research Board Annual Meeting (p. 152)

- Dixon, J. C. (2008). The shock absorber handbook. John Wiley & Sons.

- Do, M. T., Zahouani, H., & Vargiolu, R. (2000). Angular parameter for characterizing road surface microtexture. Transportation Research Record: Journal of the Transportation Research Board, 1723(1), 66-72.

- Do, M. T., & Marsac, P. (2002). Assessment of the polishing of the aggregate microtexture by means of geometric parameters. In TRB 81st Annual Meeting (Transportation Research Board) (pp. 19p-schémas).

- Do, M. T., Cerezo, V., Beautru, Y., & Kane, M. (2013). Modeling of the connection road surface microtexture/water depth/friction. Wear, 302(1-2), 1426-1435.

- Do, M. T., & Cerezo, V. (2015). Road surface texture and skid resistance. Surface Topography: Metrology and Properties, 3(4), 043001.

- Dunford, A., 2008. Measuring Skid Resistance without Contact, 2006e2007 Progress Report, Published Project Report PPR 315. Transport and Research Laboratory, Wokingham.

- Ejsmont, Grzegorz Ronowski, Beata Świeczko-Żurek & Sławomir Sommer (2017) Road texture influence on tyre rolling resistance, Road Materials and Pavement Design, 18:1, 181-198, DOI: 10.1080/14680629.2016.1160835

- EPA, (2012) "Greenhouse Gas Inventory Report".

- Ergun, M., Iyinam, S., & Iyinam, A. F. (2005). Prediction of road surface friction coefficient using only macro-and microtexture measurements. Journal of transportation engineering, 131(4), 311-319.

- Falk, K., Lang, R., & Kaliske, M. (2016). Multiscale simulation to determine rubber friction on asphalt surfaces. Tire Science And Technology, 44(4), 226-247.

- FHWA. 1980. Skid Accident Reduction Program. Technical Advisory T5040.17, Federal Highway Administration, U.S. Department of Transportation.

- Flintsch, Gerardo W., et al. "The little book of tire pavement friction." Surface Properties Consortium [online].2012.

- Ford, I. J. (1993). Roughness effect on friction for multi-asperity contact between surfaces. Journal of Physics D: Applied Physics, 26(12), 2219.

- Forster, S. W. (1981). Aggregate microtexture: Profile measurement and related frictional levels (No. FHWA-RD-81-107 Final Rpt.).

- Forster, S. W. (1989). Pavement microtexture and its relation to skid resistance. Transportation Research Record, (1215)

- Ghoreishy, M. H. R. (2008). A state of the art review of the finite element modelling of rolling tyres. Iranian Polymer Journal, 17(8), 571-597.

- Gillespie, T. D., & Sayers, M. (1981). Role of road roughness in vehicle ride. Transportation Research Record, 836, 15-20.

- Greenwood, J. A., & Tabor, D. (1958). The friction of hard sliders on lubricated rubber: the importance of deformation losses. Proceedings of the Physical Society, 71(6), 989.

- Golden. A (1981). theory of wet road-tyre friction. Wear, 71(3):307–331.

- Greenwood, J. A., & Williamson, J. B. P. (1966). Contact of nominally flat surfaces. Proceedings of the Royal Society of London. Series A. Mathematical and Physical Sciences, 295(1442), 300-319.

- Grosch, K. A. (1963, June). The relation between the friction and visco-elastic properties of rubber. In Proc. R. Soc. Lond. A (Vol. 274, No. 1356, pp. 21-39). The Royal Society.

- Hall, J. W., Smith, K. L., Titus-Glover, L., Wambold, J. C., Yager, T. J., & Rado, Z. (2009). NCHRP web-only document 108: Guide for pavement friction. Transportation Research Board of the National Academies, Washington, DC.

- Hammarström, U., Eriksson, J., Karlsson, R., & Yahya, M. R. (2012). Rolling resistance model, fuel consumption model and the traffic energy saving potential from changed road surface conditions. Statens väg-och transportforskningsinstitut.

- Hai Huang and Jiaqiang Pan. (2006) Speech pitch determination based on hilbert-huang transform. Signal Processing, 86(4):792–803.

- Heinrich, Gert, and Manfred Klüppel. (2008) "Rubber friction, tread deformation and tire traction." Wear 265.7: 1052-1060.

- Henderson, R. J., Cook, G., Cenek, P. D., Patrick, J. E., & Potter, S. M. (2006). The effect of crushing on the skid resistance of chipseal roads. Land Transport New Zealand.

- Henry, J. J., & Dahir, S. H. (1979). Effects of Textures and the Aggregates that produce them on the Performance of Bituminous Surfaces. Transportation Research Record, (712).

- Henry, John Jewett (2000). Evaluation of pavement friction characteristics. Vol. 291. Transportation Research Board

- Hernandez, Jaime Alberto (2015). Development of deformable tire-pavement interaction: contact stresses and rolling resistance prediction under various driving conditions. Diss. University of Illinois at Urbana-Champaign.

- Hertz, H. On the contact of elastic solids. J. reine angew. Math, 92(110):156–171, 1881.

- Hogervorst, D. (1974). Some properties of crushed stone for road surfaces. Bulletin of the International Association of Engineering Geology-Bulletin de l'Association Internationale de Géologie de l'Ingénieur, 10(1), 59-64.

- Holzapfel, Gerhard A. (1996)"On large strain viscoelasticity: continuum formulation and finite element applications to elastomeric structures." International Journal for Numerical Methods in Engineering 39.22: 3903-3926.

- Horne, W. B., & Leland, T. J. (1962). Influence of tire tread pattern and runway surface condition on braking friction and rolling resistance of a modern aircraft tire.

- Huang, J., Losa, M., & Leandri, P. (2018, July). Determining the effect of damping layers in flexible pavements on traffic induced vibrations. In Advances in Materials and Pavement Prediction: Papers from the International Conference on Advances in Materials and Pavement Performance Prediction (AM3P 2018), April 16-18, 2018, Doha, Qatar (p. 255). CRC Press.

- Hudson, W. R. (1981). Road roughness: its elements and measurement. Center for Transportation Research.

- Hui, C. Y., Lin, Y. Y., & Baney, J. M. (2000). The mechanics of tack: viscoelastic contact on a rough surface. Journal of Polymer Science Part B: Polymer Physics, 38(11), 1485-1495.

- Jahn, R., & Truckenbrodt, H. (2004). A simple fractal analysis method of the surface roughness. Journal of Materials Processing Technology, 145(1), 40-45.

- Jamieson, N.J. and Cenek, P.D. (1999): "Effects of Pavement Construction on the Fuel Consumption of Trucks," in Proceedings of the Options for Post Millenium Pavements Symposium, Wairekei Resort, Taupo, New Zealand, 17-19 Oct.1999

- Janssen, M. L., & Hall, G. L. (1980). Effect of ambient temperature on radial tire rolling resistance. SAE Transactions, 576-580.

- Johnson, K. L., Kendall, K., & Roberts, A. D. (1971). Surface energy and the contact of elastic solids. Proceedings of the royal society of London. A. mathematical and physical sciences, 324(1558), 301-313.

- Kane, M., Rado, Z., & Timmons, A. (2015). Exploring the texture–friction relationship: from texture empirical decomposition to pavement friction. International Journal of Pavement Engineering, 16(10), 919-928.

- Karlsson, R., Hammarström, U., Sörensen, H. & Eriksson, O. (2011). "Road surface influence on rolling resistance. Coastdown measurements for a car and an HGV". VTI Notat 24A. The Swedish Road and Transport Research Institute. Linköping.

- Kenis, W. (1995). Dynamic load effects on pavement primary response and future research. in dynamic loading of heavy vehicles and road wear mid-term seminar, Proceedings, 2-3 February 1995, Parkroyal hotel at Darling Harbour, Sydney, Australia.

- Kim, R.E., Kang, S., Spencer, B.F., Ozer, H. & Al-Qadi, I. L. (2017). "Stochastic Analysis of Energy Dissipation of a Half-Car Model on Non-deformable Rough Pavement", Journal of Transportation Engineering, Part B: Pavements, 143(4).

- Klüppel, M., & Heinrich, G. (2000). Rubber friction on self-affine road tracks. Rubber chemistry and technology, 73(4), 578-606.

- Kokkalis, A. G., & Panagouli, O. K. (1998). Fractal evaluation of pavement skid resistance variations. I: surface wetting. Chaos, Solitons & Fractals, 9(11), 1875-1890.

- Kokkalis, A. G., Tsohos, G. H., & Panagouli, O. K. (2002). Consideration of fractals potential in pavement skid resistance evaluation. Journal of transportation engineering, 128(6), 591-595.

- Kummer HW, Unified Theory of Rubber and Tire Friction, Engineering Research Bulletin B-94 Engineering Publications, The Pennsylvania State University (1966)

- Leaderman, H. (1943). Elastic and creep properties of filamentous materials and other high polymers.

- Leu, M. C., & Henry, J. J. (1978). Prediction of skid resistance as a function of speed from pavement texture measurements. Transportation Research Record, (666).

- Li, L., & Wang, K. C. (2016). Geometric texture indicators for safety on AC pavements with 1 mm 3D laser texture data. International Journal of Pavement Research and Technology, 9(1), 49-62.

- Lin, Y. J., & Hwang, S. J. (2004). Temperature prediction of rolling tires by computer simulation. Mathematics and Computers in Simulation, 67(3), 235-249.

- Lindner, M., Kröger, M., Popp, K., & Blume, H. (2004). Experimental and analytical investigation of rubber friction. Safety, 200, 300.

- Lopez, I., Blom, R. E. A., Roozen, N. B., & Nijmeijer, H. (2007). Modelling vibrations on deformed rolling tyres—a modal approach. Journal of Sound and Vibration, 307(3-5), 481-494.

- Lorenz, B., Persson, B. N. J., Dieluweit, S., & Tada, T. (2011). Rubber friction: comparison of theory with experiment. The European Physical Journal E, 34(12), 129.

- Lorenz, B., Persson, B. N. J., Fortunato, G., Giustiniano, M., & Baldoni, F. (2013). Rubber friction for tire tread compound on road surfaces. Journal of Physics: Condensed Matter, 25(9), 095007.

- Louhghalam, A., Akbarian, M. and Franz-Joseph Ulm, F-J. (2015) "Roughness-Induced Pavement–Vehicle Interactions: Key Parameters and Impact on Vehicle Fuel Consumption" Transportation Research Record: Journal of the Transportation Research Board, No. 2525, Transportation Research Board, Washington, D.C., pp. 62–70.

- Luce, Anthony David. Analysis of aggregate imaging system (AIMS) measurements and their relationship to asphalt pavement skid resistance. Diss. Texas A&M University, 2006.

- Mahboob Kanafi, M., Kuosmanen, A., Pellinen, T. K., & Tuononen, A. J. (2015). Macro-and micro-texture evolution of road pavements and correlation with friction. International Journal of Pavement Engineering, 16(2), 168-179.

- Mann, A. V., McManus, K. J., & Holden, J. C. (1997). Power spectral density analysis of road profiles for road defect assessment. Road and Transport Research, 6(3).

- Mansura, Dmytro A., Nicholas H. Thom, and Hartmut J. Beckedahl. (2017) "A Novel Multiscale Numerical Model for Prediction of Texture-Related Impacts on Fuel Consumption." Tire Science and Technology 45.1: 55-70.

- Marcondes, J., Burgess, G. J., Harichandran, R., & Snyder, M. B. (1991). Spectral analysis of highway pavement roughness. Journal of Transportation engineering, 117(5), 540-549.

- Masad, E., Rezaei, A., Chowdhury, A., & Harris, P. (2009). Predicting asphalt mixture skid resistance based on aggregate characteristics. Texas Department of Transportation and the Federal Highway Administration.

- Matilainen, M. J. & Tuononen, A. J. (2012), 'Intelligent tire to measure contact length in dry asphalt and wet concrete conditions', Seoul: AVEC 12, 1--6.

- McCool, J. I. (1986), "Comparison of Models for the Contact of Rough Surfaces," Wear, 107(1), pp 37-60.

- McLean, J., & Foley, G. (1998). Road surface characteristics and condition: effects on road users (No. ARR 314).

- Moore, D. F. (1975). The friction of pneumatic tyres.

- Mozharovskii, V. V., Shil'ko, S. V., Anfinogenov, S. B., & Khot'ko, A. V. (2007). Determination of resistance to rolling of tires in dependence on operating conditions. part 1. method of multifactorial experiment. Journal of Friction and Wear, 28(2), 154-161.

- Najafi, S., Flintsch, G. W., & McGhee, K. K. (2013). Assessment of operational characteristics of continuous friction measuring equipment (CFME). International Journal of Pavement Engineering, 14(8), 706-714.

- Nielsen, L., & Sandberg, T. (2002). A new model for rolling resistance of pneumatic tires. SAE Transactions, 1572-1579

- Nordström, O. (1998). Development and validation of BV14, a new twin track fixed slip friction tester for winter road maintenance monitoring in Sweden. InXTH PIARC INTERNATIONAL WINTER ROAD CONGRESS 16-19 MARCH 1998 IN LULEAA, SWEDEN (Vol. 3).

- Noyce, D. A., Bahia, H. U., Yambó, J. M., & Kim, G. (2005). Incorporating road safety into pavement management: maximizing asphalt pavement surface friction for road safety improvements. Midwest Regional University Transportation Center Traffic Operations and Safety (TOPS) Laboratory.

- Öberg G. Vädrets och väglagets inverkan på personbilshastigheten. VTI notat No. 62, Statens väg- och transportforskningsinstitut, Linköping, 1994.

- O'Boy, D. J., & Dowling, A. P. (2009). Tyre/road interaction noise—Numerical noise prediction of a patterned tyre on a rough road surface. Journal of Sound and Vibration, 323(1-2), 270-291.

- Pacheco, Juliana E. Lopes, Carlos Alberto Bavastri, and Jucélio Tomás Pereira. "Viscoelastic relaxation modulus characterization using Prony series." Latin American Journal of Solids and Structures 12.2 (2015): 420-445

- BN Persson. J. on the theory of rubber friction. Surface Science, 401(3):445–454, 1998.

- Persson, B. N. J. (2001), “Elastoplastic Contact between Randomly Rough Surfaces,” Physical Review Letters, 87(11), p 116101.

- Persson, B. N. (2001), 'Theory of rubber friction and contact mechanics', The Journal of Chemical Physics 115(8), 3840--3861.

- Persson, Bo NJ. (2006) "Contact mechanics for randomly rough surfaces." Surface Science Reports 61.4: 201-227.

- Persson, B. N., & Scaraggi, M. (2014). Theory of adhesion: Role of surface roughness. The Journal of chemical physics, 141(12), 124701.

- Persson, B. N. J. (2015). Ice friction: Role of non-uniform frictional heating and ice premelting. The Journal of chemical physics, 143(22), 224701.

- Persson, B., Carbone, G., Samoilov, V. N., Sivebaek, I. M., Tartaglino, U., Volokitin, A. I., & Yang, C. (2015). Contact mechanics, friction and adhesion with application to quasicrystals. In Fundamentals of Friction and Wear on the Nanoscale (pp. 249-287). Springer, Cham.

- PIARC Technical Committee on Surface Characteristics (C1) (1995). International PIARC Experiment to Compare and Harmonize Texture and Skid Resistance Measurements, Paris, France

- Pinnington, R. J. (2009). Rubber friction on rough and smooth surfaces. Wear, 267(9-10), 1653-1664.

- Preda, I., Covaciu, D., & Ciolan, G. (2010). Coast down test–theoretical and experimental approach.

- Rado, Z. and Kane, M.(2014). An initial attempt to develop an empirical relation between texture and pavement friction using the hht approach. Wear, 309(1):233–246.

- Narasimha Rao, K. V., Kumar, R. K., & Bohara, P. C. (2006). A sensitivity analysis of design attributes and operating conditions on tyre operating temperatures and rolling resistance using finite element analysis. Proceedings of the Institution of Mechanical Engineers, Part D: Journal of Automobile Engineering, 220(5), 501-517.

- Redrouthu, B. M., & Das, S. (2014). Tyre modelling for rolling resistance. Chalmers University of Technology.

- Roylance, D. (2001). Engineering viscoelasticity. Department of Materials Science and Engineering–Massachusetts Institute of Technology, Cambridge MA, 2139, 1-37

- Russ, J. (2013) Fractal surfaces. Springer Science & Business Media.

- Sabey, B. E. (1958). Pressure distributions beneath spherical and conical shapes pressed into a rubber plane, and their bearing on coefficients of friction under wet conditions. Proceedings of the Physical Society, 71(6), 979.

- Saito, K., Horiguchi, T., Kasahara, A., Abe, H., & Henry, J. J. (1996). Development of portable tester for measuring skid resistance and its speed dependency on pavement surfaces. Transportation Research Record: Journal of the Transportation Research

- Sandberg, U., & Ejsmont, J. A. (2000). Noise Emission, Friction and Rolling Resistance of Car Tires: Summary of an Experimental Study. Swedish National Road and Transport Research Institute.

- Sandberg, U., Bergiers, A., Ejsmont, J. A., Goubert, L., Karlsson, R., & Zöller, M. (2011). Road surface influence on tyre/road rolling resistance. Swedish Road and Transport Research Institute (VTI), Prepared as part of the project MIRIAM, Models for rolling resistance in road infrastructure asset management systems.

- Sandberg, U.S.I., (1990) Road Macro and Mega Texture Influence on Fuel Consumption, in Surface Characteristics of Roadways: International Research and Technologies (Astm Stp 1031), W.E. Meyer and J. Reichert, Editors. American Society for Testing and Materials: Philadelphia. p. 460-479.

- Santos, P. M., & Júlio, E. N. (2013). A state-of-the-art review on roughness quantification methods for concrete surfaces. Construction and Building Materials, 38, 912-923.

- Sayers, M.W. and S.M. Karamihas, (1996). Interpretation of Road Roughness Profile Data. Federal Highway Administration Report FHWA/RD-96/101, 177 p.

- Sayers, M. W., & Karamihas, S. M. (1998). The little book of profiling. University of Michigan.

- Scaraggi, M., & Persson, B. N. J. (2015). Friction and universal contact area law for randomly rough viscoelastic contacts. Journal of Physics: Condensed Matter, 27(10), 105102.

- Scaraggi, M., & Persson, B. N. J. (2016). The effect of finite roughness size and bulk thickness on the prediction of rubber friction and contact mechanics. Proceedings of the Institution of Mechanical Engineers, Part C: Journal of Mechanical Engineering Science, 230(9), 1398-1409.

- Serigos, P. A., Smit, A. D. F., & Prozzi, J. A. (2014). Incorporating Surface Micro-texture in the Prediction of Skid Resistance of Flexible Pavements. InTransportation Research Board 93rd Annual Meeting (No. 14-2278).

- Schwarzl, F., Staverman, A. J. (1952). Time temperature dependence of linear viscoelastic behavior. Journal of Applied Physics, 23: 838.

- Schuring, D. J., Siegfried, J. F., & Hall, G. L. (1985). Transient speed and temperature effects on rolling loss of passenger car tires. SAE Transactions, 515-523.

- Slimane, A. B., Khoudeir, M., Brochard, J., & Do, M. T. (2008). Characterization of road microtexture by means of image analysis. Wear, 264(5), 464-468.

- Srirangam, S. K. (2015)."Numerical Simulation of Tire-Pavement Interaction."

- Tourenq, C., & Fourmaintraux, D. (1971). Road surface roughness and the properties of aggregates. Bulletin de Liaison des laboratoires des ponts et chaussées, 51, 61-69.

- Ueckermann, A., Wang, D., Oeser, M., & Steinauer, B. (2015). Calculation of skid resistance from texture measurements. Journal of traffic and transportation engineering (English edition), 2(1), 3-16.

- Vorburger, T. V., Rhee, H. G., Renegar, T. B., Song, J. F., & Zheng, A. (2007). Comparison of optical and stylus methods for measurement of surface texture. The International Journal of Advanced Manufacturing Technology, 33(1-2), 110-118.

- Wallman C.G. Driver Behaviour on Winter Roads, a Driving Simulator Study. VTI rapport 419A, Statens väg- och transportforskningsinstitut, Linköping, 1995.

- Wallman, Carl-Gustaf, and Henrik Astrom. "Friction measurement methods and the correlation between road friction and traffic safety." A literature review. VTI meddelande A 911 (2001): 2001.

- Wambold, J. C., Defrain, L. E., Hegmon, R. R., Macghee, K., Reichert, J., & Spangler, E. B. (1981). State of the art of measurement and analysis of road roughness. Transportation research record, 836, 21-29.

- Wang, C., Caja, J., & Gómez, E. (2018). Comparison of methods for outlier identification in surface characterization. Measurement, 117, 312-325.

- Warren, T. L. and Krajcinovic, D. (1995), "Fractal Models of Elastic–Perfectly Plastic Contact of Rough Surfaces Based on the Cantor Set," International Journal of Solids and Structures, 32(19), pp 2907-2922.

- Wei, C., Olatunbosun, O. A., & Behroozi, M. (2016). Simulation of tyre rolling resistance generated on uneven road. Int. J. Veh. Des, 70(2), 113-136.

- Wei, C., & Olatunbosun, O. A. (2014). Transient dynamic behaviour of finite element tire traversing obstacles with different heights. Journal of Terramechanics, 56, 1-16.

- Wei, C., & Olatunbosun, O. A. (2016). The effects of tyre material and structure properties on relaxation length using finite element method. Materials & Design, 102, 14-20.

- Williams, M. L., Landel, R. F., & Ferry, J. D. (1955). The temperature dependence of relaxation mechanisms in amorphous polymers and other glass-forming liquids. Journal of the American Chemical society, 77(14), 3701-3707.

- Wong, J. Y. (2008). Theory of ground vehicles. John Wiley & Sons.

- Wullens, F., & Kropp, W. (2004). A three-dimensional contact model for tyre/road interaction in rolling conditions. Acta Acustica united with Acustica,90(4), 702-711.

- Xiong, Y., & Tuononen, A. (2013). Optical measurement of tread deformation for rolling resistance studies. In Qingdao: The 23rd International Symposium on Dynamics of Vehicles on Roads (pp. 1-10).

- Yandell, W. O. (1971). A new theory of hysteretic sliding friction. Wear,17(4), 229-244.

- Yandell, W. O., & Sawyer, S. (1994). Prediction of tire-road friction from texture measurements. Transportation Research Record, (1435).

- Yeoh, O. H. (1993)"Some forms of the strain energy function for rubber." Rubber Chemistry and technology 66.5, 754-771.

- Zaabar, I. (2010). Effect of pavement condition on vehicle operating costs including fuel consumption, vehicle durability and damage to transported goods. Michigan State University.

- Zaabar, I., Chatti, K., and Lajnef, N., (2018). Evaluation of fuel consumption models for pavement surface roughness effect Submitted to advances in materials and pavement performance prediction conference, Doha, Qatar.